2014-07-08

Small Molecule Activation at Nickel and Platinum Centers Containing Bulky Tin and TEMPO Radical Ligands

Anjaneyulu Koppaka
University of Miami, anji361@gmail.com

UNIVERSITY OF MIAMI

SMALL MOLECULE ACTIVATION AT NICKEL AND PLATINUM CENTERS CONTAINING BULKY TIN AND TEMPO RADICAL LIGANDS

By

Anjaneyulu Koppaka

A DISSERTATION

Submitted to the Faculty
of the University of Miami
in partial fulfillment of the requirements for
the degree of Doctor of Philosophy

Coral Gables, Florida

August 2014

UNIVERSITY OF MIAMI

A dissertation submitted in partial fulfillment of
the requirements for the degree of
Doctor of Philosophy

SMALL MOLECULE ACTIVATION AT NICKEL AND PLATINUM CENTERS CONTAINING BULKY TIN AND TEMPO RADICAL LIGANDS

Anjaneyulu Koppaka

Approved:

_____
Burjor Captain, Ph.D.
Professor of Chemistry

_____
Françisco M. Raymo, Ph.D.
Professor of Chemistry

_____
Jamie D. Walls, Ph.D.
Professor of Chemistry

_____
M. Brian Blake, Ph.D.
Dean of the Graduate School

_____
Ali Ghahremaninezhad-M, Ph.D.
Professor of Civil, Architectural, and
Environmental Engineering

KOPPAKA, ANJANEYULU (Ph.D., Chemistry)
Small Molecule Activation at Nickel and Platinum Centers Containing Bulky Tin and TEMPO Radical Ligands. (August 2014)

Abstract of a dissertation at the University of Miami.

Dissertation supervised by Professor Burjor Captain.
No. of pages in text. (225)

Metal complexes have long been recognized as fundamental in activating simple small molecules, which provide low-barrier reaction pathways through binding. One way to make highly reactive metal complexes is by reacting metal precursors with sterically demanding ligands that can create electronic unsaturation on the metal center, where activation can occur. A series of sterically crowded metal complexes have been synthesized by reactions of $Pt(COD)_2$ with bulky tin ligands of the type $HSnR_3$ [R = Bu^t, Ph and $C_6H_2Me_3$(mesitylene)]. These new complexes were studied for activation of small molecules like H_2, CO, C_2H_2, C_2H_4, and catalytic H_2- D_2 exchange reactions at ambient conditions. The complex $Pt(SnBu^t_3)_2(CNBu^t)_2$ was found to activate H_2 and CO reversibly in solid state, as well as in solution. It also catalyzes the H_2-D_2 exchange at room temperature. Currently, the NHC carbene compounds as ligands are one of the most highly studied in organometallic chemistry. The role of NHC carbene ligands on the reactivity of Pt-Sn bimetallic complexes has also been studied. The Pt-Sn-NHC complex, $[Pt(SnBu^t_3)(IBu^t)(H)]_2$ was found to be highly reactive and efficient in the reversible activation of H_2, and C_2H_4 at room temperature. This compound also activates CO at room temperature.

The bimetallic complexes with inexpensive metals Ni & Sn were also synthesized and studied catalytically. The coordination chemistry of TEMPO radical with Ni metal was also explored. The 16 electron unsaturated *'bow-tie'* complex, Ni(η^2-TEMPO)$_2$ was found to be highly efficient in activation of C-H bond of alkynes and also found to be highly reactive towards other small molecules such as H_2, CO, CO_2, and other coordinating solvents such as THF and CH_3CN. We were able to connect two Ni metal centers using an organic moiety in the complex Ni(η^2-TEMPO)(κ^1-TEMPOH)[κ^1-κ^1-CC(C_6H_4)CC]Ni(η^2-TEMPO)(κ^1-TEMPOH).

ACKNOWLEDGEMENTS

It is with great honor that I am able to dedicate this work to my family. Without the caring support of my mother Rangamma, father Pothuraju, brothers Satyanarayana and Nagaraju and my school teacher Subramanyam garu, there is simply no way I would be the person I am today. Equally as important, I am extremely thankful to my research mentor Dr. Burjor Captain for his constant support, guidance, encouragement, friendly nature, and the research techniques he has taught me over the course of my Ph.D. period.

I must thank my previous lab mates Dr. Lei Zhu, Dr. Derek Isrow, Dr. Veeranna Yempally and Dr. Sumit Saha for sharing their excellent research techniques and providing me a helping hand in guiding my research in a fruitful direction. It is because of these fine men that I am able to continue my research and write this work. I appreciate the help received from Dr. Stefania Impellizzeri in carrying out the photo polymerization reactions, Dr. David Hudson for NMR experiments and Edward Torres for mass spectroscopic experiments. I am grateful to Dr. Lever for teaching me key research techniques during his brief stay in our lab as a vising professor. I would like to extend my sincere thanks to my lab mates Nathaniel Westfall and Mark Enriquez for their kind support in writing my work. I also would like to thank Lydia Gonzalez, Sara Sucklal and Susana Gadanyi for their administrative support.

I am grateful to my committee members Dr. Françisco M. Raymo, Dr. Jamie D. Walls, and Dr. Ali Ghahremaninezhad-M for their assistance and guidance throughout my time in the chemistry department.

Finally, I am extremely thankful to the Department of Chemistry, College of Arts and Sciences, and the University of Miami for providing me an opportunity to do my Ph.D. program with excellent research facilities, necessary financial support and wonderful Ph.D. memories.

Anjaneyulu Koppaka
Chemistry CANE
University of Miami
Coral Gables, Florida
USA

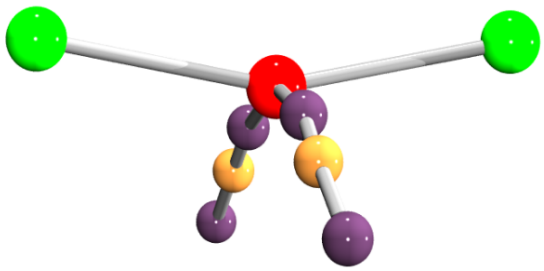

TABLE OF CONTENTS

LIST OF FIGURES

CHAPTER 1

CHAPTER 2

CHAPTER 3

CHAPTER 4

CHAPTER 5

APPENDIX A

APPENDIX C

APPENDIX D

LIST OF SCHEMES

CHAPTER 1

CHAPTER 2

CHAPTER 3

CHAPTER 4

CHAPTER 5

APPENDIX D

LIST OF TABLES

CHAPTER 1

CHAPTER 5

APPENDIX A

APPENDIX B

APPENDIX C

APPENDIX D

Chapter 1: Unsaturated Transition Metal Complexes in Activation of Small Molecules: Role of Sterics Induced by Bulky Ligands and Metal-Ligand Synergistic Effects.

1.1. Introduction.

Highly abundant simple small molecules like H_2, N_2, O_2, CO and CO_2 are incredible sources of chemical energy. These can be used in many ways, for example, molecules like H_2, N_2 and O_2 can be used to fuel biological systems,[1] and molecules like CO and CO_2 can be used as feed stocks of carbon for liquid fuels and synthesis of other useful organic compounds.[2,3] Nature uses these simple molecules to construct highly systematic complex molecules for selective processes. Despite much understanding on how nature activates and uses these simple molecules, we are still underdeveloped in activating them to produce useful synthetic products at an industrial scale.

Today's world is powered by the petroleum and natural gas industries, which generate ethylene and other products by 'cracking' the hydrocarbons; these in turn drive the chemical industry which is highly dependent on olefins and acetylenes. The understanding of the interactions of these chemicals with transition metal complexes is extremely important for the sustainability of these industries and also for the development of alternative routes for future energy sources in the wake of diminishing petroleum and natural gas resources. This is where a catalyst comes into picture and all the above mentioned issues can be addressed by well-developed catalyst industry with the understanding of the interaction of substrates, such as the above mentioned small molecules or the products of natural gas and petroleum and overcoming their significant energy barriers.

A catalyst is defined as a substance that accelerates the rates of chemical reactions without being consumed, enhances product selectivity with increased efficiency, reduces energy consumption and minimizes waste. This is the main reason why the majority of the chemical industry processes employ catalysts at certain stages during the manufacturing process. These catalysts are mainly classified in to two categories i) Heterogeneous catalysts ii) Homogeneous catalysts. The majority of the catalysts at present are heterogeneous catalysts. These catalysts include finely divided metal particles, i.e., Raney nickel, platinum black etc. On the other hand, homogeneous catalysts are operated in solution state and are usually derived from well-defined precursors; the simplest example is H^+, generated in the acid catalyzed reactions, for example, acid catalyzed esterification of carboxylic acids. Some of the well-known metal complexes that are come across frequently in the literature as catalysts and non-catalysts are shown in the Figure 1.1.

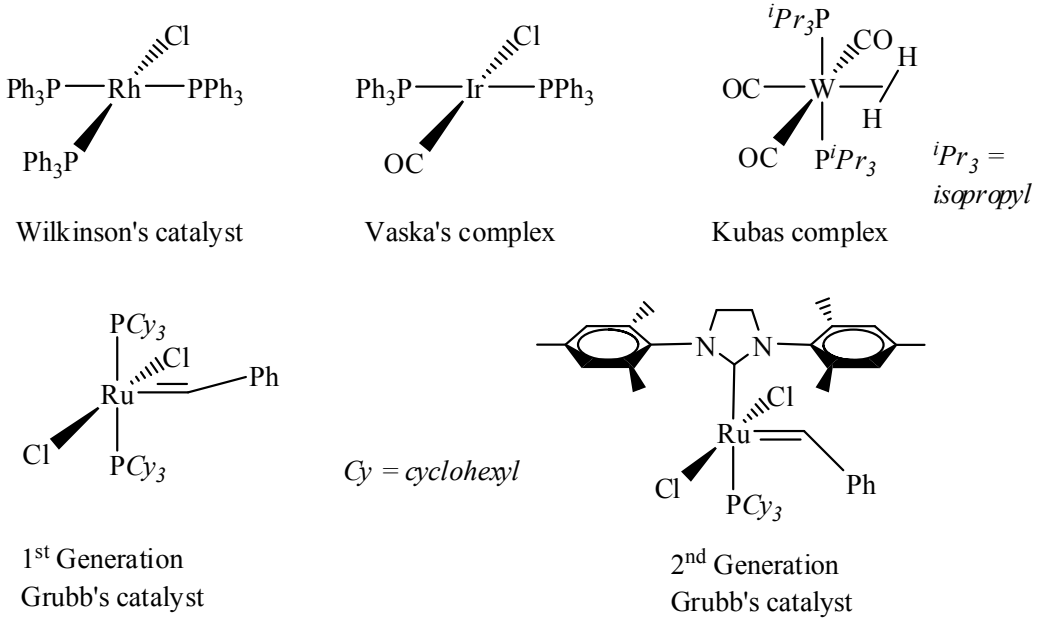

Figure 1.1. Some of the well-known transition metal complexes.

Today, the majority of the catalytic process employs heterogeneous catalysts because of the advantage of ease of catalyst re-cyclization compared to homogeneous catalyst. But, homogeneous catalysts have other advantages which are not possible with heterogeneous catalysts; such as they can be operated at mild reaction conditions, high selectivity, less sensitivity to catalyst poison, insights into catalysis mechanisms and most importantly variability in terms of steric and electronic properties for selectivity; it is where the transition metal complexes aptly fit as homogeneous catalysts for a wide variety of industrial applications.[4]

1.2. Transition metal complexes in catalysis.

Metal complexes have long been recognized as fundamental in activation and catalysis chemistry, which provides low-barrier reaction pathways through binding. The first reported synthetic organometallic complex $K[Pt(C_2H_4)Cl_3]$, synthesized by W.C. Zeise in 1827 was the activation of ethylene by $PtCl_4$.[5,6] The nickel tetracarbonyl complex, $Ni(CO)_4$ reported by Mond in 1890 led to the development of industrial process called '*Mond's process'* for the purification of nickel ores.[7,8]

Discovered in 1960s by J. W. DiLuzio and Lauri Vaska, the complex $IrCl(CO)(PPh_3)_2$ [*trans*-chlorocarbonyl*bis*(triphenylphosphine)iridium(I)] (see Figure 1.1), inspired many inorganic chemists through its ability to activate a number of small molecules (see Scheme 1.1) and led to the synthesis of similar well-known complexes that revolutionized homogeneous catalysis. It was one of the first compounds discovered which mimics the action of hemoglobin, another organometallic complex of iron. Vaska's complex reacts with O_2 and H_2 reversibly. The reaction with O_2 forms a η^2- side on-bound complex unlike the case of hemoglobin, where O_2 is end-on bound. It is a 16

electron unsaturated square planar d^8 complex, and to satisfy 18 electron configuration it can oxidatively add (where the formal oxidation of metal center increases and reverse of it is reductive elimination where the oxidation state decreases) two one-electron donating ligands or one two-electron donating ligand, to become an octahedral complex (see Scheme 1.1).

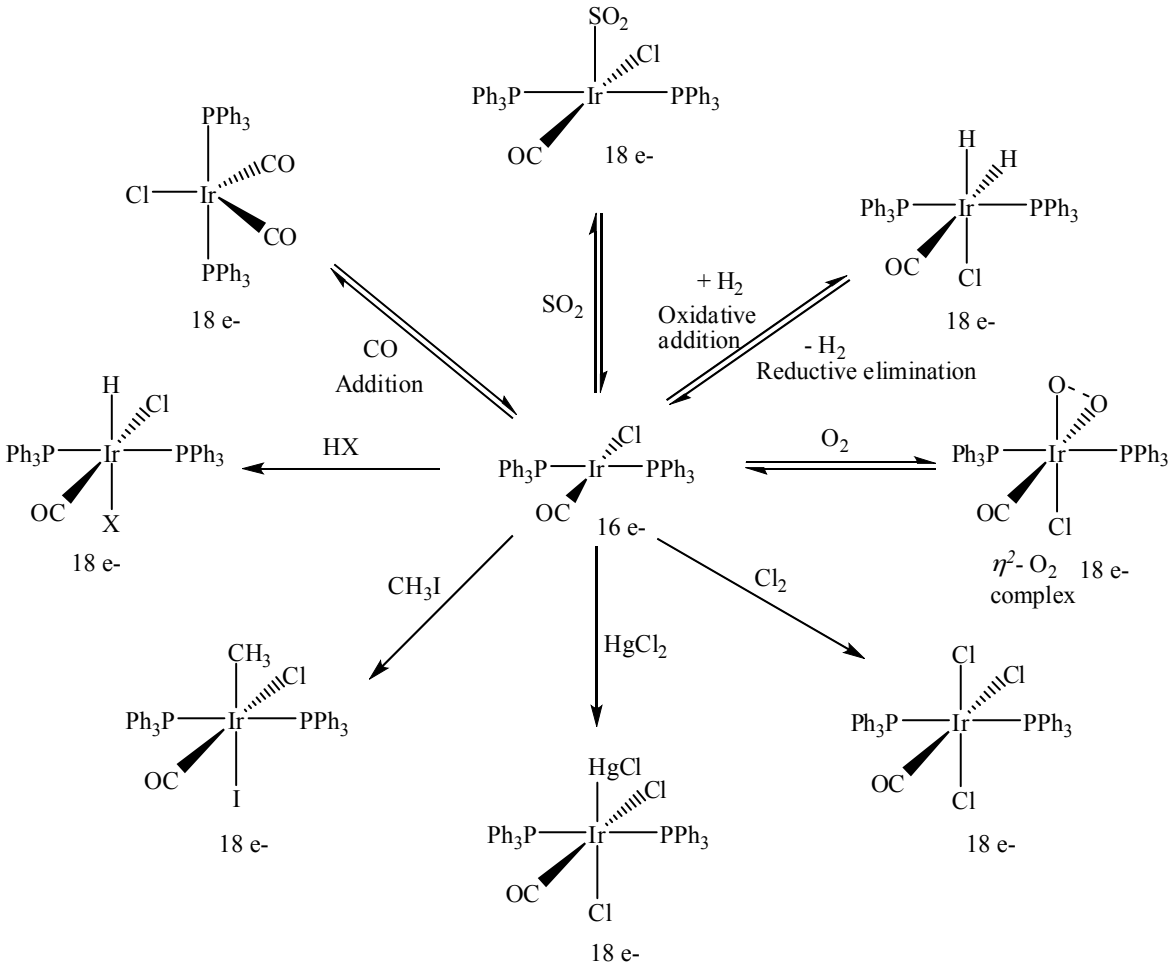

Scheme 1.1. Reaction of Vaska's complex with various small molecules.

The majority of the well-known industrially important processes use catalyst systems based on transition metals. For example, water-gas shift reaction employs

catalysts such as CuO, and ZnO for low temperature shift reaction (LTS), and Fe_2O_3 and Cr_2O_3 are used for high temperature shift reaction (HTS). The Fisher-Tropsch process, for the conversation of mixture of H_2 and CO into liquid hydrocarbons, uses a wide variety of transition metals, such as cobalt, iron, and ruthenium. Nickel is used to form methane. In the Haber Bosch process for making ammonia from N_2 and H_2, catalysts based on iron and ruthenium are used.

The water soluble vitamin B_{12}, known as coenzyme B_{12}, is the oldest known example of a naturally occurring transition metal complex which is known to aid the catalysis of 1-2 shifts in biochemical systems (see Scheme 1.2).[9]

Isomerization

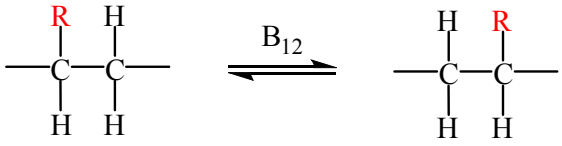

Isomerization and dehydration

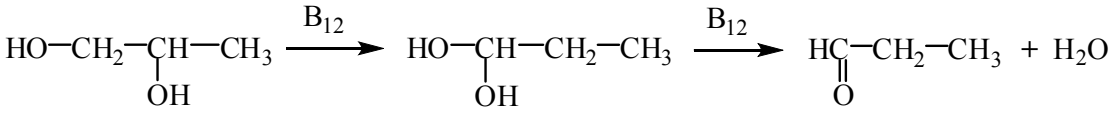

Scheme 1.2. Catalytic reactions by coenzyme B_{12}.[9]

In the homogeneous catalysis, some of the industrially important process such as hydroformylation (which involves activation of H_2 and CO),[10,11] transfer hydrogenation reactions (where dihydrogen is added to a molecule from a source other than gaseous H_2)[12], and Wacker process for the conversion of ethylene into acetaldehyde,[13] employ the transition metal organometallic complexes as catalysts. The basic principle in catalysis is activating the metal complex by creating an electronic deficiency or unsaturation on the

key central metal atom where the activation or catalysis happens. During this process, the ligands on the metal center play a key role in the form of dissociation-association from or to the metal center, migration to the other part of the complex to make way for the incoming molecule and provide stability to the molecule. Attempts were made to explain all these properties of the complexes in combination of the number of valence electrons on the metal center and molecular orbital theory.

1.3. The 18 electron rule, saturated and unsaturated transition metal complexes in activation of small molecules.

The 18 electron rule, similar to octect rule, was first proposed by Langmuir for relating the number of shared electrons or covalence (V_c) of a given atom in a compound to the number of valence electrons (e) and the number of electrons required to complete its valence shell (s), as shown in the equation 1.1.[14,15]

$$V_c = s - e \text{ (or) } V_c = 18 - e \qquad \textbf{(eq.1.1)}$$

In the beginning, the 18 electron rule was used for counting the valence electrons of the carbonyl complexes of transition metal complexes. Later, it has been extended to transition metal complexes with other ligands as well.[15,16] The 18 electron rule has been used to rationalize the stoichiometries, structures, and stability of the metal complexes. Based on the fact that the complexes that obey 18 electron rule will attain the electronic configuration of the next group 18 rare gas, it has been postulated that those complexes that obey this rule are stable and that does not obey are unstable.[17] However, it has been found that the majority of transition metal complexes do not obey this rule; yet they are stable, and no satisfactory explanation was given by the 18 electron rule for this behavior.[18]

The anomalies in stability of complexes that do not obey the rule have been explained in terms of molecular orbital theory. The Cr(0)complex, $Cr(CO)_6$, obeys the 18 electron rule (total electron count on Cr is 18, 12 electrons from 6 CO ligands and 6 electrons from Cr). If you look at the molecular orbital diagram (see Figure 1.2) of this complex, the e_g orbitals are anti-bonding and addition of electrons destabilize the complex, similarly removing the electrons from the t_{2g} bonding orbital, which are resulting from the strong π acceptor ability of CO ligands will again destabilize the complex. Ligands that are both strong σ donor and π acceptor force the energy of molecular orbitals to appear as shown in the case of $Cr(CO)_6$ (see Figure 1.2), and force the molecule to obey the 18 electron rule.

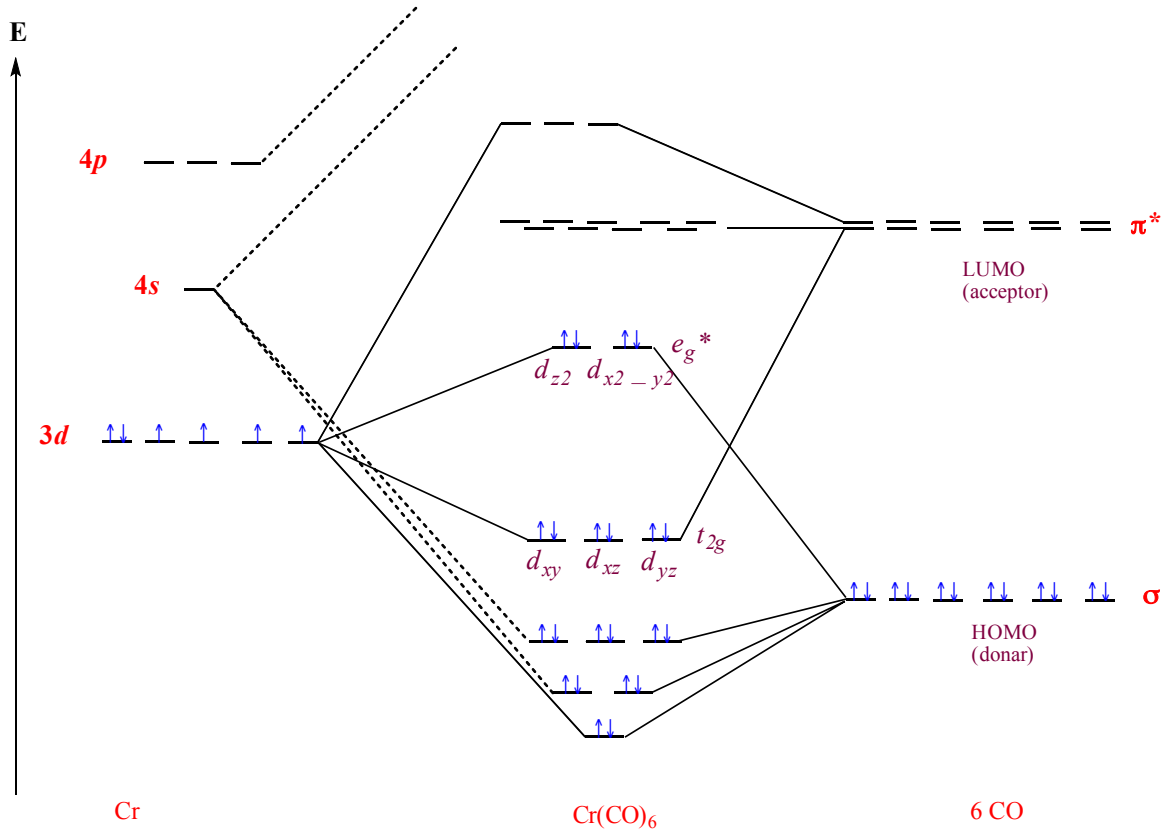

Figure 1.2. Molecular orbital diagram of $Cr(CO)_6$.[19]

The energy gap between the e_g* and t_{2g} orbital varies depending up on the type of the ligand coordinating with the metal center. The ligands which do not have the above mentioned features, as in the case of CO, may or may not force their complexes to obey the rule. Most of the organic ligands do not have these capabilities and they form the complexes that may or may not obey the 18 electron rule and their MO diagrams resemble the one shown in Figure 1.3.

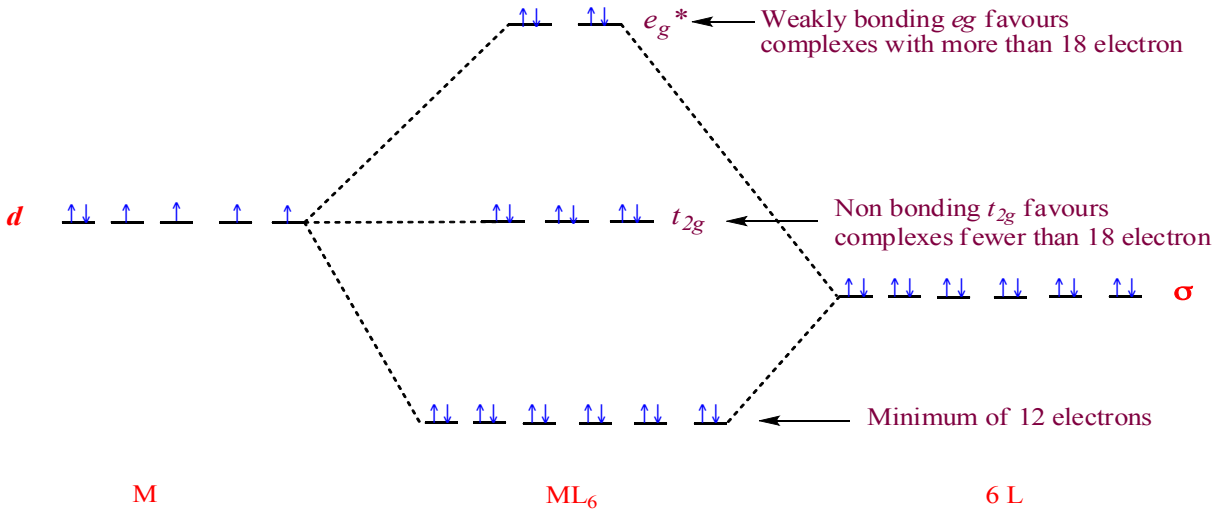

Figure 1.3. Representative MO diagram for the octahedral complexes that do not obey 18 electron rule.[19]

The 22 electron octahedral complex $[Zn(en)_3]^{2+}$ is a stable complex, though it has 4 electrons in the e_g* orbital. The en (ethylenediamine) ligand is not as good a σ donor as CO ligand, as a result, the e_g* orbitals are not as strong anti-bonding as is the case of $Cr(CO)_6$, to destabilize the complex with electrons occupying e_g* anti-bonding orbital. The complex $[Ti(F)_6]^{2-}$ is an extreme example of octahedral complex, with just 12 electrons. In this case the F^- ligand is a σ donor as well as π donor. As a result of π

donating ability, the t_{2g} orbitals becomes slightly anti-bonding, which makes the complex to have 12 electrons in the bonding 6 σ orbitals and no electrons in t_{2g} orbitals.

These arguments are generally applicable to octahedral complexes and in some cases can be extended to other geometries as well, such as trigonal bipyramidal {[$Fe(CO)_5$]} and tetrahedral complexes [$Ni(CO)_4$]. However, in the case of square planar complexes a different scenario arises where in most of the instances the 16 electron complexes are stable, particularly d^8 metal complexes. An example of MO diagram of d^8 square planar complex is shown in Figure 1.4.

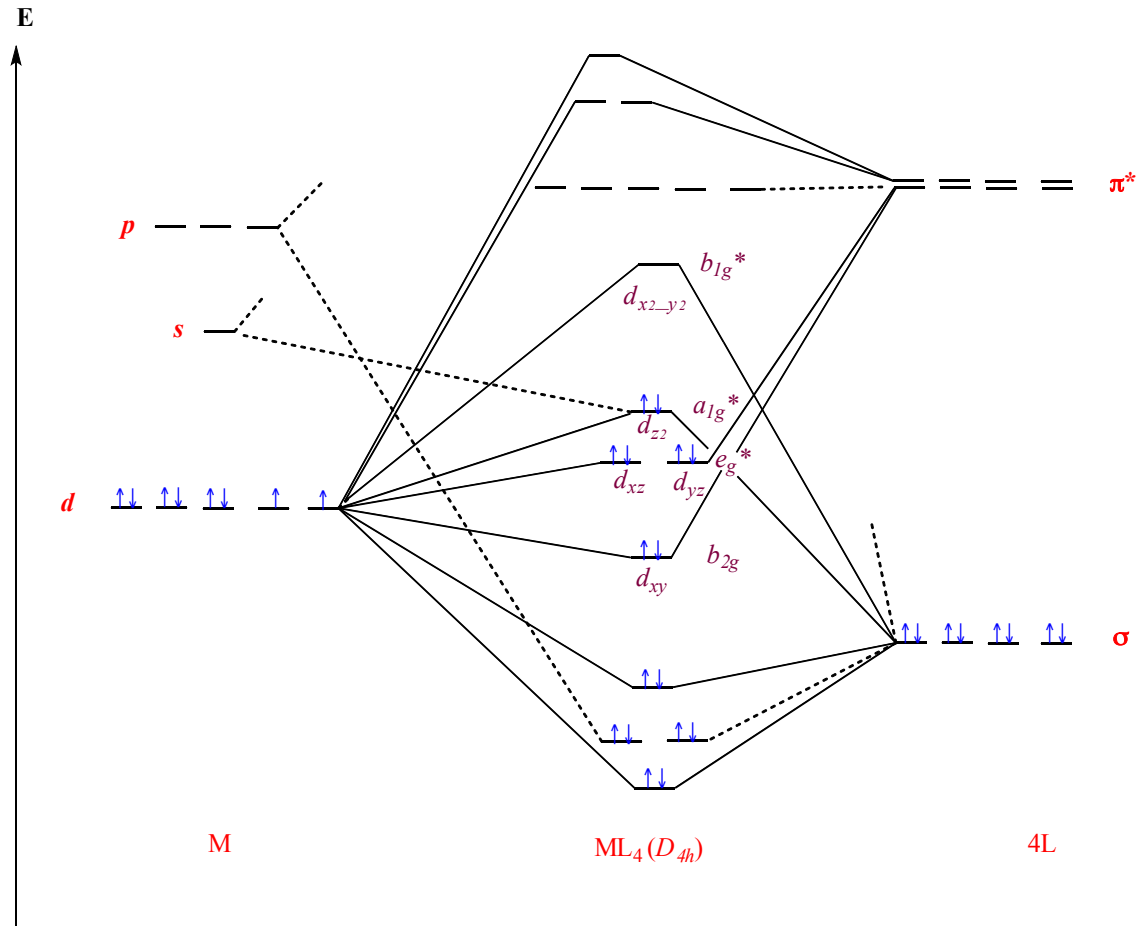

Figure. 1.4. Representative MO diagram of square planar complex.[19]

As you see in the Figure 1.4, any additional electrons go into the anti-bonding orbital b_{1g}*, which is derived from the anti-bonding interaction of $d_{x^2-y^2}$ orbital of metal with σ- donor orbitals of ligand. The b_{1g}*, anti- bonding interactions are strongest as the $d_{x^2-y^2}$ orbital points directly towards the ligand, therefore resulting in square planar geometry; complexes that have both σ-donor and π- acceptor ligands are stable with 16 electrons. In some instances, these complexes can also accept one or two-electrons along the *z*- axis vacant co-ordination sites, and that is how the 16 electron complexes like Wilkinson's catalyst and Vaska's complexes react with small molecules.

Nevertheless, in general, complexes with less than 18 valence electrons, called unsaturated, are found to be more reactive than the complexes with 18 valence electrons (18 ve), saturated complexes. This generalization is still in use for predicting the reactivity and stoichiometries of transition metal complexes. The saturated complexes, also called coordinatively saturated complexes, are generally 'exchange inert' and they react with other compounds or ligands in different ways. Some well-known mechanisms include "Dissociation-Substitution (or association)", where the formal oxidation state of the metal center remains same in the dissociative step (see Scheme 1.3), "Reductive elimination-Oxidative addition" fashion where the formal oxidation state of the metal center changes (see Scheme 1.4), and Insertion mechanism where an incoming ligand or molecule directly inserts in to the already existing metal-ligand bond (see Scheme 1.5).[20] Other possible mechanisms are also reported for the insertion reactions. These insertion reactions have potential applications in synthetic organic chemistry. These complexes generally have octahedral or tetrahedral geometry.

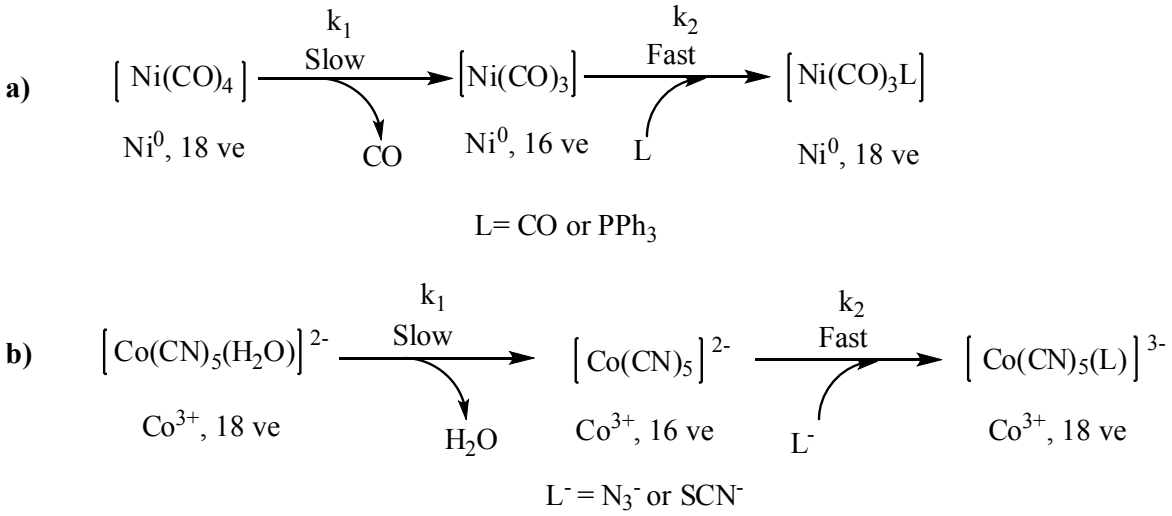

Scheme 1.3. Dissociation-Substitution by a) tetrahedral $Ni(CO)_4$, [21] and by b) octahedral $[Co(CN)_5(H_2O)]^{2-}$ complex.[22]

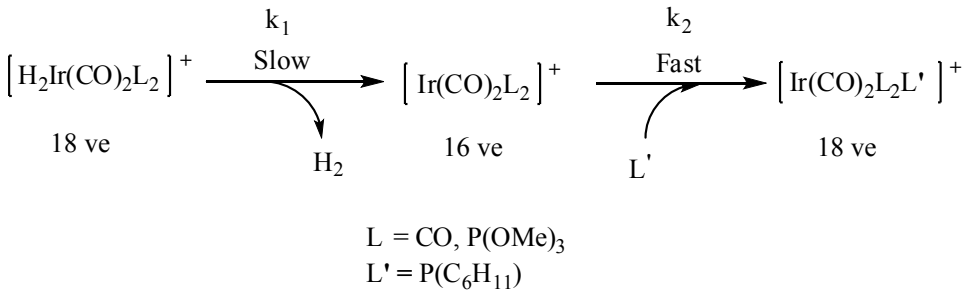

Scheme 1.4. Reductive elimination-Oxidative addition by octahedral iridium complex, $[H_2Ir(CO)_2L_2]$.[23]

The rate determining step is the dissociation step, k_1, which is slow, and no effect of k_2 on the overall rate of the reaction, was observed in these reactions (see Scheme 1.5).

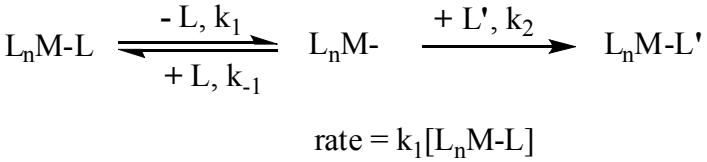

Scheme 1.5. Rate determining steps in "Dissociation-Substitution" and "Reductive elimination -oxidative addition" reactions.

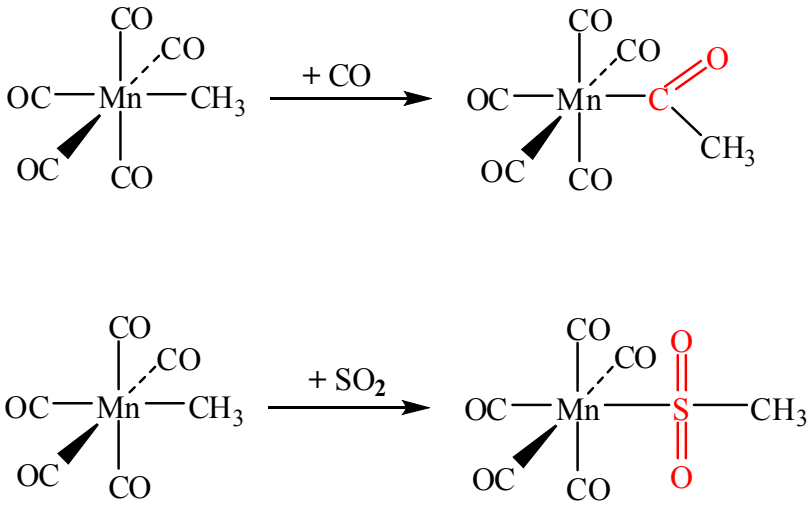

Scheme 1.6. Insertion reactions by $Mn(CO)_5(CH_3)$ complex.[20]

As mentioned earlier, the majority of transition metal complexes deviates from the 18 electron rule and are stable at ambient conditions. These complexes generally possess square planar geometry. Important examples of square-planar low-spin d^8 metal ions are Ni(II), Pd(II), and Pt(II). The well-known complexes include Vaska's complex, $[IrCl(CO)(PPh_3)_2]$, Wilkinson's complex, $[RhCl(PPh_3)_3]$, and Zeise's salt, $[PtCl_3(\eta^2\text{-}C_2H_4)]^-$. The common feature with all these complexes is they are all square planar d^8 complexes with 16 valence electrons on the central metal atom. These complexes generally undergo reactions in a wide variety of ways, which include, a) Dissociation-Association, b) Oxidative addition, c) Reductive elimination, d) Nucleophilic displacement, e) Insertion, and f) Abstraction. [24]

Many catalysts, during catalytic cycles, alternate between 16 and 14 or 18 and 16 or 14 valence electron intermediates with a series of above mentioned reactions connected in a cyclic fashion.[24] Some well-known examples are Grubb's catalyst in olefin metathesis. Olefin metathesis was first reported in 1950s, which involves the

formal exchange or redistribution of :CR_2 fragments (R= H or alkyl) between alkenes (see Scheme 1.7). Yves Chauvin, Robert H. Grubbs, and Richard R. Schrock were collectively awarded the 2005 Nobel Prize in Chemistry for the pioneering work done in this field. Robert H. Grubbs developed a series of transition metal- carbene complexes (see Figure 1.1), called Grubb's catalysts, which catalyzes these reactions.[25–28]

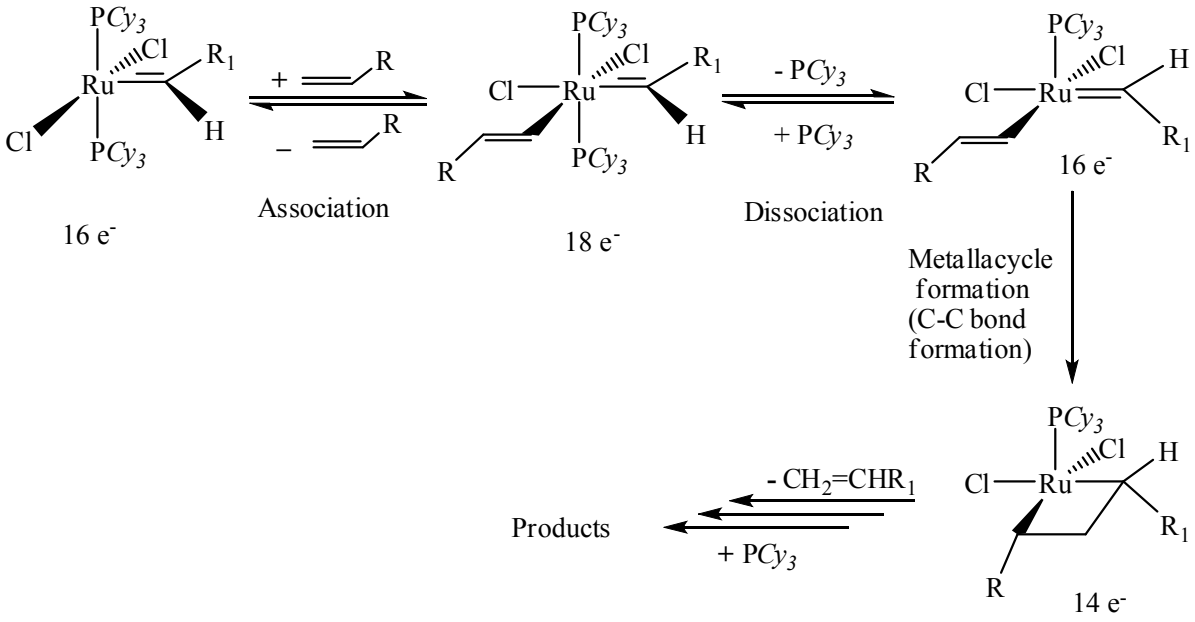

Scheme 1.7: Olefin metathesis by Grubb's catalyst.[28]

In Monsanto Acetic acid process, for the synthesis of acetic acid by catalytic carbonylation of ethanol, involves a 16 electron rhodium complex, $[Rh(CO)_2(I)_2]^-$ (see Scheme 1.8). [29]

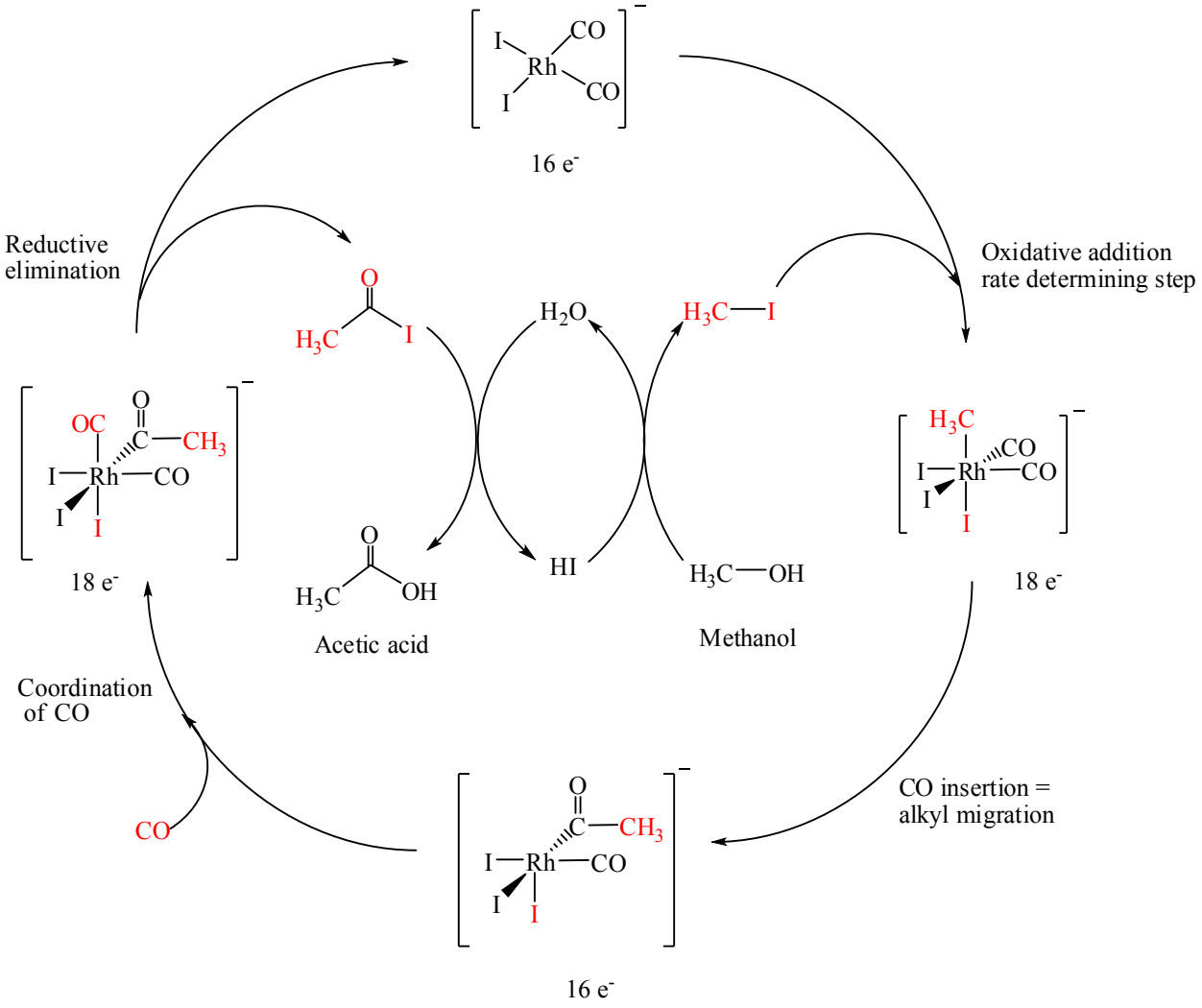

Scheme 1.8. Monsanto process of Acetic acid synthesis from methanol and CO.[29]

Similarly in the catalytic hydrogenation of alkenes using Wilkinson's catalyst $RhCl(PPh_3)_3$, the catalytic cycle involves the transition of complex between 16 valence electrons to 18 valence electrons. This catalyst is also known to selectively hydrogenate the alkenes. This is possibly due to the bulky phosphine ligands on the metal Rh (see next section). The industrial process, Wacker (or Smidt) process for the synthesis of acetaldehyde from ethylene, involves the 16 electron unsaturated palladium complex, $[PdCl4]^{2-}$.

1.4. The role of sterics induced by ligands in catalysis.

Ligands play a vital role in stabilizing transition metal complexes. The stability, as well as the reactivity of a metal in its complex form, depends upon the number, size, and the type of ligands it is bound to. Sterics imparted by the size of the ligand are found to be as equally important as electronic factors and plays a significant role in creation of unsaturation on the metal center.[30–35] Sterics greatly influence the structures, spectroscopic properties, and chemical behavior of the metal complexes.[35] By increasing the size of the ligand, one can alter the bond angle, increase the bond lengths, and favor lower coordination numbers (unsaturation) and coordination of smaller ligands. The Tolman cone angle, a concept introduced by Chadwick A. Tolman, to define the size of the ligand is highly used in homogeneous catalysis such as hydroformylation and hydrogenation reactions, to design a catalyst of specific interest to achieve selectivity.[34–36]

Tolman reported the influence of ligand size on the rate of hydrocyanation of butadiene by the nickel complex, $Ni(CO)_3L$ (see Scheme 1.9). By increasing the size of ligand, he was able to achieve greater reaction rates by increasing the rate of formation of the intermediate $HNi(CO)_{3(}CN)$.[35]

$$HCN + Ni(CO)_3L \underset{}{\overset{K}{\rightleftharpoons}} HNi(CO)_3CN + L$$

$$L = P(OEt_3),\ PPh(OEt)_2,\ P(O\text{-}o\text{-}Tolyl)$$

$$K = 0.005\ [P(OEt_3)] < 0.03\ [PPh(OEt)_2] < 10^4\ [\ P(O\text{-}o\text{-}Tolyl)_3]$$

Scheme 1.9. Effect of size of ligand on rate of hydrocyanation of butadiene.[35]

The best example for the effect of sterics on the catalysis is the Wilkinson's catalyst in the hydrogenation of alkenes. This catalyst has three bulky phosphine ligands on the Rh catalyst, which stabilizes this complex. During hydrogenation catalysis, theses ligands restrict the approach of bulky centers of the molecule being reduced towards the Rh metal center where the reduction happens. When a molecule with large number of double bonds is catalyzed, it selectively hydrogenates the double bonds which are strerically less hindered. Among a mixture of alkenes the one which is less hindered gets reduced faster compared to the other alkenes (see the equation 1.2 and Table 1.1).

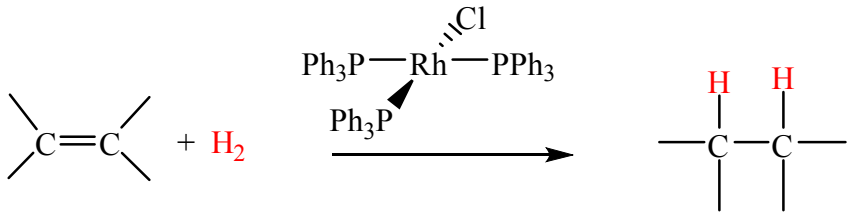

(eq. 1.2)

Compound hydrogenated	rate constant x 100 (*L / mol s*)
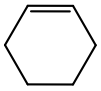	31.6
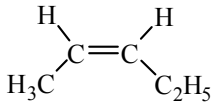	9.9
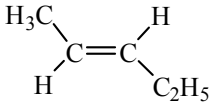	1.8
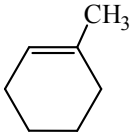	0.6
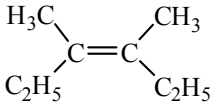	< 0.1

Table 1.1. Relative rates of hydrogenation using Wilkinson's catalyst at 25 °C.[24]

1.5. Bi metallic complexes with promising results in catalysis.

Superior synthetic methods and catalysts always evolve over time; chemists have long been interested in catalyzing reactions by using bimetallic complexes that contain two or more different metal centers rather than monometallic compounds, because of the superior catalytic performance of bimetallic compounds over monometallic compounds.[37,38] Again, the inspiration for the development of this field of inorganic chemistry is drawn from nature. Nature uses a variety of bimetallic complexes, particularly enzymes, for various functions.[39] The advantage with bimetallic complexes is that they offer a variety of reactions happening at the same time on two different active metal centers.[40] Thus, one could imagine progress of different types of oxidative-addition, reductive-elimination patterns, and the stabilization of unusual oxidation states and of ligand-bonding modes happening at same time which are not possible in monometallic complexes.

Takayuki Komatsu and co-workers used bimetallic compounds of Ni-Sn to catalyze de-hydrogenation of cyclohexane to benzene and methane.[41] Piscina, J. and co-workers found that silica supported Ni-Sn compounds catalyzes CO oxidation reaction.[42] In another example, Yuriy Román-Leshkov and co-workers found that bimetallic carbon supported copper-ruthenium (CuRu/C) catalysts are more superior than monometallic compounds, copper chromite ($CuCrO_4$) in converting 5-hydroxymethylfurfural (HMF) to 2,5-dimethylfuran (DMF), a potential liquid transportation biofuel.[43] In this reaction, Ru acts as a chloride resistant, which they introduce to purify the synthesized DMF from intermediates and other impurities. Recent work from our lab on bimetallic complex of Fe-Sn shows successful selective activation of benzylic C-H bond, and importance of the

bimetallic complexes.[44] One of the highly studied bimetallic complex systems is transition metal-tin (TM-Sn) chemistry. Tin ligands have shown versatile properties in coordination chemistry. They are used in catalytic and non-catalytic reactions. They are found to have a strong labilizing effect on their *trans* ligands, and by themselves they are also labile and thus can provide necessary vacant coordination sites in the catalysis and also can promote the migratory insertions reactions.[45,46] These ligands are also found to accomplish oxidative addition and subsequent reductive elimination processes with ease. Most importantly a variety of organo-tin compounds are available for catalysis with the flexibility of varying bulkiness on the tin center. Various transition metal–tin hetero bimetallic catalysts were synthesized and studied effectively in the catalytic and non-catalytic fields of hydrogenation, isomerization of olefins, polymerization, hydroformylation, and coupling reactions. A review by Marks S. Holt, William L. Wilson, and John H. Nelson efficiently summarized the application of TM-Sn bimetallic complexes for various applications in chemistry.[47]

1.6. Statement of purpose.

The aim of the work that has been presented here is to synthesize electronically unsaturated, inexpensive bimetallic complexes aided by sterically demanding ligands that can exclusively activate the small molecules. The above detailed Schemes and reactions represent the underlying principles in successful synthesis of the reactive unsaturated transition metal (TM) complexes stabilized by bulky ligands. As discussed above tin has been found to display a variety of properties that can aid in the activation of small molecules. By using tin as both ligand and hetero metal, we wanted to probe the cooperative reactivity between two metals in the resulting TM-Sn bimetallic complexes.

Interestingly, these complexes were found to successfully activate small molecules, and, do so in some instances, catalytically. The initial work reported here comprises of Pt-Sn bimetallic complexes. Though Pt is an expensive metal, we employed this metal to test its ability to activate small molecules in homogenous catalysis, because of its superior catalytic properties. We also used other bulky ligands such as carbenes in combination with tin to test their reactivity towards small molecules. Later we tried to replace the Pt metal with inexpensive Ni metal to mimic the reactivity of Pt-Sn bimetallic complexes. The Ni-Sn complexes were found to be photo sensitive and indicated the formation of radicals in the presence of light they also displayed some interesting catalytic properties in polymerization.

The stable radical TEMPO is a well-known radical trap and its applications as a coordinating ligand are very few. It is known to coordinate to metal centers in different modes. Here, in the last chapter, the unexpected complexes of this seemingly bulky TEMPO radical as ligand and its unexpected Ni-TEMPO complexes and their synergistic reactivity to activate carbon-hydrogen bond of small organic molecules have been discussed.

Chapter 2: Activation of Small Molecules by Sterically Crowded Pt-Sn Bimetallic Complexes: Synthesis, Structures, and Reactivity.

2.1 Background.

Transition metal – tin chemistry has been quite well known for some time now, and one way to prepare transition metal – tin complexes is by using triaryl and trialkyl stannanes (R_3SnH). R_3SnH reacts readily with transition metals via oxidative addition of the Sn-H bond to the metal atom. Tin compounds have been used extensively as modifiers of the platinum group metals, and platinum-tin bimetallic heterogeneous catalysts have been shown to be highly efficient for use by the petroleum industry for a number of processes vital to petroleum reforming, catalytic hydrogenations[48–51] and dehydrogenations.[52,53] Under homogeneous conditions, tin complexes have also been shown to catalyze many important reactions such as hydrogenation and isomerization of olefins, the water gas shift reaction, and also to improve the product selectivities of the reactions[47,54–56]. Recently, it was reported that the trimetallic tin containing catalyst $PtRu_5Sn$, exhibited the highest selectivity for formation of unsaturated alcohols in the hydrogenation of citral.[57]

We have been interested in investigating bulky tin compounds as a reagent in organometallic chemistry. The sterically encumbered stannane, tri-*tert*-butyltinhydride, Bu^t_3SnH, has great potential, however, there isn't much chemistry associated with this compound in the literature. To demonstrate the versatility of this new ligand, we have already prepared a few metal complexes from reactions of Bu^t_3SnH with metal carbonyl compounds. For example, the reaction of Bu^t_3SnH with $Pt_2Ru_4(CO)_{18}$ yields the new trimetallic Pt/Ru/Sn mixed metal cluster $Pt_2Ru_2(CO)_9(SnBu^t_3)_2(\mu\text{-}H)_2$, which was shown

to be a hydrogenation catalyst when supported on mesoporous silica.[58] In addition to our work with precious metals, preliminary investigations of the coordination chemistry of bulky tin ligands with less expensive metals such as cobalt,[59] nickel[59] and iron[44,60] have begun. We recently communicated the facile reversible activation of hydrogen by the bimetallic Pt-Sn complex $Pt(SnBu^t_3)_2(CNBu^t)_2$, that occurs both in solution and in the solid state.[61]

The Pt(0) compound, $Pt(COD)_2$ (COD= cyclooctadiene), is a highly reactive compound. It is moisture sensitive, air sensitive, and temperature sensitive in solution state and is highly efficient in activation of the Sn-H bond at room temperature. The bulky stannane ligand Bu^t_3SnH is also a reactive compound sensitive to moisture and air. The complexes synthesized from the reaction of these two reagents are unsaturated and stabilized by the sterics imparted by the bulky *tert*-butyl groups.

Here this chapter reported the synthesis and characterization of a series of hetero bimetallic complexes that were obtained by reacting $Pt(COD)_2$ with bulky tri-*tert*- butyl stannane (Bu^t_3SnH), trimesityl stannane {$(2,4,6\text{-}Me_3C_6H_2)_3SnH$ or Mes_3SnH} and triphenyl stannane, (Ph_3SnH) reagents. Here is also presented the reactivity of these complexes towards small molecules such as H_2, CO and catalyzation of H_2-D_2 exchange reaction at room temperature and at depressed temperatures of -78 °C.

2.2 Results and discussion.

Reaction of $Pt(COD)_2$ with one equivalent of Bu^t_3SnH: When one equivalent of Bu^t_3SnH was added drop wise to hexane solution of $Pt(COD)_2$ at room temperature under argon atmosphere, the solution immediately changed color to dark reddish-brown to yield

a mononuclear 16electron Pt(II) complex Pt(COD)(SnBu$^t_3$)(H), **2.1**. Structure of **2.1** is shown in Figure 2.1 (further crystallographic data can be found in Appendix A, Table A.1).

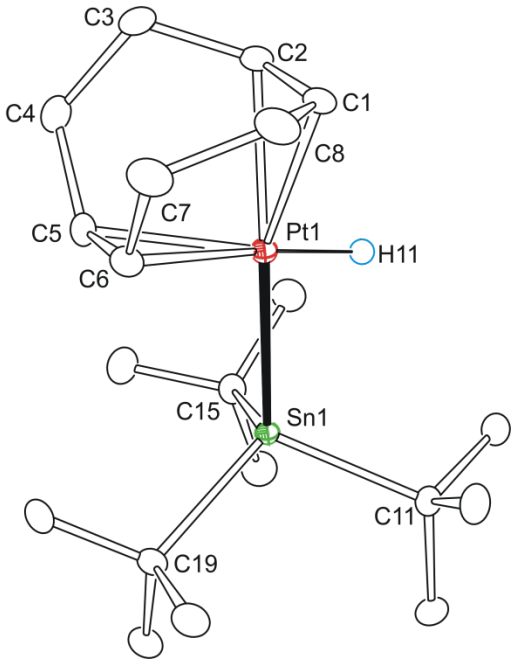

Figure 2.1. An ORTEP of the molecular structure of Pt(COD)(SnBu$^t_3$)(H), **2.1**, showing 50% probability thermal ellipsoids. Selected interatomic distances (Å) and angles (deg) are as follows: Pt(1)-Sn(1)=2.5984(2); Pt(1)-H(11)=1.45(3); Pt(1)-C(1)=2.289(2); Pt(1)-C(2)=2.324(2); Pt(1)-C(5)=2.245(2); Pt(1)-C(6)=2.266(2); Sn(1)-Pt(1)-H(11)=74(1); Sn(1)-Pt(1)-C(1)=160.11(6); Sn(1)-Pt(1)-C(5)=101.70(5).

It is evident from the structure that compound **2.1** is formed by the elimination of one COD ligand and oxidative addition of Sn-H bond to the Pt metal center as shown in equation 2.1.

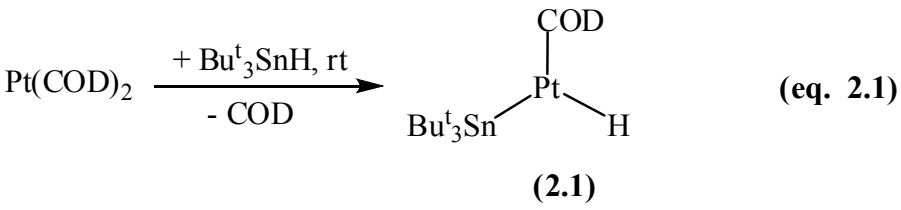

(eq. 2.1)

(2.1)

The complex **2.1** was characterized by the combination of ^{1}H NMR and single crystal X-ray crystallography. The COD ligand is slightly bent away from the Pt center to accommodate the terminal hydride ligand. The isolation of **2.1** is tedious, as it is always associated with some unidentified oily products. The Pt-Sn bond length in compound **2.1** is 2.598(18) Å, and Pt-H bond length is 1.45(3) Å, which is consistent with reported Pt-Sn single bond in Pt(II) complexes.[10,62] The hydride ligand is located and refined during crystallographic data collected at 100 K. The presence of the hydride ligand was also confirmed by ^{1}H NMR spectroscopy, where it shows up at -3.74 ppm in C_6D_6 solvent with appropriate one-bond coupling to Pt ($^{1}J_{Pt\text{-}H}$ =1223.2 Hz) and two-bond coupling to Sn ($^{2}J_{Sn\text{-}H}$ = 48.2 Hz). Compound **2.1** is a 16 electron highly reactive unsaturated Pt-Sn bimetallic complex, it is sensitive to air, moisture and temperature. It can be used as a precursor to synthesize a variety of complexes by the substitution of easily replaceable COD ligand with another $Bu^{t}_{3}SnH$ group.

Addition of one more equivalent of $Bu^{t}_{3}SnH$ to compound 2.1: The aim here was to isolate a 14 electron unsaturated Pt(IV) complex with two terminal $Bu^{t}_{3}Sn$ ligands and two hydride ligands, $Pt(Bu^{t}_{3}Sn)_2(H)_2$, **2.2** (see equation 2.2) by replacing the COD ligand. Very few 14 electron neutral Pt complexes are characterized and reported in literature.[63–65] These complexes are highly unsaturated, unstable, and highly reactive. They also have the tendency to form dimers to gain stability.

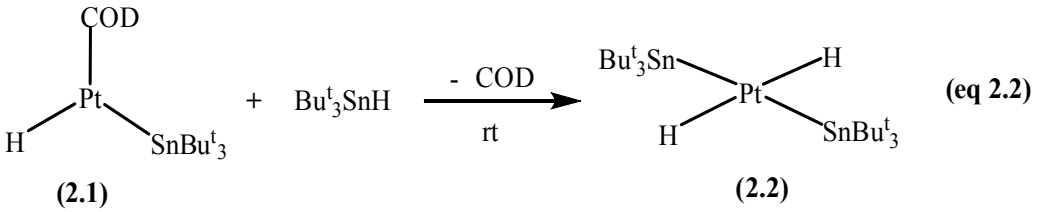

(2.1) **(2.2)** **(eq 2.2)**

When the reaction was carried out by adding an equivalent of Bu^t_3SnH to compound **2.1** in C_6D_6 solvent, new peaks were observed in ^{1}HNMR spectroscopy in the hydride region at -7.8 ppm. However, these complexes were not identified and were not able to be isolated. Interestingly, when the reaction mixture was dissolved in dichloromethane and plated on TLC to collect a yellow band, gave an unexpected new Pt-Sn cluster complex $[Pt(SnBu^t_3)(\mu\text{-}SnBu^t_2)(H)_2]_2$, **2.3**, upon crystallization in hexane solvent at -20 °C. The molecular structure of **2.3** is shown in Figure 2.2 (further crystallographic data can be found in Appendix A, Table A.1). The compound **2.3** is characterized by the combination of ^{1}H NMR, single crystal X-ray crystallography and mass spectrometry. The yield was low due to decomposition on the TLC plate. Compound **2.3** can also be prepared by reacting excess Bu^t_3SnH with $Pt(COD)_2$ as discussed below.

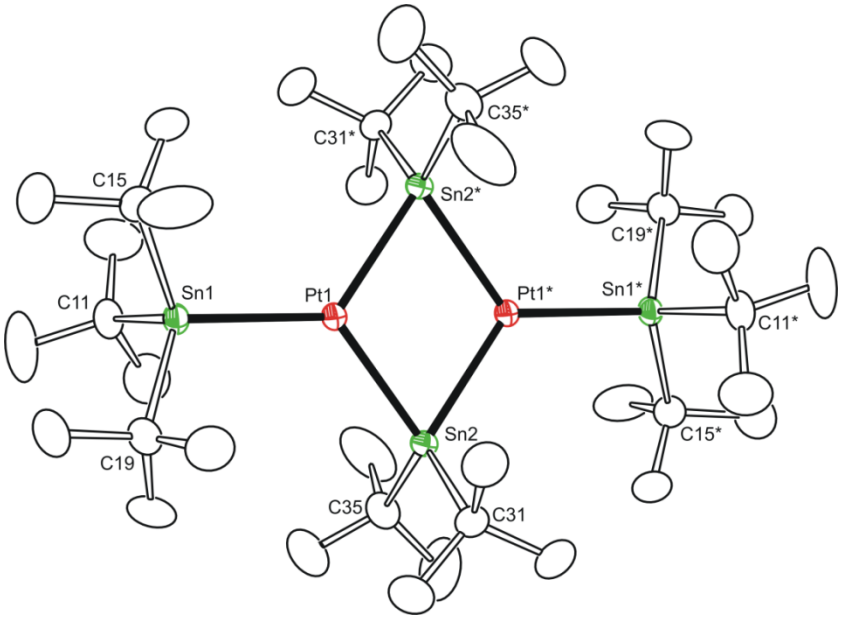

Figure 2.2. An ORTEP of the molecular structure of $[Pt(SnBu^t_3)(\mu\text{-}SnBu^t_2)(H)_2]_2$, **2.3,** showing 50% probability thermal ellipsoids. Selected interatomic distances (Å) and angles (deg) are as follows: Pt(1)-Sn(1)=2.6550(4), Pt(1)-Sn(2)=2.6353(4), Sn(1)-Pt(1)-Sn(2)=126.19(1); Sn(1)-Pt(1)-Pt(1*)=178.04(1); Sn(2)-Pt(1)-Pt(1*)=54.09(1); Pt(1)-Sn(2)-Pt(1*)=71.78(1).

Extensive research has been done in the activation of group14 Element-H bonds using late transition metal complexes with emphasis on activation of Sn-H and Ge-H bonds. Pt-Sn and Pt-Ge complexes similar to complex **2.3** were reported in the literature. The Pt-Sn complex $[(Ph_3P)_2(H)Pt(\mu\text{-}SnPh_2)\ (\mu\text{-}\eta^2\text{-}H\text{-}SnPh_2)Pt(PPh_3)]$ (see Scheme 2.1) reported is the first example of unsymmetrical diplatinum complex with bridging ($\mu\text{-}\eta^2$-H-$SnPh_2$) ligand.[66,67]

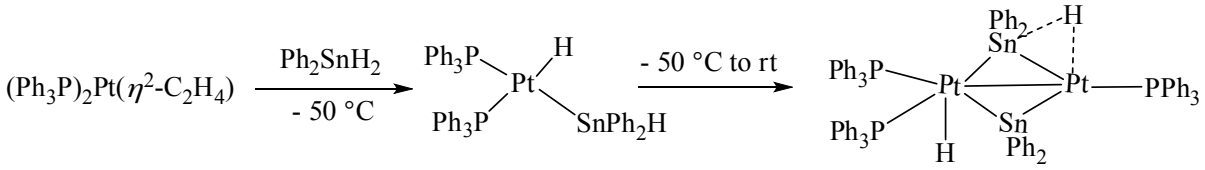

$[(Ph_3P)_2(H)Pt(\mu\text{-}SnPh_2)(\mu\text{-}\eta^2\text{-}H\text{-}SnPh_2)Pt(PPh_3)]$

Scheme 2.1. Sn bridged dinuclear Pt complex $[(Ph_3P)_2(H)Pt(\mu\text{-}SnPh_2)\ (\mu\text{-}\eta^2\text{-}H\text{-}SnPh_2)Pt(PPh_3)]$. [66,67]

Reaction of $Pt(COD)_2$ with excess of Bu^t_3SnH: The reaction of $Pt(COD)_2$ with Bu^t_3SnH is further explored to make new unsaturated Pt-Sn complexes like compound **2.3.** Drop wise addition of benzene solution of excess Bu^t_3SnH to $Pt(COD)_2$ at room temperature in a glove box, followed by slow evaporation of solvent, afforded light yellow crystals covered with brown oily residue. Crystals were washed with dichloromethane several times to yield pure crystals of compound **2.3**, (crystal structure shown in Figure 2.2 and line drawing shown in Figure 2.3), which was previously obtained by reacting $Pt(COD)_2$ with two equivalents of Bu^t_3SnH, but this time the yields are decent but still very low, about 5%. These low yields can be attributed to the

formation of unidentified oily bi-products. Apart from compound **2.3,** no new Pt-Sn complexes were isolated from this reaction.

Compound **2.3** is an unsaturated symmetrical dinuclear Pt complex, with a Pt-Pt bond that is bridged by two $SnBu^t_2$ groups. There is a terminal $SnBu^t_3$ ligand on each Pt atom. The complex also contains four hydride ligands, (see Figure 2.3), two on each Pt, that were confirmed by ^{1}H NMR spectroscopy

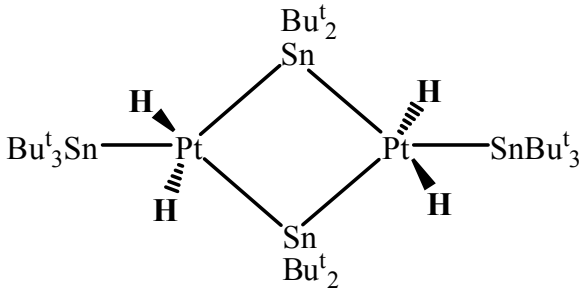

Figure 2.3. The line drawing of Pt(IV) complex $[Pt(SnBu^t_3)(\mu\text{-}SnBu^t_2)(H)_2]_2$, **2.3**.

The presences of hydrides in **2.3** were confirmed by ^{1}H NMR taken in toluene-d_8 solvent. The hydride peaks resonance appears at -3.45 ppm with appropriate one-bond coupling to Pt ($^1J_{Pt\text{-}H}$ = 905 Hz) and two-bond coupling to Sn ($^2J_{Sn\text{-}H}$ = 32 Hz). The Pt-Pt bond length in compound **2.3** is 3.0877 Å, longer than the average Pt-Pt single bond distance of 2.70 Å.[68–70] In the analogous Pt-Ge dinuclear complex $[(GePh_3)(CO)Pt(\mu\text{-}GePh_2)]_2$, a Pt-Pt bond distance of 2.8394 (3) Å was reported.[68] The longer bond length in **2.3** can be attributed to the sterics induced by bulky $SnBu^t_2$ ligands which are even bigger than $GePh_2$ ligands.

The Pt(IV) tetrahydride complex **2.3** is stable towards moisture and air in the solid state, and poorly soluble in most organic solvents. Solubility can be increased by heating

the solution and is stable in solution up to 100 °C for four hours but on prolonged heating the *tert*-butyl groups cleave off from the tin, producing isobutane gas and other un-identified tin bi-products.

Proposed reaction mechanism for the formation of compound 2.3: Based on the experimental observations, the following reaction mechanism (Scheme 2.2) has been proposed for the formation of compound **2.3**. The first step is the oxidative addition of two equivalents of Bu^t_3SnH to the Pt center, followed by reductive elimination of the COD ligand to yield the unstable, highly reactive intermediate compound **2.2**. The second step is the cleavage of one *tert*-butyl group from the Bu^t_3Sn group to yield the proposed intermediate compound ***I*** accompanied by the abstraction of a hydride by the cleaved *tert*-butyl group to produce isobutane gas. Peaks corresponding to free isobutane in the ^1H NMR spectrum were observed when the reaction was performed in toluene-d_8 solution in the NMR tube. Cleavage of an alkyl group from organotin ligands bonded to transition metals has been previously observed.[71,72] Intermediate ***I*** dimerizes at room temperature to afford another unsaturated intermediate $[(H)Pt(\mu\text{-}SnBu^t_2)(SnBu^t_3)]_2$, ***II*****,** a 28 electron unsaturated dinuclear Pt-Sn bimetallic complex. The unusual electronic unsaturation at the platinum metal center in intermediate ***II*** initiates the abstraction of hydride from excess Bu^t_3SnH to yield compound **2.3.** The activation of Si-H and C-H bonds is a common feature of unsaturated Pt complexes.[73,74] An increase in the product yield in the presence of excess Bu^t_3SnH also supports this reaction mechanism as the excess Bu^t_3SnH provides the necessary proton for the formation of compound **2.3**. We have not been able to isolate any of the above proposed intermediates.

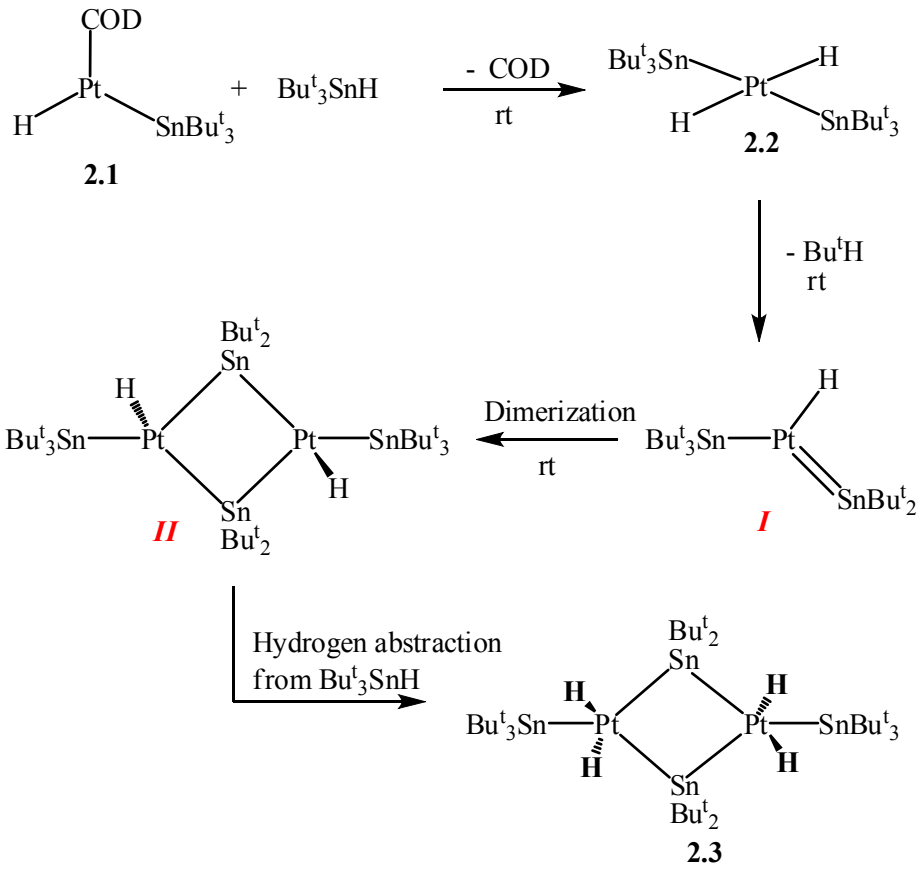

Scheme 2.2. Proposed mechanism for the formation of compound **2.3.**

Reaction of [Pt(μ-SnBu$^t_2$)(SnBu$^t_3$)(H)$_2$]$_2$, 2.3, with CO: The dinuclear Pt-Sn complex **2.3** reacts with CO gas reversibly at room temperature both in solid state as well as in solution state, to give corresponding CO added product [Pt(SnBu$^t_3$)(μ-SnBu$^t_2$)(CO)(H)$_2$]$_2$, **2.4**, see Figure 2.4, (further crystallographic data can be found in Appendix A, Table A.1). When CO gas is purged through the hexane solution of **2.3** at room temperature, the solution turns to dark yellow instantaneously to afford **2.4**. Compound **2.4** is moderately stable. Removal of the CO atmosphere by applying vacuum or introducing argon gas results in regeneration of the starting compound **2.3** in quantitative yield (see

equation 2.3). The solubility of dinuclear Pt-Sn carbonyl complex **2.4** is better than that of compound **2.3**, but it decomposes rapidly when exposed to air while in solution.

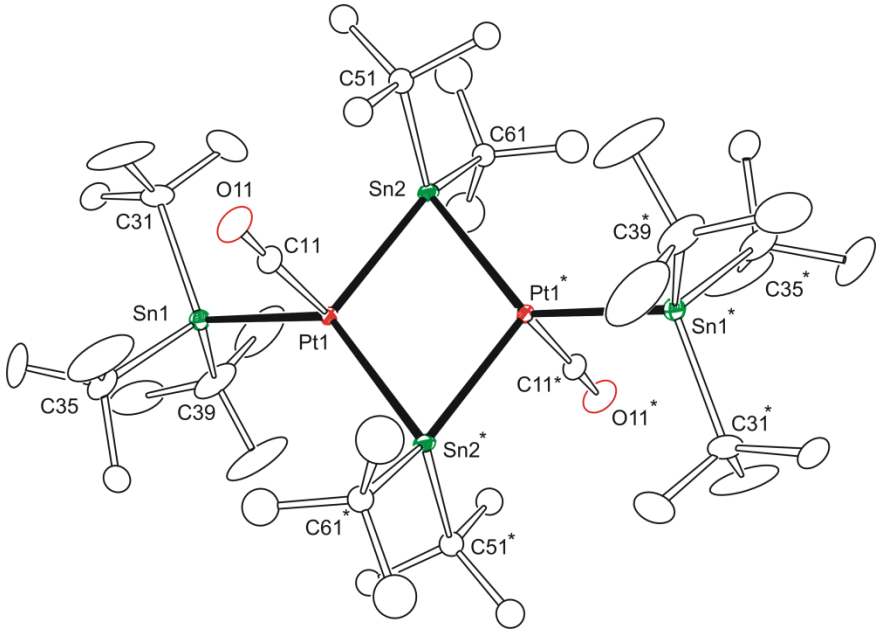

Figure 2.4.The molecular structure for $[Pt(SnBu^t_3)(\mu\text{-}SnBu^t_2)(CO)(H)_2]_2$, **2.4**.

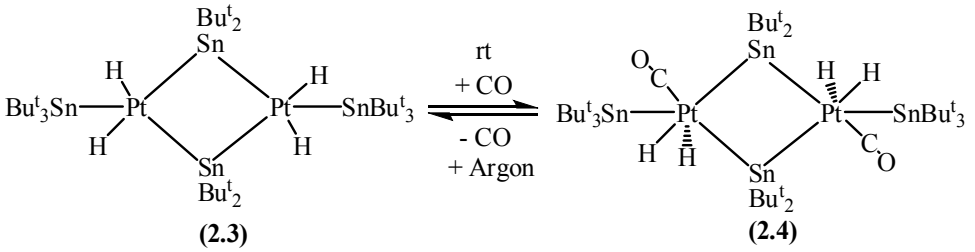

(2.3) **(2.4)** **(eq. 2.3)**

Compound **2.4** is a 34 electron dinuclear Pt-Sn cluster complex. Its structure is similar to compound **2.3** except that the CO ligands are added in *trans*-positions to each other. The Pt-Pt bond distance is 3.1894 (6) Å, slightly longer than that observed in compound **2.3** (3.0149 A). The Pt1-C11(1.929 Å) bond distance is consistent with the known Pt-C distance in Pt-carbonyl complexes (1.888 Å).[68] The CO groups lie perpendicular to the plane of Pt_2Sn_2 square to avoid steric repulsion from tin ligands.

Compound **2.4** was also characterized by the combination of ^{1}H NMR, single crystal X-ray crystallography, and IR spectroscopy.

The hydride ligands were identified by the ^{1}H NMR where they show up at -12.77 ppm with appropriate one bond coupling to Pt($^{1}J_{Pt-H}$ = 702 Hz), and their number was identified by appropriate integration with respect to other proton resonances. Interestingly, with the addition of CO to the compound **2.3,** there is a dramatic shift in the hydride resonance of hydride ligands in the ^{1}H NMR. In toluene-d_8 solution, for compound **2.3** the hydride resonance appears at -3.71 ppm ($^{1}J_{Pt-H}$ = 905 Hz), and for compound **2.4** the resonance appears at -12.77 ppm ($^{1}J_{Pt-H}$ = 702 Hz) (Figure 2.5).

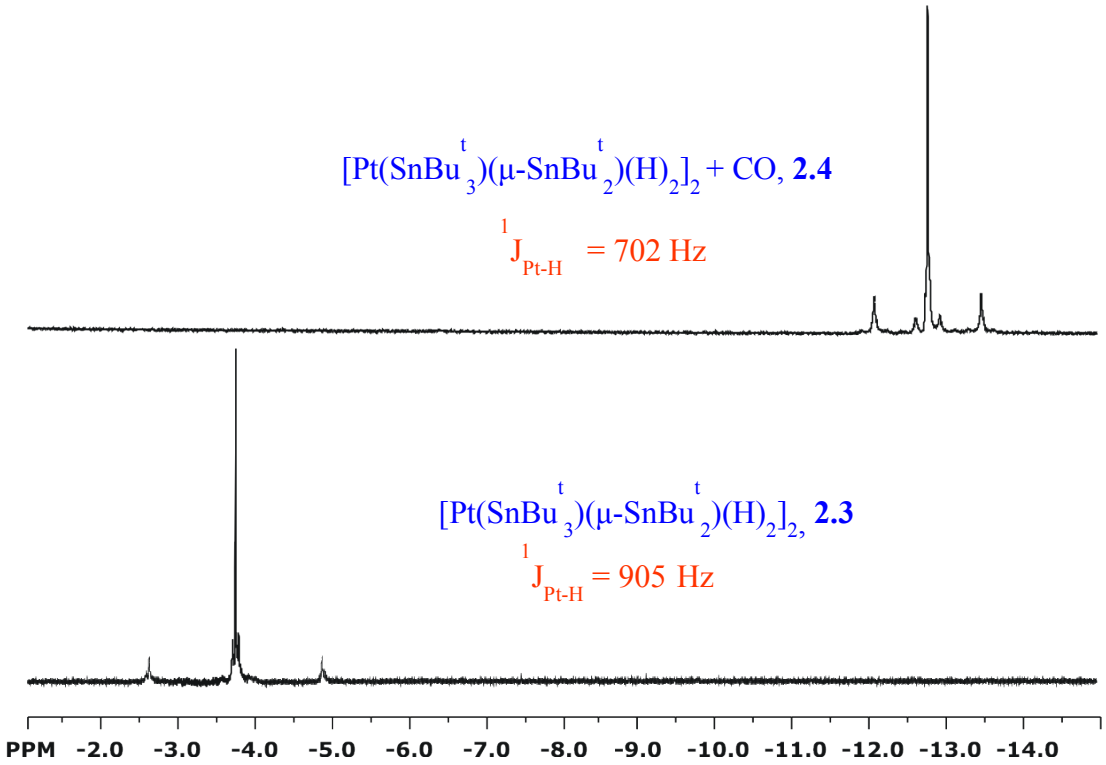

Figure 2.5. ^{1}H NMR spectrum in hydride region for compound **2.3** and compound **2.4**.

The more-up field appearance of hydrides resonance could be due to the increased electron density around platinum metal center by the back donation of electrons from the

CO ligands which in turn increases the electron density around hydride ligands, which causes the hydrides to resonate more up-field compared to the hydrides resonance in compound **2.3**.

Reaction of $Pt(COD)_2$ with Bu^t_3SnH in the presence of $CNBu^t$: The reaction of $Pt(COD)_2$ with one equivalent of Bu^t_3SnH and two equivalents of *tert*-butylisocyanide, $CNBu^t$, at room temperature afforded the dihydrido Pt-Sn complex $Pt(SnBu^t_3)_2(CNBu^t)_2(H)_2$, **2.5**, in 32 % yield. High yields can be obtained by performing the reaction at -78 °C. Compound **2.5** was characterized by the combination of ^1H NMR, mass spectrometry, and single crystal x-ray diffraction analyses and IR spectroscopy. An ORTEP showing the molecular structure of **2.5** is shown in Figure 2.6, (further crystallographic data can be found in Appendix A, Table A.2).

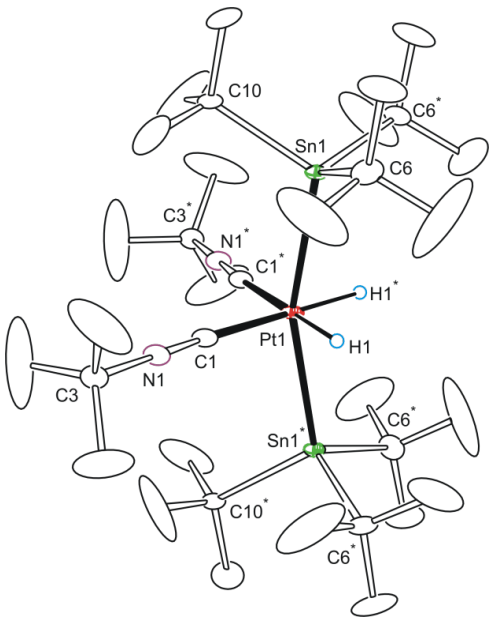

Figure 2.6. An ORTEP of the molecular structure of $Pt(SnBu^t_3)_2(CNBu^t)_2(H)_2$, **2.5,** showing 30% probability thermal ellipsoids. Selected interatomic distances (Å) and angles (deg) are as follows: Pt(1) – Sn(1) = 2.6718(5); Pt(1) – C(1) = 2.014(8); Pt(1)-H(1) = 1.65(9); Sn(1)-Pt(1)-Sn(1*) = 161.35(3); C(1)-Pt(1)-C(1*) = 102.5(4); C(1)-Pt(1)-Sn(1) = 95.82(3); Sn(1)-Pt(1)-H(1) = 84.2(4).

For the formation of compound **2.5,** it is proposed that the addition of 2 equivalents of Bu^t_3SnH to $Pt(COD)_2$ first gives the highly reactive 14 electron complex $Pt(SnBu^t_3)_2(H)_2$, **2.2**, via oxidative addition of the Sn-H bond (see Scheme 2.3). This unsaturated complex then adds 2 equivalents of $CNBu^t$ to afford the 18 electron complex **2.5**.

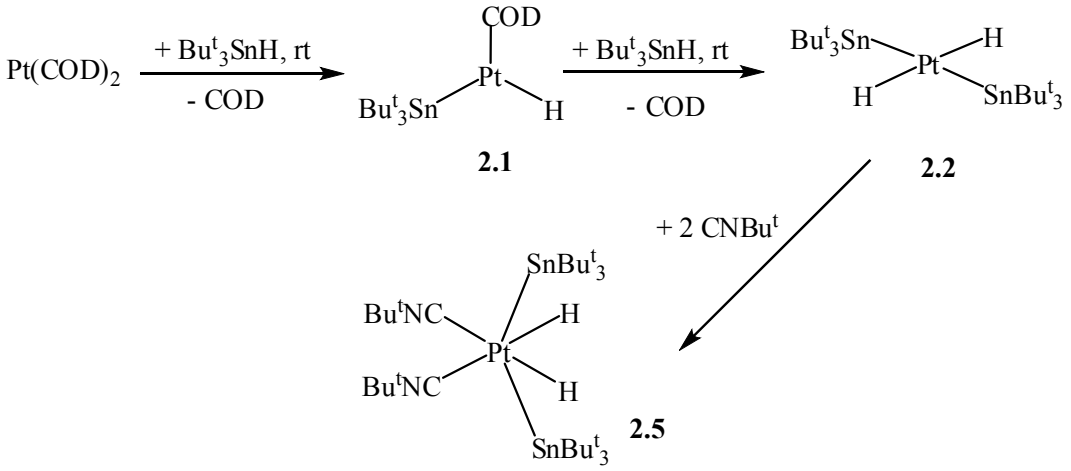

Scheme 2.3. Proposed pathway for the formation of $Pt(SnBu^t_3)_2(CNBu^t)_2(H)_2$, **2.5.**

Compound **2.5** is an 18 electron mono nuclear platinum complex with distorted octahedral geometry and over all possesses a C_{2v} symmetry. The hydride ligands are located and refined in the structural analysis performed at 100 K. Their presence was further confirmed by ^1H NMR, which shows one resonance for both the hydrides at -13.52 ppm in C_6D_6 with appropriate one bond coupling to Pt ($^1J_{Pt\text{-}H}$ = 697 Hz) and two bond coupling to Sn ($^2J_{Sn\text{-}H}$ = 34 Hz). The Pt-Sn bond distance in **2.5** is 2.6718(5) Å and the Pt-H bond distance is 1.65(9) Å. The Pt-Sn bond length is consistent with the

literature value for mononuclear octahedral Pt(IV) complexes {2.554 Å for Pt-stannaborate isocyanide complex}.

Compound 2.5 reversibly loses both the hydrides in solution and solid state: Both the hydride ligands in **2.5** can be displaced at room temperature. When argon gas is purged through the compound **2.5** both in the solution state and in solid state, it loses both the hydrides to furnish the complex $Pt(SnBu^t_3)_2(CNBu^t)_2$, **2.6**, in very high yields. Compound **2.6** activates hydrogen gas both in solid state and in solution state. Compound **2.6** was also characterized crystallographically and its structure in the solid state is shown in Figure 2.7, (further crystallographic data can be found in Appendix A, Table A.2).

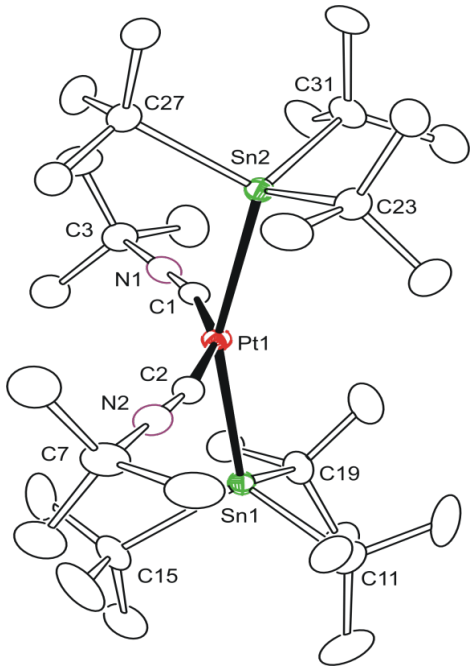

Figure 2.7. An ORTEP of the molecular structure of $Pt(SnBu^t_3)_2(CNBu^t)_2$, **2.6,** showing 50% probability thermal ellipsoids. Selected interatomic distances (Å) and angles (deg) are as follows: Pt(1)–Sn(1) = 2.6765(3); Pt(1)-Sn(2) = 2.6851(3); Pt(1)–C(1) = 1.932(3); Pt(1)-C(2) = 1.929(3); Sn(1)-Pt(1)-Sn(2) = 159.539(8); C(1)-Pt(1)-C(2) = 158.69(13).

The loss of the hydride ligands gives a 16 electron configuration around the Pt atom in **2.6** with a formal oxidation state of +2. The complex as seen in Figure 2.7 is

not planar, as expected for Pt(II) d^8 complexes, and could be considered as more of a "saw-horse" type structure, due to the sterics imparted by the bulky Bu^t groups.

Analysis of the X-ray crystal structures reveals how the ligands in **2.6** rearrange to accommodate hydride ligands upon addition of hydrogen. The C2-Pt1-C1 bond angle in compound **2.6** is 158.69(13)°, whereas the C1-Pt1-C1* bond angle in compound **2.5** is squeezed significantly to 102.5(4)° to accommodate the two hydride ligands (see Figure 2.8).[61] Such a rearrangement of coordination geometry of ligands is common in the addition of hydrogen or CO to the transition metal carbonyl clusters.[75–77] There is no considerable change in the Sn-Pt-Sn bond angle upon addition of H_2 to compound **2.6**. Similarly, the Pt-Sn bond lengths also remain essentially the same after addition of H_2.

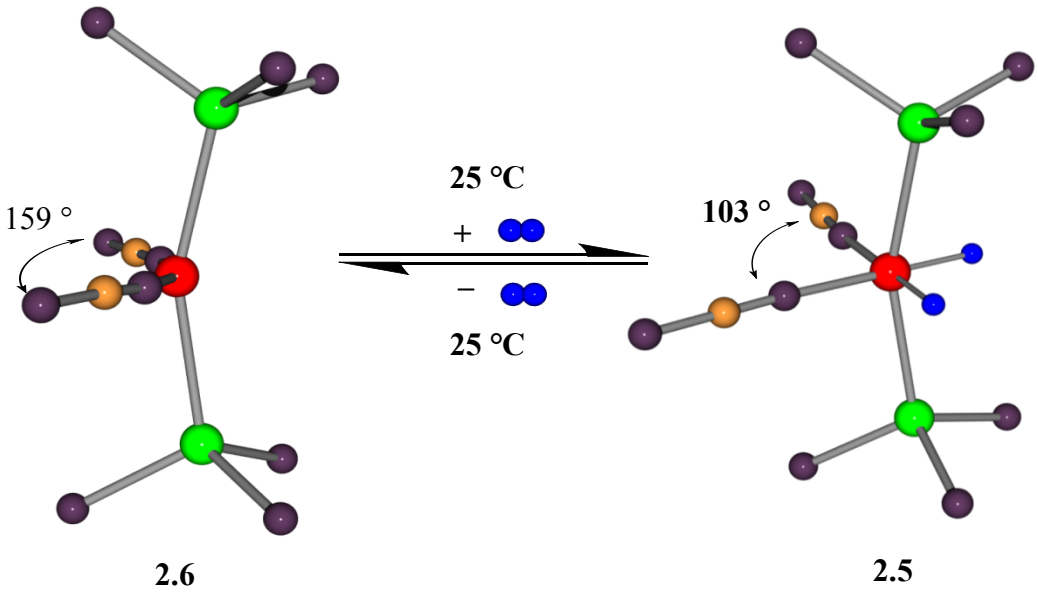

Figure 2.8. Change in coordination geometry of ligands after addition of H_2 to **2.6**.

Compounds **2.5** and **2.6** also display a marked difference in the IR resonances of CN stretches. The ν_{CN} stretching frequency for **2.6** in hexane solution shows a sharp peak

around 2112 cm^{-1}, slightly out of the literature reported range of 2225-2170 cm^{-1}, common for Pt(II)-bound isocyanide complexes.[78] The IR spectrum of compound $Pt(SnBu^t_3)_2(CNBu^t)_2(H)_2$, **2.5** in hexane solution shows two peaks, one weak intensity peak at 2112 cm^{-1} corresponding to the two terminal hydrides (ν_{Pt-H} stretching frequency) and one sharp peak at 2139 cm^{-1} corresponding to ν_{CN} stretching of the $CNBu^t$ ligands. Upon addition of hydride ligands to Pt(II) isocyanide complex **2.6**, there is a slight shift in ν_{CN} stretching frequency (2112 cm^{-1}, **2.5**) this might be due to increase in electron density around the Pt-metal center in **2.5**. The absorption peak of ν_{Pt-H} for Pt(IV)hydride complex $[PtH_2(SnPh_3)_2(PMe_2Ph)_2]$ synthesized by Eaborn et al. several years ago also has ν_{Pt-H} values in the same range(2085, and 2115 cm^{-1}).[86]

Activation of H_2 by compound $Pt(SnBu^t_3)_2(CNBu^t)_2$, 2.6 in solid state: As mentioned earlier compound **2.6** activates hydrogen not only in the solution state but also in the solid state at room temperature and also at -78 °C. Upon exposing the purple-colored crystals of compound **2.6** to H_2 atmosphere, the colorless crystals of compound **2.5** formed over a period of 10 minutes in almost quantitative yield, consistent with the solid state structure of **2.5** for two hydride ligands. Removing the hydrogen gas and placing the colorless crystals of compound **2.5** in vacuum for 12 hours regenerates purple crystals of compound **2.6**. A similar phenomena of crystal to crystal transformation during the activation of small molecules (H_2, CO, and C_2H_4, NH_3) by [Ir]-N_2 pincer complex (see Figure 2.9) was reported by the Brookhart group.[79] Here the crystal structure remains intact during the ligand exchange reactions, without decaying to microcrystalline powder form.

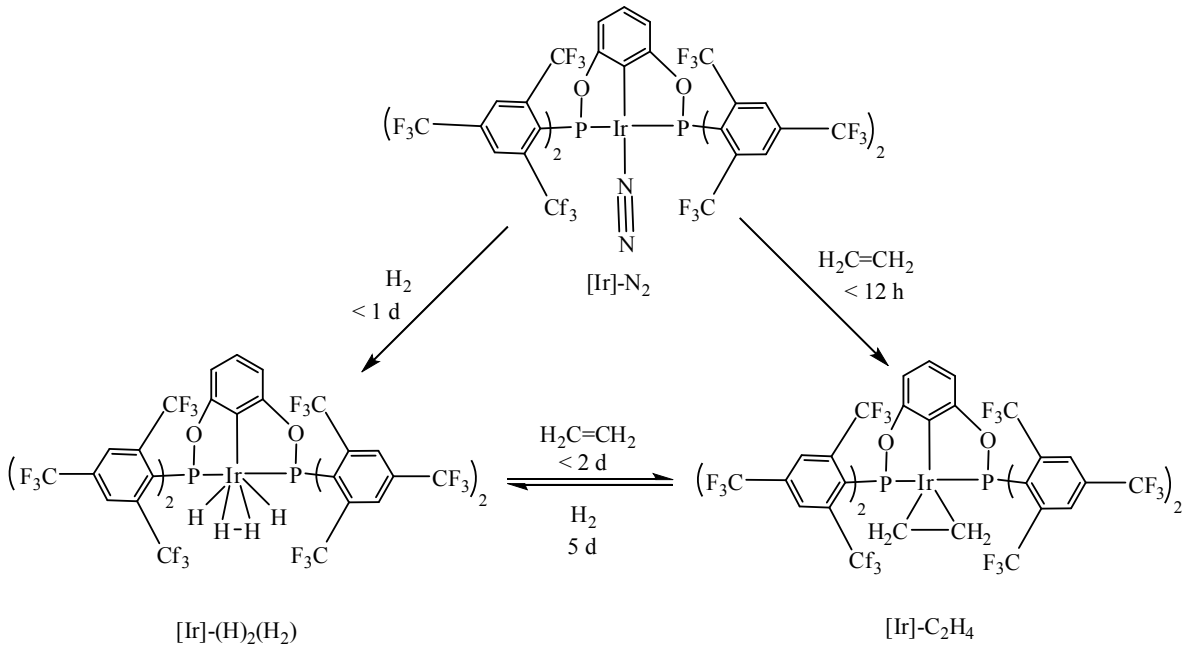

Figure 2.9. Line drawing for crystal to crystal transformations of [Ir]-pincer complexes of N_2, H_2 and C_2H_4, reported by Brookhart group.[79]

Nature of hydride ligands of 2.5, reaction of compound $Pt(SnBu^t_3)_2(CNBu^t)_2$, 2.6 with HD gas: Compound **2.5**-d_1 was prepared by the reaction of **2.6** with HD gas to test for the existence of direct H-H interactions in **2.5**, i.e., to know whether it is a molecular hydrogen H-H or two terminal hydrides attached to Pt metal center. The ^{1}H NMR spectrum of **2.5**-d_1 did not show any H-D coupling, suggesting that there is no significant H-D interaction, which is consistent with the crystal structure analysis of **2.5**. In addition to the resonance of **2.5**-d_1, the hydride resonance for **2.5** was also present in the ^{1}H NMR spectrum (see Figure 2.10). The small shift difference in the spectrum in Figure 2.10 (top) is due to isotope shift effects.

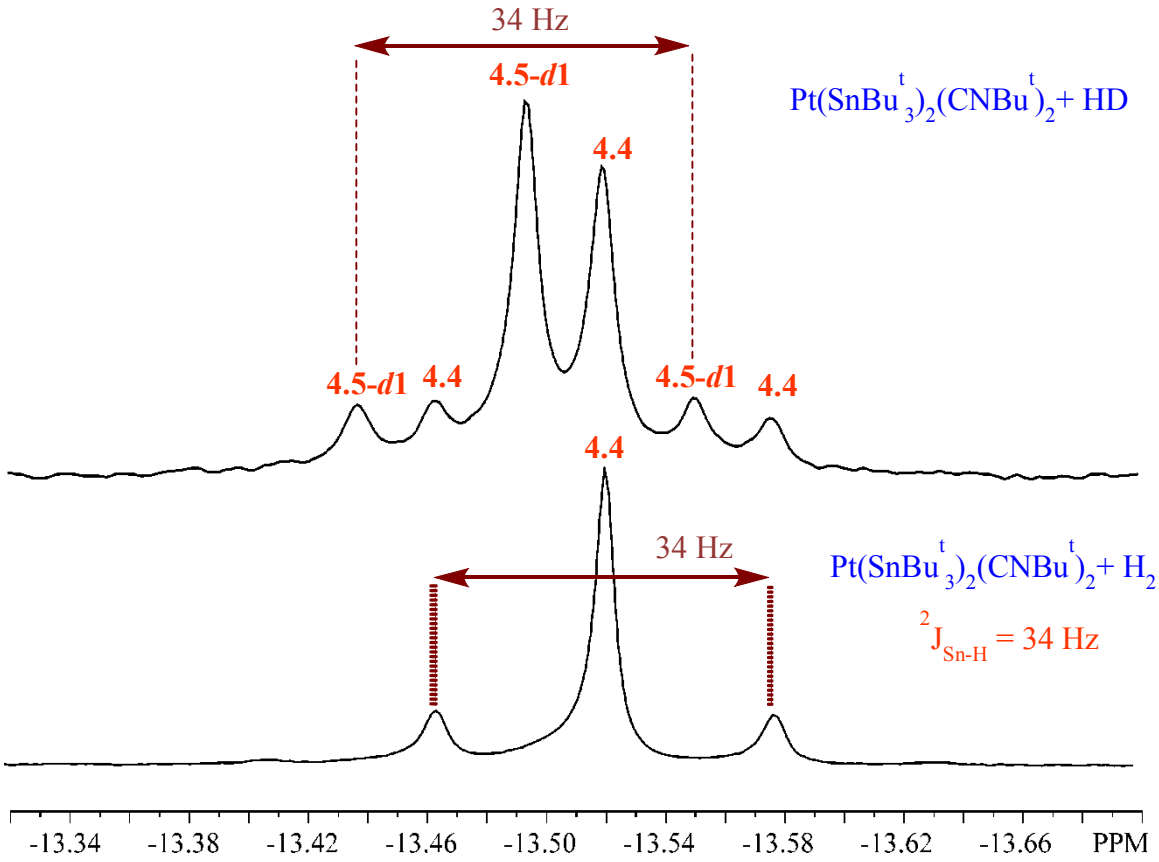

Figure 2.10. Overlay of ^{1}H NMR spectra of the hydride region (bottom) for **2.5** from the addition of H_2 to **2.6** and (top) for the addition of HD to **2.6**. Pt-H one-bond couplings are not shown.

Compound Pt(SnBu$^t_3$)$_2$(CNBu^t)$_2$, 2.6 catalyzes H_2-D_2 exchange: In solution, compound **2.6** catalyzes the H_2-D_2 exchange to give HD gas at room temperature (see Figure 2.11), which was monitored by ^{1}H NMR (see Figure 2.12). Also the three possible isotopomers of **2.5** are also observed in the ^{1}H NMR**.** Unlike activation of H_2 in solid state, compound **2.6** catalyzes the H_2-D_2 exchange only in the solution state and not in the solid state.

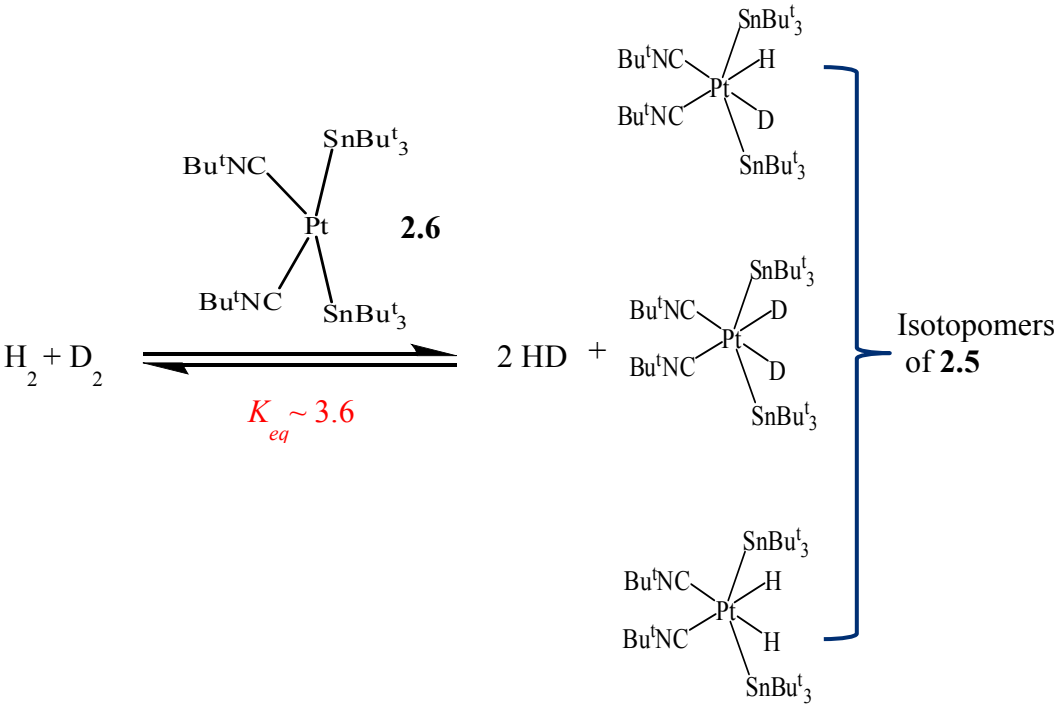

Figure 2.11. Catalytic H_2- D_2 exchange by $Pt(SnBu^t_3)_2(CNBu^t)_2$, **2.6**.

The catalysis of H_2-D_2 exchange is not uncommon with transition metal complexes. Several years ago, HD gas was reported to be formed both from $[CpRu(PPh_3)(Bu^tNC)(H_2)]^+$ and D_2 in dichloromethane,[80] and in thermal H_2-D_2 exchange reactions of $Cr(CO)_4(H_2)_2$ in liquid xenon.[81] Kubas et al. also observed H_2-D_2 exchange over their $M(CO)_3(PR_3)_2(H)_2$ complex to produce HD gas both in solution and in solid state.[82]

The catalytic H_2-D_2 exchange reaction with **2.6** is monitored in C_6D_6 solvent at room temperature by ^{1}H NMR. Mixture of H_2-D_2 gas is purged through the solution of **2.6** using syringe, followed by vigorous shaking for 15 minutes, the ^{1}H NMR indicated the formation of HD gas. The ^{1}H NMR of a 1:1 molar ratio of H_2-D_2 mixture without catalyst **2.6** shows a single peak for free hydrogen (see Figure 2.12). The ^{1}H NMR

spectrum also indicates that the $H_2 + D_2 \rightleftharpoons 2HD$ equilibrium has been reached (as there was no change in the integration ratio of the peaks even after 5days) and appropriately integration of the peaks is consistent with $K_{eq} \sim 3.6$.[83]

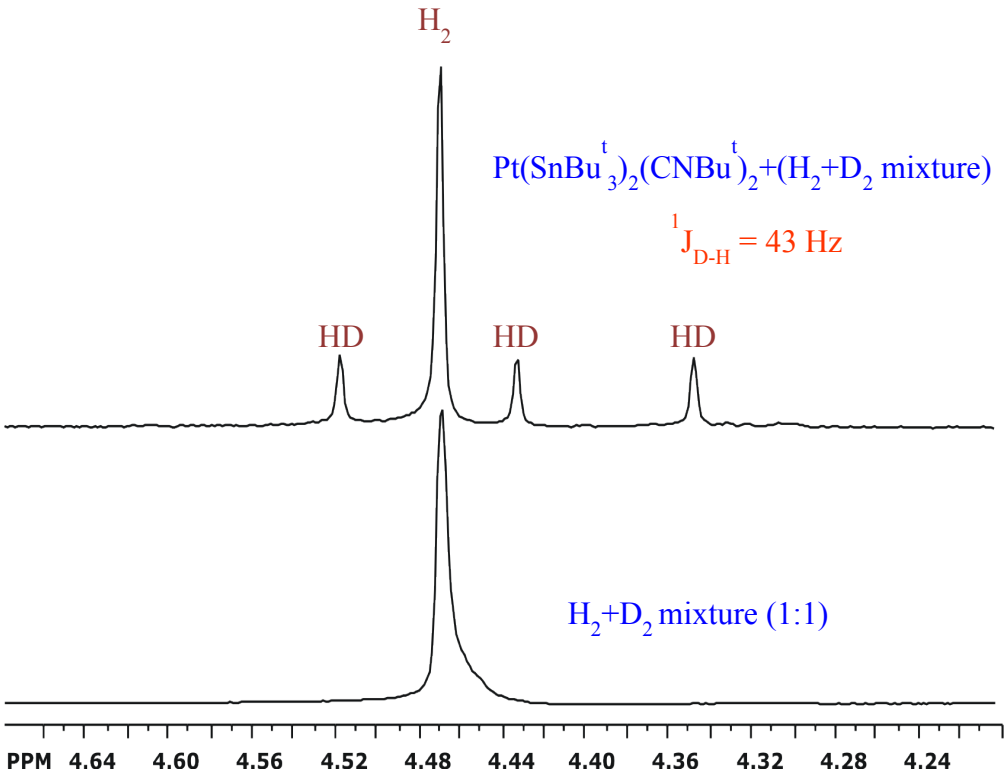

Figure 2.12. ^1H NMR spectra in C_6D_6 for catalytic H_2-D_2 scrambling by $Pt(SnBu^t_3)_2(CNBu^t)_2$, **2.6**.

Mechanism of H_2-D_2 exchange: The fact that compound $Pt(SnBu^t_3)_2(CNBu^t)_2$, **2.6** catalyzes H_2-D_2 exchange, and that its reaction with H-D gas afforded a mixture of isotopomers of $Pt(SnBu^t_3)_2(CNBu^t)_2(H)_2$, **2.5**, prompted us to understand this exchange mechanism on the Pt center. Addition of H_2 to **2.6** gives **2.5** which is an 18 electron, formally Pt(IV) complex in an octahedral geometry. Thus addition of D_2 to an intact **2.5** would increase the oxidation state from IV to VI and the coordination number on

platinum to 20 electrons which is highly unlikely, so the H_2-D_2 exchange process should be accompanied by ligand loss in **2.5**. An alternate could be that once complex **2.5** is formed by addition of H_2, reductive elimination of Bu^t_3SnH could occur providing intermediate ***I*** with vacant coordination sites (see equation 2.4) for the addition of D_2. With both hydride and deuteride coordinated to platinum, reductive elimination of HD could then proceed.

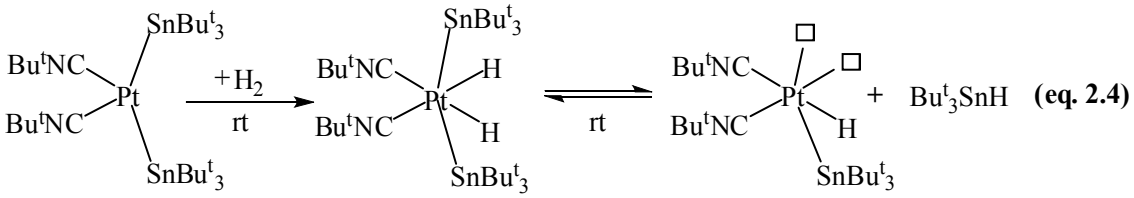

2.6 **2.5** ***I*** **(eq. 2.4)**

To test if the rate of H_2 addition to **2.6** is affected by the presence of free Bu^t_3SnH, there was no detectable decrease in the rate of H_2 addition in the presence of a 32-fold excess of Bu^t_3SnH at room temperature. Since the H_2 addition reaction is instantaneous at room temperature, the addition of H_2 to **2.6** in the presence of excess Bu^t_3SnH was carried out at lower temperatures. Even at -78 °C, no detectable decrease in the rate was observed, perhaps suggesting that H_2 addition could proceed without ligand dissociation. To further dwell on the possibility of Bu^t_3SnH elimination from **2.5**, the reaction was carried out in the presence of another R_3SnH reagent, namely Ph_3SnH, to see if the complex $Pt(SnBu^t_3)(SnPh_3)(CNBu^t)_2(H)_2$, could be isolated, where one of the $SnBu^t_3$ groups in **2.5** is replaced by a $SnPh_3$ group. If the $SnBu^t_3$ group is replaced by the other SnR_3 group in the presence of H_2 gas with the formation of free $HSnBu^t_3$, then the proposed mechanism in equation 2.4 is pretty much proved. The mechanistic pathway of

loss of $CNBu^t$ in the presence of H_2/D_2 has been ruled out as a new rose colored product $Pt(SnBu^t_3)_2(CNBu^t)_3$, **2.7** (see Figure A.1 in Appendix A) has been isolated in the presence of excess $CNBu^t$ and H_2/D_2 indicating the strong binding capability of $CNBu^t$ with Pt metal center. A similar compound with Ni metal has also been synthesized in our lab.[84]

Exchange of $SnBu^t_3$ group in $Pt(SnBu^t_3)_2(CNBu^t)_2$, 2.6 with Ph_3Sn group: When 3 fold excess Ph_3SnH, which is less bulky than $SnBu^t_3H$, is added to the hexane solution of **2.6** in the presence of H_2 gas (where compound **2.5** will be formed immediately), an immediate white colored precipitate was observed in the reaction mixture. Residue was filtered in the glove box and recrystallized in CH_2Cl_2/Hexane solvent mixture at -30 °C to give colorless crystals of $Pt(SnPh_3)_3(CNBu^t)_2(H)$, **2.8** in 90% yield. Wherein both the Bu^t_3Sn ligands in **2.5** were replaced by two Ph_3Sn ligands, a third Ph_3Sn ligand is also coordinated the Pt metal center and there is also a hydride ligand on the Pt metal center to from an 18 electron Pt(IV) complex in an octahedral geometry. Compound **2.8** can also be prepared even in the absence of H_2 gas. We believe it is a highly strained structure given the steric crowdedness around the Pt metal center. Very few literature examples were reported with three or more tin ligands on the same Pt metal center but there are only two examples with three bulky tin ligands on the same Pt metal center in an octahedral symmetry.[85,86] Compound **2.8** can also be prepared by reacting $Pt(COD)_2$ with two equivalents of $CNBu^t$ and 3 equivalents of Ph_3SnH at -78 °C in the presence of inert atmosphere. An ORTEP showing the molecular structure of **2.8** is shown in Figure 2.13, (further crystallographic data can be found in Appendix A, Table A.2). Compound **2.8** is

characterized by the combination of IR, ^{1}H NMR, elemental and single crystal x-ray diffraction analyses.

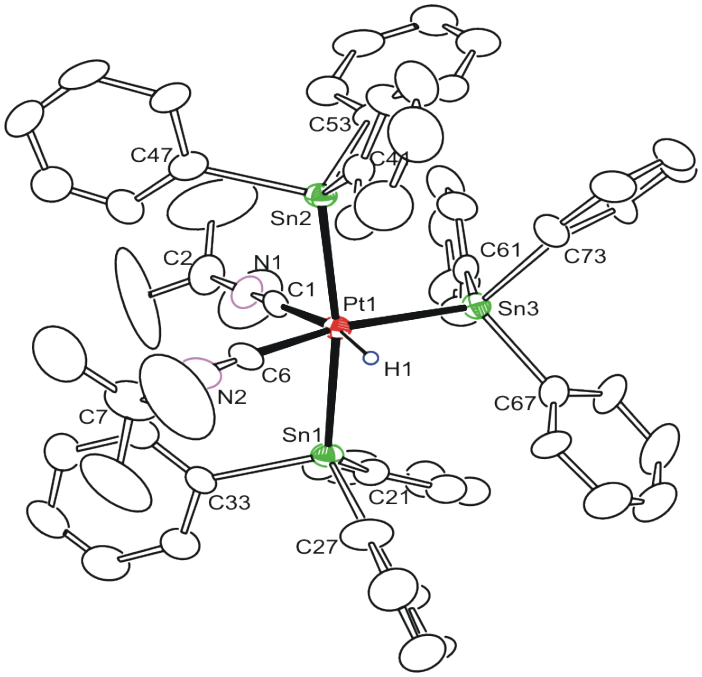

Figure 2.13. An ORTEP of the molecular structure of $Pt(SnPh_3)_3(CNBu^t)_2(H)$, **2.8** showing 30% probability thermal ellipsoids. Selected interatomic distances (Å) and angles (deg) are as follows: Pt(1)-Sn(1) = 2.6761(8), Pt(1)-Sn(3) = 2.6140(7), Pt(1)-C(1) = 2.03(1), Pt(1)-H(1) = 1.65(6) Sn(1)-Pt(1)-Sn(2) = 171.07(3), Sn(2)-Pt(1)-Sn(3)=93.32(2), C(1)-Pt(1)-Sn(3) = 94.1(3), C(1)-Pt(1)-C(6) = 102.8(4), Sn(2)-Pt(1)-C(1) = 89.2(3), Sn(1)-Pt(1)-(C6) = 85.0(3), C(6)-Pt(1)-H(1) = 66(2), Sn(3)-Pt(1)-H(1) = 97(2).

The ^{1}H NMR of $Pt(SnPh_3)_3(CNBu^t)_2(H)$, **2.8** displayed some interesting temperature dependent dynamics in solution (see Figure 2.14). The ^{1}H NMR in toluene showed two broad resonances in the hydride region at 25 °C (δ = -6.42, and -11.91). As the temperature was decreased to -20 °C, two distinct hydride resonances were observed showing coupling to both platinum and tin (δ = -6.62, $J_{119Sn-H}$ = 679 Hz, $J_{117Sn-H}$ = 647Hz, $^{1}J_{Pt-H}$ = 775 Hz, and δ = -11.90, $^{1}J_{Pt-H}$ = 665 Hz, $^{2}J_{119Sn-H}$ = 26.68 Hz, $^{2}J_{117Sn-H}$ = 13.95 Hz) which is consistent with the presence of isomers in solution. As the temperature is

raised from -20 °C, the two hydride signals start to broaden and coalesce; however, the averaged fast exchange limit could not be obtained as the complex decomposes above 30°C.

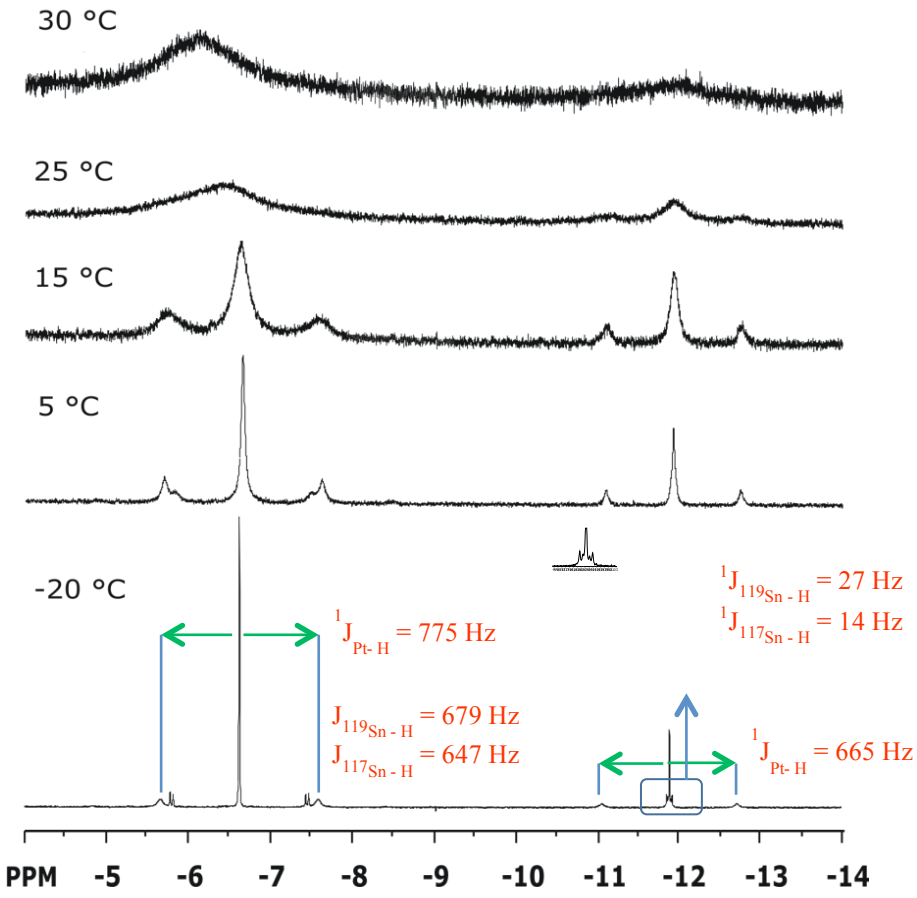

Figure 2.14. VT ^{1}HNMR overlay of $Pt(SnPh_3)_3(CNBu^t)_2(H)$, **2.8.**

As shown in Figure 2.14, both the hydride resonances show one bond coupling to platinum. The hydride resonance at -11.90 ppm has a Sn coupling of 27Hz (^{119}Sn) which is consistent with the two bond coupling value, indicating this resonance could be due to the structure **2.8** (compound **2.8),** where the H1 atom is *cis* to the Sn3 atom (Figure 2.13). The resonance at -6.62 ppm also shows coupling to Sn, with $J_{119Sn-H}$ = 679 Hz, which we are not sure about the order of coupling, as this value is far off from the one bond ^{119}Sn-H

coupling (as the $^{1}J_{119Sn\text{-}H}$ in Ph_3SnH is 1936 Hz) and also far higher to be a two bond coupling. But there is a possibility that this unusual Sn coupling could be due to a resonance structure where the hydride bridges a Sn and Pt metal centers (see Scheme 2.4 a). However subsequent literature searches lead to the belief that this could indeed be due to two bond Sn coupling as suggested by Prof. Richard Adams, where hydride is two bond *trans* to the Sn[87–90] (see Scheme 2.4 b).

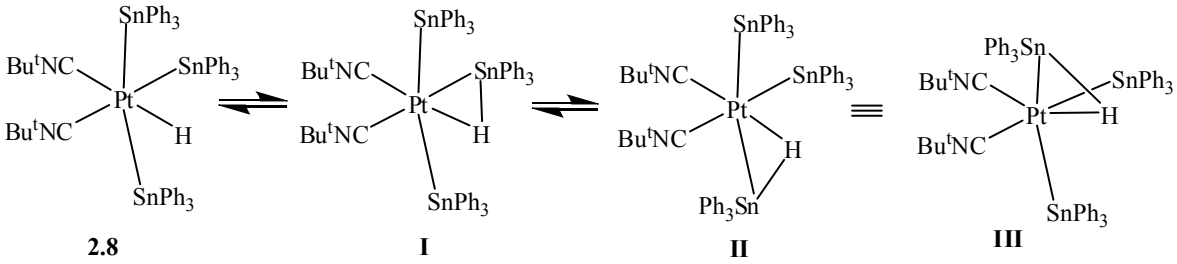

2.8 **I** **II** **III**

$J_{119Sn\text{-}H}$ = 679 Hz (complex **2.8**) (vs) $^{1}J_{119Sn\text{-}H}$ = 1936 Hz (Ph_3SnH)

a

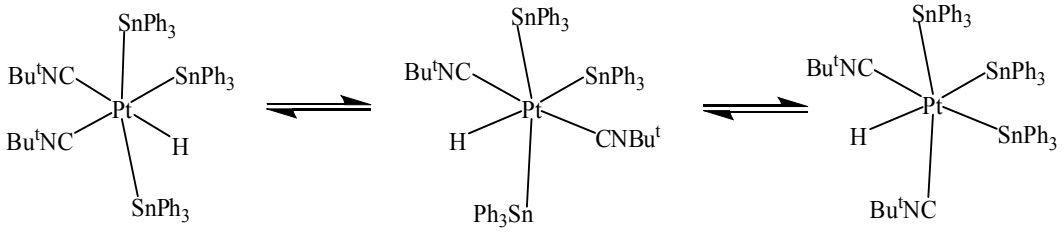

2.8 **IV** **V**

$J_{119Sn\text{-}H}$ = 679 Hz (complex **2.8**) (vs) $^{2}J_{119Sn\text{-}H}$ ~ 800 to 1000 Hz (*trans*)

b

Scheme 2.4: a) Proposed resonance structures with bridging hydride. b) Proposed *cis/trans* isomers.

Efforts to identify the hydride bridging isomer by ^{119}Sn NMR spectroscopy failed as the proton coupled spectra was too broad and did not show any possible doublets due

to hydride couplings. The only possible solution to this is to crystallize the isomers and study them using single crystal x-ray spectroscopy. At this point it is unclear about the existence of type of isomerism/isomer in the solution of **2.8,** and further research is underway to identify the isomer at -6.62 ppm.

As expected, compound $Pt(SnPh_3)_3(CNBu^t)_2(H)$, **2.8** is unstable in air and loses hydride as H_2 and Ph_3Sn ligand as $Ph_3SnSnPh_3$ and $(Ph_3)_4Sn$ and forms a stable yellow colored compound $Pt(SnPh_3)_2(CNBu^t)_2$, **2.9.** An ORTEP diagram of the molecular structure of **2.9** is shown in Figure 2.15, (further crystallographic data can be found in Appendix A Table A.3).

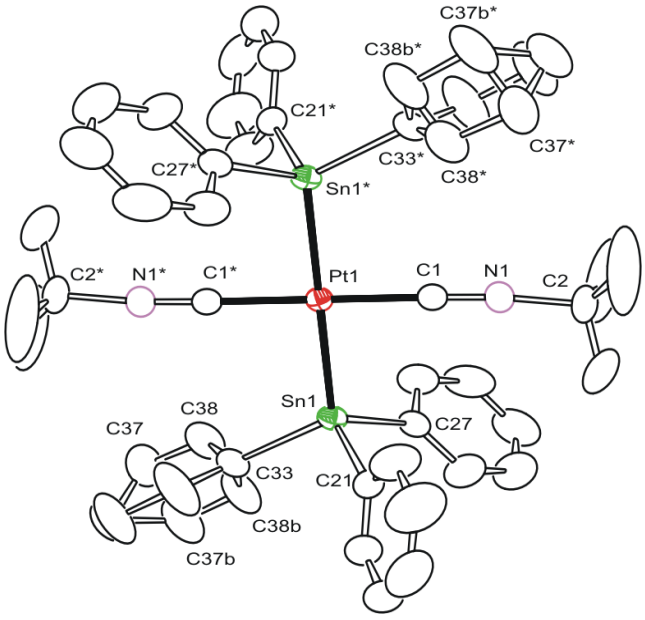

Figure 2.15. An ORTEP of the molecular structure of $Pt(SnPh_3)_2(CNBu^t)_2$, **2.9** showing 30% probability thermal ellipsoids. Selected interatomic distances (Å) and angles (deg) are as follows: Pt(1)-Sn(1) = 2.6231(3), Pt(1)-C(1) = 1.936(5). Sn(1)-Pt(1)-Sn(1^*) = 180.00, Sn(1)-Pt(1)-C(1) = 87.5(1), Sn(1)-Pt(1)-C(1^*)=92.5(1), C(1)-Pt(1)-C(1^*)=180.0(2).

Compound $Pt(SnPh_3)_2(CNBu^t)_2$, **2.9** is a d^8 square planar, 16 electron Pt(II) compound. Compound **2.9** is characterized by the combination of IR, ^{1}H NMR, elemental

and single crystal x-ray diffraction analyses. Compound **2.9** can also be prepared by reacting $Pt(COD)_2$ with two equivalents each of Ph_3SnH and $CNBu^t$ at -78°C. Interestingly, compound **2.9** is stable towards H_2 or CO addition, but reacts with Ph_3SnH under inert atmosphere to generate back compound $Pt(SnPh_3)_3(CNBu^t)_2(H)$, **2.8**.

Exchange of $SnBu^t_3$ group with Mes_3Sn group: Reaction of compound **2.6** with Ph_3SnH didn't give much insight into the mechanism of H_2-D_2 exchange as it reacts by itself even in the absence of H_2 gas to give the compound **2.8**. So the exchange reaction was carried with other Sn ligand Mes_3SnH, trimesityl stannane {$(2,4,6\text{-}Me_3C_6H_2)_3SnH$ or Mes_3SnH} which is bulkier than Bu^t_3SnH. There was essentially no reaction of compound **2.6** with a 3 fold excess of Mes_3SnH at room temperature (^1H NMR of the reaction mixture shows only very trace amounts of product and reaction takes 7 days for completion at room temperature). However when H_2 gas is introduced to the reaction system (which first forms compound **2.5**), the reaction proceeds faster to afford $Pt(SnBu^t_3)(SnMe_3)(CNBu^t)_2$, **2.10** (see Scheme 2.5). This is imaginable as in case of **2.5** there is a readily available hydride on Pt, which can be bonded to $SnBu^t_3$ group to be removed as Bu^t_3SnH. But in the case of **2.6,** in the absence of H_2 gas the hydride has to come from Mes_3SnH which is a time consuming process with relatively high energy barrier compared to previous route.

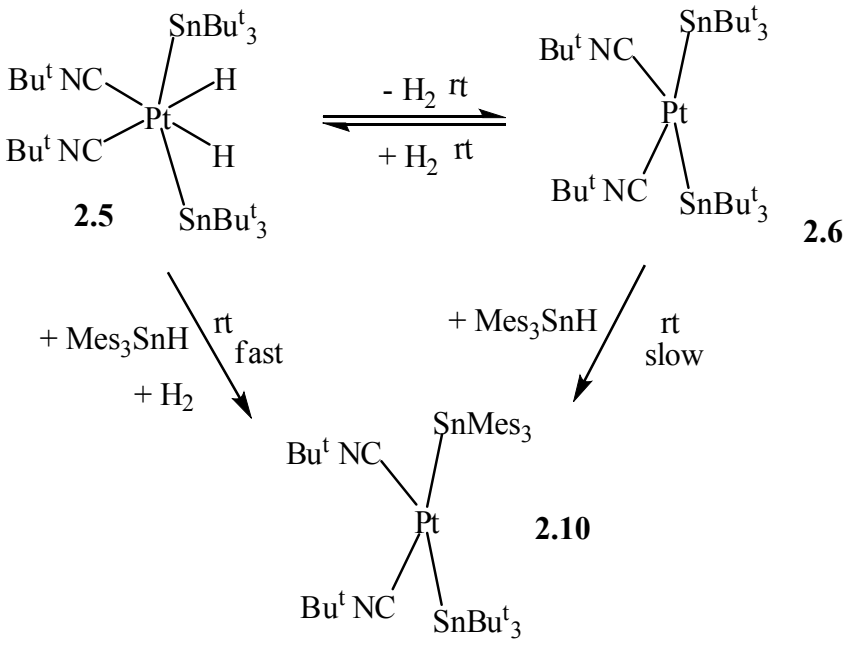

Scheme 2.5. Formation of compound **2.10** from compounds **2.5** and **2.6.**

Crystal structure for **2.10** is shown in Figure 2.16 (further crystallographic data can be found in Appendix Table A.3). In the absence of H_2 gas, the formation of $Pt(SnBu^t_3)(SnMes_3)(CNBu^t)_2$, **2.10** from **2.6** in fact proceeds through complex **2.5,** where complex **2.5** forms first and then the reductive elimination of Bu^t_3SnH takes place (which is evident from ^{1}HNMR where peaks corresponding to both compound **2.5** and Bu^t_3SnH were observed) to facilitate the oxidative addition of Mes_3SnH. A variety of exchange reactions at the Pt metal center are reported in the literature,[91–95] but to our knowledge this is the first example of an exchange reaction where we have successfully replaced a single tin ligand with a different tin ligand to furnish a stable complex that has two different terminal tin ligands coordinated to a Pt metal center.

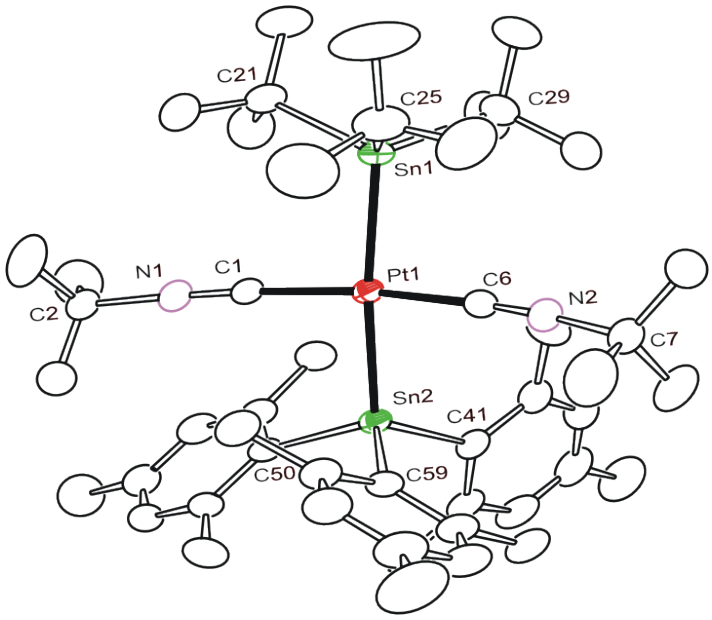

Figure 2.16. An ORTEP of the molecular structure of $Pt(SnMes_3)(SnBu^t_3)(CNBu^t)_2$, **2.10** showing 30% probability thermal ellipsoids. Selected interatomic distances (Å) and angles (deg) are as follows: Sn(1)-Pt(1)=2.6797(5), Sn(2)-Pt(1)=2.6775(5), C(1)-Pt(1) =1.947(6), C(6)-Pt(1)=1.945(6), Sn(1)-Pt(1)-Sn(2)=171.50(2), C(1)-Pt(1)-C(6) = 167.1(3), C(6)-Pt(1)-Sn(1) =92.1(2), C(1)-Pt(1)-Sn(1)=93.3(2), C(1)-Pt(1)-Sn(2)=89.3(2), C(6)-Pt(1)-Sn(2)=87.0(2).

Compound **2.10** is similar in structure to **2.6** where in place of one of the $SnBu^t_3$ there is a $SnMes_3$ group. The complex is not square planar but at the same time not as distorted to a "sawhorse" type structure as in **2.6,** [C(1)-Pt(1)-C(6) = 167.1(3) °, Sn(1)-Pt(1)-Sn(2)=171.50(2)]. Complex **2.10** does not contain any hydride ligands, but it can be assumed that the dihydride complex $Pt(SnBu^t_3)(SnMes_3)(CNBu^t)_2(H)_2$ first forms, which in turn loses H_2 to give **2.10**. Considering how labile the hydride ligands are in **2.5,** it is not surprising that $Pt(SnBu^t_3)(SnMes_3)(CNBu^t)_2(H)_2$, could not be detected. Furthermore, addition of H_2 or CO to **2.10** does not occur as in the case with **2.5** at room temperature and is highly stable to exchange other Bu^t_3Sn even with excess Mes_3SnH.

Efforts to exchange the other $SnBu^t_3$ ligand from compound $Pt(SnMes_3)(SnBu^t_3)(CNBu^t)_2$, **2.10** with the excess of Mes_3SnH to form the compound $Pt(SnMes_3)_2(CNBu^t)_2$, **2.11** were unsuccessful at room temperature. However, we were able to make the $Pt(SnMes_3)_2(CNBu^t)_2$, **2.11** directly from the reaction of $Pt(COD)_2$ with two equivalents of each $CNBu^t$ and Mes_3SnH at -78 °C in 80% yield. A crystal structure of **2.11** is shown in Figure 2.17, (further crystallographic data can be found in Appendix Table A.3). Compound **2.11** is highly stable and similar in structure to compound **2.10**, except compound **2.11** is highly sterically encumbered and it is also unreactive towards H_2 or CO at room temperature as in the case of $Pt(SnBu^t_3)(SnMes_3)(CNBu^t)_2$, **2.10.**

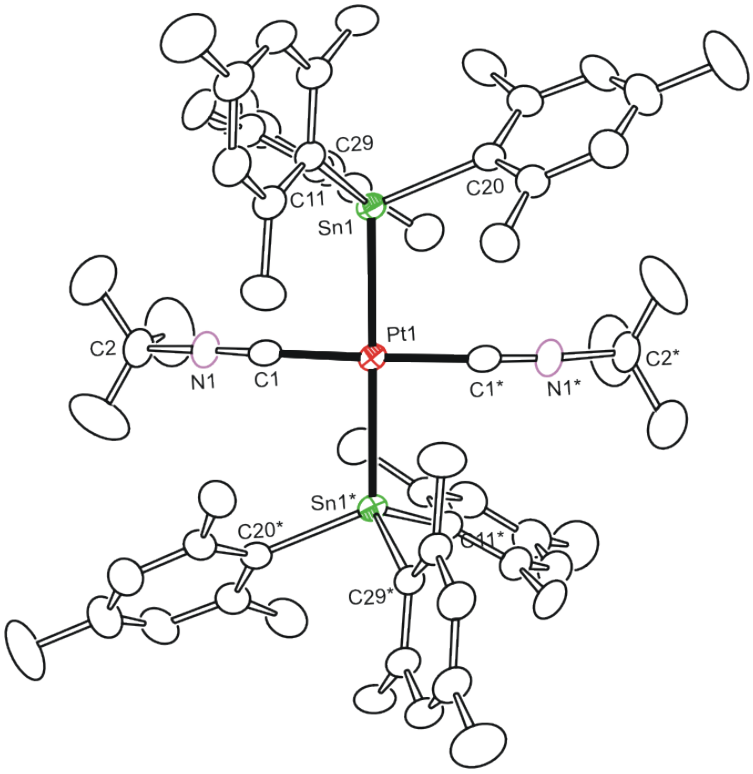

Figure 2.17. An ORTEP of the molecular structure of $Pt(SnMes_3)_2(CNBu^t)_2$, **2.11,** showing 30% probability thermal ellipsoids. Selected interatomic distances (Å) and angles (deg) are as follows: Sn(1)-Pt(1) = 2.6615(6), C(1)-Pt(1) = 1.92(1). Sn(1)-Pt(1)-Sn(1*) = 175.74(3), Sn(1)-Pt(1)-C(1) = 89.0(3), C(1)-Pt(1)-C(1*)= 164.2(4).

Exchange between $Pt(SnBu^t_3)_2(CNBu^t)_2(D)_2$, 2.5-*d*$_2$ and free Bu^t_3SnH: While the experiment conducted with Mes_3SnH and **2.6**, shows exchange of the tin groups, it can be assumed that reductive elimination of Bu^t_3SnH should occur from **2.5**. To further prove this, we performed the reaction of the dideuteride complex $Pt(SnBu^t_3)_2(CNBu^t)_2(D)_2$, **2.5-*d*$_2$** and free Bu^t_3SnH. When an equimolar mixture of **2.5-*d*$_2$** and Bu^t_3SnH was carried out in an NMR tube with C_6D_6 solvent, $^2H\{^1H\}$ NMR revealed formation of Bu^t_3SnD showing appropriate one bond coupling to both ^{119}Sn and ^{117}Sn, (δ = 5.62, $^1J119_{Sn\text{-}D}$ = 213 Hz and $^1J117_{Sn\text{-}D}$ = 203 Hz). The deuteride region showed a peak at δ = -13.48, $^1J_{Pt\text{-}H}$ = 106 Hz due to **2.5-*d*$_2$** and **2.5-*d*$_1$**, and appropriately ^1H NMR showed a resonance at (δ = -13.49 for **2.5-*d*$_1$** and -13.52 for **2.5)** (see Figure 2.18).

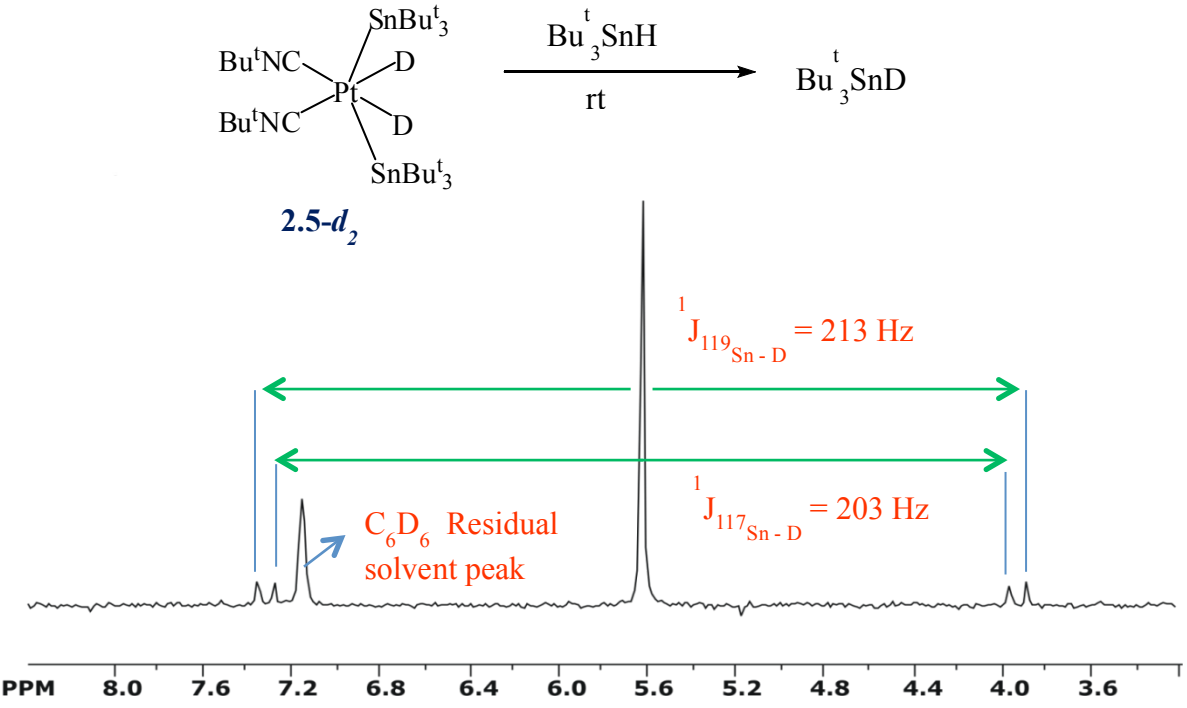

Figure 2.18: $^2H\{^1H\}$ NMR of Bu^t_3SnD in the reaction mixture of $Pt(SnBu^t_3)_2(CNBu^t)_2(D)_2$, **2.5-*d*$_2$**, and Bu^t_3SnH.

These exchange experiments further support the proposed mechanism in equation 2.4, for reductive elimination of $SnBu^t_3H$ in the presence of H_2/D_2 gas to facilitate the exchange to form HD gas. Based upon these experimental results the following mechanism (see Scheme 2.6) has been proposed for the catalytic formation of HD gas from H_2-D_2 in the presence of compound **2.5.**

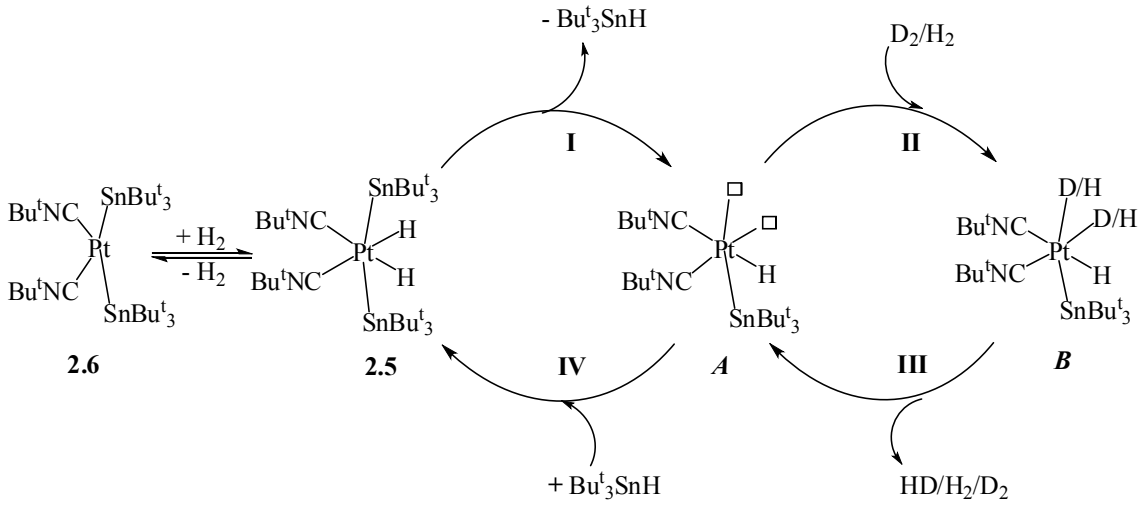

Scheme 2.6. Proposed mechanism for the catalytic formation of HD gas from H_2-D_2 in the presence of compound **2.5.**

The catalysis begins with the formation of **2.5**, followed by the reductive elimination of free Bu^t_3SnH from **2.5,** to form intermediate ***A*** with two vacant co-ordination sites. Step **I** is believed to be the rate determination step. Then H_2/D_2 adds to the intermediate ***A*** in oxidative addition fashion to form another intermediate ***B***. It is where H_2-D_2 exchange happens to form HD gas and the intermediate ***A*.** The catalytic steps **II** and **III** keep on going until there reaches equilibrium between $HD/H_2/D_2$. Once equilibrium is attained the catalysis stops and the cycles proceeds to step **IV** where the

free Bu^t_3SnH formed during step **I,** adds to intermediate ***A*** in an oxidative addition fashion to form back the compound **2.5.**

Reaction of CO gas with reaction mixture of $Pt(COD)_2$ and Bu^t_3SnH: The hydride ligands in the compound **2.5** are labile and can be eliminated under mild conditions. We were fortunate to isolate complex **2.5** in pure form and obtain its crystal structure. However, we were unable to isolate the analogous carbonyl complex $Pt(SnBu^t_3)_2(CO)_2(H)_2$ when the reaction of one equivalent of $Pt(COD)_2$ with two equivalents of Bu^t_3SnH was carried out at room under an atmosphere of carbon monoxide gas (in place of $CNBu^t$). Instead, new compound $Pt(CO)_2(SnBu^t_3)_2$, **2.12**, was isolated from the reaction mixture. When CO gas is purged at room temperature through the brownish-red colored reaction mixture of two equivalents of Bu^t_3SnH and one equivalent of $Pt(COD)_2$ in hexane solution, the color of the solution turned to green within 10 minutes. The IR spectra showed new peaks corresponding to the CO stretching. The reaction mixture was filtered through silica plug to yield a green colored 16 electron Pt(II) compound $Pt(CO)_2(SnBu^t_3)_2$, **2.12**, in 91% yield which does not contain any hydride ligands. The structure of **2.12** is shown in Figure 2.18, (further crystallographic data can be found in Appendix Table A.4). As expected for platinum complexes in d^8 configuration the molecular geometry is square planar. The ligands are *trans* to each other and that the structure of **2.12** deviates considerably from planarity is due to the sterics of the $CNBu^t$ ligands versus the CO ligands as seen in Figure 2.19. The Pt-Sn bond length is 2.7317 Å, slightly longer than that observed in compound **2.5**. The Pt1-C1 bond length (1.894 Å) is in the same range as reported for similar Pt-carbonyl complexes.[68]The complex **2.12** is stable in solid state at room temperature for few hours,

but decomposes upon prolonged exposure to air. Compound **2.12** was characterized by the combination of ^{1}H NMR, single crystal X-ray crystallography, and IR spectroscopy.

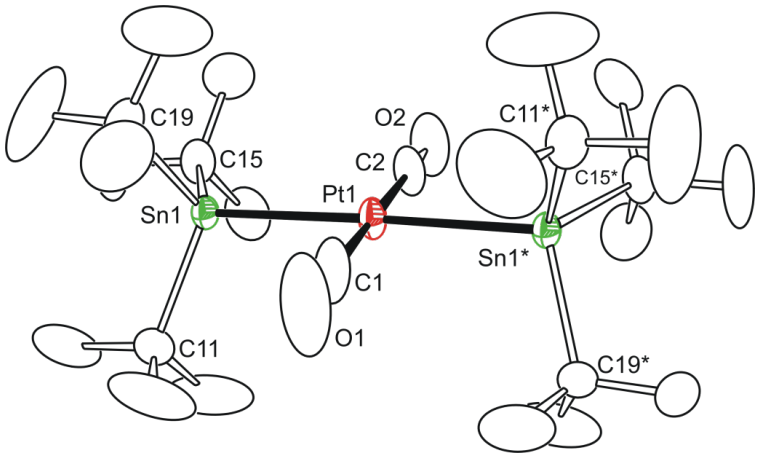

Figure 2.19. An ORTEP of the molecular structure of $Pt(SnBu^{t}_{3})_2(CO)_2$, **2.12,** showing 40% probability thermal ellipsoids. Selected interatomic distances (Å) and angles (deg) are as follows: Pt(1)–Sn(1) = 2.7317(4); Pt(1)–Sn(1*) = 2.7317(4); Pt(1)-C(1) = 1.847(1); Pt(1)–C(2) = 1.894(1); Sn(1)-Pt(1)-Sn(1*) = 176.08(2); C(1)-Pt(1)-C(2) = 180.0(6); Sn(1)-Pt(1)-C(1) =88.0(5); Sn(1)-Pt(1)-C(2)=92.0(4).

Compound **2.12** is electronically similar to compound $Pt(SnBu^{t}_{3})_2(CNBu^{t})_2$, **2.6**, except the bulky isocyanides force geometrical distortion from square planarity as evidenced by the "X" shape in **2.12**, and the sterics in **2.6** force the molecule to adopt a see-saw type geometry. Compound **2.12** is also analogous to the hypothized compound **2.2**, and can be assumed that it is formed by the replacement of both the hydride ligands in $Pt(SnBu^{t}_{3})_2(H)_2$, **2.2** by two CO ligands (Scheme 2.7). Adams et al. recently reported a similar Pt(II) carbonyl complex with $GePh_3$ ligands, $Pt(CO)_2(GePh_3)_2$,[68] and Braunschweig group prepared an analogous Pt(0) carbonyl complex with phosphine ligands $Pt(Cy_3P)_2(CO)_2$.[96]

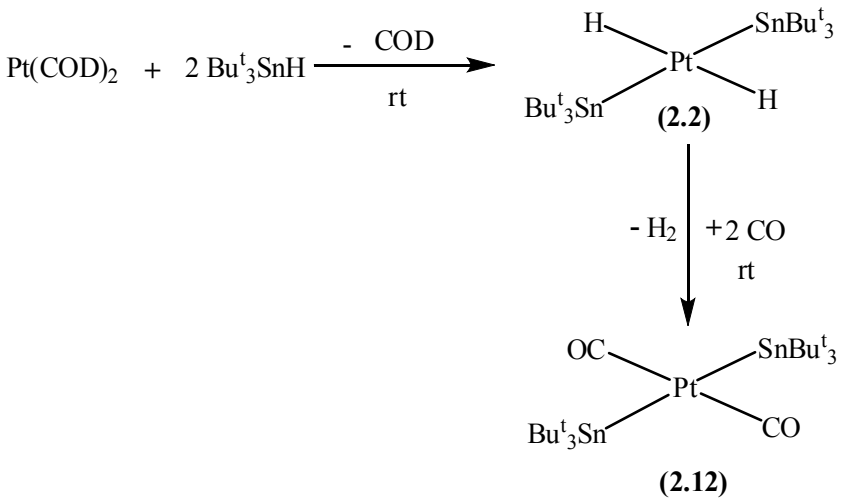

Scheme 2.7. Proposed pathway for the formation of $Pt(SnBu^t_3)_2(CO)_2$, **2.12.**

The IR spectrum of **2.12** in hexane solution shows a single strong absorption peak corresponding to a υ_{CO} stretching frequency at 2007 cm^{-1} in agreement with a *trans*-conformation. The CO ligands on $Pt(SnBu^t_3)_2(CO)_2$, **2.12** are found to be labile and they can be substituted with other ligands.

Reaction of compound $Pt(SnBu^t_3)_2(CO)_2$, 2.12 with $CNBu^t$: The carbonyl ligands in **2.12** can be replaced with $CNBu^t$ groups to give compound **2.6**, however *en route* to **2.6**, we obtained the complex $Pt(SnBu^t_3)_2(CNBu^t)_2(CO)$, **2.13,** in 96 % yield at room temperature. Addition of two equivalents of $CNBu^t$ to the green-colored solution of the $Pt(SnBu^t_3)_2(CO)_2$, **2.12,** in hexane resulted in evolution of the CO gas from the reaction mixture and formed a colorless precipitate of the intermediate Pt(II)-monocarbonyl complex, $Pt(SnBu^t_3)_2(CNBu^t)_2(CO)$, **2.13**, The structure of **2.13** is shown in Figure 2.20, (further crystallographic data can be found in Appendix Table A.4). Compound **2.13** is

characterized by the combination of ^{1}H NMR, and single crystal X-ray crystallography and, IR spectroscopy

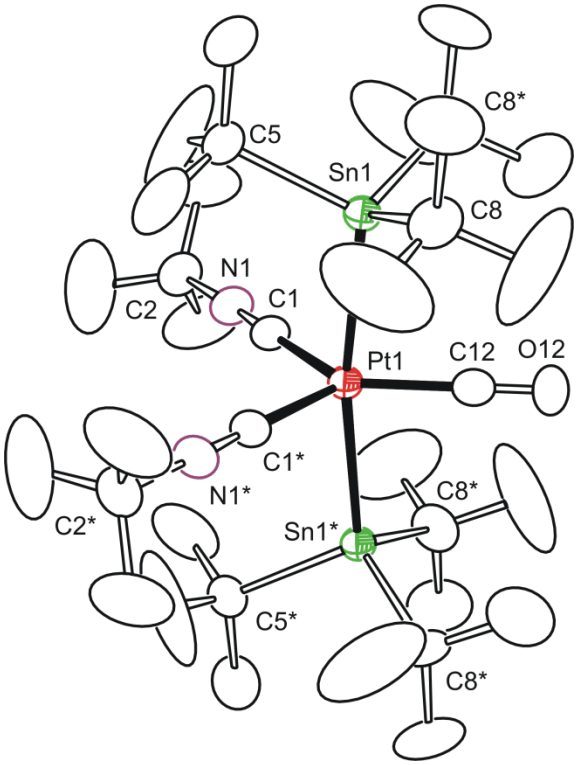

Figure 2.20. An ORTEP of the molecular structure of $Pt(SnBu^{t}_{3})_2(CNBu^{t})_2(CO)$, **2.13,** showing 30% probability thermal ellipsoids. Selected interatomic distances (Å) and angles (deg) are as follows: Pt(1)–Sn(1) = 2.7147(6); Pt(1)-C(1) = 2.02(1); Pt(1)–C(12) = 1.89 (2); Sn(1)-Pt(1)-Sn(1*) = 170.66(3); C(1)-Pt(1)-C(12) = 128.2(6); Sn(1)-Pt(1)-C(1) =92.9(3); Sn(1)-Pt(1)-C(12)=85.3(5); C(1)-Pt(1)-C(1*) = 103.7(4).

The molecular geometry of complex **2.13** is trigonal bipyramidal, in which the two $SnBu^{t}_{3}$ groups occupy both of the axial positions, while the two $CNBu^{t}$ and one CO ligand lie in the in the equatorial plane. The geometry around the Pt(II) metal center in **2.13** is slightly distorted from trigonal bipyramidal geometry due to sterics induced by $SnBu^{t}_{3}$ ligands. The Pt-Sn and Pt-CO bond lengths remain almost the same as observed in precursor complex **2.12**. The Pt-Sn bond length in complex **2.13** is 2.714 (8) Å,

slightly longer than Pt-Sn bond length in complex **2.5**. The C1-Pt-C1* bond angle in **2.13** is the same as in compound **2.5**.

Reversible activation of CO by compound 2.6: Compound **2.13** is stable in the solid state for approximately 24 hours. In hexane solution, compound **2.13** rearranges to **2.6** over a period of 12 hours at room temperature even under argon atmosphere with the elimination of a CO ligand. Compound **2.6** in hexane solution activates the CO molecule at room temperature to afford $Pt(CO)(SnBu^t_3)_2(CNBu^t)_2$, **2.13** in quantitative yield (see equation. 2.6).

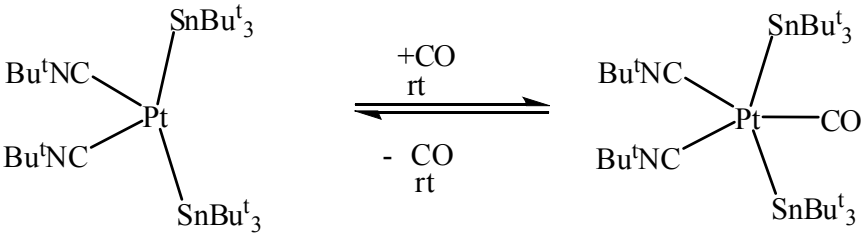

(2.6) **(2.13)** **(eq. 2.6)**

The addition of CO gas to compound **2.6** is reversible in the solid state as well; as observed in the addition of H_2. The purple crystals of **2.6** turn colorless upon exposure to CO atmosphere in 15 minutes at room temperature to yield **2.13** quantitatively. Similarly, colorless crystals of **2.13** turn purple under argon flow after 24 hours, yielding quantitative amounts of **2.6**. Interestingly, the CO ligand in **2.13** can also be exchanged with the hydride ligands. Addition of H_2 to compound **2.13** affords Pt(IV) isocyanide complex **2.5** at room temperature. A similar phenomenon of inter conversion between CO complex to $(H)_2$ complex was observed by M. J. Mays and co. in their iridium complex . The reversible activation of H_2 and CO molecules by the 16 electron Pt(II) isocyanide complex **2.6** are summarized in Scheme 2.8.

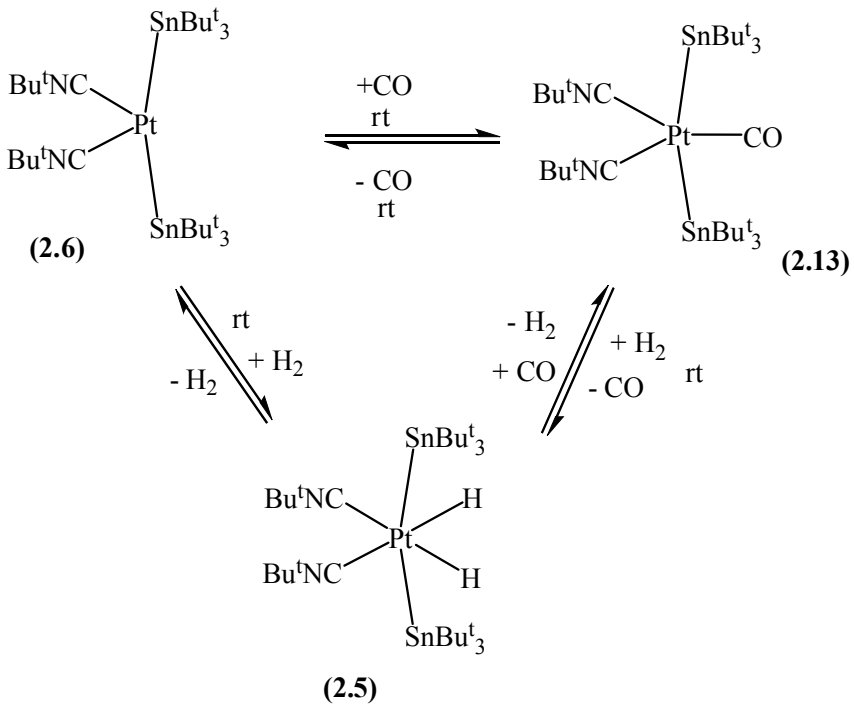

Scheme 2.8. Interconversion between compounds **2.6, 2.5** and **2.13.**

2.3 Summary and conclusions.

Scheme 2.9 presents the summary of synthesis of various saturated and unsaturated Pt-Sn bimetallic complexes discussed in this chapter. This project has been started with the aim of synthesizing sterically crowded Pt-Sn unsaturated complexes to activate small molecules. Reaction of $Pt(COD)_2$ with one equivalent Bu^t_3SnH yielded highly reactive unsaturated compound **2.1.** Efforts to synthesize compound **2.2** with two equivalents of Bu^t_3SnH were unsuccessful. However the reaction of $Pt(COD)_2$ with presence of excess Bu^t_3SnH yielded the compound **2.3** believed to be formed from **2.2**. When $Pt(COD)_2$ was reacted with Bu^t_3SnH in the presence of $CNBu^t$, it formed di hydride Pt(IV) compound **2.5**, which reversibly loses both the hydrides to furnish Pt(II) compound **2.6.** Compound **2.6** activates hydrogen reversibly even at -78 °C and it also catalyzes H_2-D_2 exchange. Compounds **2.6** and **2.5** are inter-convertible even in the solid

state. The $SnBu^t_3$ group from **2.5** can be replaceable with Ph_3Sn to give Pt(IV) compound **2.8** and with Mes_3Sn to give compound **2.10.** The proposed mechanism for the H_2-D_2 exchange involves the reductive elimination of a free Bu^t_3SnH to create vacant sites on the Pt metal center, which in turn are attacked by H_2/D_2 for the exchange to happen.

Compound **2.8** displays fluxional behavior in the solution, which was attributed to the *cis-trans* isomerization in the solution, and we were not able to isolate the *trans* isomer of compound **2.8.** Compound **2.8** is highly strained and loses a Ph_3Sn ligand and the hydride to form stable Pt(II) compound **2.9**. Compound **2.10** is stable towards exchanging the Bu^t_3Sn ligand to form compound **2.11**, even in the presence of excess Mes_3SnH under refluxing conditions. However, compound **2.11** was directly synthesized from the reaction of $Pt(COD)_2$ with two equivalents of Mes_3SnH. The reaction of $Pt(COD)_2$ with Bu^t_3SnH in the presence of CO gas yielded Pt(II) compound **2.12.** Compound **2.12** in the presence of $CNBu^t$ loses a CO ligand and forms compound **2.13.** Compound **2.13** reversibly loses the CO ligand to from compound **2.6** both in solid state and solution state.

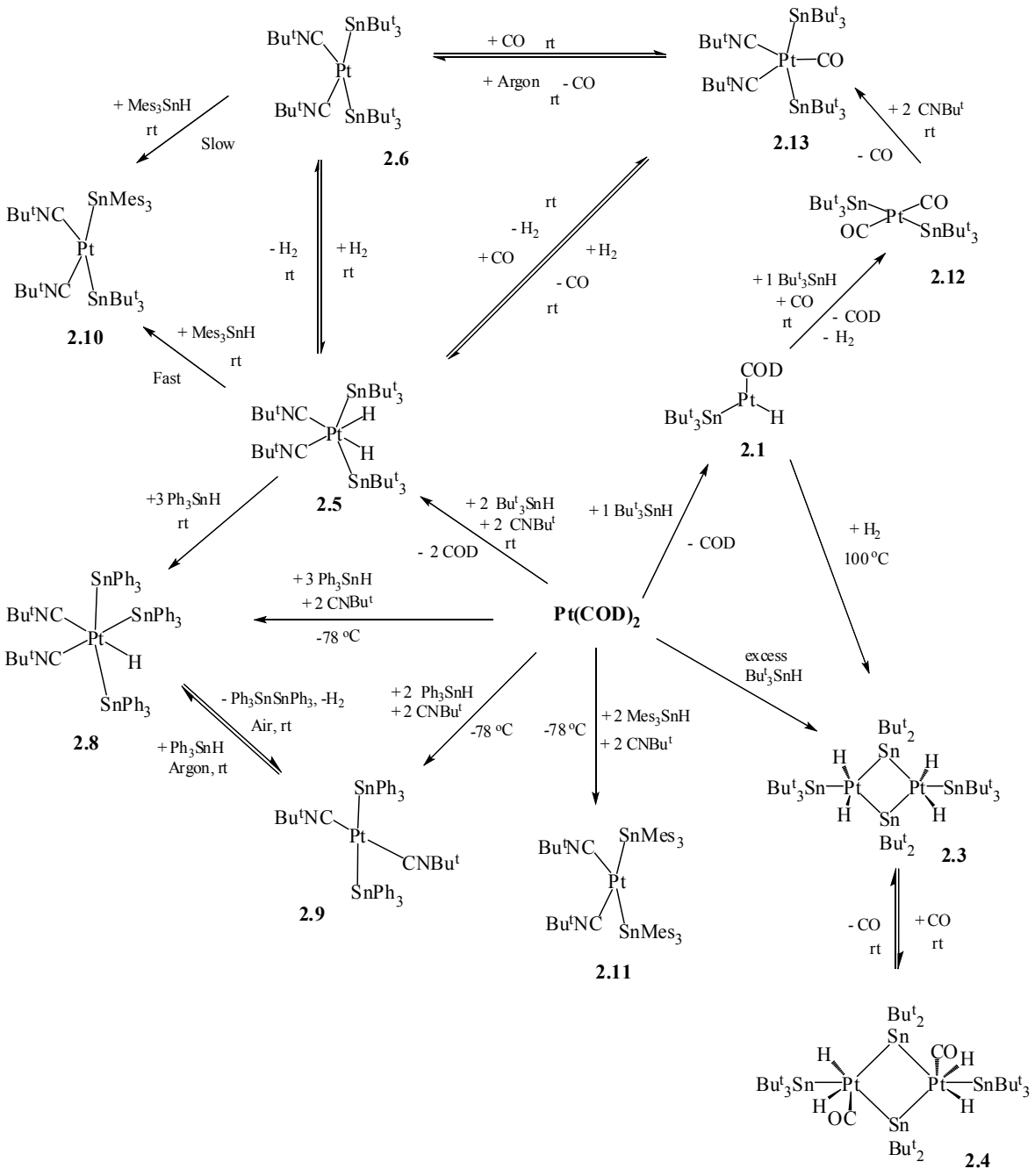

Scheme 2.9. Summary of reactions discussed in chapter 2.

2.4 Experimental section.

General Data: Unless indicated otherwise, all reactions were performed under an atmosphere of Argon. Reagent grade solvents were dried by the standard procedures and were freshly distilled prior to use. Infrared spectra were recorded on a Nicolet 380 FT-IR spectrophotometer. ^{1}H NMR were recorded on a Bruker 300 and 400 spectrometer operating at 300.13 MHz and 399.99 MHz respectively. Elemental analyses were performed by Columbia Analytical Services (Tuscon, AZ). Mass spectrometric measurements performed by a direct–exposure probe using electron impact ionization (EI) were made on a VG 70S instrument at the University of South Carolina, Columbia, SC. Tertiary butylisocyanide, $CNBu^{t}$, was purchased from Sigma-Aldrich and used without further purification. Triphenyltin hydride was purchased from Alfa Aesar and used without further purification. Bis(1,5-cyclooctadiene)platinum, $Pt(COD)_2$,[97] tri-*tert*-butylstannane, $Bu^{t}_{3}SnH$,[44,60] Mes_3SnH[98] were prepared according to the published procedures. Silica gel (60-200 μm, 70-230 mesh) used for chromatographic separations was purchased from Silicycle.

Synthesis of $Pt(SnBu^{t}_{3})(COD)(H)$, 2.1: In a glove box, under an atmosphere of argon, 25mg of $Bu^{t}_{3}SnH$ (0.086 mmol) dissolved in 3mL of freshly distilled hexane was added to 30.0 mg of $Pt(COD)_2$ (0.073 mmol). The reaction mixture immediately turned dark brown. The reaction mixture stirred at room temperature for an additional 10 min and was filtered through kimwipe and the solvent was evaporated completely dry under argon gas flow. The yellowish-brown solid residue was redissolved in diethylether and placed in -20 °C freezer overnight which gave crystalline $Pt(SnBu^{t}_{3})(COD)(H)$, **2.1**, covered with black oily residue. After washing the crystalline product with isopropyl alcohol (3 x

0.3 mL), 13.2 mg (30 % yield) of **2.1** was obtained. Spectral data for **2.1**: ^{1}H NMR (C_6D_6, rt, in ppm): δ = 5.80 (m, $^{2}J_{Pt\text{-}H}$ = 51.4 Hz, $^{3}J_{Sn\text{-}H}$ = 5.0 Hz, 2H; CH- cod), 5.45 (m, $^{2}J_{Pt\text{-}H}$ = 44.7 Hz, $^{3}J_{Sn\text{-}H}$ = 6.5 Hz, 2H; CH- cod), 1.82-1.51 (broad m, 8H; CH_2-cod); 1.53 (s, $^{3}J_{Sn\text{-}H}$ = 52.5 Hz, 27H, $SnBu^{t}_3$); -3.74 (s, $^{1}J_{Pt\text{-}H}$ =1223.2 Hz, $^{2}J_{Sn\text{-}H}$ = 48.2 Hz, 1H, hydride).

Synthesis of [Pt(SnBu$^{t}_3$)(μ-SnBu$^{t}_2$)(H)$_2$]$_2$, 2.3: In a glove box, under an atmosphere of argon, 583 mg of Bu^{t}_3SnH (2.000 mmol) dissolved in 1mL of freshly distilled toluene was added slowly drop wise to 103 mg of $Pt(COD)_2$ (0.250 mmol) over a period of 20 min at room temperature with continuous stirring. The solvent was allowed to evaporate in dry box overnight. The black oily residue was washed with dichloromethane solvent several times until the solution was colorless, yielding 34 mg of **7** (19 % yield). Yield is low because of unidentified side products. Spectral data for **2.3**: ^{1}H NMR (C_7D_8, rt, in ppm): δ = 1.58(s, 36 H, $SnBu^{t}_2$, $^{2}J_{Sn\text{-}H}$ = 64 Hz), 1.50 (s, 54H, $SnBu_3^{t}$, $^{3}J_{Sn\text{-}H}$ = 60 Hz), -3.71(s, 4H, hydride, $^{1}J_{Pt\text{-}H}$ = 905 Hz, $^{2}J_{Sn\text{-}H}$ = 32 Hz). Mass Spec. EI/MS *m*/*z*. 1383 (M^{+}-Bu^{t}), 1326(M^{+}-2Bu^{t}). The isotope pattern is consistent with the presence of two platinum and four tin atoms.

Synthesis of [Pt(SnBu$^{t}_3$)(μ-SnBu$^{t}_2$)(CO)(H)$_2$]$_2$, 2.4: In a 10 ml schlenk tube, under atmosphere of argon, 25 mg (0.017 mmol) of **2.3** dissolved in 3 ml of hexane/dichloromethane (1:1 mixture) was transferred. The reaction mixture was colorless and turbid. With the purging of CO gas through solution at room temperature for 10 min, solution color turned to dark yellow and solution became clear. The reaction mixture filtered through Kim wipe and crystallized in ice bath (0 °C) under CO gas stream to obtain 20 mg (78% yield) of yellow crystals of **2.4** (after washing 2 times with

small portions of hexane). ^{1}H NMR (C_7D_8, rt, in ppm): δ = 1.69(s, 36 H, $SnBu^t_2$, $^{2}J_{Sn-H}$ = 72 Hz), 1.45 (s, 54 H, $SnBu^t_3$, $^{3}J_{Sn-H}$ = 61 Hz), -12.77(s, 4H, hydride, $^{1}J_{Pt-H}$ = 702 Hz, $^{2}J_{Sn-H}$ = 28 Hz). IR ν_{CO} (cm^{-1} in hexane): 2163(w), 2027(vs), 2008 (m). Elemental Anal, calc.: C, 33.72; H, 6.33 % Found: C, 34.18; H, 5.92 %.

Conversion of $[Pt(SnBu^t_3)(\mu\text{-}SnBu^t_2)(CO)(H)_2]_2$, 2.4 to $[Pt(SnBu^t_3)(\mu\text{-}SnBu^t_2)(H)_2]_2$, 2.3 in solution: In a 10 mL schlenk tube, 10.0 mg of **2.4** (0.0067 mmol) was dissolved in 2 mL of hexane. The solvent was removed overnight in glove box during which time the color of the solution changed from yellow to colorless. This yielded 9.0 mg (94 % yield) of crystalline **2.3**.

Synthesis of $Pt(SnBu^t_3)_2(CNBu^t)_2(H)_2$, 2.5: In a glove box, under an atmosphere of argon, 49.5 mg of Bu^t_3SnH (0.170 mmol) dissolved in 5 mL of freshly distilled hexane was added to 35.0 mg of $Pt(COD)_2$ (0.085 mmol). The reaction mixture was stirred at room temperature for 5 min after which time 14.0 mg of $CNBu^t$ (0.170 mmol) was added and the reaction mixture was stirred at room temperature for an additional 10 min. The solution was then filtered, and the filtrate was placed in a -20 °C freezer overnight which gave crystalline $Pt(SnBu^t_3)_2(CNBu^t)_2(H)_2$, **2.5**. After washing the crystalline product with approx. 2 mL of acetonitrile, 26 mg (32 % yield) of **2.5** was obtained. Spectral data for **2.5**: ^{1}H NMR (C_6D_6, rt, in ppm): δ = 1.57 (s, 54 H, $SnBu^t_3$, $^{3}J_{Sn-H}$ = 51 Hz), 0.96 (s, 18H, Bu^t); –13.52 (s, 2H, hydride, $^{1}J_{Pt-H}$ = 697 Hz, $^{2}J_{Sn-H}$ = 34 Hz). ^{119}Sn NMR (C_6D_6, rt, in ppm): δ = 81.50 (s, 2 Sn, $^{1}J_{Pt-Sn}$ = 3604 Hz). IR (cm^{-1} in Hexane): ν_{CN} 2139(s), ν_{Pt-H} 2112(m). Mass Spec. EI/MS *m*/*z*. 942 (M^+), 883 (M^+-H_2-Bu^t). Mass Spec. EI/MS *m*/*z*. 942 (M^+), 883 (M^+-H_2-Bu^t). The isotope pattern is consistent with the presence of one platinum and two tin atoms.

Conversion of $Pt(SnBu^t_3)_2(CNBu^t)_2(H)_2$, 2.5 to $Pt(SnBu^t_3)_2(CNBu^t)_2$, 2.6 in solution: A 15.0 mg amount of **2.5** (0.016 mmol) was dissolved in 50 mL of distilled hexane. With stirring, argon was then allowed to purge through the solution at 25 °C for approximately 20 h. Within minutes the colorless solution starts to turn violet. ^{1}H NMR of the reaction mixture showed complete conversion of the starting **2.5** to **2.6.** The solvent was removed *in vacuuo*, and the purple color residue was crystallized by evaporation of a benzene/acetonitrile solvent mixture under a stream of argon at room temperature to yield 13.2 mg (88 %) of crystalline **2.6.** Spectral data for **2.6**: ^{1}H NMR (C_6D_6, rt, in ppm): δ = 1.60 (s, 54 H, $SnBu^t_3$, $^3J_{Sn\text{-}H}$ = 49 Hz), 1.15 (s, 18 H, Bu^t). IR (cm^{-1} in Hexane): ν_{CN} 2112(s). Mass Spec. EI/MS *m*/*z*. 940 (M^+), 883 (M^+-Bu^t). The isotope pattern is consistent with the presence of one platinum and two tin atoms.

Conversion of $Pt(SnBu^t_3)_2(CNBu^t)_2$, 2.6 to $Pt(SnBu^t_3)_2(CNBu^t)_2(H)_2$, 2.5 in solution: In a 10 mL schlenk tube, 28.0 mg of **2.6** (0.030 mmol) was dissolved in 5 mL of hexane. The solvent was removed under a slow stream of hydrogen gas (approx. 3 h) during which time the color of the solution changed from violet to colorless. This yielded 26.2 mg (93 % yield) of crystalline **2.5**.

Conversion of $Pt(SnBu^t_3)_2(CNBu^t)_2(H)_2$, 2.5 to $Pt(SnBu^t_3)_2(CNBu^t)_2$, 2.6 in the solid state: In a 10 mL schlenk tube containing 10.0 mg of colorless crystalline **2.5** (0.011 mmol), argon gas was purged through the system for 24 h in the dark at room temperature, at which time the color of the crystalline **2.5** turned to violet. ^{1}H NMR indicated complete consumption of starting **2.5** in quantitative yield to $Pt(SnBu^t_3)_2(CNBu^t)_2$, **2.6**.

Conversion of $Pt(SnBu^t_3)_2(CNBu^t)_2$, 2.6 to $Pt(SnBu^t_3)_2(CNBu^t)_2(H)_2$, 2.5 in the solid state: In a 10 mL schlenk tube containing 12.0 mg of violet crystalline **2.6** (0.013 mmol), hydrogen gas was purged through the system for 15 min in the dark at room temperature, at which time the color of the crystalline **2.6** turned to colorless. ^{1}H NMR indicated complete consumption of starting **2.6** in quantitative yield to **2.5**.

Synthesis of $Pt(SnPh_3)_3(CNBu^t)_2(H)$, 2.8: A 20 mg (0.049mmol) amount of $Pt(COD)_2$ was transferred into 50 ml schlenk tube and the flask was evacuated and refilled with argon several times . To this, 10 mL of distilled hexane was added under argon at -78°C. While maintaining -78°C, a mixture of 51.2 mg of Ph_3SnH (0.146 mmol, 3 equ) and 8.08 mg of ^{But}NC (0.097 mmol, 2equ) dissolved in 15 mL of distilled hexane solvent was added drop wise to $Pt(COD)_2$ solution under argon. The reaction mixture was stirred at -78°C for 10 min, after which slowly allowed to warm to the room temperature, during which time a white insoluble precipitate was observed. The reaction mixture was stirred at RT for an additional 1 hr. The solution was filtered through glass frit in glove box. The white colored residue was washed three times with 2 mL portions of distilled hexane. The residue was dissolved CH_2Cl_2/hexane mixture, filtered through Kim wipe and crystallized at -30°C in the glove box to obtain 60mg (86 % yield) of color less crystals. Spectral data for $Pt(SnPh_3)_3(CNBu^t)_2(H)$, **2.8**: Note: Compound exhibits fluxional behaviour in solution. ^{1}H NMR (Toluene-d_8, –20 °C, in ppm): δ = 7.8 – 6.9 (m, Ph), 0.83 (s, $CNBu^t$), 0.51 (s, $CNBu^t$), 0.44 (s, $CNBu^t$), 0.44 (s, $CNBu^t$), -6.63 (s, hydride, $^1J_{119Sn-H}$ = 679 Hz, $^1J_{117Sn-H}$ = 647Hz, $^1J_{Pt-H}$ = 775 Hz,), -11.91 (s, hydride, $^1J_{Pt-H}$ = 665 Hz, $^2J_{119Sn-H}$ = 26.68 Hz, $^2J_{117Sn-H}$ = 13.95Hz). IR ν_{CN} (cm^{-1} in CH_2Cl_2): 2190(vs). Elemental Anal, calc.: C, 54.42; H, 4.57; N, 1.98 %. Found: C, 53.94; H, 4.88; N, 1.82 %.

Conversion of $Pt(SnBu^t_3)_2(CNBu^t)_2$, 2.6 to $Pt(SnPh_3)_3(CNBu^t)_2(H)$, 2.8 in solution in glove box: In a 10 mL schlenk tube, 10 mg of **2.6** (0.011 mmol) was dissolved in 3 mL of freshly distilled hexane. To which 13.52 mg of Ph_3SnH (0.039 mmol, 3.5 equ)) dissolved in 3 mL of hexane solvent was added drop wise over a period of 10 minutes while stirring the reaction mixture, during which time violet colored solution turned color less and a white colored precipitate was observed at the bottom of the schlenk tube. The precipitate was washed three times with 2 mL portions of distilled cold hexane. The residue was dissolved in mixture of CH_2Cl_2/ hexane solvent, filtered through Kim wipe and crystallized at -30°C in the glove box to obtain 14 mg (90 % yield) of $Pt(SnPh_3)_3(CNBu^t)_2(H)$, **2.8.**

Synthesis of $Pt(SnPh_3)_2(CNBu^t)_2$, 2.9: A 20 mg (0.049 mmol) amount of $Pt(COD)_2$ was transferred into 50 mL schlenk tube and flask was evacuated and refilled with argon several times . To this, 10 mL of distilled hexane was added under argon at -78°C. While maintaining -78°C, a mixture of 34.12 mg of Ph_3SnH (0.097 mmol, 2 equ) and 8.08 mg of Bu^tNC (0.097 mmol, 2 equ) dissolved in 15 mL of distilled hexane solvent was added drop wise to $Pt(COD)_2$ solution under argon while maintaining the reaction mixture at -78°C. The reaction mixture was stirred at -78°C for 10 min, after which was slowly allowed to warm to the room temperature, during which time solution color changed to cloudy yellow. The reaction mixture was stirred at RT for an additional 12 hrs. The solvent was removed *in vacuuo*, and the residue was dissolved in CH_2Cl_2/Hexane solvent mixture, filtered through Kim wipe and crystallized at -30°C in the glove box to obtain 44 mg (84 % yield) of yellow colored crystals.. Spectral data for $[Pt(SnPh_3)_2(CNBu^t)_2]$, **2.9**: ^{1}H NMR (CD_2Cl_2, rt, in ppm): δ = 0.883 (s, 18 H, 2 $CNBu^t$), δ = 7.22-7.7 (m, 30 H,

2 Ph_3Sn). IR ν_{CN} (cm^{-1} in CH_2Cl_2): 2165 (vs). Elemental Anal, calc.: C, 52.05; H, 4.56; N, 2.64 %. Found: C, 52.10; H, 4.74; N, 2.61 %.

Conversion of $Pt(SnPh_3)_2(CNBu^t)_2$, 2.9 to $Pt(SnPh_3)_3(CNBu^t)_2(H)$, 2.8 to in solution: In glove box, 20 mg of $Pt(SnPh_3)_2(CNBu^t)_2$, **2.9** (0.019 mmol) was transferred in to a 10 mL schlenk tube containing 3 mL of hexane. To which, Ph_3SnH (7 mg, 0.02 mmol) dissolved in minimum amount of hexane solvent was added drop wise while stirring the contents. The solution became color less over a period of 5 minutes and a white insoluble precipitate of compound **2.8** was obtained at the bottom of the schlenk tube. The precipitate was washed three times with 2 mL portions of cold hexane. The residue was dissolved in a mixture of CH_2Cl_2/ hexane solvent, filtered through Kim wipe and crystallized at -30°C in the glove box to obtain 18 mg (90 % yield) of $Pt(SnPh_3)_3(CNBu^t)_2(H)$, **2.8.**

Conversion of $Pt(SnPh_3)_3(CNBu^t)_2(H)$, 2.8 to $Pt(SnPh_3)_2(CNBu^t)_2$, 2.9 in solution: In a 10 mL vial, 20 mg of $Pt(SnPh_3)_3(CNBu^t)_2(H)$, **2.8** (0.014 mmol) was dissolved in 3 mL of CH_2Cl_2/octane solvent mixture and crystallized at RT while exposing it to the air to obtain 9 mg (60 % yield) of the yellow crystals of $Pt(SnPh_3)_2(CNBu^t)_2$, **2.9.**

Synthesis of $Pt(SnMes_3)(SnBu^t_3)(CNBu^t)_2$, 2.10: In a 50 mL schlenk flask, 80 mg of $Pt(SnBu^t_3)_2(CNBu^t)_2$, **2.6** (0.085 mmol) was dissolved in 20 mL of distilled hexane. To which, 40.6 mg of Mes_3SnH (0.085 mmol) dissolved in 10 mL of distilled hexane solvent was added drop wise over a period of 10 minutes while stirring the reaction mixture. Then, the reaction mixture was stirred for another 1 hr at RT under a slow stream of H_2 gas purge through the solution to give an orange colored solution. After which H_2, gas flow was stopped, and the reaction flask was sealed under H_2 gas and stirred for an

additional 12 hrs at RT. After which the solvent was removed *in vacuuo*, to give an orange colored residue. The residue was washed three times with 2 mL portions of cold pentane. Then the residue was re dissolved in a mixture of CH_2Cl_2/ hexane solvent, filtered through Kim wipe and crystallized at -30°C in the glove box to obtain 53 mg (55 % yield). Spectral data for $Pt(SnMes_3)(SnBu^t_3)(CNBu^t)_2$, **2.10**: ^1H NMR (C_6D_6, rt, in ppm): δ = 0.80 (s, 18 H, 2 $CNBu^t$), δ = 1.61 (s, 27H, Bu^t_3Sn), δ = 2.16 (s, 9H, 3-*p*CH_3, Mes_3Sn), δ = 2.60 (s, 18H, 6-*o*CH_3,Mes_3Sn), δ = 6.78 (s, 6CH, Mes_3Sn). IR ν_{CN} (cm^{-1} in CH_2Cl_2): 2138(vs). Mass spectroscopy: EI/MS *m*/*z*. 1071 (M^+-Bu^t), 837 (M^+-Bu^t_3Sn).

Synthesis of $Pt(SnMes_3)_2(CNBu^t)_2$, 2.11: A 20 mg (0.049mmol) amount of $Pt(COD)_2$ was transferred into 50 mL schlenk tube and the flask was evacuated and refilled with argon several times . To this, 10 mL of distilled hexane was added under argon at -78°C. To this, a mixture of 46.4 mg of Mes_3SnH (0.097 mmol, 2equ) and 8.08 mg of Bu^tNC (0.097 mmol, 2equ) dissolved in 15 mL of distilled hexane solvent was added drop wise under argon while maintaining the reaction mixture at -78°C. The reaction mixture was stirred at -78°C for an additional 10 min, after which was slowly allowed to warm to the room temperature, during which time solution color changed to orange. Reaction mixture was stirred at RT for 1 hr. The solvent was removed *in vacuuo*, and the residue was dissolved in CH_2Cl_2 and plated on a TLC silica gel in hexane solvent and the top yellow colored product band was collected and crystallized in hexane solvent at -30°C to obtain 52 mg (80 % yield) of crystalline yellow colored product. Spectral data for $Pt(SnMes_3)_2(CNBu^t)_2$, **2.11**: ^1H NMR (C_6D_6, rt, in ppm): δ = 0.53 (s, 18 H, 2 $CNBu^t$), δ = 2.17 (s, 18H, 6-*p*CH_3,2Mes_3Sn), δ = 2.67 (s, 36H, 12-*o*CH_3, 2Mes_3Sn), δ = 6.82 (s, 12CH, 2Mes_3Sn). IR ν_{CN} (cm^{-1} in CH_2Cl_2): 2154(vs). Mass spectroscopy ES^+/MS

calculated for [M^+] =1313; found 1313. The isotope distribution is consistent with the presence of one Pt atom.

Synthesis of $Pt(SnBu^t_3)_2(CO)_2$, 2.12: A 53 mg (0.129 mmol) amount of $Pt(COD)_2$ was transferred into 10 ml schlenk tube and the flask was evacuated and refilled with argon several times. A 80 mg of Bu^t_3SnH (0.274 mmol) dissolved in 8 mL of distilled hexane solvent was added to $Pt(COD)_2$ under argon. The brown color reaction mixture was stirred at room temperature for 5 min after which time CO gas was bubbled through the solution for additional 30 min. The solution was filtered through silica plug to give a green color solution. The solvent was removed in vacuo to obtain 98 mg (91 % yield) of green solid. Spectral data for **2.12**: ^{1}H NMR ($CDCl_3$, rt, in ppm): δ = 1.38 (s, 54 H, $SnBu^t_3$, $^3J_{Sn\text{-}H}$ = 59 Hz. ^{1}H NMR (C_6D_6, rt, in ppm): δ = 1.44 (s, 54 H, $SnBu^t_3$, $^3J_{Sn\text{-}H}$ = 59 Hz IR ν_{CO} (cm^{-1} in hexane): 2007(vs). Elemental Anal, calc.: C, 37.57; H, 6.55 % Found: C, 37.77; H, 6.42 %.

Synthesis of $Pt(SnBu^t_3)_2(CNBu^t)_2(CO)$, 2.13: In a glove box, under an atmosphere of argon, a 40.0 mg (0.480 mmol) amount of $CNBu^t$ was added to 195 mg of $Pt(SnBu^t_3)_2(CO)_2$, **2.12** (0.235 mmol) dissolved in 2 mL of freshly distilled hexane at room temperature. With the addition of $CNBu^t$ the CO gas evolves from the reaction mixture (gas bubbles can be seen), and the green color solution slowly turns into colorless solution, and the colorless crystals crashes out of the solution. The solution is then placed in -20 °C freezer overnight to obtain more crystals. The solvent is removed and colorless crystals were washed with 0.2 ml of hexane to afford 219 mg (96 % yield). The crystals turn to violet color on prolonged exposure to air. Spectral data for **2.13**: ^{1}H NMR (C_6D_6, rt, in ppm): δ = 1.57 (s, 54 H, $SnBu^t_3$, $^3J_{Sn\text{-}H}$ = 51 Hz), 0.96 (s, 18H, Bu^t).

Note: NMR spectra recorded under a CO atmosphere. IR ν_{CO} (cm^{-1} in hexane): 2144(w), 2112 (vs), 1966 (s).

Conversion of $Pt(SnBu^t_3)_2(CNBu^t)_2(CO)$, 2.13 to $Pt(SnBu^t_3)_2(CNBu^t)_2$, 2.6 in solution: A 17.0 mg amount of **2.13** (0.0175 mmol) was dissolved in 10 mL of distilled hexane. With stirring, argon gas was then allowed to purge through the solution at 25 °C for approximately 10 min. Within minutes the colorless solution starts to turn violet. IR of the reaction mixture showed complete conversion of the starting **2.13** to **2.6.** The solvent was removed *in vacuuo*, and the purple color residue was crystallized by evaporation of a benzene/acetonitrile solvent mixture under a stream of argon gas at room temperature to yield 15.0 mg (91 %) of crystalline **2.6.**

Conversion of $Pt(SnBu^t_3)_2(CNBu^t)_2$, 2.6 to $Pt(SnBu^t_3)_2(CNBu^t)_2(CO)$, 2.13 in solution: A 17.0 mg amount of **2.6** (0.0181 mmol) was dissolved in 25 mL of distilled hexane. With stirring, CO gas was then allowed to purge through the solution at 25 °C for approximately 10 min. Within minutes the purple solution starts to turn colorless. IR of the reaction mixture showed complete conversion of the starting **2.6** to **2.13.** The solvent was removed *in vacuuo*, and the purple color residue was crystallized by evaporation of a benzene/acetonitrile solvent mixture under a stream of CO gas at room temperature to yield 15.0 mg (85 %) of crystalline **2.13.**

Conversion of $Pt(SnBu^t_3)_2(CNBu^t)_2$, 2.6 to $Pt(SnBu^t_3)_2(CNBu^t)_2(CO)$, 2.13 in the solid state: In a 10 mL schlenk tube containing 10.0 mg of purple crystalline **2.6**, CO gas was purged through the system for 1 hr in the dark at room temperature, at which time the color of the crystalline **2.13** turned to colorless. ^1H NMR indicated complete consumption of starting **2.6** in quantitative yield to $Pt(SnBu^t_3)_2(CNBu^t)_2(CO)$, **2.13**.

Conversion of $Pt(SnBu^t_3)_2(CNBu^t)_2(CO)$, 2.13 to $Pt(SnBu^t_3)_2(CNBu^t)_2$, 2.6 in solid state: In a 10 mL schlenk tube containing 10.0 mg of colorless crystalline **2.13**, argon gas was purged through the system for 16 hr in the dark at room temperature, at which time the color of the crystalline **2.13** turned to violet. ^1H NMR indicated complete consumption of starting **2.13** in quantitative yield to $Pt(SnBu^t_3)_2(CNBu^t)_2$, **2.6**.

2.5 Crystallographic analysis.

Colorless crystals of $Pt(SnBu^t_3)(COD)(H)$, **2.1** suitable for diffraction analysis were grown by slow evaporation of a solution of **2.1** in hexane solvent under a slow stream of argon gas at 0 °C (ice-water bath). Colorless crystals of $[Pt(SnBu^t_3)(\mu\text{-}SnBu^t_2)(H)_2]_2$, **2.3** suitable for diffraction analysis were grown by slow evaporation of a solution of **2.3** in hexane solvent under a slow stream of argon gas at 0 °C (ice-water bath). Light yellow color crystals of $[Pt(SnBu^t_3)(\mu\text{-}SnBu^t_2)(CO)(H)_2]_2$, **2.4** suitable for diffraction analysis were grown by slow evaporation of a solution of **2.4** in dichloromethane/hexane solvent mixture under a slow stream of CO gas at room temperature.

Colorless crystals of $Pt(SnBu^t_3)_2(CNBu^t)_2(H)_2$, **2.5** suitable for diffraction analysis were grown by slow evaporation of a solution of $Pt(SnBu^t_3)_2(CNBu^t)_2$, **2.6** in diethyl ether solvent under a slow stream of hydrogen gas at 0 °C (ice-water bath). Violet colored crystals of $Pt(SnBu^t_3)_2(CNBu^t)_2$, **2.6** suitable for diffraction analysis were grown by slow evaporation of solvent from a hexane solution at –20 °C in a glove box.

Colorless colored crystals of $Pt(SnPh_3)_3(CNBu^t)_2(H)$, **2.8,** suitable for diffraction analysis were grown by slow evaporation of a solution of **2.8** in a mixture of CH_2Cl_2/

hexane solvent at -30 °C in glove box. Yellow colored crystals of $Pt(Ph_3Sn)_2(CNBu^t)_2$, **2.9,** suitable for diffraction analysis were grown by slow evaporation of a solution of **2.9** in a mixture of CH_2Cl_2/ hexane solvent at -30 °C in glove box.

Orange colored crystals of $Pt(Mes_3Sn)(Bu^t_3Sn)(CNBu^t)_2$, **2.10,** suitable for diffraction analysis were grown by slow evaporation of a solution of **2.10** in a mixture of CH_2Cl_2/ hexane solvent at -30 °C in glove box. Yellow colored crystals of $Pt(Mes_3Sn)_2(CNBu^t)_2$, **2.11,** suitable for diffraction analysis were grown by slow evaporation of a solution of **2.11** in hexane solvent at -30 °C in glove box.

Green colored crystals of $Pt(SnBu^t_3)_2(CO)_2$, **2.12** suitable for diffraction analysis were grown by slow evaporation of solvent from a hexane solution in –80 °C freezer. Colorless crystals of $Pt(SnBu^t_3)_2(CNBu^t)_2(CO)$, **2.13** suitable for diffraction analysis were grown by slow evaporation of solvent from a hexane solution at –20 °C in a glove box.

The data crystal for $Pt(SnBu^t_3)(COD)(H)$, **2.1,** $[Pt(SnBu^t_3)(\mu\text{-}SnBu^t_2)(CO)(H)_2]_2$, **2.4**, $Pt(SnBu^t_3)_2(CNBu^t)_2(H)_2$,**2.5** and $Pt(SnBu^t_3)_2(CNBu^t)_2$, **2.6** was mounted onto the end of a thin glass fiber using Paratone-N.

The data crystal for $[Pt(SnBu^t_3)(\mu\text{-}SnBu^t_2)(H)_2]_2$, **2.3**, $Pt(SnPh_3)_3(CNBu^t)_2(H)$, **2.8,** $Pt(SnPh_3)_2(CNBu^t)_2$, **2.9** $Pt(Mes_3Sn)(Bu^t_3Sn)(CNBu^t)_2$, **2.10**, $Pt(Mes_3Sn)_2(CNBu^t)_2$, **2.11**, $Pt(SnBu^t_3)_2(CO)_2$, **2.12** and $Pt(SnBu^t_3)_2(CNBu^t)_2(CO)$, **2.13**, was glued onto the end of a thin glass fiber. X-ray intensity data were measured by using a Bruker SMART APEX2 CCD-based diffractometer using Mo Kα radiation (λ = 0.71073 Å).[99] The raw data frames were integrated with the SAINT+ program by using a narrow-frame integration algorithm.[99] Corrections for Lorentz and polarization effects were also applied with

SAINT+. An empirical absorption correction based on the multiple measurement of equivalent reflections was applied using the program SADABS. Both structures were solved by a combination of direct methods and difference Fourier syntheses, and refined by full-matrix least-squares on F^2, by using the SHELXTL software package.[100,101] Crystal data, data collection parameters, and results of the analyses are listed in Appendix A Tables A.1-A.4 in the supporting information.

Compound Pt(COD)($SnBu^t_3$)(H), **2.1** crystallized in the monoclinic crystal system. The systematic absences in the intensity data identified the unique space group $P2_1/n$. The hydride ligand was located from the difference map but refined on its positional parameters with a fixed isotropic thermal parameter.

Compound [Pt($SnBu^t_3$)(μ-$SnBu^t_2$)$(H)_2]_2$, **2.3** crystallized in the monoclinic crystal system. The systematic absences in the intensity data identified the unique space group $P2_1/n$. With Z = 4, there is half a formula equivalent of the molecule present in the asymmetric unit that has crystallographic center of inversion symmetry.

Compound [Pt($SnBu^t_3$)(μ-$SnBu^t_2$)(CO)$(H)_2]_2$, **2.4** crystallized in the triclinic crystal system. The space group $P\bar{1}$ was assumed and confirmed by the successful refinement and solution of the structure. The CO-Pt-Pt-CO core in the molecule is disordered over two orientations which were refined with fixed site-occupancy factors in the ratio 50/50. The two orientations are mirror images of each other and the CO-Pt-Pt-CO core as seen in Figure 1 are offset by an angle of 12.07°. Atoms Pt1 and Pt1* lie above and below the Sn1-Sn2-Sn1*-Sn2*plane at a distance of 0.4411(4) Å, while atoms Pt2 and Pt2* lie above and below the Sn1-Sn2-Sn1*-Sn2* plane at a distance of 1.0020(4) Å. The carbon atoms of the two Bu^t groups attached to atom Sn2 are also

disordered. The disorder components in the Bu^t groups were located from the difference map and refined with fixed site-occupancy factors in the ratio 50/50. The hydride ligand was not located and included in the refinement. There is still minor disorder present in the structure which was not accounted for due to satisfactory low R values (R1 = 3.91%) during the final stages of the refinement cycles.

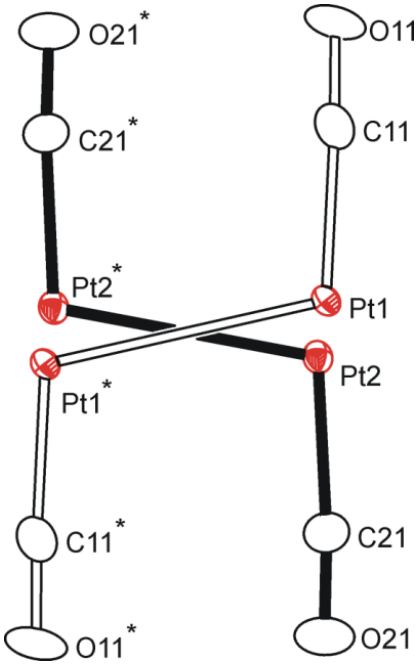

Figure 2.21. An ORTEP of the disordered CO-Pt-Pt-CO core in **2.4**.

Compound $Pt(SnBu^t_3)_2(CNBu^t)_2(H)_2$, **2.5** crystallized in the orthorhombic crystal system. The systematic absences in the intensity data were consistent with either of the space groups $Pmn2_1$ or *Pmmn*. The centrosymmetric space group *Pmmn* was assumed and confirmed by the successful solution and refinement of the structure. With Z = 2 there is half a formula equivalent of the molecule in the asymmetric crystal unit about a site of *mm*2 symmetry. Half a molecule of diethyl ether from the crystallization solvent,

co-crystallized with the complex on a crystallographic *mm*2 symmetry cite. The hydride ligand was located and refined with an isotropic thermal parameter. All non-hydrogen atoms were refined with anisotropic displacement parameters. Hydrogen atoms were placed in geometrically idealized positions and included as standard riding atoms during the least-squares refinements.

Compound $Pt(SnBu^t_3)_2(CNBu^t)_2$, **2.6** crystallized in the monoclinic crystal system. The space group $P2_1/n$ was confirmed on the basis of the systematic absences in the data. All non-hydrogen atoms were refined with anisotropic displacement parameters. Hydrogen atoms were placed in geometrically idealized positions and included as standard riding atoms during the least-squares refinements.

Compound $Pt(SnPh_3)_3(CNBu^t)_2(H)$, **2.8** crystallized in the orthorhombic crystal system. The space group $P2_12_12_1$ was confirmed on the basis of the systematic absences in the data for compound **12**. The hydride ligand was located and refined with geometric restraints.

Compound $Pt(SnPh_3)_2(CNBu^t)_2$, **2.9** crystallized in the Triclinic crystal system. The space group $P\ \bar{1}$ was assumed and confirmed by the successful refinement and solution of the structure. The molecule is crystallographically centrosymmetric. Two C atoms (C37 and C38) of one the phenyl rings are disordered. The disorder was modelled and refined in a 50:50 ratio.

Compound $Pt(SnMes_3)(SnBu^t_3)(CNBu^t)_2$, **2.10** crystallized in the monoclinic crystal system. The systematic absences in the intensity data were consistent with the space groups $P2_1/n$.

Compound $Pt(SnMes_3)_2(CNBu^t)_2$, **2.11** crystallized in the trigonal crystal system. The systematic absences in the intensity data were consistent with either of the space groups *P*3*c*1 or *P* $\bar{3}$c1. The latter space group was chosen and confirmed by the successful refinement and solution of the structure. Only half a molecule of the complex is present in the asymmetric crystal unit which lies about a 2-fold rotation site.

Compound $Pt(SnBu^t_3)_2(CO)_2$, **2.12** crystallized in the monoclinic crystal system. The systematic absences in the intensity data identified the unique space group *C*2/*c*. With Z = 4, there is half a formula equivalent of the molecule present in the asymmetric unit that has crystallographic center of inversion symmetry.

Compounds $Pt(SnBu^t_3)_2(CNBu^t)_2(CO)$, **2.13** crystallized in the orthorhombic crystal system. The systematic absences in the intensity data were consistent with either of the space groups $Pmn2_1$ or *Pmmn*. The centrosymmetric space group *Pmmn* was assumed and confirmed by the successful solution and refinement of the structure. With Z = 2 there is half a formula equivalent of the molecule in the asymmetric crystal unit about a site of *mm*2 symmetry.

Chapter 3: Pt-Sn-NHC Complexes in Activating Small Molecules: Synthesis, Structure and Reactivity.

3.1 Background.

Carbene is a molecule with two unshared valence electrons and N-Heterocyclic carbene (NHC) is a cyclic carbene with at least one α-amino substituent as shown in the Figure 3.1.

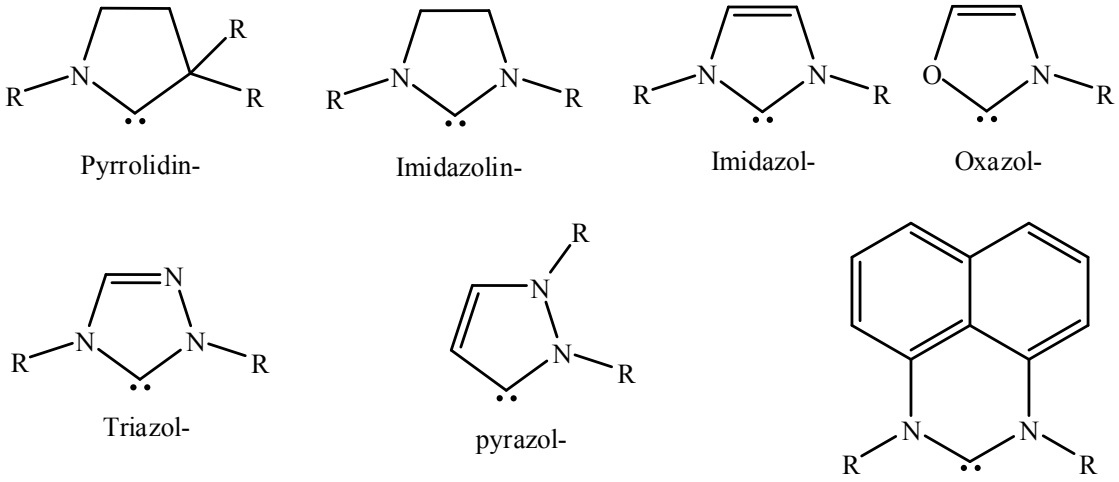

Figure 3.1. Structures of some of the highly encountered N-Heterocyclic Carbene subclasses. The Suffix "ylidene" should be added to obtain the generic name of each NHC subclass.[102]

Though Öfele[103] and Wanzlick[104] first reported the TM- NHC (TM = transition metal) complexes in 1968, followed by significant contributions from Lappert,[105] the chemistry of TM-NHC exploded only after the synthesis of first stable "bottle-able" carbene by Arduengo et al.,[106] in 1991. Since then a wide variety of TM-NHC complexes have been reported and studied as catalysts.[107–109] The Hermann group extensively researched on use of NHC ligands for synthesis of low coordinate transitional metal

complexes and also as potential substitute for electron rich organophosphanes.[110] The ever increasing applications of these NHCs as supporting ligands in catalysis is attributed to the strong σ-electron-donating properties,[30,111] which helps form a strong NHC-metal bond,[112,113] where a carbon atom with unshared electrons bonds to the metal atom, and thus prevents the decomposition of the metal complex - an essential property of a successful catalyst. As it can be seen in the Figure 3.1, NHCs are also flexible to varying bulkiness on the heteroatom (N) by modifying the 'R' group substituents. This is an added advantage for synthesizing highly unsaturated and reactive TM-NHC complexes.

These TM-NHC complexes have been successfully studied in catalytic activation of C-H bond and in formation of C-H, C-C, C-N, and C-O bonds. Palladium complexes of NHC ligand have been extensively studied in catalysis. In fact, the initial reports of catalytically active TM-NHC complexes involved Pd metal, in Heck coupling of aryl bromides and aryl halides,[114] followed by Suzuki and Sonogashira coupling reactions.[115,116] Grubbs[26,117,118] , Nolan[32,119–121] extensively studied the field of olefin metathesis using NHC substituted metal complexes, and Organ[122–124] also made significant contributions in cross coupling reactions using these Pd-NHC complexes. Later TM-NHC chemistry had been extended to other metals as well.[102]

The past decade has seen extensive research in the field of organic syntheses using these TM-NHC complexes. More recently focus is laid on the activation of small molecules using electronically unsaturated TM-NHC complexes (TM = Ir, Rh, Pd, Ni)[125–127] which is also our field of interest. Nolan group activated H_2 using the complex Pd(IPr)(PCy3), a 14 electron mononuclear Pd-NHC complex[128] and Hazari group activated the CO_2 using Ni-NHC complex.[129] The NHC complexes of Co, Rh, Ir, Pd, and

Au are all well studied, and their catalytic activity is known to be superior to corresponding phosphine complexes.[11,102,130–132] The Co-NHC complex reported by Llewellyn and coworkers not only activates both CO and H_2 it also gave promising results in the hydroformylation of 1-octene as shown in the Scheme 3.1.[133]

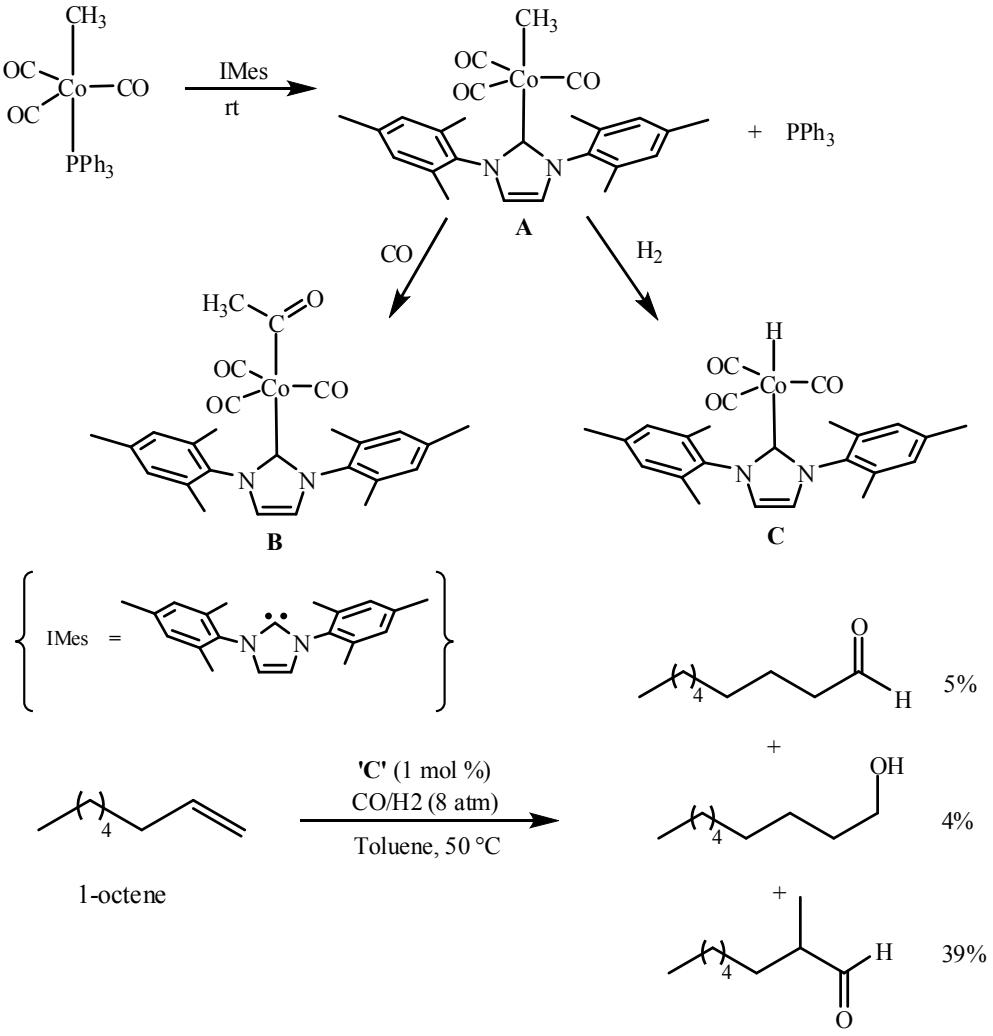

Scheme 3.1. Activation of CO and H_2 by Co-NHC complex, [Co(IMes)$(CO)_3$(Me)], **A** and hydroformylation of 1-octene by hydrido Co-NHC complex **'C'**.

A significant number of Pt-NHC complexes were synthesized and studied catalytically. Much emphasis was laid on mono nuclear Pt-NHC complexes which were shown as outstanding in the catalytic hydrosilylation of olefins with high selectivity and efficiencytic,[134] and also in reductive cyclization of diynes.[135]

Though mononuclear Pt-NHC complexes are studied well, much less work was done on Pt-NHC complexes coupled to a hetero metal, particularly group 14 metals. Only two Pt-Sn-NHC complexes with established crystal structure were reported in the literature.[135,136] It is worth to examining the effect of NHC ligands on the reactivity of Pt-Sn complexes in homogeneous catalysis. The bimetallic synergetic effect in Pt-Sn-NHC complexes has to be explored further to identify efficient homogeneous catalysts for hydroformylation and small molecule activation. The synthesis of bimetallic NHC carbene complexes will sure aid us in understanding the role of electronic and steric effects exerted by an additional metal on the Pt-NHC complexes.

In the previous chapter a series of sterically crowded unsaturated Pt-Sn bimetallic complexes in the activation of small molecules have been discussed. The driving force there is the unsaturation created by the bulky *tert*-butyl groups. As the literature suggests, these NHCs not only make a stable bond with the metals, but also aid in the synthesis of highly reactive unsaturated complexes which can be engineered to exclusively activate small molecules. This prompted us to synthesize Pt-Sn-NHC complexes to activate a variety of small molecules. In this chapter, a bulky two-electron donating N,N′-di-*tert*-butylimidazol-2-ylidene (IBu^t carbene) ligand has been used to study the effect of NHC on the reactivity of Pt-Sn complexes for potential catalytic application in the fields of small molecule activation, hydro-formylation and hydrogenation catalysis.

3.2. Results and discussion.

Reaction of compound (H)Pt(COD)($SnBu^t_3$), 2.1 with IBu^t carbene: In the previous chapter, synthesis of highly reactive unsaturated compound (H)Pt(COD)($SnBu^t_3$), **2.1** was discussed, which was shown to react readily by losing the four electron donating COD ligand. When a toluene solution of bulky NHC carbene ligand, N, N′-di-*tert*-butylimidazol-2-ylidene (IBu^t) was added at room temperature in a drybox to a hexane solution of Pt(COD)($SnBu^t_3$)(H), **2.1**, a red solid precipitate was observed at the bottom of the reaction flask. Precipitate was separated and washed with cold hexane to give Pt-Sn carbene complex, $[Pt(SnBu^t_3)(IBu^t)(H)]_2$, **3.1**, in 75% yield. This compound can also be prepared directly by reacting $Pt(COD)_2$, Bu^t_3SnH and IBu^t at room temperature. However, clean product and higher yield can be achieved when the reaction was performed at -78 °C. The possible pathway for the formation of compound **3.1** is shown in Scheme 3.2. The aim here was to synthesize the 14 electron Pt(II)-NHC complex Pt($SnBu^t_3$)(IBu^t)(H), **3.2**, by replacing the COD ligand in compound **2.1** with IBu^t carbene. But we were unable to isolate compound **3.2**, instead we ended up making dinuclear Pt complex **3.1**, which we believe is formed by the dimerization of complex **3.2** which is highly unsaturated and highly reactive. This work has been done in collaboration with Prof. Carl. D. Hoff at the University of Miami.

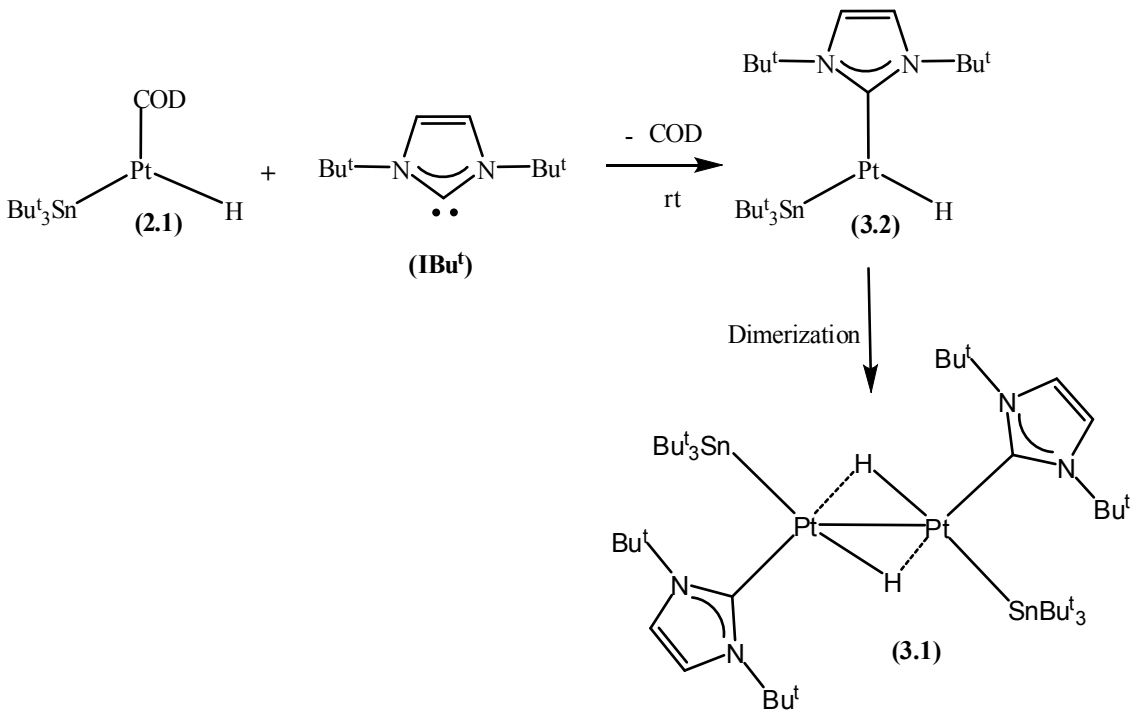

Scheme 3.2. Proposed pathway for the formation of compound **3.1.**

The complex $[Pt(SnBu^t_3)(IBu^t)(H)]_2$, **3.1**, is stable in air in the solid state, but decomposes slowly in solution state at room temperature on prolonged exposure to air. The molecular structure of **3.1** is shown in Figure 3.2 (further crystallographic data is provide in Appendix Table B.2). Compound **3.1** has two terminal $SnBu^t_3$ groups and two IBu^t groups positioned *trans* to each other. The Pt-Pt metal bond is bridged by two hydride ligands which are equivalent. Presence of both the hydride ligands was confirmed by ^1H NMR where they show up at -5.61 ppm (in THF-d_8) with appropriate one and two bond couplings to Pt ($^1J_{Pt\text{-}H}$ = 652 Hz, $^2J_{Pt\text{-}H}$ = 205 Hz), and two-bond coupling to Sn ($^2J_{Sn\text{-}H}$ = 55.0 Hz) (see Figure 3.5).

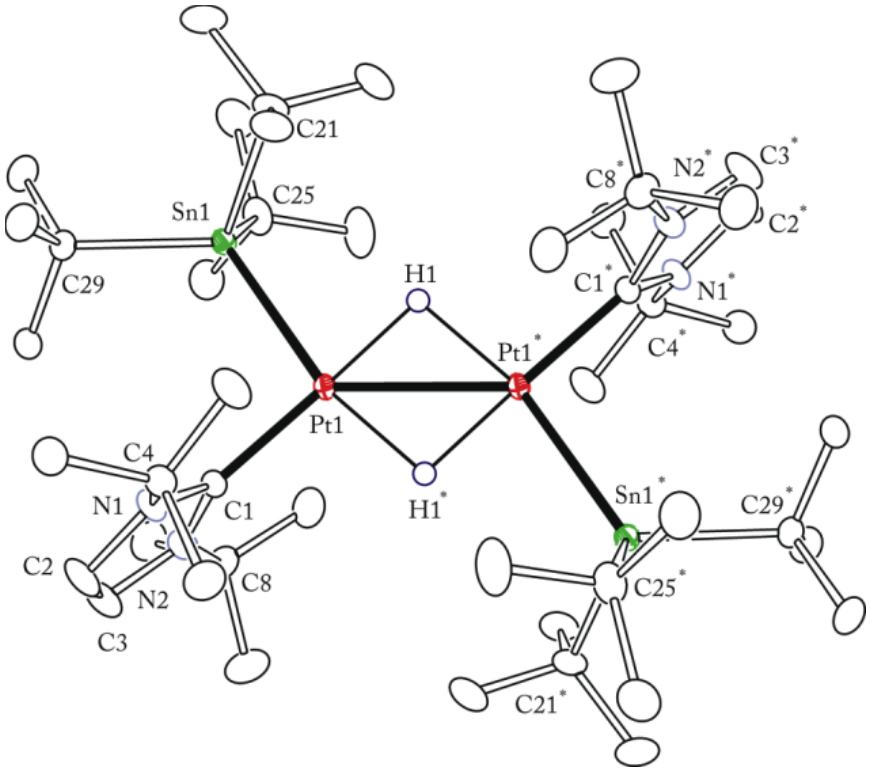

Figure 3.2. The molecular structure of $[Pt(SnBu^t_3)(IBu^t)(H)]_2$, **3.1**. Showing 30% probability thermal ellipsoids. Selected interatomic distances (Å) and angles (deg) are as follows: Pt(1)-Pt(1)* = 2.6715(1), Pt(1)-H(1) =1.75(3), Pt(1)-H(1)* = 1.87(3), Pt(1)-Sn(1)=2.5933(2), Pt(1)-C(1) =2.021(2). C(1)-Pt(1)-Sn(1)=97.61(6),C(1)-Pt(1)-H(1)*=96.5(8), C(1)-Pt(1)-H(1) =176.3(9), C(1)-Pt(1)-Pt(1)* =137.01(6), Sn(1)-Pt(1)-H(1)=81.4(9), Sn(1)-Pt(1)-H(1)*=165.5(8), Sn(1)-Pt(1)-Pt(1)*= 125.38, Pt(1)-H(1)-Pt(1)*= 95(1), H(1)-Pt(1)-H(1)*=85(1).

As is evident from the structure, the Pt1 –H1 and Pt1*- H1 bond lengths are not same (same applies to H1*) and one would expect two different sets of one bond coupled Pt satellites for the resonance at -5.61 ppm. But that was not the case as we see only one set of one bond coupled Pt satellites, indicating some sort of fluxional process between these two bonds, which also explains why the satellites are a bit broader. The Pt-Pt bond length in compound **3.1** is 2.6715 Å and is consistent with Pt-Pt single bond reported by Stone and co., for a similar complex $[Pt(\mu\text{-}H)(SiR_3)PR_3]_2$, with a Pt-Pt bond distance of 2.692 Å.[137]

Compound **3.1** is an unsaturated 28 electron dinuclear Pt complex. We performed Fenske-Hall molecular orbital calculations on compound **3.1** to obtain a clear picture of its unsaturation.[138,139] These molecular orbital calculations revealed the presence of a low lying unoccupied molecular orbital, LUMO, which could accommodate two valence bonding electrons to bring the electron count to 30, making the cluster saturated. The contours of the LUMO orbital, shown in Figure 3.3, are predominantly concentrated on the platinum atoms. Based on these observations, we believe that the addition or activation of small molecules will occurr at the Pt metal center. Experimental results also suggested the same, where the compound **3.1** reacts with small molecules by breaking the cluster into two monomers to accommodate the incoming molecule, indicating the high reactivity of the Pt-Pt metal bond.

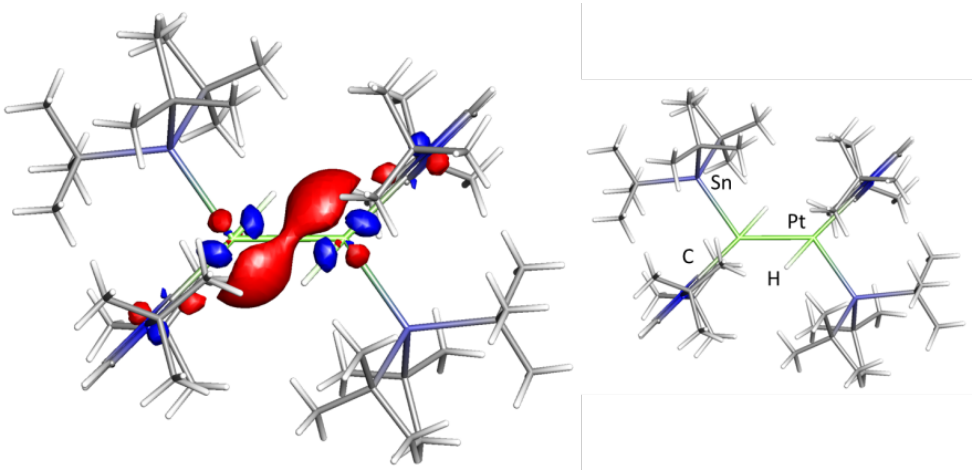

Figure 3.3. The LUMO orbital for $[Pt(SnBu^t_3)(IBu^t)(H)]_2$, **3.1**.

Reaction of complex $[Pt(SnBu^t_3)(IBu^t)(H)]_2$ 3.1, with CO: When compound **3.1** was exposed to CO atmosphere at room temperature, the orange-red colored solution of **3.1** in toluene solvent turned to light yellow instantaneously to yield mono nuclear Pt-NHC compound $Pt(SnBu^t_3)(IBut_2)(CO)(H)$, **3.3**, in a quantitative yield (90%) as shown in

equation 3.1. The molecular structure of **3.3** is shown in Figure 3.4 (further crystallographic data is provided in the Appendix Table B.2).It is evident from the structure that the Pt-Pt bond in the starting dinuclear complex breaks with the addition of CO to afford the mononuclear Pt(II)-carbonyl compound $Pt(SnBu^t_3)(IBut_2)(CO)(H)$, **3.3**, as shown in equation 3.1.

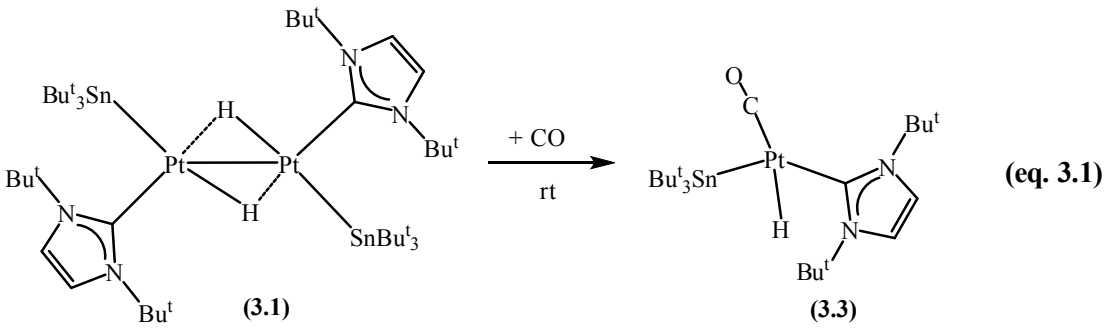

(eq. 3.1)

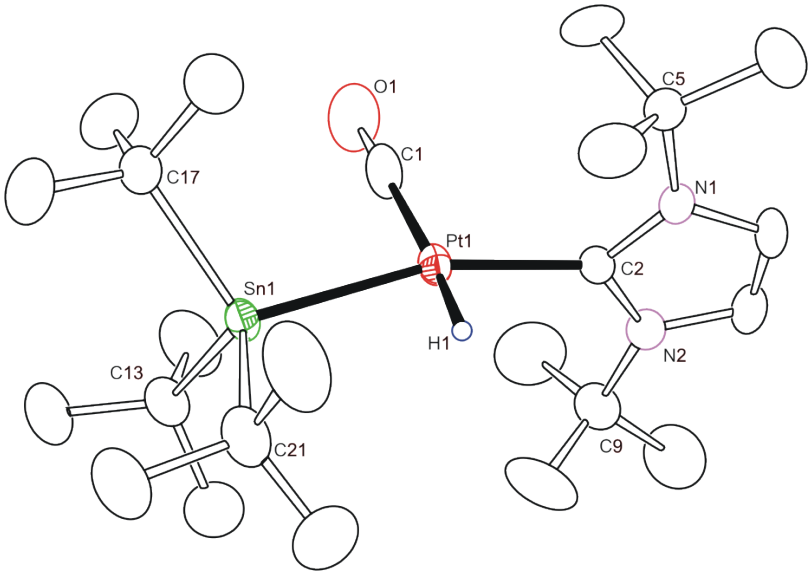

Figure 3.4. The molecular structure of $Pt(SnBu^t_3)(IBut_2)(CO)(H)$, **3.3**. Showing 50% probability thermal ellipsoids. Selected interatomic distances (Å) and angles (deg) are as follows: Sn(1)-Pt(1)=2.6112(3), H(1)-Pt(1)=1.37(6), C(1)-Pt(1)= 1.885(5), C(2)-Pt(1) = 2.091(4). Sn(1)-Pt(1)-C(2)= 160.0(1), Sn(1)-Pt(1)-H(1)= 78(3), Sn(1)-Pt(1)-C(1)= 94.8(2), C(1)-Pt(1)-H(1)= 170(3), C(1)-Pt(1)-C(2)= 105.1(2).

Compound **3.3** is characterized by the combination of ^{1}H NMR spectroscopy, single crystal X-ray diffraction technique, and IR spectroscopy. Compound **3.3** is a 16 electron mononuclear Pt (II) complex with the CO and hydride ligands positioned *trans* to each other. The position of the hydride ligand was determined and refined crystallographically, and its presence was further confirmed by ^{1}H NMR where its resonance shows up at -2.48 ppm with appropriate one bond coupling to Pt with $^{1}J_{Pt\text{-}H}$ = 891.8 Hz, and two bond coupling to Sn with $^{2}J_{Sn\text{-}H}$ = 18.4 Hz. The C(1)-Pt(1)-Sn(1) bond angle in compound **3.3** is 94.79^{o} and the C(1)-Pt(1)-C(2) bond angle is 105.06^{o}. As is evident from these bond angles, compound **3.3** is distorted from square planar geometry which can be attributed to the small unbalanced sterics of the hydride compared to the larger sterics of *trans* CO ligand with bulky Bu^{t} groups.

Compound **3.3** is stable at room temperature in the solid state, and can be handled in air. Addition of CO to compound **3.1** is irreversible. The IR spectrum of **3.3** in hexane solution shows a medium intensity peak at 2104 cm^{-1} for $\upsilon_{Pt\text{-}H}$ stretching frequency and a very strong peak for the Pt-bound carbonyl group at 1979 cm^{-1}. Pt complexes with terminal hydride ligands are known to have a $\upsilon_{Pt\text{-}H}$ stretching frequency in the range of 2050-2120 cm^{-1}.[140,141]

Reversible activation of H_2 by complex 3.1 to form Pt- tri hydride complex: When H_2 gas is purged through the solution of compound **3.1** (3.1 is highly soluble in THF and CH_2Cl_2, moderately soluble in benzene, toluene and insoluble in hexane), a slight change in color of the solution was observed (from red to red orange). Attempts to isolate and crystallize the product were unsuccessful as we were able to isolate only the starting complex **3.1**, indicating the high instability of the product.

Reaction was also monitored by ^{1}H NMR. After purging H_2 gas through the anhydrous THF-d_8 solution of complex **3.1** in a sealed NMR tube followed by vigorous shaking for 5 minutes, ^{1}H NMR was recorded. Which indicated the disappearance of the hydride resonance peaks corresponding to complex **3.1**, and appearance of a new hydride resonances showing one-bond coupling to Pt and two-bond coupling to Sn (see Figure 3.5). Appropriate integration of the proton peaks, lead us to postulate the structure $Pt(SnBu^t_3)(IBu^t_2)(H)_3$, **3.4**, as shown in the equation 3.2.

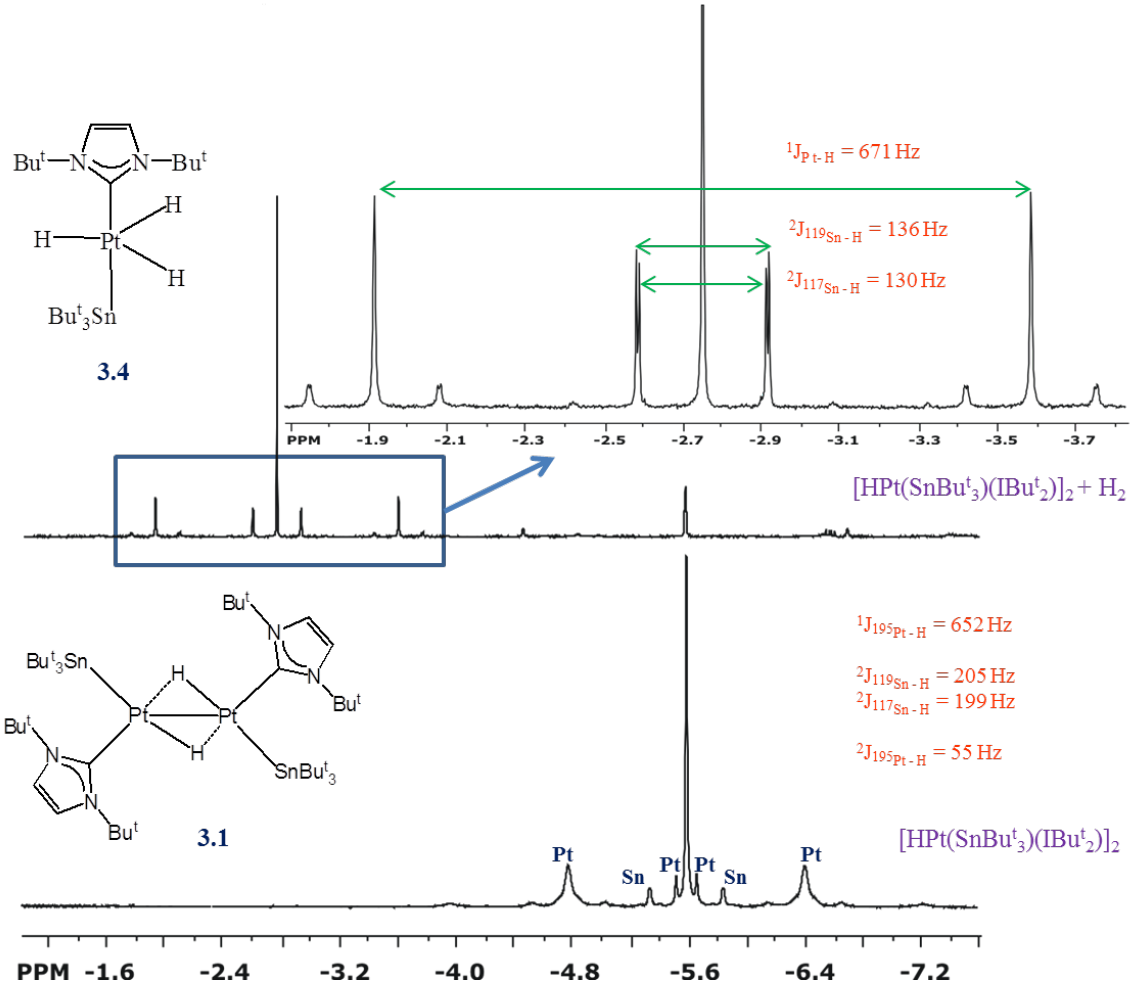

Figure 3.5. ^{1}H NMR spectrum showing the hydride region of compounds **3.1**and **3.3** in THF-d_8.

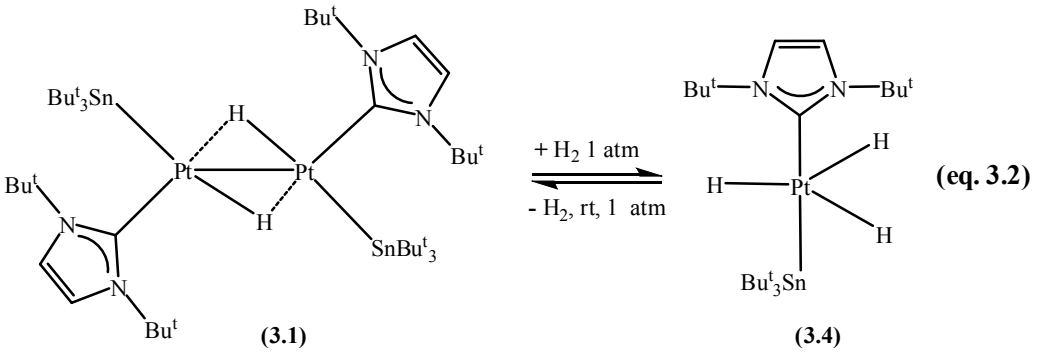

(3.1) **(3.4)** **(eq. 3.2)**

It is evident from Figure 3.5 that both the hydrides of the compound $[Pt(SnBu^t_3)(IBu^t_2)(H)]_2$, **3.1** show up at -5.59ppm with a set of one bond coupled ^{195}Pt satellites ($^1J^{195}_{Pt-H}$ = 652 Hz), one set each of two bond coupled ^{119}Sn and ^{117}Sn satellites ($^2J^{119}_{Sn-H}$ = 205 Hz, $^2J^{117}_{Sn-H}$ = 199 Hz) and one set of two bond coupled ^{195}Pt satellites ($^2J^{195}_{Pt-H}$ = 55 Hz) (at the base of the hydride) consistent with the structure **3.1**. But when H_2 gas is purged through the solution of compound **3.1,** a shift in the hydride resonances was observed. The new resonances now show up at -2.75 ppm with one set of one bond coupled ^{195}Pt satellites ($^1J^{195}_{Pt-H}$ = 671 Hz), one set each of two bond coupled ^{119}Sn and ^{117}Sn satellites ($^2J^{119}_{Sn-H}$ = 136 Hz, $^2J^{117}_{Sn-H}$ = 130 Hz). Interestingly, now the two bond coupled ^{195}Pt satellites are missing, indicating that the structure could be a mononuclear Pt complex, as was expected.

To further confirm the nuclearity and the number of hydrides on the Pt metal center, ^{195}Pt NMR and ^{119}Sn NMR experiments haves been carried out on the reaction mixture of $[Pt(SnBu^t_3)(IBu^t_2)(H)]_2 + H_2$ (see Figure 3.6).

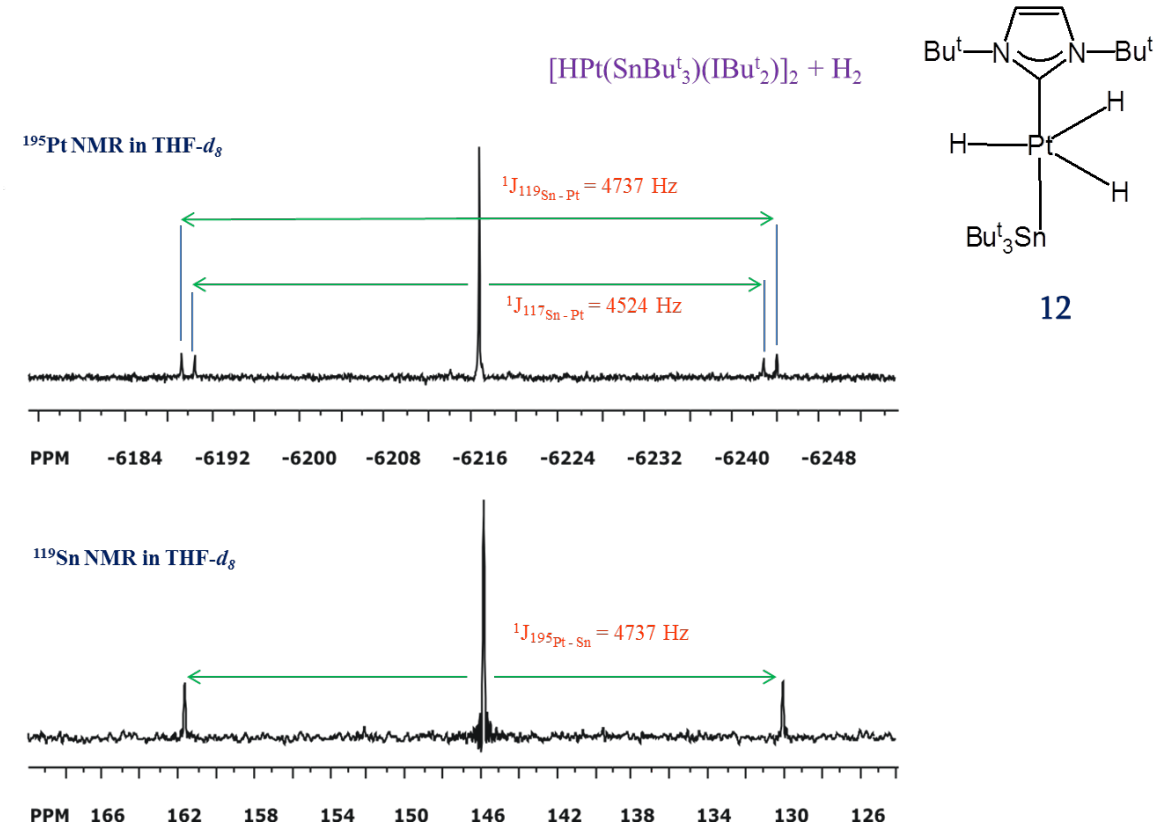

Figure 3.6. Overlay of ^{195}Pt and ^{119}Sn NMR spectra of [Pt(SnBu$^t_3$)(IBu$^t_2$)(H)]$_2$ + H$_2$ in THF-d_8.

The proton decoupled ^{195}Pt NMR showed one peak corresponding to ^{195}Pt at -6216.70 ppm with both one bond coupled ^{119}Sn and ^{117}Sn satellites ($^1J^{119}_{Sn-Pt}$ = 4737 Hz, $^2J^{117}_{Sn-Pt}$ = 4524 Hz). Similarly, the proton decoupled ^{119}Sn NMR showed one peak corresponding to ^{119}Sn at 145.84 ppm with one bond coupled ^{195}Pt satellites ($^1J^{195}_{Pt-Sn}$ = 4737 Hz). The second order or other multi order couplings are not observed, consistent with the presence of one Pt and one Sn in the new product.

As predicted, the proton coupled spectra of ^{195}Pt NMR showed a quartet for the Pt resonance at -6216.70 ppm with $^1J_{H-}{}^{195}_{Pt}$ = 671 Hz, (see Figure 3.7, tin satellites are shown as Sn) exactly matching the one bond coupled ^{195}Pt *J* value from ^{1}H NMR, see Figure 3.5. This indicates that we are looking at the same proton-Pt couple in both ^{1}H and

^{195}Pt NMR spectra. However, the proton coupled ^{119}Sn NMR did not show any distinct resonances due to two bond coupling to proton as the resonances, due to the fact that one bond coupling to ^{13}C were prominent and broad (in $SnBu^t_3$, Sn is one bond coupled to three 'C' atoms of three Bu^t groups).

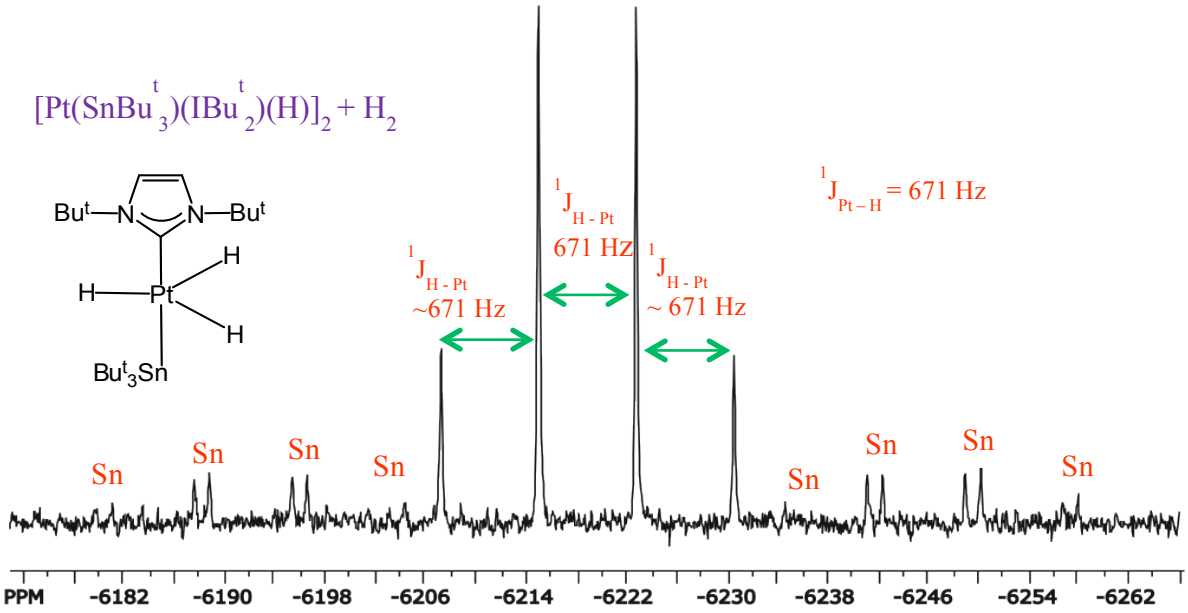

Figure 3.7. Proton coupled ^{195}Pt NMR spectra of [Pt(SnBu$^t_3$)(IBu$^t_2$)(H)]$_2$ + H_2 in THF-d_8.

Similar to addition of CO to compound **3.1**, addition of H_2 also proceeds through the breaking of Pt-Pt bond in dinuclear Pt(II)-NHC complex **3.1** to afford the proposed mononuclear complex Pt(SnBu$^t_3$)(IBu$^t_2$)(H)$_3$, **3.4.** Apart from the NMR data which was consistent with the structure **3.4,** and visual color change upon purging H_2 gas through the solution of complex **3.1**, we don't have any other experimental evidence to prove the existence of structure **3.4** in solution, as isolation of products from the reaction mixture of compound **3.1** + **H_2** is extremely sensitive to moisture, temperature, air and also to H_2 atmosphere. Upon removal of H_2 atmosphere we observed regeneration of compound **3.1** in solution as shown in equation 3.2, and the reaction mixture showed a large number of

unidentified hydride peaks when either wet solvents or oxygenated solvents were used. To our knowledge, Pt-carbene complexes with three hydrides are unknown; no precedent examples exist for comparison. However, Pt-NHC complexes with dihydrides are known. Recently, Nolan et al. prepared an analogous 14 electron Pd(0) dihydride complex $Pd(Ipr)(H)_2(PCy_3)$ with IPr NHC ligand.[128] Crabtree et al. also reported a similar dihydride Ir-NHC carbene complex.[142] We were unable to isolate and characterize the compound **3.4** crystallographically, but it's presence has been proved in the solution through combination of ^{195}Pt, ^{119}Sn and ^{1}H NMR.

Activation of ethylene by Pt-Sn NHC complex 3.1: In a similar fashion to the addition of CO to compound **3.1**, ethylene addition also yields a mononuclear Pt-carbene complex. Ethylene is bound to Pt metal center in an η^2 mode through C=C π-bond to yield a 16 electron Pt-NHC-ethylene complex, $Pt(SnBu^t_3)(IBu^t)(C_2H_4)(H)$, **3.5**. The addition of ethylene to **3.1** is also reversible both in the solid state and in solution state at room temperature. Replacing the ethylene atmosphere with argon gas or by applying vacuum, compound **3.5** regenerates compound **3.1**. Crystals suitable for X-ray diffraction were also grown under ethylene atmosphere. Compound **3.5** was characterized by the combination of ^{1}H NMR and single crystal X-ray diffraction techniques. The molecular structure of compound **3.5** is shown in Figure 3.8 (further crystallographic data is given in the Appendix B Table B.2).

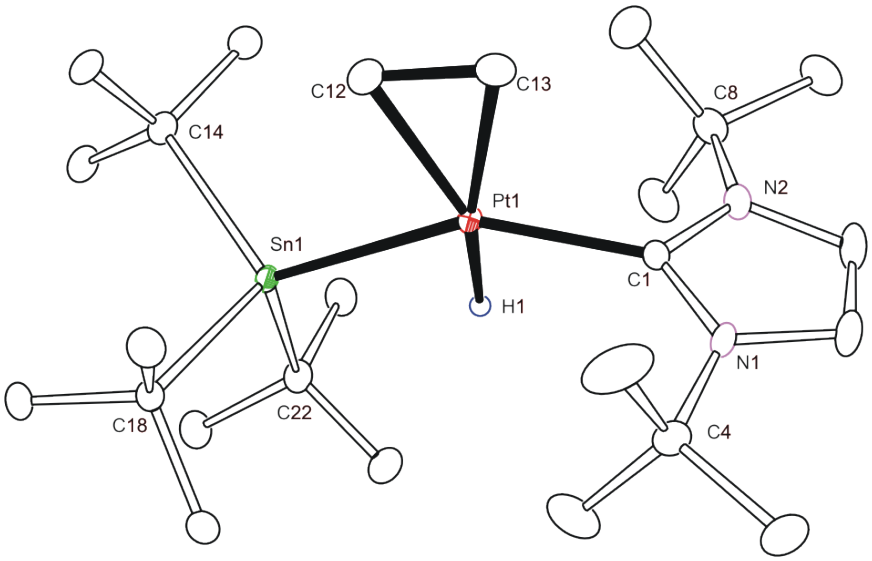

Figure 3.8. Molecular structure of $Pt(SnBu^t_3)(IBu^t)(C_2H_4)(H)$, **3.5**. Showing 30% probability thermal ellipsoids. Selected interatomic distances (Å) and angles (deg) are as follows: Pt(1)-Sn(1) = 2.6293(4), Pt(1)-H(1) = 1.60(5), Pt(1)-C(1)=2.078(4), Pt(1)-C(12)=2.163(6), Pt(1)-C(12)=2.161(6), C(13)-C(12)= 1.410(8). C(1)-Pt(1)-Sn(1) =146.6(2), C(1)-Pt(1)-H(1) = 81(2), Sn(1)-Pt(1)-H(1) = 67(2).

Interestingly, the position of ethylene in **3.5,** is similar to that of CO in **3.3,** both are added in the *trans* position to the hydride ligand. The position of the hydride ligand in **3.5** was determined and refined crystallographically using the data collected at 100 K. The presence of the hydride ligand was also confirmed by ^{1}H NMR spectroscopy, where the proton resonance of the hydride ligand appears at -3.57 ppm with appropriate one bond coupling to Pt (s, $^1J_{Pt\text{-}H}$ = 891.8 Hz) and two-bond coupling to Sn ($^2J_{Sn\text{-}H}$ = 18.4 Hz). The C12-C13(ethylene) bond distance in compound **3.5** is 1.410 Å (in free ethylene it is 1.339 Å), which is close to the reported C=C bond distance of 1.434 Å in a similar ethylene-bound mononuclear Pt-complex $Pt(PPh_3)_2(C_2H_4)$.[143]

Attempted catalytic hydroformylation of ethylene with compound 3.1: As shown above, we have successfully activated CO, H_2, and ethylene using compound **3.1** which is

an essential requirement of a hydroformylation catalyst in homogeneous catalysis. This led us to attempt the hydroformylation of ethylene using compound **3.1.** We carried out this experiment in a small Parr-reactor. Initially, reactor was loaded with toluene solution of compound **3.1**. Then, the reactor was pressurized with ethylene gas to yield compound **3.5**. Then an equimolar mixture of H_2 and CO gas (1:1 ratio) was introduced at room temperature and the reactor was sealed. Reactions were carried out from a total pressure of 75 psi to 150 psi with varying amounts of ethylene and H_2+CO mixture. The progresses of the reactions were monitored by ^{1}H NMR spectroscopy. After 24 hours we observed the disappearance of peaks corresponding to ethylene compound **3.5** and complete conversion of compound **3.5** into Pt-carbonyl compound **3.3**. Unfortunately, we were unable to identify peaks corresponding to any products resulting from hydroformylation in the ^{1}H NMR spectra of the reaction mixture. Even at the refluxing temperatures of toluene we have not observed any products of hydroformylation. Probably varying experimental conditions or modification of substituents on the nitrogen atom of the NHC ligand may promote hydroformylation of olefins. Further studies on hydroformylation of other alkenes in the presence of compound **3.1** are underway.

3.3. Summary and conclusions.

Reaction of IBu^t carbene with compound Pt(COD)(SnBu$^t_3$)(H), **2.1**, gave a stable but highly reactive dinuclear Pt compound [Pt(SnBu$^t_3$)(IBu^t)(H)]$_2$, **3.1**,. Efforts to synthesize the proposed intermediate Pt(SnBu$^t_3$)(IBu^t)(H), **3.2** were unsuccessful with IBu^t carbene. Probably it is possible with more sterically demanding carbenes. Compound **3.1** successfully activated CO, ethylene and H_2 molecules at room temperature. The reactions with ethylene and H_2 are reversible. However, the reaction of

compound **3.1** with H_2 is highly sensitive to air, moisture, and temperature, and we could not isolate the proposed trihydride-Pt product **3.4**. Its presence in solution has been proven by NMR spectroscopy. Summary of the complexes is given in Scheme 3.3.

Compound **3.1** has all the required properties of a hydroformylation catalyst as it successfully activated CO, C_2H_4 (alkene), and H_2; but the efforts to hydroformylate C_2H_4 were unsuccessful, indicating the need to alter the reaction conditions. It might also work on a different alkene. More research has been planned along these lines. Efforts to activate other small molecules such as N_2 and CO_2 were unsuccessful and further research is required in synthesizing the Pt-NHC complexes that can activate these molecules.

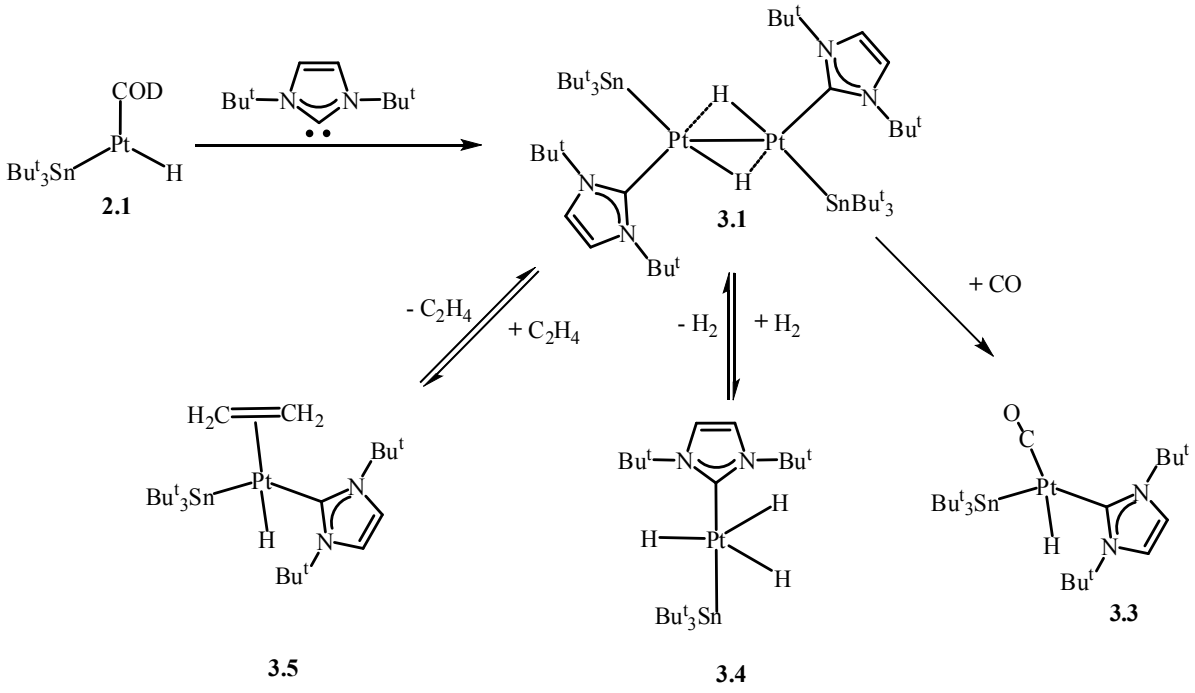

Scheme 3.3. Summary of NHC complexes synthesized**.**

3.4. Experimental section.

General Data: Unless otherwise indicated, all reactions were performed under an atmosphere of Argon. Reagent grade solvents were dried by standard procedures and were freshly distilled prior to use. Infrared spectra were recorded on a Nicolet 380 FT-IR spectrophotometer. ^{1}H NMR were recorded on Bruker 300 and 400 spectrometer operating at 300.13 MHz and 399.99 MHz respectively. Elemental analyses were performed by Columbia Analytical Services (Tuscon, AZ). Mass spectrometric measurements performed by a direct–exposure probe using electron impact ionization (EI) were made on a VG 70S instrument at the University of South Carolina, Columbia, SC. The NHC carbenes IBu^{t} and IPr were purchased from Strem chemicals and used without further purification. Ethylene, CO, and CO_2, H_2 gases of 99.9% purity were purchased from Air gas south and used without further purification. Tertiary butylisocyanide, $CNBu^{t}$, was purchased from Sigma-Aldrich and used without further purification. Bis(1,5-cyclooctadiene)platinum, $Pt(COD)_2$,[97] and tri-*tert*-butylstannane ($Bu^{t}_{3}SnH$),[44] were prepared according to the published procedures. Silica gel (60-200 μm, 70-230 mesh) used for chromatographic separations was purchased from Silicycle.

Synthesis of $[Pt(SnBu^{t}_{3})(IBu^{t})(H)]_2$, 3.1: In a glove box, under an atmosphere of argon, 30.0 mg of $Bu^{t}_{3}SnH$ (0.103 mmol) dissolved in 3mL of freshly distilled hexane was added to 40.0 mg of $Pt(COD)_2$ (0.097 mmol). The reaction mixture immediately turned dark brown. The reaction mixture was stirred at room temperature for an additional 10 minutes then 17.0 mg of IBu^{t} dissolved in 0.5 ml of toluene solution was added to dark brown reaction mixture. The reaction mixture immediately turned red. The reaction was stirred for 30 minutes, after which solvent was reduced to *c.a.* 1 mL. The solid was

filtered and washed with 3x 3.0 mL of pentane to yield 48 mg (yield 75%) of cherry red powder. Spectral data for **3.1**: ^{1}H NMR (THF-d_8, rt, in ppm): δ = 7.33 (s, 4H; imid), 2.03 (s, 36H; $C(CH_3)_3$), 1.09 (s, 54H; $^{2}J_{Sn-H}$ = 49.3 Hz, $C(CH_3)_3$); -5.61 (s, $^{1}J_{Pt-H}$ = 652 Hz, $^{2}J^{119}_{Sn-H}$ = 205 Hz, $^{2}J^{117}_{Sn-H}$ = 119 Hz, $^{2}J_{Pt-H}$ = 55.0 Hz, 2H, hydride). ^{1}H NMR (C_6D_6, rt, in ppm): δ = 6.60 (s, 4H; imid), 1.94 (s, 36H; $C(CH_3)_3$), 1.42 (s, 54H; $^{2}J_{Sn-H}$ = 49.3 Hz, $C(CH_3)_3$); -5.61 (s, $^{1}J_{Pt-H}$ = 652 Hz, $^{2}J_{Sn-H}$ = 205 Hz, $^{2}J_{Pt-H}$ = 55.0 Hz, 2H, hydride). ^{195}Pt NMR (THF-d_8, rt, in ppm): δ = -3789.16 (s, proton decoupler on), proton decoupler off, δ = -3789 [triplet (1:2:1), $^{1}J_{Pt-Pt}$ = 650.84 Hz]. ^{119}Sn NMR Spectral data for **3.1:** (THF-C_6D_6, rt, in ppm): -17.85 (s, $^{1}J^{195}_{Pt-Sn}$ = 12815 Hz, $^{2}J^{195}_{Pt-Sn}$ = 5714 Hz). Elemental analysis, Calc: C, 41.45; H, 7.26; N, 4.20 %, Found: C, 41.47; H, 7.41; N, 4.09 %.

Synthesis of Pt($SnBu^{t}_3$)(IBu^{t})(CO)(H), 3.3: A 25 mL schlenk tube was charged with 30 mg of **3.1** (0.023 mmol) which was subsequently dissolved in 4.0 mL of toluene. The red solution was under an atmosphere of *c.a.* 10 psi CO and shaken vigorously. The resultant solution turned light orange immediately. The solvent was removed under reduced pressure. The solid was then washed with 3x 0.25 mL heptane and yielded 28.6 mg (90% yield) of a khaki-colored powder. Spectral data for **3.3**: ^{1}H NMR (C_6D_6, rt, in ppm): δ = 6.60 (s, $^{4}J_{Pt-H}$ = 8.8 Hz, 2H; imid), 1.67 (s, 27 H, $SnBu^{t}_3$, $^{3}J_{Sn-H}$ = 51.8 Hz), 1.37 (s, 18 H, $C(CH_3)_3$); -2.48 (s, $^{1}J_{Pt-H}$ = 891.8 Hz, $^{2}J_{Sn-H}$ = 18.4 Hz, 1H, hydride). IR ν_{CO} (cm^{-1} in hexane): 1979(vs), 2104(m).

Reaction of 3.1 with H_2 gas, compound 3.4: ^{1}H NMR; A 5 mL NMR tube was charged with 10.0 mg of **3.1** which was subsequently dissolved in 0.5 mL of toluene-d_8. The NMR tube was sealed under argon, and the red solution was exposed to an atmosphere of *c.a.* 1 atm H_2 and shaken vigorously. The resultant solution turned light orange

immediately to yield mononuclear Pt-Sn carbene complex with the three hydride ligands. Spectral data for **3.4**: ^{1}H NMR (C_6D_6, rt, in ppm): δ = 6.60 (s, $^{4}J_{Pt-H}$ = 8.8 Hz, 2H; imid), 1.56 (s, 27 H, $SnBu^{t}_{3}$, $^{3}J_{Sn-H}$ = 62.1 Hz), 1.41 (s, 18 H, $C(CH_3)_3$); -4.36 (s, $^{1}J_{Pt-H}$ = 726.5 Hz, $^{2}J_{Sn-H}$ = 127.5 Hz, 3H, hydride). ^{1}H NMR (THF- d_8, rt, in ppm): δ = -2.75 (s, $^{1}J_{Pt-H}$ = 671 Hz, 3H, hydride, $^{1}J^{119}_{Sn-H}$ = 136 Hz, $^{1}J^{117}_{Sn-H}$ = 130 Hz),

^{195}Pt NMR: A 5 mL NMR tube was charged with 40 mg of **3.1** which was subsequently dissolved in 0.5 mL of THF-d_8. The NMR tube was sealed under argon, and the red solution was exposed to an atmosphere of *c.a.* 1 atm H_2 and shaken vigorously. The resultant solution turned light orange immediately to yield mononuclear Pt-Sn carbene complex with the three hydride ligands. ^{195}Pt NMR spectral data for **3.4:** (THF-d_8, rt, in ppm): -6216.70 (s, decoupler on, $^{1}J^{119}_{Sn-Pt}$ = 4736 Hz, $^{1}J^{117}_{Sn-Pt}$ = 4524 Hz), decoupler off, quartet (1:3:3:1), -6216.70 ($^{1}J_{Pt-Pt}$ = 667 Hz). **^{119}Sn NMR:** (THF-d_8, rt, in ppm): 145.83 (s, $^{1}J^{195}_{Pt-Sn}$ = 4737 Hz).

Synthesis of $Pt(SnBu^{t}_{3})(IBu^{t})(C_2H_4)(H)$, **3.5**: A 25 mL schlenk tube was charged with 30.0 mg (0.023 mmol) of **3.1** which was subsequently dissolved in 4.0 mL of toluene. The red solution was under an atmosphere of *c.a.* 10 psi ethylene and shaken vigorously. The resultant solution turned light yellow immediately. The solvent was removed under slow flow of ethylene gas to yield 26.6 mg (85% yield) of a light yellow-colored powder. Spectral data for **3.5**: ^{1}H NMR (toluene-d_8, rt, in ppm): δ = 6.60 (s, $^{4}J_{Pt-H}$ = 8.8 Hz, 2H; imid), 2.45 (s, 4H, ethylene), 1.88 (s, 27 H, $SnBu^{t}_{3}$, $^{3}J_{Sn-H}$ = 51.8 Hz), 1.63 (s, 18 H, $C(CH_3)_3$); -3.57 (s, $^{1}J_{Pt-H}$ = 891.8 Hz, $^{2}J_{Sn-H}$ = 18.4 Hz, 1H, hydride).

Reaction of 3.1 with a mixture of H_2 and CO (1:1 mole ratio): In a typical reaction, a 3 mg of compound **3.1**, 1 mL of anhydrous toluene or toluene-d_8 and a magnetic stir bar

were sealed in a Parr reactor under ethylene atmosphere of 25psi. The Parr reactor was pressurized with 25 psi of H_2 and 25 psi of CO gas at room temperature. The reaction was monitored by ^{1}H NMR at different time intervals. Every time experiment was setup with fresh sample and fresh gases. The reaction was monitored at room temperature and at refluxing temperature of toluene from 75psi to 150psi pressures. After 24 hours the ^{1}H NMR of reaction mixture showed peaks corresponding to compound **3.3** and free ethylene. No peaks were observed corresponding to acetaldehyde. The Parr reactor was then placed in an oil bath with a stir bar that was pre-heated to 120 ºC. The reaction was monitored by ^{1}H NMR at different time intervals. After two days, the ^{1}H NMR of reaction mixture showed peaks corresponding to compound **3.3** and free ethylene. There was no product observed resulting from hydroformylation of ethylene.

3.5. Crystallographic analyses.

Red-colored crystals of **3.1** suitable for diffraction were grown by slow evaporation of toluene solution at room temperature in a glove box. Yellow crystals of **3.3** were grown by evaporation of hexane solution of **3.1** at 0 °C under the slow stream of the CO gas. Light yellow crystals of **3.5** of suitable quality for diffraction were grown by slow evaporation of hexane solution under a stream of ethylene gas in an ice bath (0 °C). Orange-colored crystals of **3.6** were grown by evaporation of hexane solution in glove box at room temperature.

Each data crystal was mounted onto the end of a thin glass fiber using Paratone-N. X-ray intensity data were measured by using a Bruker SMART APEX2 CCD-based diffractometer using Mo Kα radiation (λ = 0.71073 Å).[99] The raw data frames were

integrated with the SAINT+ program by using a narrow-frame integration algorithm.[99] Corrections for Lorentz and polarization effects were also applied with SAINT+. An empirical absorption correction based on the multiple measurement of equivalent reflections was applied using the program SADABS. Both structures were solved by a combination of direct methods and difference Fourier syntheses, and refined by full-matrix least-squares on F^2, by using the SHELXTL software package.[101] Crystal data, data collection parameters, and results of the analyses are listed in Tables B.2- B.4 in Appendix B.

The compound **3.1** crystallized in triclinic system. The space group $P\ \bar{1}$ was assumed and confirmed by the successful refinement and solution of the structure. The hydride ligand was located from the difference map but refined on its positional parameters with a fixed isotropic thermal parameter. Compound **3.3** crystallized in monoclinic system. The space group *P21/c* was confirmed on the basis of the systematic absences in the data. With Z= 8, there were two molecules in the structure and the hydride ligand was located from the difference map but refined on its positional parameters with a fixed isotropic thermal parameter.

Compound **3.5** crystallized in triclinic system. The space group $P\ \bar{1}$ was confirmed on the basis of the systematic absences in the data. The ether solvent molecule co-crystallized with the compound **3.5**. The hydride ligand was located from the difference map but refined on its positional parameters with a fixed isotropic thermal parameter.

Chapter 4. Photo Sensitive Radical Generating Ni-Sn Complexes: Synthesis, Structure and Reactivity.

4.1. Background.

The complexes of precious transition metals such of platinum group metals (PGM) are used as catalysts for a wide variety of industrial processes, such as in hydrogenation reactions.[144] Though platinum is one of the highly used metals in various catalytic processes, it is one of the rarest metals available in the earth's crust and highly expensive. There is a need for cost effective alternatives to make an industrial process sustainable amid frequent financial meltdowns. This can be achieved by replacing expensive methods with economical ones, and this represents the incredible opportunity to develop processes which involve non-precious metals. It is where the inexpensive organometallic complexes of Ni fit aptly with the catalytic applications competitive to those of PGM.

Nickel is one of the most highly abundant transition metals in the earth's crust, and it is also an inexpensive (at present, Ni is 2555 times cheaper than Pt) metal compared to platinum. Nickel is used as hydrogenation catalyst in many important industrial reactions.[145,146] It also plays an important role biologically.[147]

The organometallic chemistry of Ni had been started in 1890 with the dramatic discovery of $Ni(CO)_4$ by Mond, Langer, and Quincke.[7] This had been later employed in industry to purify Ni metal, called *Mond's process*.[8] It is the first carbonyl of a zerovalent metal to be made. Nickel also forms zero-valent and stable complexes with other strong π- acceptors such as isocyanides and carbenes.[148,149] This had led to use these complexes as catalysts in organic synthesis as carbonylation[150] (see Scheme 4.1), hydrocyanation[33] and hydrosilylation[151] reagents. Nickel also has a strong tendency to from complexes

with alkenes and alkynes, and this leads to the development of catalytically active Ni complexes that can perform oligomerization of alkenes,[152] hydrogenation of alkenes,[153] alkene isomerization,[154] and also alkyl-aryl cross coupling reactions.[155–157] It was also found that Ni oxidatively couples carbon dioxide to unsaturated compounds such as alkynes, alkenes, dienes, conjugated dienes, cumulenes, imines or aldehydes and converts carbon dioxide into a variety of useful organic products.[158–161]

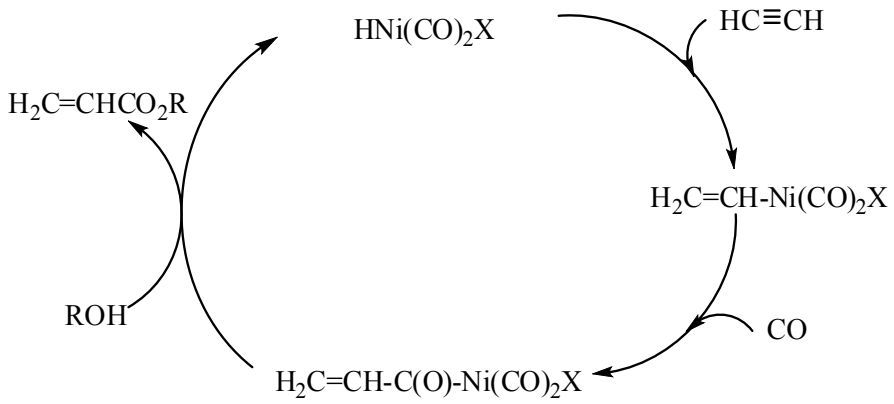

Scheme 4.1. Reppe carbonylation (addition of CO and HX to alkyne or alkene) of acetylene to produce acrylate ester using Ni complex (X= halide).

Organometallic compounds of nickel are also found to be photolytically active. The cluster complex Ni_3 (μ_3-I) $_2$(dppm) $_3$, was shown to reduce CO_2 photochemically,[162] yielding the radical anion $CO_2^{\bullet -}$. This reaction selectively produces the industrial feed stock chemical 1, 2-cyclohexanedicarboxylic acid. Such reactions of photochemical activation and transformation of abundant atmospheric gasses like CO_2, O_2, and N_2 into useful chemical products may dominate the future technologies.

As mentioned earlier, tin is extensively used as a modifier of the platinum group metals, to increase the catalytic efficiency. Similarly, Ni–Sn bimetallic complexes are

also shown to display promising results in catalysis. Ni-Sn complexes, supported on silica were shown to catalyze CO oxidation reactions,[42] as well as the dehydrogenation of cyclohexene[41] compared to mono Ni complexes. Recently, Raney Ni-Sn catalyst has been used very efficiently for the production of H_2 from biomass derived hydrocarbons.[52]

$Ni(COD)_2$ is a highly reactive yellow crystalline solid. It is extremely sensitive to air, moisture and temperature. The COD ligands on Ni metal center are highly labile and can be easily replaced by the isocyanide ligands at ambient conditions. This chapter presets the efforts that have been placed to synthesize the Ni-Sn analogues of Pt-Sn complexes and the reactivity of resultant complexes.

4.2. Results and discussion.

In the previous two chapters, synthesis of Pt-Sn complexes and their reactivity towards small molecules have been discussed. As mentioned earlier, this project has been started with the aim of replacing the expensive Pt metal with Ni and carryout the activation of mall molecules. The initiation for this chapter comes from chapter 2, where a series of exciting Pt-Sn complexes and the reaction of these complexes with small molecules have been discussed. Emphasis was laid on the synthesis of the Ni analogues of complexes $Pt(SnBu^t_3)_2(H)_2$, **2.2**, $Pt(SnBu^t_3)_2(Bu^tNC)_2(H)_2$, **2.5** and $Pt(SnBu^t_3)_2(Bu^tNC)_2(CO)$, **2.13** for carrying out the reversible activation of H_2 and CO.

Reaction of $Ni(COD)_2$ with Bu^t_3SnH and $CNBu^t$: From the reaction of $Pt(COD)_2$ with Bu^t_3SnH and $CNBu^t$, a simple unsaturated Pt-Sn complexe $Pt(SnBu^t_3)_2(CNBu^t)_2(H)_2$, **2.5** was made,[84] and the proposed pathway for the formation was shown in the equation 4.1.

Nevertheless, the nickel analogue of this platinum-ditin-dihydride compound was not made and attempts to synthesize the intermediate were also unsuccessful.

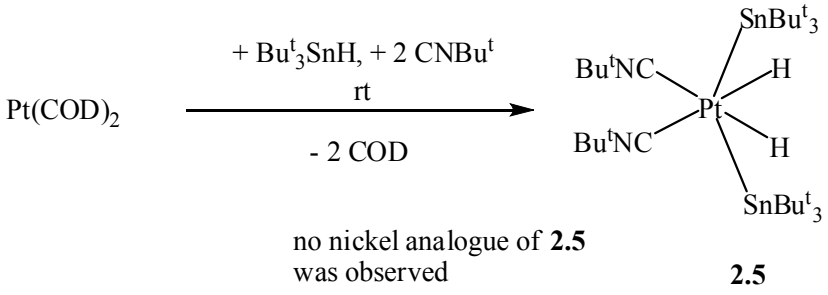

(eq. 4.1)

no nickel analogue of **2.5** was observed

2.5

However, when one equivalent of $Ni(COD)_2$ was reacted with two equivalents of $^tBu_3SnH$ and two equivalents of $CNBu^t$ under argon atmosphere in hexane solution, a red dark solution was formed. The FTIR spectra of this solution showed new broad stretches in the isocyanide region with no appreciable decrease in the amount of free tin hydride but complete consumption of free $CNBu^t$, and when the reaction mixture was brought to 68 °C the solution quickly changed color from dark red to gold, and the volatiles were removed in *vacuo*. The residues were re-dissolved in a methylene chloride/hexane mixture and filtered through silica gel. Slow evaporation of solvent yielded orange block crystals which were determined by X-ray crystallographic analysis to be $Ni(SnBu^t_3)_2(CNBu^t)_3$, **4.1** (see Figure 1.1). Further crystallographic data is listed in Appendix C Table C.1. The compound $Ni(SnBu^t_3)_2(CNBu^t)_3$, **4.1** was characterized by a combination of ^1H NMR, FTIR, UV-Vis, elemental analysis, mass spectrometry, and single crystal X-ray diffraction.

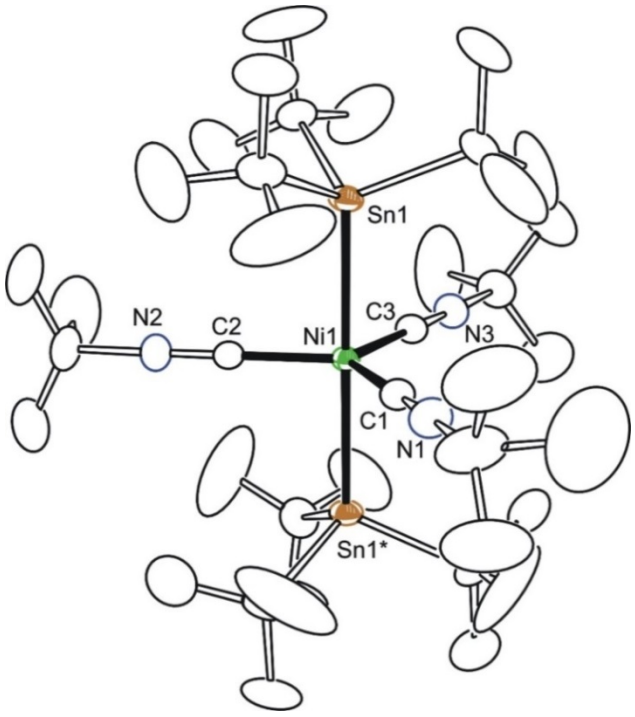

Figure 4.1. An ORTEP showing the molecular structure of $Ni(SnBu^t_3)_2(CNBu^t)_3$, **4.1** at 30 % thermal ellipsoid probability. Selected interatomic distances (Å) and angles (deg) are as follows: Ni1-C1= 1.862, Ni1-Sn1=2.6108; Sn1-Ni1-Sn1* = 179.24, C2-Ni1-C1= 120.9, Sn1-Ni1-C1=90.3.

Compound **4.1** is an $18e^-$ saturated complex. The FTIR spectrum of $Ni(Sn^tBu_3)_2(^tBuNC)_3$, **4.1** shows two distinct isocyanide resonances, as opposed to the theoretical one ν_{CN} for trigonal bipyramidal $M(L)_2(L^{\square})_3$ with axial L. It is still unknown why there is an extra FTIR active stretch, but evidence for sterically induced symmetry distortion in solution is provided below. The FTIR disagreement with normal symmetry theory is the first of many unusual pieces of information found in this work. The platinum analogue $Pt(Sn^tBu_3)_2(^tBuNC)_3$ (see chapter 5) and the palladium analogue $Pd(Sn^tBu_3)_2(^tBuNC)_3$ are also synthesized in our lab.[163]

The pathway for the formation of complex **4.1** is shown in Scheme 4.2. Complex $Ni(CNBu^t)_4$ will be formed first then it releases a $CNBu^t$ ligand to react with two Bu^t_3SnH to form complex $Ni(SnBu^t_3)_2(CNBu^t)_3$, **4.1**. Indeed this analogy was proved

later where $Ni(SnBu^t_3)_2(CNBu^t)_3$ is readily formed from the reaction of $Ni(CNBu^t)_4$ with two equivalents of Bu^t_3SnH in refluxing hexane, as shown in equation 4.1, with the release of H_2 gas and $CNBu^t$.[84] The reaction proceeds at room temperature as well but much more slowly.

The proposed mechanism for the formation of $Ni(SnBu^t_3)_2(CNBu^t)_3$, **4.1** involves the formation of intermediate $Ni(RNC)_3$ first, as the reactivity of the complexes of the type $Ni(RNC)_4$ proceed via ligand dissociation yielding reactive trigonal planar $Ni(RNC)_3$ intermediates.[164] After the formation of $Ni(RNC)_3$ intermediate, the Bu^t_3SnH ligand adds to it stepwise, as shown in Scheme 4.2. A concerted mechanism to produce $Ni(SnBu^t_3)_2(CNBu^t)_3$, **4.1** with release of H_2 has been ruled out due to steric restraints.

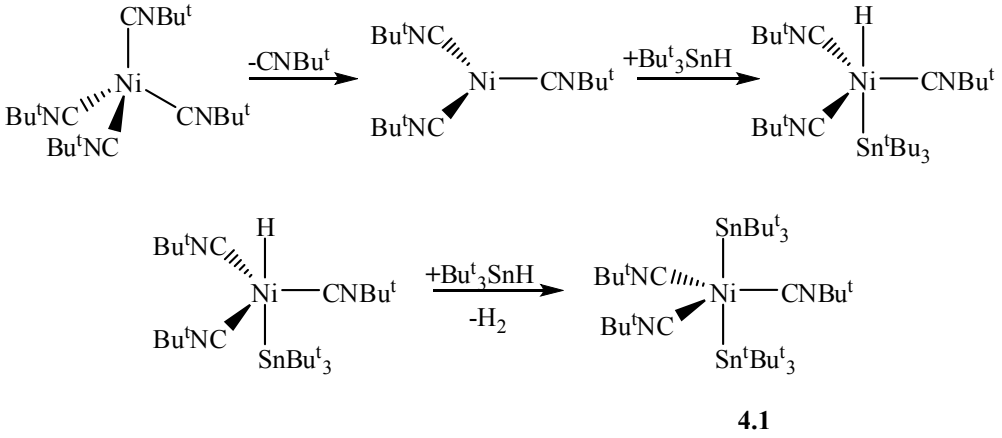

4.1

Scheme 4.2. Line drawing of proposed formation for $Ni(SnBu^t_3)_2(CNBu^t)_3$, **4.1**.

Slow and drop wise addition of one equivalent of diluted Bu^t_3SnH to a solution of $Ni(CNBu^t)_4$ at any temperature will afford only a mixture of $Ni(SnBu^t_3)_2(CNBu^t)_3$, **4.1** and $Ni(CNBu^t)_4$. Unsuccessful detection of any hydride in the reaction mixture suggests a rapid reaction to form the product **4.1,** once initiated by the first tin binding. The initial reaction conditions described earlier used only 2eq of $CNBu^t$ and formed a dark red

intermediate. A literature search determined that this afforded the nickel cluster $Ni_4(CNBu^t)_7$ which also apparently reacts with Bu^t_3SnH to give the same product $Ni(SnBu^t_3)_2(CNBu^t)_3$ but in understandably lower yield due to deficiency of isocyanide.[165]

Reaction of $Ni(SnBu^t_3)_2(CNBu^t)_3$, 4.1 with Carbon Monoxide, CO: When CO gas is purged through the room temperature gold colored hexane solution of $Ni(SnBu^t_3)_2(CNBu^t)_3$, **4.1** a color change to light-yellow was observed. FTIR spectroscopy analysis of the reaction mixture confirmed the presence of a free $CNBu^t$ and resonances of a new compound displaying both CN and CO stretches. Solvent was removed under *vacuo* and the residue was crystallized in a mixture of CH_2Cl_2/Hexane solvent at -25 °C. Analyzing the resultant crystals using X-ray crystallography yielded a molecular structure of $Ni(SnBu^t_3)_2(CNBu^t)_2(CO)$, **4.2** shown in Figure 4.2. Further crystallographic data is found in Appendix C Table C.1. The complex $Ni(SnBu^t_3)_2(CNBu^t)_2(CO)$, **4.2** was characterized by a combination of ^1H NMR, ^{13}C-CO NMR, FTIR, UV-Vis, mass spectrometry, and single crystal X-ray diffraction.

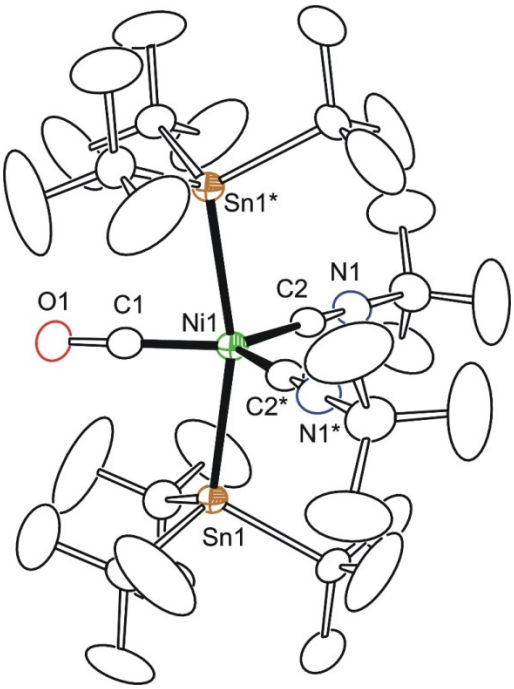

Figure 4.2. An ORTEP showing the molecular structure of $Ni(SnBu^t_3)_2(CNBu^t)_2(CO)$, **4.2** at 30 % thermal ellipsoid probability. Selected interatomic distances (Å) and angles (deg) are as follows: Ni1-C1= 1.736, Ni1-Sn1=2.6087, Ni1-C2= 1.875; Sn1-Ni1-Sn1* = 164.33, C2-Ni1-C1= 123.6, Sn1-Ni1-C1=82.2, Sn1-Ni1-C2 = 94.3, C2-Ni1-C2*=112.9.

The symmetry distortion due to steric repulsion between the bulky Bu^t groups is clearly evident from the crystal structure shown in Figure 4.2. The structure of $Ni(SnBu^t_3)_2(CNBu^t)_2(CO)$, **4.2** is very similar to the mono CO platinum complex $Pt(SnBu^t_3)_2(CNBu^t)_2(CO)$, **2.13** discussed in the chapter 2, which reversibly loses CO to regenerate complex $Pt(SnBu^t_3)_2(CNBu^t)_2$, **2.6**. The axial tin groups seen in **4.2** bend away from the bulky equatorial isocyanides in an attempt to relieve steric strain. The *tert*-butyl groups even arrange themselves appropriately *anti* to further reduce any molecular tension. Both the compounds $Ni(SnBu^t_3)_2(CNBu^t)_3$, **4.1** and $Ni(SnBu^t_3)_2(CNBu^t)_2(CO)$, **4.2** are stable in air in solid state and in solution state for extended periods of time.

When CO gas is purged through either $Ni(SnBu^t_3)_2(CNBu^t)_3$, **4.1** or $Ni(SnBu^t_3)_2(CNBu^t)_2(CO)$, **4.2** in refluxing hexane or THF, formation of an almost 50:50

mixture of $Ni(SnBu^t_3)_2(CNBu^t)_2(CO)$,**4.2** and $Ni(SnBu^t_3)_2(CNBu^t)_2(CO)_2$, **4.3** was observed (see Scheme 4.3). These two compounds are extremely similar, and their separation requires large amounts of time and resources. Compound, **4.3** is characterized by FTIR, ^{1}H NMR, and X-ray crystallographic analysis, but we did not pursue further its reactivity or photochemical properties due to difficulty involved in isolation and purification. The synthesis and characterization of **4.3** can be found here.[84]

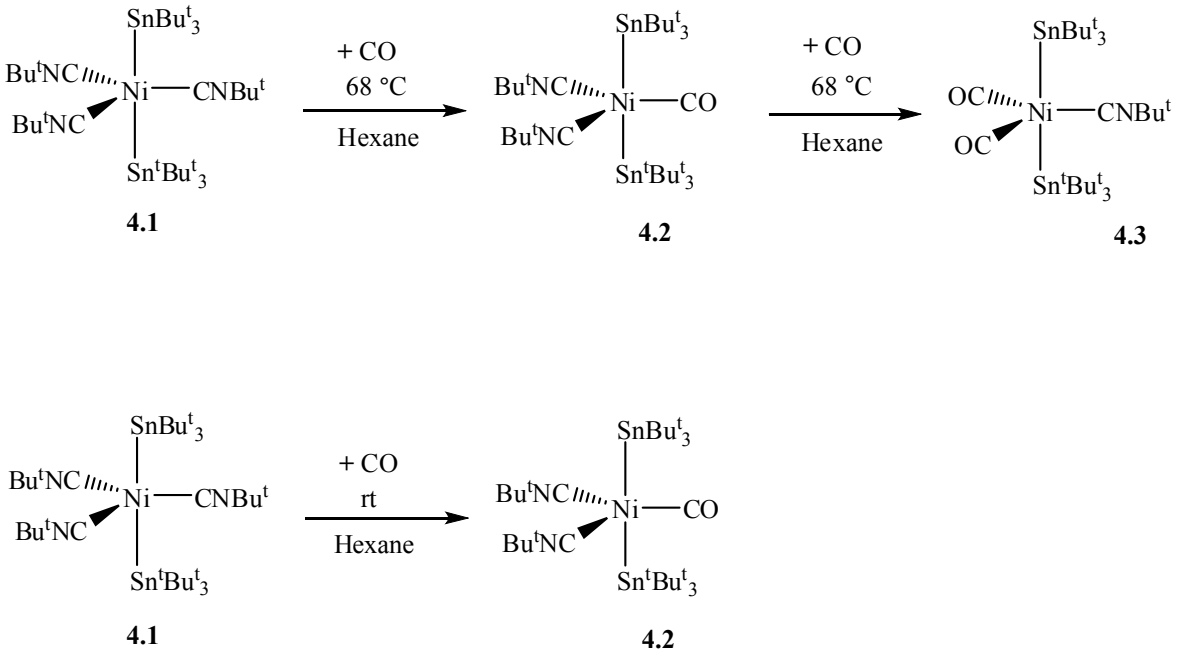

Scheme 4.3. Formation of compounds **4.2** and **4.3** from **4.1.**

Compound $Ni(SnBu^t_3)_2(CNBu^t)_2(CO)$, 4.2, is photo active: The compound $Ni(SnBu^t_3)_2(CNBu^t)_2(CO)$, **4.2**, was found to be highly light sensitive. When an oxygen-free yellow colored hexane solution of **4.2** was exposed to incandescent light, a quick color change to metallic purple occurred, as shown in Figure 4.3.

Figure 4.3. Photographs showing the color change of $Ni(SnBu^t_3)_2(CNBu^t)_2(CO)$, **4.2**, Before photolysis (left), after photolysis (right).

As mentioned, compound **4.2** is very sensitive to light. Exposure to sunlight or even under normal tube light it changes the color to purple. That was how Dr. Derek Isrow discovered the photolytic activity of this compound when he was walking in the sunlight with a solution of this compound in an NMR tube, and the compound became purple from yellow and this led to a series of experiments to characterize its photolytic activity.

Initially, the photolytic activity was thought to be due to the induced elimination of CO producing $Ni(SnBu^t_3)_2(CNBu^t)_2$, the Ni analogue of the platinum-tin complex $Pt(SnBu^t_3)_2(CNBu^t)_2$, **2.6** from chapter 2. As the CO dissociation is a very common mechanism in metal-carbonyl photochemical reactions,[166] carbon monoxide gas is purged through the purple colored solution to check for regeneration of the starting material, however, the purple solution was relatively stable to CO, as well as hydrogen gas. We

were unable to produce either the complex $Ni(SnBu^t_3)_2(CNBu^t)_2$ or its di-hydride product $Ni(SnBu^t_3)_2(CNBu^t)_2(H)_2$ as shown in equation 4.2.

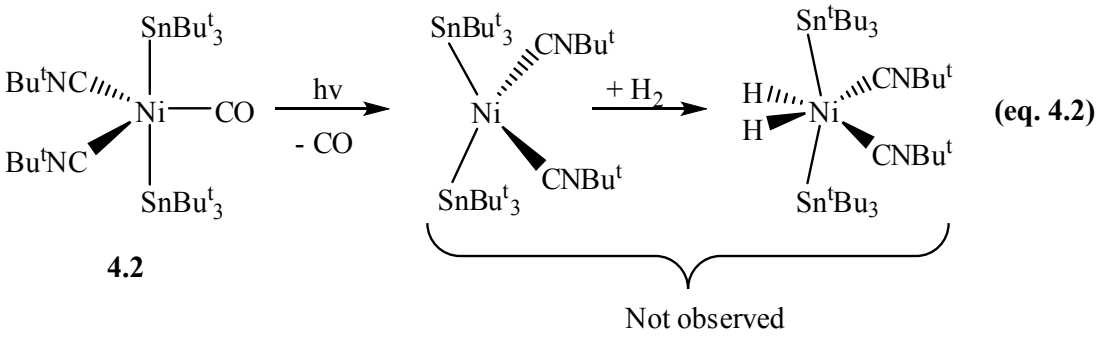

4.2 **(eq. 4.2)**

The purple colored product is highly sensitive to air and moisture. It was also found that lower temperatures increases the rate of formation of this purple colored product. Crystallization of this purple colored product is very difficult, and after repeated attempts, product was finally crystallized as dichroic purple/green colored crystals by slow evaporation of concentrated diethyl ether solutions at -20 °C under argon atmosphere. Crystallographic analysis yielded the dimeric structure of $[Ni(SnBu^t_3)(CNBu^t)_2(CO)]_2$, **4.4** as shown in Figure 4.4. Further crystallographic data is provided in Appendix C Table C.1. The compound $[Ni(SnBu^t_3)(CNBu^t)_2(CO)]_2$, **4.4**, was characterized by the combination of ^{1}H NMR, ^{13}C-CO NMR, FTIR, UV-Vis, ESR, elemental and single crystal X-ray diffraction analyses. It is stable in the solid state in air for an extended period of time, but will quickly decolorize to yellow in both oxygenated and oxygen free room temperature solution state even under argon atmosphere. As it is evident from the structure the Sn-Ni-Ni-Sn back bone adopted a zigzag pattern with *anti*-configuration to relieve equatorial strain between bulky *tert*-butyl groups.

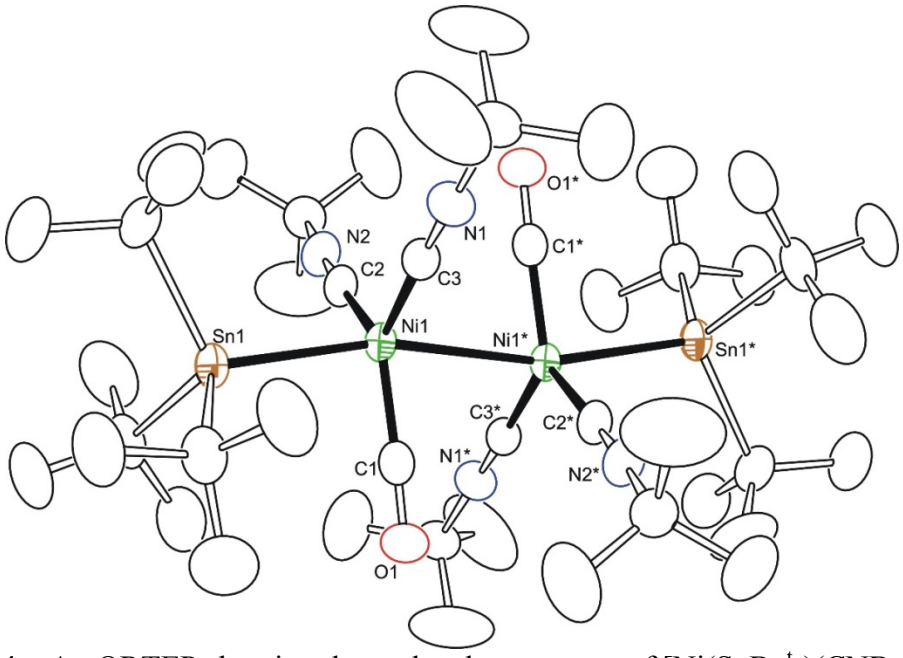

Figure 4.4. An ORTEP showing the molecular structure of $[Ni(SnBu^t_3)(CNBu^t)_2(CO)]_2$, **4.4,** at 30 % thermal ellipsoid probability. Selected interatomic distances (Å) and angles (deg) are as follows: Sn1-Ni1=2.5639(4), Ni1-Ni1*=2.6515(4), Ni1-C1=1.747(3), Ni1-C2= 1.858(3), Ni1-C3= 1.863(3); Sn1-Ni1-Ni1*=166.26(2), Sn1-Ni1-C1= 89.0(1), Sn1-Ni1-C2= 94.29(9), Ni1*-Ni1-C1= 77.3(1), Ni1*-Ni1-C2= 91.87 (9).

Radical mechanism for the formation of $[Ni(SnBu^t_3)(CNBu^t)_2(CO)]_2$, 4.4: As it can be seen in the Figure 4.4, the crystal structure of compound **4.4** still displays CO ligands which were not lost as proposed in the equation 4.3, but rather Ni-Sn bonds were cleaved and a new Ni-Ni bond was formed. The ^1H NMR analysis of the $Ni(SnBu^t_3)_2(CNBu^t)_2(CO)$, **4.2** solution after photolysis indicated the presence of hexa-*tert*-butyl-di-stannane, $Bu^t_3Sn\text{-}SnBu^t_3$, a known compound and later it has been isolated from the crystallization of the photolysis product.[167] Which was believed to be formed by combining two Bu^t_3Sn moieties and these di-stannanes are known to produce tri-alkyl tin radicals by thermolysis at elevated temperatures.[168] If extreme care is not taken to eliminate as much oxygen from the reaction mixture as possible, another known compound, $Bu^t_3Sn\text{-}O\text{-}SnBu^t_3$ is detected and isolated as colorless plates.[169]

Based on these experimental evidences a radical mechanism has been proposed (see Scheme 4.4) for the formation of product $[Ni(SnBu^t_3)(CNBu^t)_2(CO)]_2$, **4.4**, with photolytic generation of the elusive and paramagnetic tetrahedral Ni^I radical[170] ● $Ni(SnBu^t_3)(CNBu^t)_2(CO)$ and the planar ● Sn^tBu_3 radical.

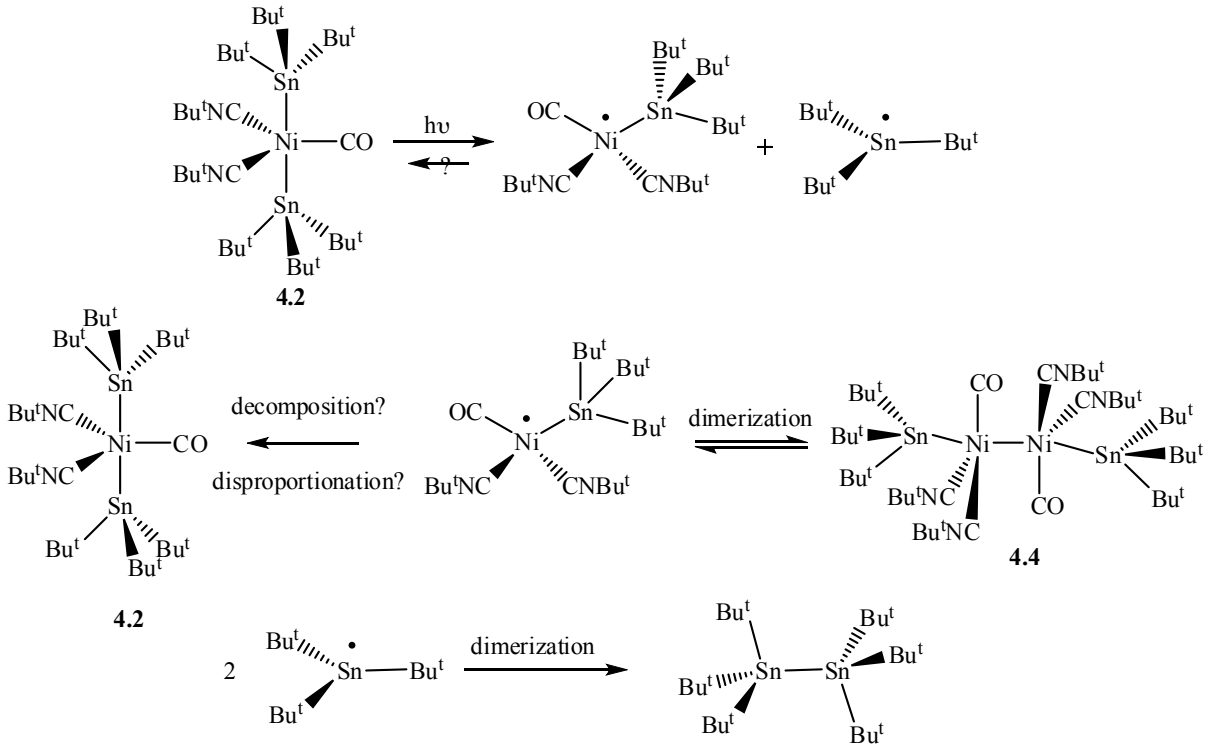

Scheme 4.4. Proposed mechanism for photolysis of $Ni(SnBu^t_3)_2(CNBu^t)_2(CO)$, **4.2** to $[Ni(SnBu^t_3)(CNBu^t)_2(CO)]_2$, **4.4** with generation of $Bu^t_3Sn\text{-}SnBu^t_3$.

The proposed tetrahedral Ni^I species ● $Ni(SnBu^t_3)(CNBu^t)_2(CO)$ is unsaturated by one electron and apparently dimerizes forming the compound $[Ni(SnBu^t_3)(CNBu^t)_2\text{-}(CO)]_2$, **4.4**. Though the existence and stability of the radical ● $Ni(SnBu^t_3)(CNBu^t)_2(CO$) in solution is still mostly unclear to us presently.

ESR studies on $[Ni(SnBu^t_3)(CNBu^t)_2(CO)]_2$, 4.4: After proposing the radical mechanism for the formation of $[Ni(SnBu^t_3)(CNBu^t)_2(CO)]_2$, **4.4** we set out to prove the

existence of radicals in solution. When ESR studies were performed on toluene solution of **4.4** at 134 K, an ESR signal with g = 2.059 was observed which is in good agreement with the literature reported g value for the Ni^{I} centered radicals.[171] Typical g-values for Sn-centered radicals range from 1.988 to 2.027.[172] The ^{13}CO-$[Ni(SnBu^{t}_{3})(CNBu^{t})_2(CO)]_2$ spectrum is shown below in Figure 4.5 and the ^{12}CO spectrum is shown in Appendix C Figure C.3.

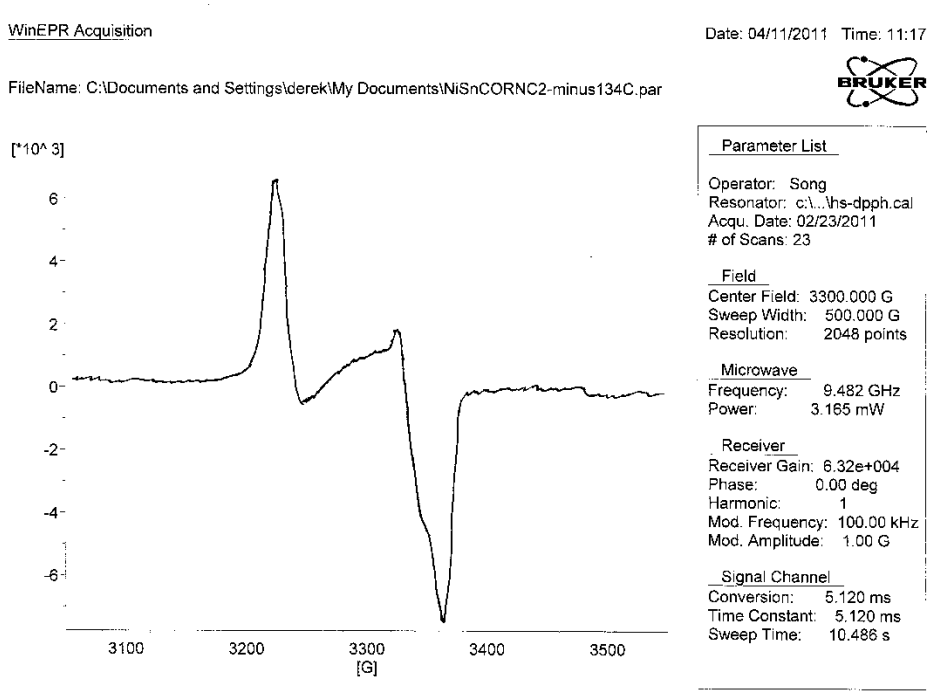

Figure 4.5. ESR spectra of ^{13}CO-$[Ni(SnBu^{t}_{3})(CNBu^{t})_2(CO)]_2$ at 134 K. g = 2.059.

Efforts to trap proposed radical species: After learning from ESR experiments that the complex **4.2** is generating paramagnetic species in solutions when exposed to the light, we carried out few more experiments to further confirm the generation of radicals in solution. In the first experiment we wanted to capture the radicals using a well know radical trap (2,2,6,6-Tetramethylpiperidin-1-yl)oxyl, TEMPO (see Figure 4.6). [173,174] This

widely used radical trap has many other industrial application such as polymerization initiation, catalytic oxidation, etc., which will be discussed in the next chapter.

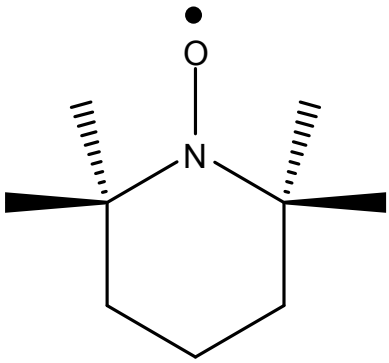

Figure 4.6. Line structure of (2,2,6,6-Tetramethylpiperidin-1-yl)oxyl, TEMPO, radical.

When the yellow colored solution of the compound $Ni(SnBu^t_3)_2(CNBu^t)_2(CO)$, **4.2** was exposed to the light in the presence of three equivalents of TEMPO radical , the solution did not change to the characteristic purple color of the dimer, but rather darkened slightly to a brownish yellow. Similar color change was observed with $Ni(SnBu^t_3)_2(CNBu^t)_3$, **4.2** as well. Evacuation of volatiles and recrystallization of the solid residue from diethyl ether at -25 °C yielded brown yellow crystalline blocks of $Ni(\eta^2\text{-TEMPO})(SnBu^t_3)(CNBu^t)$, **4.5** (see Figure 4.7) in 54 % yield. It was characterized by a combination of ^1H NMR, FTIR, and single crystal X-ray diffraction. Further crystallographic data is found in Appendix C Table C.1.

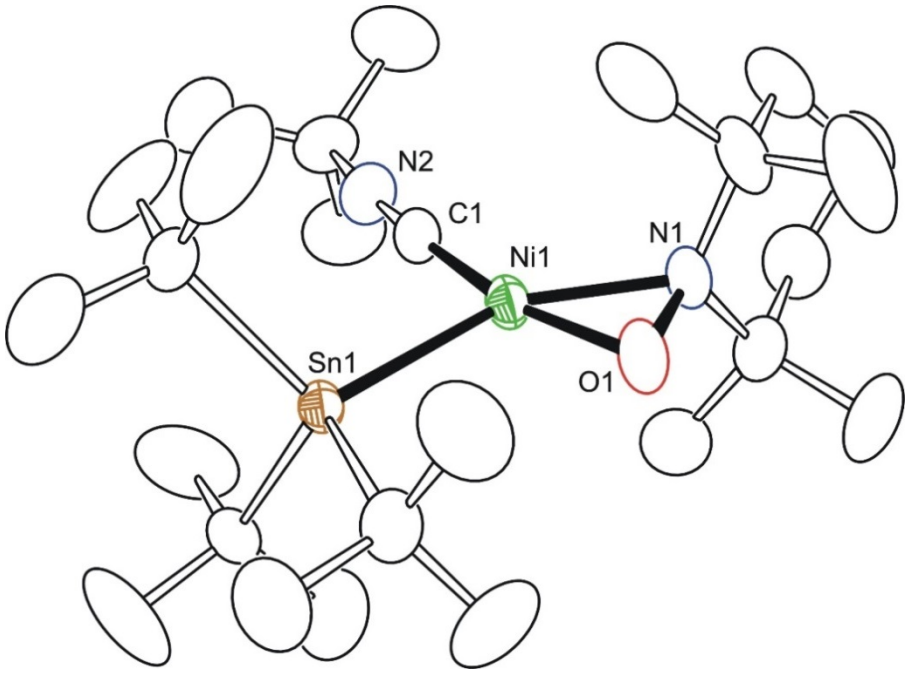

Figure 4.7. An ORTEP showing the molecular structure of Ni(η^2-TEMPO)($SnBu^t_3$)($CNBu^t$), **4.5** at 30% thermal ellipsoid probability. Selected interatomic distances (Å) and angles (deg) are as follows: Ni1-Sn1=2.4964(3), Ni1-N1=1.957(2), Ni1-O1= 1.825(2), Ni1-C1=1.760(2), N1-O1= 1.409(3); Sn1-Ni1-C1= 94.00(8), Sn1-Ni1-O1=101.70(7), Ni1-O1-N1= 73.2(1), Ni1-N1-O1=63.2(1),N1-Ni1-O1= 43.57(9), N1-Ni1-C1= 120.7(1)

It is evident from the Figure **4.7** that a CO ligand and a $CNBu^t$ are missing from the Ni metal center. After careful consideration and study of the molecule and reaction the following mechanism (see Scheme 4.5) has been proposed for the formation of Ni(η^2-TEMPO)($SnBu^t_3$)($CNBu^t$), **4.5**. TEMPO is known to bind to metal centers through $\eta^1$and η^2 modes (further discussed in the next chapter 5). Here, we believe TEMPO initially binds to the Ni^I radical center through oxygen atom in η^1 mode to form the intermediate *I*, which results in $1e^-$ reduction of TEMPO to its monoanion and oxidation of Ni^I back to Ni^{II}. This is followed by repulsive elimination of isocyanide to form the tetrahedral $16e^-$ intermediate Ni(η^1-TEMPO)($SnBu^t_3$)($CNBu^t$)(CO), *II*. Then TEMPO transforms to its $3e^-$ η^2 binding mode, displacing a CO ligand (or a second isocyanide for

●$Ni(SnBu^t_3)(CNBu^t)_3$) due to steric interactions and favorable heats of formation, forcing a $16e^-$ distorted square planar final product. The N1-O1 bond distance of 1.409(1) Å is longer than that found in free TEMPO which is 1.283(9) Å. The geometry around the N1 atom is pyramidal [O1-N1-C22 = 117.75(4) °, O1-N1-C26 = 111.16(7) °, C26-N1-C22 = 119.25(1) °] and the Ni1-N1 and Ni1-O1 bond distances are short [Ni1-N1 = 1.958(2) Å, Ni1-O1 = 1.825(4) Å]. All of these structural parameters are consistent with a bidentate η^2-TEMPO coordination mode and formulation of a reduced TEMPO radical as a monoanionic TEMPO ligand according to the literature.[175]

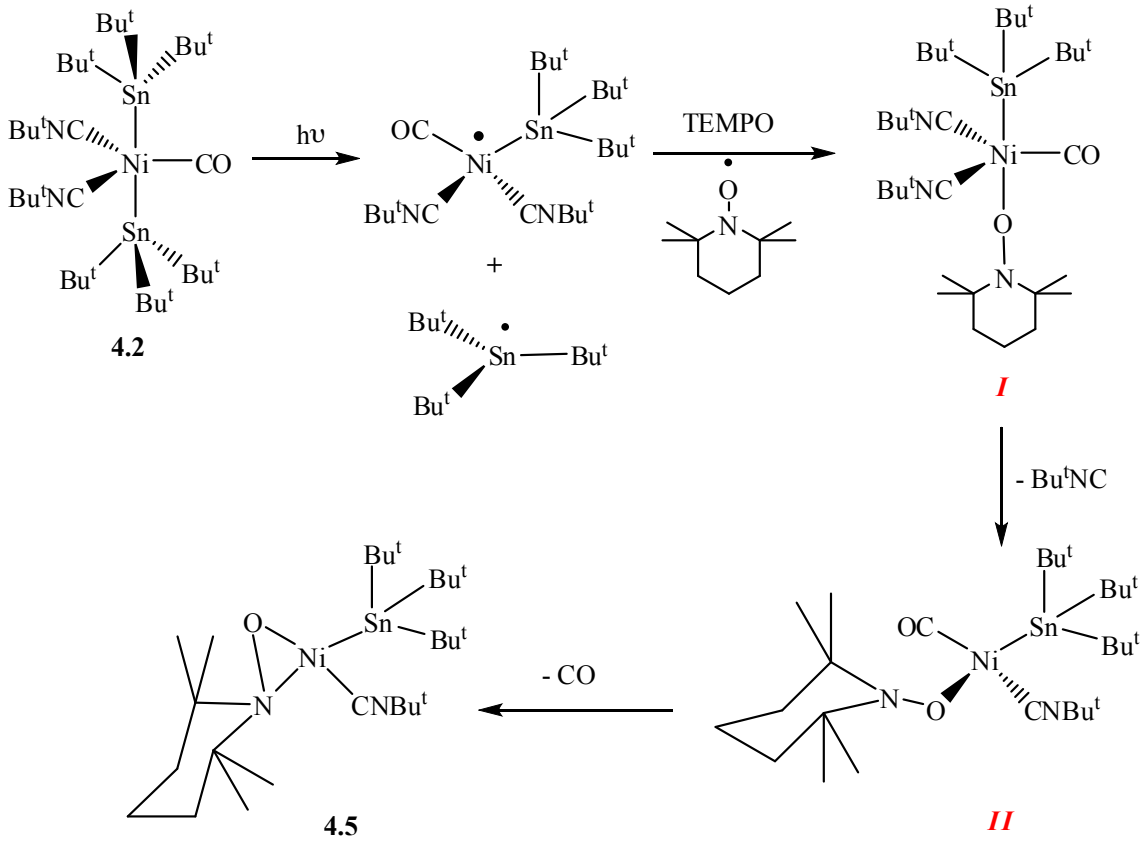

Scheme 4.5. Proposed mechanism for the formation of Ni(η^2-TEMPO)($SnBu^t_3$)($CNBu^t$), **4.5**.

TEMPO also reacts with non-radical metal centers in a similar fashion to form $\eta^1$and η^2 TEMPO bound products[170,176–178] that will be discussed in detail in the next chapter. In this case it is also possible that TEMPO is reacting with a non-radical Ni compound, but ESR studies, peak broadening at low temperature in ^{1}H NMR and isolation of Bu^tSn-O-$SnBu^t$ product from the photolyzed raction mixture in the presence oxygen, where oxygen is known to react with radicals, supports the radical mechanism shown in Scheme 4.4, and also the formation of Ni(η^2-TEMPO)($SnBu^t_3$)($CNBu^t$),**4.5** shown in Scheme 4.5. Further study on the reactivity of complex **4.5** is currently under way in our lab.

In the Scheme 4.4, dimer dissociation of [Ni($SnBu^t_3$)($CNBu^t$)$_2$(CO)]$_2$, **4.4** into two ●Ni($SnBu^t_3$)($CNBu^t$)$_2$(CO) radicals has also been proposed. To test this mechanism two equivalents of TEMPO radical was added to the pure crystalline **4.4** dissolved in C_6D_6. Solution quickly decolorized to brownish yellow in ambient light. ^{1}H NMR spectroscopy of the reaction mixture confirmed the presence of mixture of Ni(η^2-TEMPO)($SnBu^t_3$)($CNBu^t$), **4.3** and free isocyanide**.** The formation of Ni(η^2-TEMPO)($SnBu^t_3$)($CNBu^t$),**4.5** compound indicates that TEMPO is reacting with the same compound that is being generated in the solution of [Ni($SnBu^t_3$)($CNBu^t$)$_2$(CO)]$_2$, **4.4**, which is also present in the photolysed solution of Ni($SnBu^t_3$)$_2$($CNBu^t$)$_2$(CO), **4.2**. This seems to support the dissociation of **4.4** into the radical monomers, which then reacts with the TEMPO radical to form compound Ni(η^2-TEMPO)($SnBu^t_3$)($CNBu^t$), **4.5**.

Though we haven't successfully captured the proposed ●Ni($SnBu^t_3$)($CNBu^t$)$_2$(CO) radical as such using TEMPO radical we have got some evidence for the existence of the radicals in the solution in the form of radical polymerization catalysis.

Attempt to capture the other proposed radical $^{\bullet}SnBu^{t}_{3}$ were partially successful. These radical are known to exist in planar geometry[179] and Dr. Derek was able to isolate them as a polymer $[(^{t}Bu_3Sn)(PF_4)]_{\infty}$ with trapped planar $SnBu^{t}_{3}$ in between PF_4^- moiety.[84] Efforts are still under way to capture both the proposed radicals of Ni and Sn from the photolyzed reaction mixture of compound **4.2**.

Sunlight triggered photo polymerization catalysis with $Ni(SnBu^{t}_{3})_2(CNBu^{t})_2(CO)$: Photo polymerization using transition metal complexes is well known in the literature.[180–183] Ni complexes are also shown to catalyze photo polymerization.[184–186] After being learned that compound **4.2** forms radical species photolytically, we performed some polymerization reactions. When 1% (w/w) solution of compound **4.2** in trimethyl propane ethoxylate triacrylate in the presence of triethanolamine, a coinitiator[187] was exposed to either flood light lamp or sunlight, it rapidly, almost instantaneously polymerized to give the polytrimethyl propane ethoxylate triacrylate (TPET) (see Scheme 4.6). The presence of co-initiator is required as when we tried to perform the reaction without co-initiator we were not able to trigger the polymerization process. But, the polymerization of methylmethacrylate (MMA) with compound **4.2** is not as rapid as in the case of TPET monomer polymerization. Interestingly there was no characteristic purple coloration, that we observe when compound **4.2** undergoes photolysis. Probably there was no sufficient time to form dimeric compound **4.4**. We are still in the process of understanding the mechanistics of the polymerization processes.

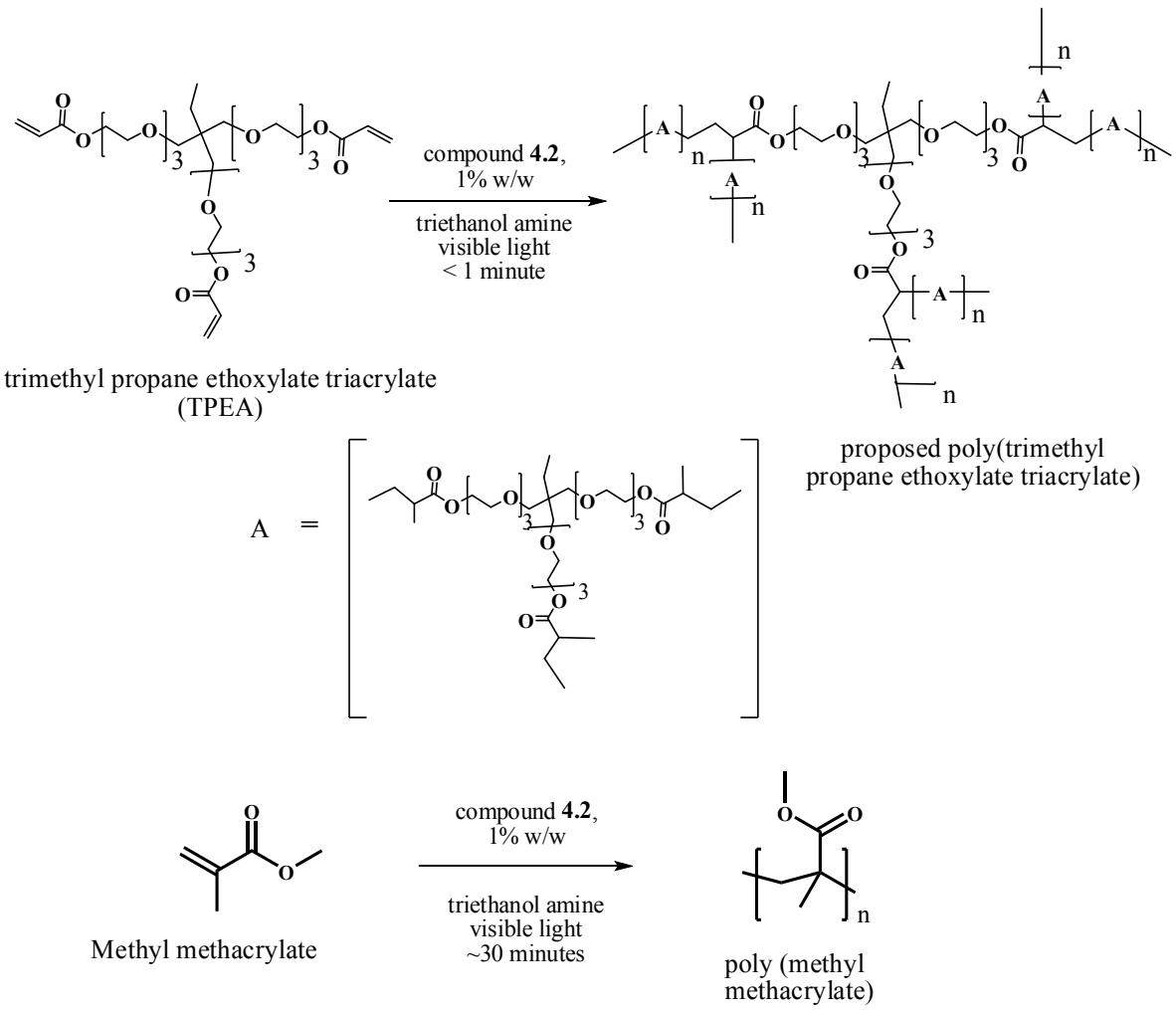

Scheme 4.6. Polymerization reactions with compound **4.2** in the presence of visible light.

When, benzophenone (BP), a well-known photo initiator of the polymerization reactions, was used in place of compound **4.3**, the same monomer was polymerized in 30 minutes. This indicates the efficiency of compound **4.3** in polymerization of TPET. The process involved in the polymerization of monomer MMA using benzopheneone and triethanol amine is reported in the literature by Merlin André and co. (see Scheme 4.7).[187]

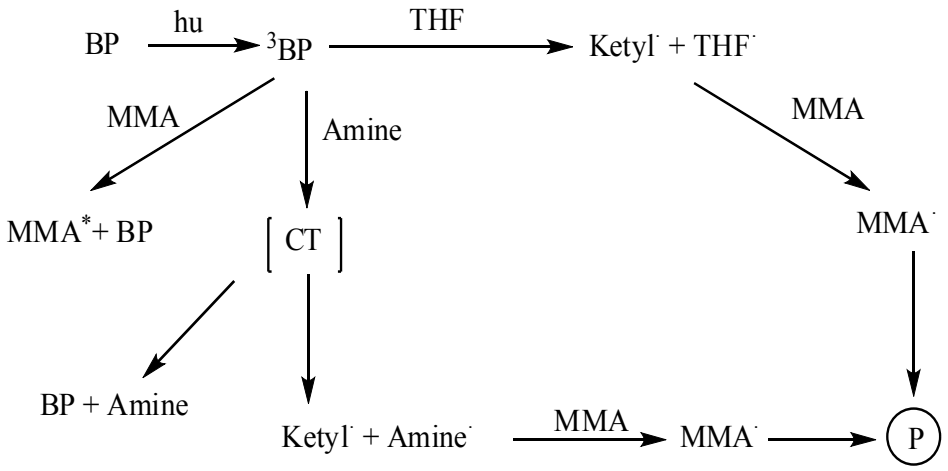

Scheme 4.7. Process involved in the photo polymerization of methylmethacrylate (MMA) using benzophenone (BP) and triethanol amine (Amine).[187]

Based on the above shown mechanism we believe compound **4.2** is also playing a similar role as that of benzophenone. As mentioned before we did not observe the characteristic purple color of the dimer, this indicates that dimerization is not happening in the polymerization reaction. In such case there is a good chance of isolating the radical moiety as such. More research is required to understand the exact role of compound **4.2** in the above discussed polymerization reactions.

4.3. Summary and conclusions.

We have reported the successful synthesis of new heterobimetallic Ni-Sn compounds containing the sterically encumbered $SnBu^t_3$ ligand: $Ni(SnBu^t_3)_2(CNBu^t)_3$,**4.1**, $Ni(SnBu^t_3)_2(CNBu^t)_2(CO)$, **4.2**, $Ni(SnBu^t_3)_2(CNBu^t)(CO)_2$, **4.3**, $[Ni(SnBu^t_3)(CNBu^t)_2(CO)]_2$, **4.4** and $Ni(\eta^2$-TEMPO$)(SnBu^t_3)(CNBu^t)$, **4.5.** Compound $Ni(SnBu^t_3)_2(CNBu^t)_2(CO)$, **4.2** is found to be photo active. Compound $[Ni(SnBu^t_3)(CNBu^t)_2(CO)]_2$, **4.4** has been isolated from the photolysis reaction of

$Ni(SnBu^t_3)_2(CNBu^t)_2(CO)$, **4.2**. A radical mechanism has been proposed for the formation of compound **4.5.** ESR, NMR and polymerization studies support the formation of both nickel and tin centered radicals due to initial bond photolysis generating $\bullet Ni(SnBu^t_3)(CNBu^t)_2(CO)$ and $\bullet Sn^tBu_3$ as well as dissociation of the Ni-Ni bond in $[Ni(SnBu^t_3)(CNBu^t)_2(CO)]_2$, **4.5** yielding two $\bullet Ni(SnBu^t_3)(CNBu^t)_2(CO)$. Attempted trapping of $\bullet Ni(SnBu^t_3)(CNBu^t)_2(CO)$ or $\bullet Ni(SnBu^t_3)(CNBu^t)_3$ with the stable TEMPO radical afforded the $16e^-$ square planar $Ni(\eta^2\text{-TEMPO})(SnBu^t_3)(CNBu^t)$, **4.5**.

Compound **4.2**, has shown some extraordinary catalytic activity. It catalyzed the monomer polytrimethyl propane ethoxylate triacrylate (TPET) just under 1 minute in the presence of visible light. This reaction also supports the proposed radical formation by compound **4.2** in the presence of light. $Pd(Sn^tBu_3)_2(^tBuNC)_3$ and $Pt(Sn^tBu_3)_2(^tBuNC)_3$ have also been synthesized in our laboratory, however neither of these precious metal analogues showed any signs of photo sensitivity, this displays the unusual reactivity of Ni-Sn complexes. Indeed, Ni-Sn bimetallic compounds do exhibit useful functionality and may yield future complexes which reduce the need for platinum, palladium and other precious metals. Further study of all reported compounds is under way.

4.4. Experimental section.

General Data: Unless otherwise stated, all reactions were carried out under an argon atmosphere in Schlenk flasks or an MBraun Unilab inert atmosphere glovebox. Reagent grade solvents were dried according to standard procedures and freshly distilled before use. Infrared spectra were recorded on a Nicolet 380 FT-IR spectrophotometer. Single crystal FTIR spectra were recorded on a Perkin Elmer Spectrum 400 using a Perkin

Elmer Universal ATR Sampling Accessory. ^{1}H and ^{13}C NMR spectra were recorded on a Bruker 400 spectrometer operating at 399.993 MHz. UV-Vis spectra were recorded on a Varian Cary 100 Bio Spectrophotometer using screw-cap quartz cuvettes with 1 cm path lengths. Mass spectrometric measurements performed by direct–exposure probe using electron impact ionization (EI) were made on a VG 70S instrument at the University of South Carolina, Columbia, SC, and electrospray mass spectrometric measurements were obtained on a Bruker microTOF-Q II at the University of Miami. ESR spectra were recorded on a Bruker EMX ESR Spectrometer. Elemental analyses were performed by Columbia Analytical Services (Tucson, AZ). Photolysis was accomplished with a 150 W Sylvania flood lamp. Bis(1,5-cyclo-octadiene) nickel, $Ni(COD)_2$, was purchased from Strem Chemicals and used without further purification. Tri-iron dodecacarbonyl, $Fe_3(CO)_{12}$, was purchased from Aldrich and used without further purification. *Tert*-butyl isocyanide, $CNBu^t$, trityl hexafluorophosphate, $Ph_3C^+ PF_6^-$, and TEMPO radical were purchased from Alfa Aesar and used without further purification. Argon, carbon monoxide, hydrogen, and carbon dioxide gasses were purchased from AirGas Supplies. ^{13}CO was kindly provided to us by Dr. Carl Hoff and his group. Triethanolamine and Methylmethacrylate were provided by Dr. Francisco Raymo and his group. Tri-*tert*-butyl tin hydride, Bu^t_3SnH,[44,60] was synthesized according to the published procedure. For the synthesis of compounds **4.3**, see the reference.[84]

Synthesis of $Ni(SnBu^t_3)_2(CNBu^t)_3$, 4.1: A 100 mg (0.36 mmol) sample of $Ni(COD)_2$ and 215 mg (0.74 mmol) of Bu^t_3SnH were loaded into a sidearm Schlenk flask equipped with a water cooled condenser. Under flow of argon, 50 mL of hexane was added by cannula and the mixture was stirred to dissolve all solids. 100 mg (1.25 mmol) of $CNBu^t$ was

added resulting in an immediate color change to pale yellow. The solution was stirred for 10 minutes and heated to a brief reflux, resulting in a color change to gold, before removing the volatiles in *vacuo*. The solid residue was redissolved in methylene chloride and passed down a column of silica gel. The solution was evacuated to dryness, redissolved in 4ml of a 1:1 methylene chloride/hexane solution, filtered into a glass vial, and placed in a -25 °C freezer in the drybox. Slow evaporation of solvent resulted in 239 mg (74% yield) of orange blocks of $Ni(SnBu^t_3)_2(CNBu^t)_3$. A similar yield can be obtained by room temperature reaction after approximately 12 hours. Spectral data for $Ni(SnBu^t_3)_2(CNBu^t)_3$, **4.1 :** ^{1}H NMR (C_6D_6 in ppm): δ= 1.676 (s, $^3J_{Sn-H}$ = 47 Hz, 54 H, Sn-Bu^t), 1.191 (s, 27 H, CN-Bu^t). FTIR in hexane- ν_{CN} cm^{-1}: 2034 (s), 2062 (w). UV-Vis= 392 nm. Elemental analysis: Found = C 51.98 %, H 9.12 %, N 4.46 %; Calculated = C 52.75 %, H 9.19 %, N 4.73 %. EI Mass Spec shows major peak at 598 m/z which is $Ni(SnBu^t_3)_2(CNBu^t)_3$- ($SnBu^t_3$)= 888 - 290= 598. Spectral pattern is consistent with the presence of 1 Ni and 1 Sn atom.

Synthesis of $Ni(SnBu^t_3)_2(CNBu^t)_2(CO)$, 4.2: A 50 mg (0.0056 mmol) sample of $Ni(SnBu^t_3)_2(CNBu^t)_3$, **4.1,** was loaded into a sidearm Schlenk flask. Under flow of argon, 30 mL of hexane was added by cannula and the mixture was stirred to dissolve all solids. The argon atmosphere was evacuated and replaced by carbon monoxide, CO. The stirred solution changed color from dark gold to light yellow over a period of several minutes. The solution was evacuated to dryness and the solid residue was redissolved in 2ml of a 1:1 methylene chloride/hexane solution, filtered into a glass vial, and placed in a -25 °C freezer in a drybox. Slow evaporation of solvent resulted in 38 mg (82% yield) of yellow blocks of $Ni(SnBu^t_3)_2(CNBu^t)_2(CO)$, **4.2**. A sample of ^{13}CO- $Ni(SnBu^t_3)_2(CNBu^t)_2(CO)$

was prepared for ^{13}C NMR by using ^{13}CO in the same procedure. Spectral data for $Ni(SnBu^t_3)_2(CNBu^t)_2(CO)$**:** ^1H NMR (C_6D_6 in ppm): δ= 1.642 (s, 54H, Sn-Bu^t, $^3J_{Sn-H}$= 52 Hz), 1.037 (s, 18H, CN-Bu^t). ^{13}C-CO NMR (toluene-d_8)= 197.27 ppm (s, 1C, $^2J_{Sn-C}$= 127 Hz at 25°C) and 197.40 ppm (s, 1C, $^2J_{Sn-H}$= 127 Hz at -80°C). FTIR in hexane- ν_{CN} cm^{-1} : 2092 (s), 2114 (m). ν_{CO} cm^{-1} : 1935 (s). Single Crystal FTIR- ν_{CN} cm^{-1}: 2094 (s), 2118 (m). ν_{CO} cm^{-1}: 1920 (s). UV-Vis= 375 nm. EI Mass Spec shows major peaks at 832, 775 and 747 m/z which are $Ni(SnBu^t_3)_2(CNBu^t)_2(CO)$, $Ni(SnBu^t_3)_2(CNBu^t)_2(CO) - Bu^t = 832 - 57 = 775$ and $Ni(SnBu^t_3)_2(CNBu^t)_2(CO) - Bu^t - CO = 832 - 57 - 28 = 747$, respectively. Spectral pattern is consistent with the presence of 1 Ni and 2 Sn atoms.

Synthesis of $[Ni(SnBu^t_3)(CNBu^t)_2(CO)]_2$, 4.4: A 30 mg (0.0036 mmol) sample of compound $Ni(Sn^tBu_3)_2(^tBuNC)_2(CO)$, **4.2** was loaded into a sidearm Schlenk flask. Under flow of argon, 30ml of hexane was added by cannula and the mixture was stirred to dissolve all solids. The flask was placed under slight vacuum and then irradiated with a 150W Sylvania flood lamp. The solution began to change color from light yellow to pink to deep purple over the period of one minute. The light was extinguished and the mixture was evacuated to dryness. The purple solid residue was redissolved in 2ml of diethyl ether, filtered into a glass vial, and placed in a -25 °C freezer in a drybox. Slow evaporation of solvent resulted in 6.25 mg (32 % yield) of purple blocks of $[Ni(SnBu^t_3)(CNBu^t)_2(CO)]_2$, 4.5. A sample of ^{13}CO-$[Ni(SnBu^t_3)(CNBu^t)_2(CO)]_2$, **4.4** was prepared for ^{13}C NMR by using ^{13}CO-$Ni(SnBu^t_3)_2(CNBu^t)_2(CO)$ in the same procedure. Spectral data for $[Ni(SnBu^t_3)(CNBu^t)_2(CO)]_2$**:** ^{13}C-CO NMR (toluene-d_8 in ppm)= 205 (s, 1C, -80°C). Single Crystal FTIR- ν_{CN} cm^{-1}: 2096 (s), 2063 (m). ν_{CO} cm^{-1}: 1906 (s).

UV-Vis= 564 nm. Elemental analysis: Found= C 50.12 %, H 8.40 %, N 4.87 %; Calculated= C 50.81 %, H 8.35 %, N 5.15 %.

Synthesis of Ni(η^2-TEMPO)($SnBu^t_3$)($CNBu^t$), 4.5: A 30 mg (0.0036 mmol) sample of $Ni(SnBu^t_3)_2(CNBu^t)_2(CO)$, **4.2** and 17 mg (0.0108 mmol) of TEMPO were loaded into a sidearm Schlenk flask. Under flow of argon, 30ml of hexane was added by cannula and the mixture was stirred to dissolve all solids. The flask was placed under slight vacuum and then irradiated with a 150 W Sylvania flood lamp. The solution began to change color from light yellow to brownish yellow over the period of one minute. The light was extinguished and the volatiles were removed in *vacuo*. The brownish yellow solid residue was redissolved in 2ml of diethyl ether, filtered into a glass vial, and placed in a -20 °C freezer in a drybox. Slow evaporation of solvent resulted in 11.5 mg (54 % yield) of brownish yellow blocks of Ni(η^2-TEMPO)($SnBu^t_3$)($CNBu^t$), **4.5.** Spectral data for compound **4.5:** ^{1}H NMR (C_6D_6 in ppm): δ= 1.639 (s, $^3J_{Sn-H}$= 49 Hz, 27H, Sn-Bu^t), 0.954 (s, 9H, CN-Bu^t), 1.784 (s, 6H, $(CH_3)_2$-TEMPO), 1.213 (s, 6H, $(CH_3)_2$-TEMPO). FTIR in hexane- ν_{CN} cm^{-1}: 2086 (s).

4.5. Crystallographic analysis.

Single crystals of $Ni(SnBu^t_3)_2(CNBu^t)_2(CO)$, **4.2,** $[Ni(SnBu^t_3)(CNBu^t)_2(CO)]_2$**,** **4.4,** and Ni($\eta^2$-TEMPO)($SnBu^t_3$)($CNBu^t$), **4.5**, suitable for diffraction analysis were grown by slow evaporation of concentrated diethyl ether solutions at – 20 °C. The data crystal for $Ni(SnBu^t_3)_2(CNBu^t)_3$, **4.1** was grown by slow evaporation of a concentrated benzene solution at 5 °C. All data crystals were glued onto the end of a thin glass fiber and collected under ambient atmosphere at room temperature.

X-ray intensity data were measured using a Bruker SMART APEX2 CCD-based diffractometer using Mo Kα radiation (λ = 0.71073 Å).[99] The raw data frames were integrated with the SAINT+ program by using a narrow-frame integration algorithm.[99] Corrections for Lorentz and polarization effects were also applied with SAINT+. An empirical absorption correction based on the multiple measurement of equivalent reflections was applied using the program SADABS. All structures were solved by a combination of direct methods and difference Fourier syntheses, and refined by full-matrix least-squares on F^2, by using the SHELXTL software package.[100,101] All non-hydrogen atoms were refined with anisotropic displacement parameters. Hydrogen atoms were located from the difference map and refined with isotropic thermal parameters. Crystal data, data collection parameters, and results of the analyses are listed in Appendix C Tables C.1.

The compound $Ni(SnBu^t_3)_2(CNBu^t)_3$, **4.1** crystallized in the orthorhombic crystal system. The systematic absences in the intensity data were consistent with the unique space group *Cmca*. $Ni(Sn^tBu_3)_2(^tBuNC)_3$ crystallized with a molecule of benzene solvent in the unit cell.

The compound $Ni(SnBu^t_3)_2(CNBu^t)_2(CO)$, **4.2** crystallized in the orthorhombic crystal system. The systematic absences in the intensity data were consistent with the unique space group *Pmmn*. $Ni(SnBu^t_3)_2(CNBu^t)_2(CO)$ crystallized with a molecule of diethyl ether in the unit cell.

The compound $[Ni(SnBu^t_3)(CNBu^t)_2(CO)]_2$**, 4.4** crystallized in the monoclinic crystal system. The systematic absences in the intensity data were consistent with the unique space group $P2_1/n$.

The compound Ni(η^2-TEMPO)($SnBu^t_3$)($CNBu^t$), **4.5** crystallized in the monoclinic crystal system. The systematic absences in the intensity data were consistent with the unique space group $P2_1/c$.

Chapter 5: Novel Complexes of Ni with TEMPO Radical: Synthesis, Structures, and Metal – Ligand Synergistic Effects in Activating Small Molecules.

5.1 Background.

The stable tetraalkylnitroxyl radical TEMPO (2,2,6,6-tet-ramethylpiperidine-1-oxyl) is a well-known oxidation catalyst first synthesized by Lebedev and Kazarnowskii in 1960.[173] Since then it has been not only used in a wide variety of industrial applications[188] but also gained constant attention in academia as well.[175,188–197] This solid, red-orange, sublimable heterocyclic radical is prepared by oxidation of the 2,2,6,6-tetramethylpiperidine, as shown in equation 5.1. Oxidation generally involves the use of hydrogen peroxide and tungsten based catalyst such as sodium-tungstate or phosphotungstic acid.

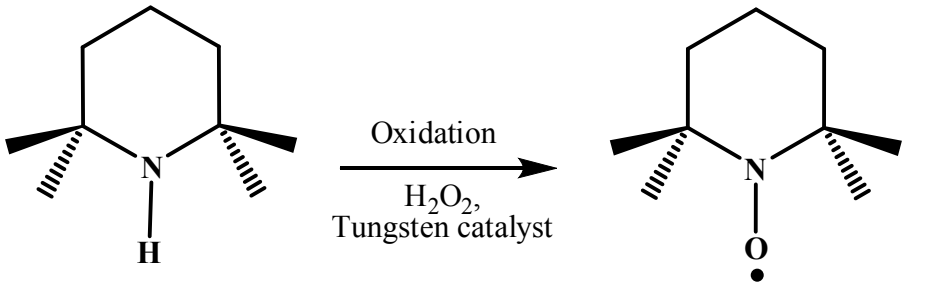

(Eq. 5.1)

2,2,6,6-tetramethylpiperidine

(2,2,6,6-tetramethylpiperin-1-yl)oxyl
TEMPO

TEMPO is a stable persistent free radical. Stability of this radical is attributed to the steric crowding imparted by the four methyl groups around the oxygen radical center. It is commonly used as radical trap and also widely used in the fields of controlled radical polymerization initiation reactions,[198–201] oxidation reactions, catalysis,[178,202–210] as well as a spin-probe/label in ESR studies to understand the environment of complex chemical and biochemical systems.[189,211–215] TEMPO radical is a mild oxidation reagent and is a

widely used catalyst in selective oxidation of primary alcohols to aldehydes and carboxylic acid.[216]

Though the chemistry of TEMPO as a reagent in the fields of catalysis, oxidation and in ESR studies is well investigated, its coordination chemistry is less studied. The coordination chemistry of this paramagnetic species with metal complexes is found to be interesting as it has been shown that the TEMPO ligand is able to coordinate through both η^1 and η^2 bonding motifs.[170,175–177,195,196,217–225]

Recently a few attention-grabbing metal-TEMPO complexes exhibiting catalytic and non-catalytic reactions have been reported.[193,194,226–230] Hayton and co-workers reported the 1e- oxidative homolysis of the Ni−NO bond and subsequent evolution of NO gas from the reaction of TEMPO with [Ni(NO)(bipy)][PF6] to form [(bipy)Ni(η2-TEMPO)][PF6] complex.[194] In this complex TEMPO makes a η^2 coordination with Ni center. This is one of the few reported examples of NO dissociation upon oxidation of a metal nitrosyl complex. The transition metal /TEMPO catalytic systems are currently receiving increased attention for oxidation of alcohols. The η^1 coordinated TEMPO to Lewis acids such as FeCl3 reported by Hayton and co-workers[193] was shown to oxidize 9, 10-dihydroanthraquinone and also primary and secondary alcohols via a mechanism involving concerted proton-coupled electron transfer (CPET) in which proton from C-H bond of the substrate transfers to the nitrogen atom of the η^1 coordinated TEMPO, much like the systems that we recently reported[231] wherein a proton from the substrate transfers to the nitrogen atom of the η^2 coordinated TEMPO ligand, subsequently forming η^1 coordinated TEMPO containing N-H bond. Stahl and co-workers recently reported a (bpy) Cu^I / TEMPO catalyst system with NMI (bpy =2,2′-bipyridine, TEMPO = 2,2,6,6-

tetramethylpiperidine-N-oxyl, NMI = N-methylimidazole) for the aerobic oxidation of alcohols to aldehydes and ketones.[226,232] This catalyst system was shown to overcome nearly all the limitations of using Pd(II) as catalyst for the aerobic oxidation of alcohols and also found to be superior in catalytic activity at least an order of magnitude than the homogeneous Pd(II) catalysts upon which much attention has been focused. In another example, an Fe-TEMPO complex has been investigated for the oxidation of 9, 10-dihydroanthraquinone and also primary and secondary alcohols, with a mechanism involving H atom transfer from the organic substrate to the nitrogen atom of the η^1 coordinated TEMPO ligand.[193] A recent report also shows the oxygen atom transfer capability of an Fe-TEMPO complex, which leads to formation of an Fe(III) oxo intermediate.[230]

Very few metal-TEMPO compounds have been synthesized and studied among them there is only one literature reported example of an organometallic complex possessing exclusively TEMPO ligands, and this dinuclear lanthanide complex, $[(\eta^1\text{-}ONC_5H_6Me_4)_2Sm(\mu\text{-}\eta^1\text{: }\eta^2\text{-}ONC_5H_6Me_4)]_2$, contains η^1, η^2, and μ_2-TEMPO ligands.[149] Very few examples of Group 10 metal-TEMPO compounds with Ni and Pd were reported in the literature but there are no reported platinum-TEMPO compounds.

The inspiration for all the work that has been presented in this chapter comes from the unsuccessful attempt to trap the proposed photolytically generated Ni radical $\bullet Ni(SnBu^t_3)(CNBu^t)_2(CO)$ with TEMPO radical, that was discussed in chapter 4. There we isolated the $16e^-$ square planar complex $Ni(\eta^2\text{-TEMPO})(SnBu^t_3)(CNBu^t)$, **4.5** with a distorted square planar structure, as shown in Figure 5.1.

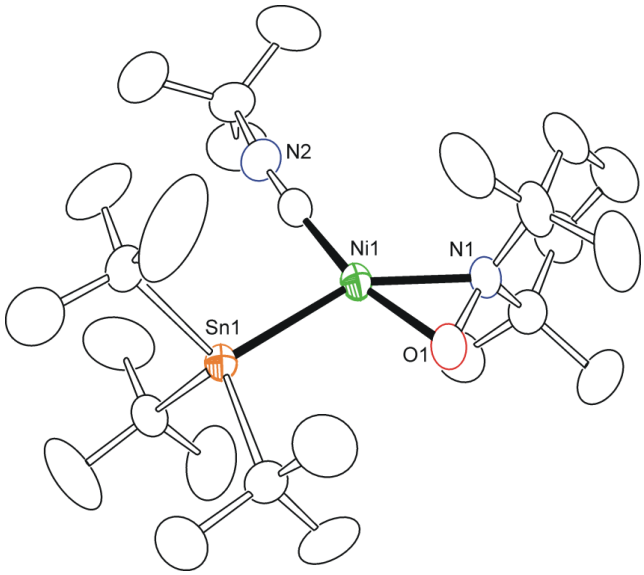

Figure 5.1. An ORTEP showing the molecular structure of Ni(η^2-TEMPO)($SnBu^t_3$)($CNBu^t$), **4.5** at 30 % thermal ellipsoid probability.

As it can be seen in Figure 5.1, the TEMPO ligand is coordinated to Ni center in an η^2 mode by inducing the elimination of both an isocyanide and CO ligand from tetrahedral •Ni($SnBu^t_3$)($NCBu^t$)$_2$(CO) to form Ni(η^2-TEMPO)($SnBu^t_3$)($CNBu^t$), **4.5** This Ni-O-N metallacycle is remarkably stable to subsequent reactions with *tert*-butyl isocyanide, Bu^tSnH, or carbon monoxide, even in great excess. The preferential binding of TEMPO radical with Ni center as 3e$^-$ donating η^2- TEMPO to form a 16e$^-$ square planar geometry as opposed to the η^1-O-TEMPO may be due to some thermodynamic preference as suggested in literature .[233] All of the published Ni or Pd-TEMPO compounds are square planar and possess this η^2- TEMPO ligand.[170,177,194,195,234–236] As mentioned before the interesting complex **4.5** (see Figure 5.1) led us to start an excited chemistry exclusively with the TEMPO radical as ligand. Reported in this chapter is the synthesis and characterization of Ni(η^2-TEMPO)$_2$, the first example of 16 e$^-$ unsaturated mononuclear transition metal complex supported exclusively by the TEMPO ligand

system and detailed reactivity study of Ni(η^2-TEMPO)$_2$ with a wide variety of chemical reagents as depicted in Scheme 5.1 , where the reactivity of the complex Ni(η^2-TEMPO)$_2$ is assisted by the TEMPO ligand to transform from an η2 binding mode to an η1 binding mode. Here is also reported detailed computational mechanistic studies on the reactivity of Ni(η^2-TEMPO)$_2$.

Note: All complex designations were suffixed with a ***t*** or ***c*** to distinguish between the two isomeric possibilities, *trans* and *cis* of Ni(η^2-TEMPO)$_2$ and its complexes with various reagents.

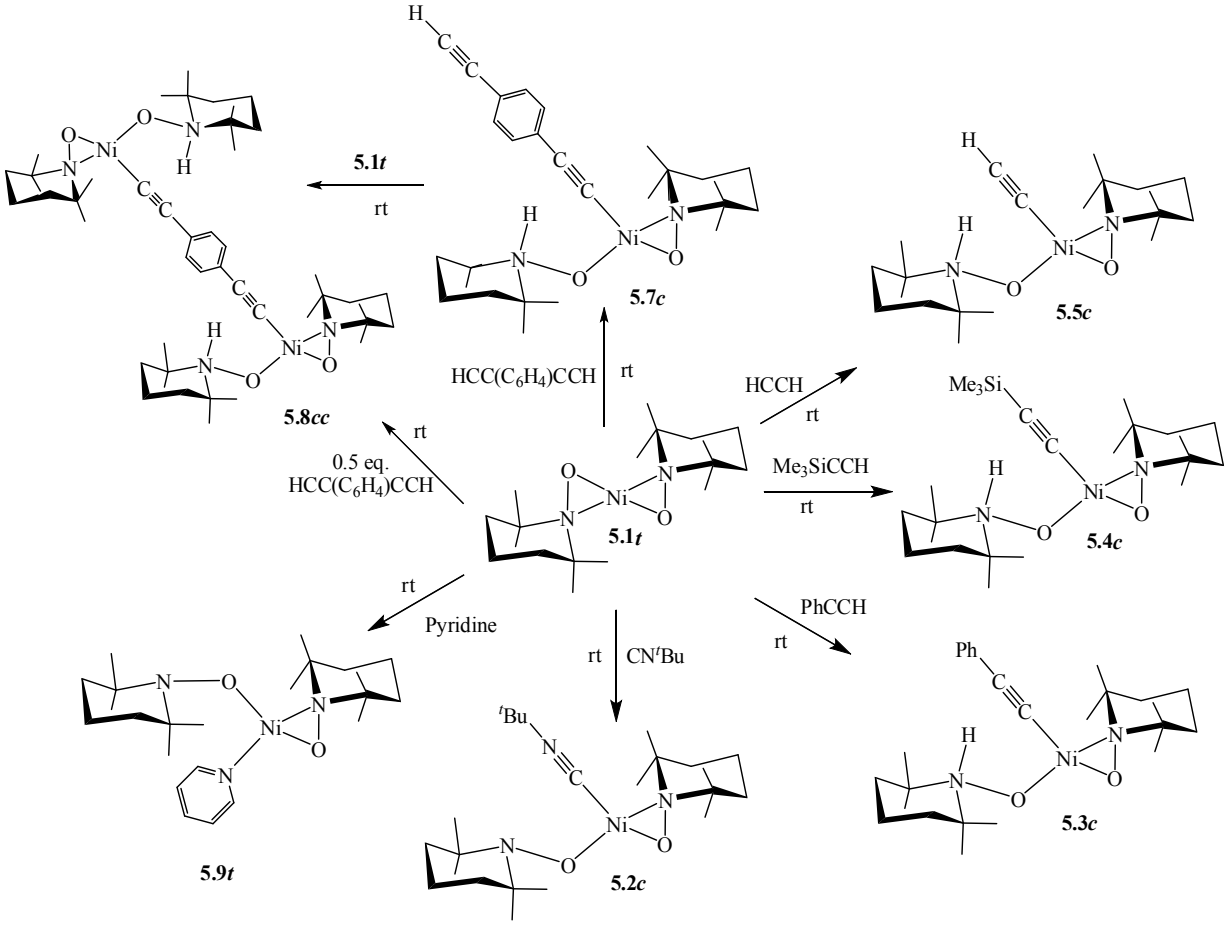

Scheme 5.1. Products of Ni(η^2-TEMPO)$_2$, **5.1*t*** with various reagents.

5.2 Computational methods.

Computational studies on all the compounds discussed in this chapter were performed in collaboration with Charles Edwin Webster, Department of Chemistry, University of Memphis. All computations were performed using the Gaussian09 software package.[237] Gas-phase energies, optimized geometries, and unscaled harmonic vibrational frequencies were obtained using density functional theory (DFT).[238] The hybrid B3LYP[239,240] and pure PBEPBE[241] functionals were used with default grid parameters (the PBEPBE functional will be referred to as PBE throughout the article, default pruned fine grids (75 radial shells, 302 angular points) for energies and default pruned course grids for gradients and Hessians (35 radial shells, 110 angular points). There are few qualitative differences between the structural and energetic PBE and B3LYP results. Therefore, all discussion in the text will refer to the PBE functional, and B3LYP data will be presented as Supporting Information. The basis set for nickel was the Hay and Wadt basis set and effective core potential (ECP) combination (LANL2DZ),[242,243] as modified by Couty and Hall (Ni: 341/341/41),[244] where the two outermost p functions have been replaced by a split of the optimized Ni 4p function, respectively. All C, N, O, and H atoms utilized the 6-31G(d′) basis set,[245,246]{The 6-31G(d′) basis set has the d polarization functions for C,N, and O taken from the 6-311G(d) basis set, instead of the original arbitrarily assigned value of 0.8 used in the 6-31G(d) basis set}. Spherical harmonic d-functions were used throughout; i.e., there are five angular basis functions per d-function. The Hessian of the energy was computed at all stationary points to designate them as either minima or transition states (first-order saddle points). Zero-point energies (ZPE) and thermal enthalpy/free energy corrections

were computed at 1 atm and 298.15 K. Aqueous solvation energies were computed using the SMD model with standard cavity parameters for n-hexane.[247] For the major reactants and products investigated, the computed singlet energies were generally lower by 8−10 kcal mol−1 than corresponding geometry-optimized triplet states. Therefore, all reported mechanisms and relative energies refer to closed-shell singlet species (except for the free TEMPO radical).

Note: Mechanistic pathways of addition reactions of the various adducts (*tert*-butyl isocyanide, phenylacetylene, pyridine, acetylene, 1, 4-diacetylenebenzene, and trimethylsilyl acetylene, respectively) are discussed in the section: Kinetics, Thermodynamics, and Possible Isomerization Mechanisms.

5.3. Results and discussion.

Reaction of Ni(COD)$_2$ with TEMPO radical: When two equivalents of (2,2,6,6-tetramethylpiperidin-1-yl)oxyl, TEMPO, radical were added to the hexane solution of one equivalent of (1,5-biscyclooctadiene) nickel, Ni(COD)$_2$, under argon atmosphere at room temperature, a color change from light orange to deep purple occurred over a period of approximately 10 minutes. The reaction was found to be almost instantaneous at 68 °C. Removal of volatiles in *vacuo* and crystallization of the solid residue from diethyl ether yielded purple colored block crystals of Ni(η^2-TEMPO)$_2$, **5.1*t*** in 78 % yield. The ORTEP diagram of complex **5.1*t*** is shown in Figure 5.2. Complex **5.1*t*** was characterized by ^{1}H NMR, mass spectroscopy, and X-ray diffraction analysis. Further crystallographic data can be found in Appendix D Table D.1. Complex **5.1*t*** is highly air and moisture sensitive and crystallographic analysis data was collected at 100 K under flow of N_2 to avoid fast crystal decomposition.

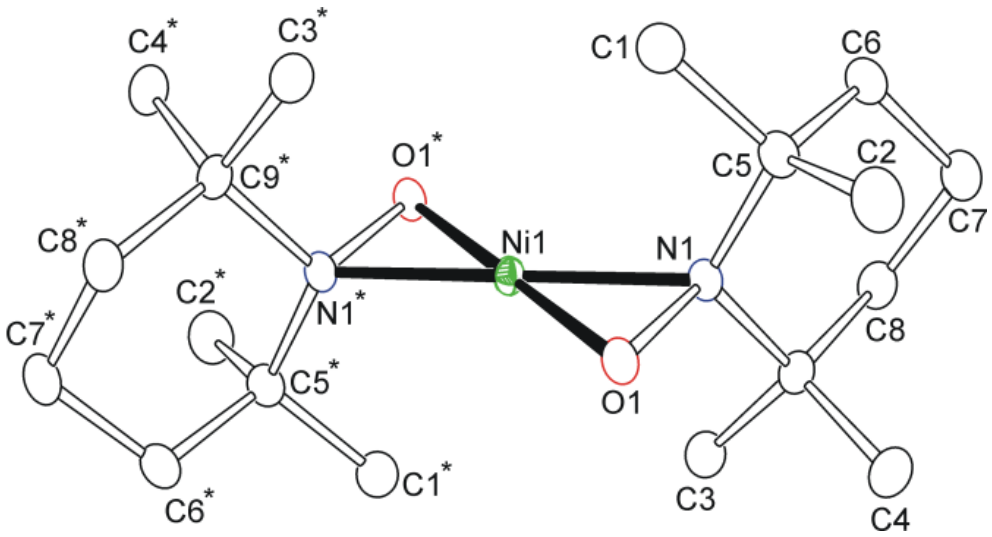

Figure 5.2 An ORTEP of the molecular structure of Ni(η^2-TEMPO)$_2$, **5.1*t*** showing 50 % thermal ellipsoid probability. Selected bond distances (Å) and angles (°) are: Ni1-O1=1.8404(11), Ni1-N1=1.9360(10), N1-O1=1.4136(12), N1-C5=1.5240(16), N1-C5=1.5240(16), O1-Ni1-O1* =180.0, N1-Ni1-N1*=180.0, N1-Ni1-O1=43.88(4), N1-Ni1-O1*=136.12(4), N1-O1-Ni1=71.66(6), O1-N1-Ni1=64.47(6), C5-N1-O1=110.83(9), C5-N1-Ni1=119.99(8).

As you see in Figure 5.2 the nickel, nitrogen, and oxygen atoms all lie in the same plane creating a "bow-tie" type rectangular planar structure. In the solid state, the molecule lies about an inversion center and can be viewed to overall possess approximately C_{2h} symmetry. The N-O bond distance is 1.4136(12) Å, which is longer than that found in free TEMPO [1.283(9) Å]. The N-Ni-O angle is 43.88(4)°. The geometry around the nitrogen atom is pyramidal [O1-N1-C5 = 110.83(9)°, O1-N1-C9 = 110.97(9)°, C5-N1-C9 = 116.59(9)°], and the Ni-N and Ni-O bond distances are short [Ni1-N1= 1.9360(10) Å, Ni1-O1=1.8404(11) Å]. These structural parameters are consistent with the bidentate monoanionic reduced TEMPO radical, which are known to act as neutral 3e$^-$ or anionic 4e$^-$ donors.[231,233] These observations conclude that the complex **5.1*t*** is a 16e$^-$ unsaturated complex with a formal oxidation of +2 on the Ni metal center.

The DFT optimized structure of **5.1*t*** was also found to possess C_{2h} symmetry with structural parameters in reasonable agreement with those of the X-ray crystal structure (Table 5.1). The metal-ligand bond distances are slightly longer than experimental results (0.020 for $r_{e\text{-}Ni\text{-}O}$ and 0.044 Å for $r_{e\text{-}Ni\text{-}N}$). Typical of DFT results, intraligand bond distances (C−C, N−O TEMPO bonds) are shorter than the X-ray crystal structure parameters of **5.1*t*.**

Ni(η^2-TEMPO)$_2$	**Theory 5.1*t***	**Expt. 5.1*t***
Ni-O r_e	1.8870 Å	1.8404 Å
Ni-N r_e	1.9733 Å	1.9360 Å
N-O TEMPO r_e	1.3882 Å	1.4136 Å
N-Ni-O angle	41.89°	43.88°
O-N-C angle	112.13°	110.83°
C-N-C angle	116.46°	116.59°
free TEMPO ligand N-O r_e	1.2798 Å	1.283[a]
free TEMPO anion N-O r_e	1.3966 Å	

Table 5.1. Geometric parameters of compound **5.1*t*** using the PBE level of theory. [a] see the reference for the data.[233]

The "cis" complex with C2 point group symmetry has also been theoretically determined which we are not able to isolate experimentally (**5.1*c***; see Scheme 5.2). Scheme 5.3 also shows 2D illustrations and a simplified interpretation of the 2D structural skeleton of **5.1** that will be used throughout further schemes. In the *cis* structure, the Ni−O bond is shortened, while the Ni−N bond is elongated. For all substituted complexes (vide infra) as well as complex **5.1**, only a single isomer has been isolated and characterized experimentally

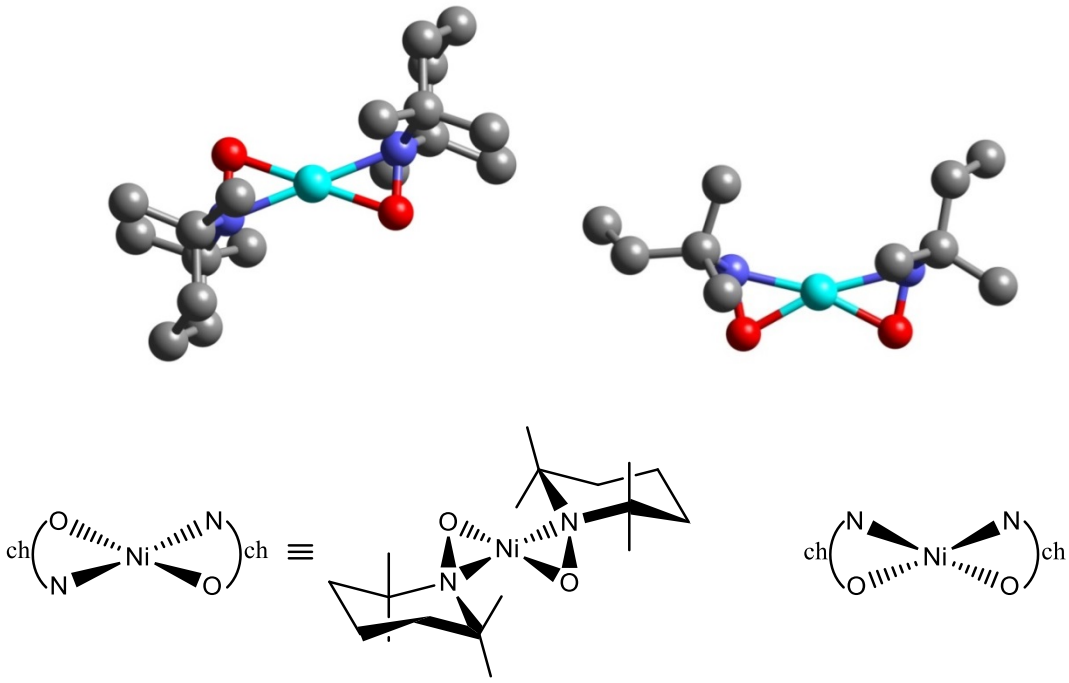

5.1*t* **5.1*c***

Scheme 5.2. Structures of **5.1*t*** and **5.1*c*.**[a] ([a] Hydrogen atoms omitted for clarity).

Two monoanionic η^2 -TEMPO ligands can each serve as 4 e^- donors giving the Ni atom a 16 electron configuration and a formal oxidation state of 2+ (d^8). Proton NMR study of this purple compound confirmed that the solid state η^2 binding mode persists in solution, displaying magnetically inequivalent methyl groups of the TEMPO as two distinct sets exist on differing sides of the N-O bonds. Even at extreme temperatures these acute Ni-O-N metallacycles appear to be stable as little change was found in the variable temperature ^{1}H NMR spectrum from -80 °C to 90 °C in toluene-d_8. However , as stated earlier, **5.1*t*** is extremely air and moisture sensitive and exposure to either one results in rapid decomposition to colorless products which are insoluble in all the tested solvents.

Reaction of Ni(η^2-TEMPO)$_2$, 5.1*t*, with *tert*-Butyl Isocyanide, Bu^{t}NC: When one equivalent of CNBu^t was added to the hexane solution of **5.1*t***, a very quick color change from purple to dark red was observed. After which, the reaction mixture was stirred for 10 minutes and the volatiles were removed in *vacuo*. Crystallization of the solid residue from diethyl ether gave red colored blocks of Ni(η^2-TEMPO)(η^1-TEMPO)(κ^1-CNBu^t), **5.2*c***, in 90 % yield. X-ray crystallographic analysis of these crystals yielded the distorted square planar structure for **5.2*c*** shown in Figure 5.3. Further crystallographic information is provided in Appendix D, Table D.1.

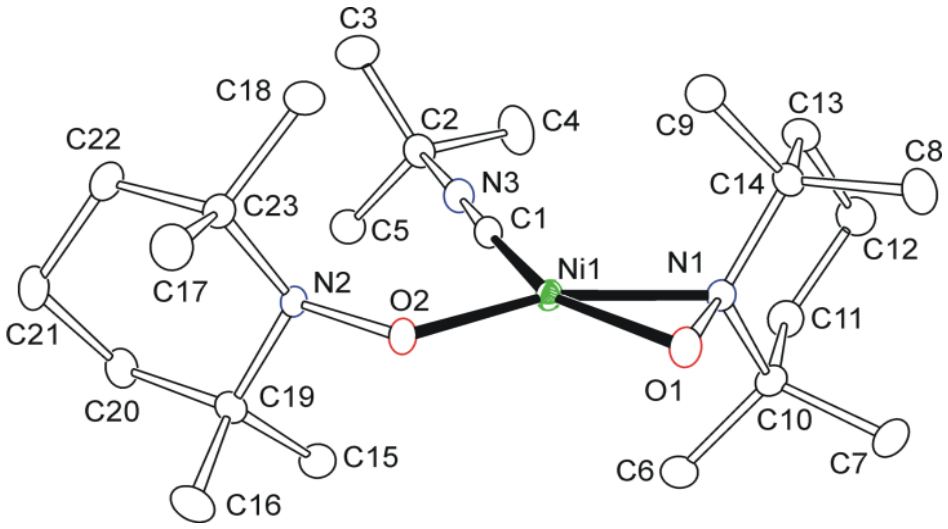

Figure 5.3. An ORTEP showing the molecular structure of Ni(η^2-TEMPO)(η^1-TEMPO)(κ^1-CNBu^t), **5.2*c*** at 50 % thermal ellipsoid probability. Selected bond distances (Å) and angles (°) are: Ni1-O1=1.8796(7), Ni1-N1=1.8801(8), Ni1-O2=1.8378(7), Ni1-C1=1.8210(10), N1-O1=1.3851(10), N2-O2=1.4354(10), C1-N3=1.1544(13), N1-Ni1-O1=43.23(3), O1-Ni1-C1=153.50(4), C1-Ni1-O2=100.59(4), N1-Ni1-C1=110.27(4), O1-Ni1-O2=105.90(3),N2-O2-Ni1=115.02(5),Ni1-N1-O1=68.37(4), Ni1-O1-N1=68.40(4).

Compound **5.2*c*** was characterized by the combination of ^{1}H NMR, FTIR, mass spectroscopy, and X-ray crystallographic analysis. Compound **5.2*c*** is also highly air and moisture sensitive like **5.1*t*** and to avoid rapid crystal decomposition, crystallographic data was collected at 100 K under flow of N_2 gas.

As is evident from Figure 5.3, compound **5.2*c*** has a distorted square planar structure, but more importantly the complex has isomerized to a *cis* form and one of the η^2-TEMPO ligands in the starting complex **5.1*t*** has now become an η^1-bonding ligand. The electron count around nickel remains at 16 with the CNBu^t and η^1-TEMPO groups each, acting as two electron donors. The two TEMPO ligands remain reduced to their monoanionic TEMPO forms in **5.2*c***, giving a formal oxidation state of 2+ on the nickel metal center. The computed geometric parameters of *cis*-Ni(η^2-TEMPO)(k^1-TEMPO)(κ^1-CN^{t}Bu), **5.2*c*** are also in reasonable agreement with those of the X-ray crystal structure (Table 5.2).

Ni(η^2-TEMPO)(k^1-TEMPO)(κ^1-CNBu^t)	**Theory 5.2*c***	**Expt. 5.2*c***
Ni-O η^1-TEMPO r_e	1.8613 Å	1.8378 Å
Ni-O η^2-TEMPO r_e	1.9423 Å	1.8796 Å
N-O η^1-TEMPO r_e	1.3769 Å	1.4354 Å
N-O η^2-TEMPO r_e	1.3648 Å	1.3851 Å
Ni-C κ^1 - CNBu^t r_e	1.7780 Å	1.8210 Å

Table 5.2. Geometric parameters of compound **5.2*c*** using the PBE level of theory.

The companion *trans* structure (**5.2*t***) has not been isolated. No square pyramidal Ni(η^2-TEMPO)(k^1-TEMPO)(κ^1-CNBu^t) complexes were located, which corresponds to the hypothesis of steric crowding from the incoming CNBu^t ligand,[231] and all the computations were collapsed to either **5.2*c*** or **5.2*t***. To better understand these sterics, space filling models are also prepared (see Figure 5.4). As is evident from the Figure 5.4 the axial sites above and below the N1-O1-N1*-O1* square plane are simply not accessible as the bulky methyl groups are shielding the Ni atom (shown in green) completely. However, the Ni atom can be accessible from equatorial position as the shielding from methyl groups is not that effective in the equatorial position. The

mechanistic pathway for the formation of **5.2*c*** is discussed in the section: Kinetics, Thermodynamics, and Selectivity of Substituted Species.

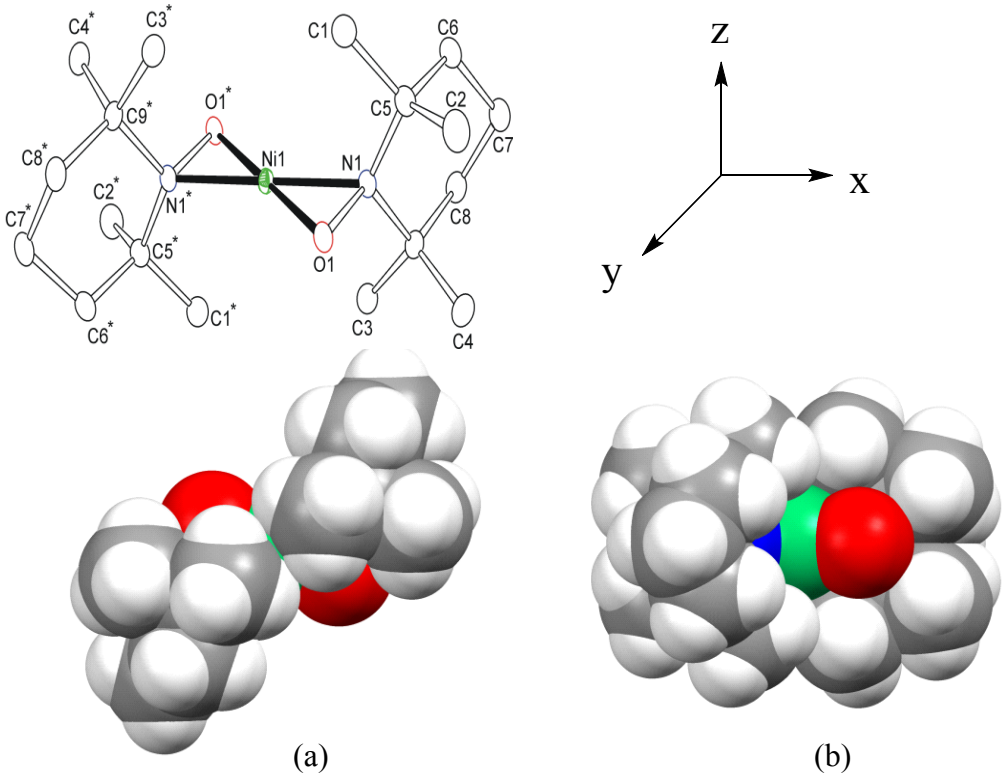

Figure 5.4. Space-filling model of Ni(η^2-TEMPO)$_2$, **5.1*t*** seen from (a) down the C_2 (Z) axis above the square plane and (b) down the XY plane perpendicular to the C_2 (Z) axis. Atomic dimensions are the van der Waals radii. Nickel is shown in green, oxygen in red, nitrogen in blue, carbon in gray, and hydrogen in white.

The ^{1}H NMR spectrum of complex **5.2*c*** at room temperature consists of a series of broad overlapping peaks indicative of some dynamical processes occurring in solution. Variable temperature ^{1}H NMR spectra in the range of 25° to 90 °C resulted in some sharpening of the peaks, however, as shown in Appendix D Figure D.1, peak broadening stayed even at the high temperature of 90 °C. Above 90 °C the complex decomposes.

Similar fluxional processes were observed in the ^{1}H NMR spectra of complex **5.9*t*,** a complex of **5.1*t*** with pyridine,that will be discussed later in this chapter. These fluxional processes appear to be due to equilibrium formation in solution due to weak bonding interactions between the reagents. Though it is clear that some exchange occurs within this molecule, the exact nature of the fluxional process remains unresolved presently.

Reaction of Ni(η^2-TEMPO)$_2$, 5.1*t* with Phenylacetylene, HC≡CPh: Nickel complexes are known to catalytically activate C≡C bonds.[248,249] Keeping this in mind, we wanted to see how complex **5.1*t*** reacts with the alkynes, as alkynes are well known to coordinate with the metal centers in two different ways, "side-on" η^2 or "end-on" $k^1(\eta^1)$. When 1eq of phenylacetylene was added to a hexane solution of Ni(η^2-TEMPO)$_2$, **5.1*t*** a color change from purple to red occurred over a period of less than 1 hour. The reaction is almost instantaneous at 68 °C reflux. Removal of volatiles in *vacuo* and crystallization from diethyl ether resulted in light red bars of Ni(η^2-TEMPO)(κ^1-TEMPOH)(κ^1-CCPh), **5.3*c*** in 73 % yield. X-ray crystallographic analysis generated distorted square planar structure for **5.3*c***, as shown in Figure 5.5. Further crystallographic information is provided in Appendix D Table D.2. This complex was characterized by the combination of ^{1}H NMR, FTIR, mass spectroscopy, and X-ray crystallographic analysis. Complex **5.3*c*** is moderately air and moisture sensitive and crystallographic data was collected at 100 K under flow of N_2 to avoid crystal decomposition.

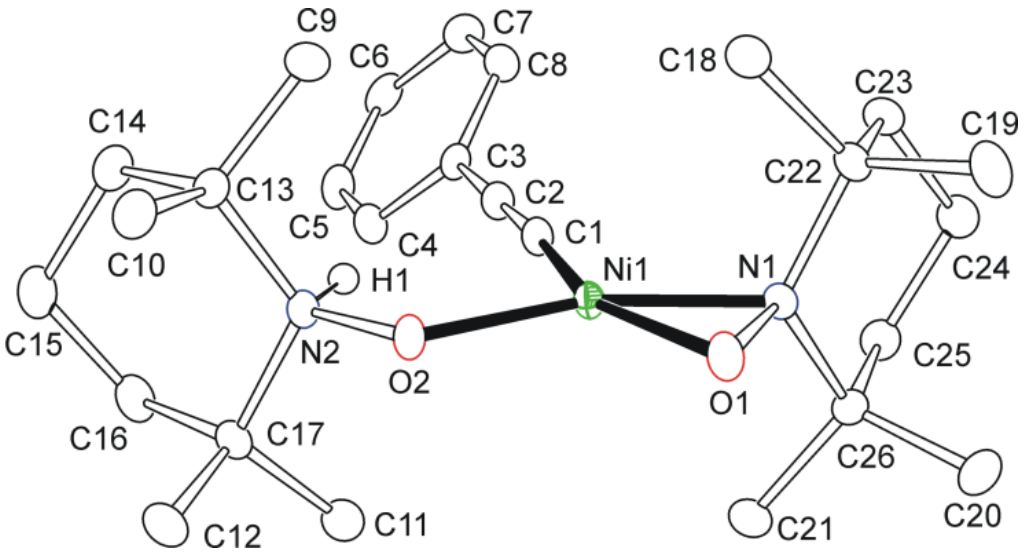

Figure 5.5. An ORTEP showing the molecular of Ni(η^2-TEMPO)(κ^1-TEMPOH)(κ^1-CCPh), 5.3*c* at 50 % thermal ellipsoid probability. Selected bond distances (Å) and angles (°) are: Ni1-O1=1.8868(7), Ni1-N1=1.8608(8), Ni1-O2=1.8927(7), Ni1-C1=1.8648(10), N1-O1=1.3869(10), N2-O2=1.4048(10), C1-C2=1.2205(14), N1-Ni1-O1=43.43(3), O1-N1-C22=112.57(7), O1-N1-C26=112.92(7), C22-N1-C26=118.21(7), O2-N2-C13=110.87(7), O2-N2-C17=110.52(7), C13-N2-C17=118.06(7).

As evident from Figure 5.5, the phenylacetylene reagent did not bind to the Ni atom in side-on, η^2 mode but has rather been transformed into an "end-on" phenylacetylide group, k^1-C≡CPh. This reaction is an unusual example of sp hybridized C-H bond activation (~ 130 kcal/mol)[250,251] by a group 10 organometallic complex which is somewhat uncommon for that group. Very few complexes of the type Ni(k^1-CCPh) were reported in the literature and nearly all of them were synthesized using salt metathesis or other intricate procedures.[252–256] Even most of the published Pt and Pd phenylacetylides require several step syntheses or intense UV photolysis.[56,256–261] The facile room temperature activation of a sp hybridized C-H bond and formation of an η^1-CCPh phenylacetylide was unusual, surprising, and shows unexpected chemical reactivity of the non-precious nickel metal.

Based on the X-ray crystal structure data collected at 100 K, the position of the H atom on the atom N2 that was coming from PhCC-**H** was located and refined satisfactorily. Further, it was also monitored by ^{1}H NMR which showed a peak at 7.62 ppm with an appropriate integration of one H. The location of the H atom on nitrogen was further established by 2D [^{1}H, ^{15}N] HSQC NMR which showed a direct correlation between atoms N2 and H1 with an observed $^{1}J(^{15}$N-H) coupling constant of 78 Hz, see Appendix D Figure D.2.[262–264]

When the complex **5.1*t*** was reacted with phenylacetylene-d_1 (99 %), it gave the complex **5.3*c*-*d*$_1$** and its ^{1}H NMR spectrum showed all the appropriate resonances for **5.3*c***, with the exception of the peak at 7.62 ppm which was almost totally absent (see Appendix D Figure D.3). Compound **5.3*c*** remains a 16 electron Ni(II) complex, with the κ^1-TEMPOH ligand acting as a 2 electron donor neutral ligand. The κ^1-TEMPOH ligand is now protonated at nitrogen and can be viewed as a monoanionic TEMPO, as in the tautomeric form of free TEMPOH (where H is bonded to O). This type of bonding mode for κ^1-TEMPOH is rather rare in transition metal complexes and there are only few other crystallographically characterized examples.[193,265,266] Interestingly, the structure of **5.3*c*** is also *cis*-disposed compared to the unsubstituted complex **5.1*t***. Computed geometries of **5.3*c*** (see Table 5.3) show excellent structural agreement with the experimental crystal structure due to an elongated Ni−O η^2- TEMPO bond and a much shorter Ni−N η^2-TEMPO optimized bond length. In free TEMPO, the N−O bond length is 1.283(9) Å,19 while, once coordinated, the N−O bond length is elongated (by more than ~0.1 Å), which is expected for a reduced monoanionic ligand with a pyramidal geometry about the nitroxyl N atom. Interestingly, in the compounds **5.2*c*** and **5.3*c*** (along with the other

following complexes), the side-bound η^2-TEMPO always has a shorter N−O bond than the end-bound k^1-TEMPO. These results suggest the k^1-TEMPO ligand is more anionic than the η^2- TEMPO ligand, possibly depopulating a N−O antibonding orbital in the η^2 case, with the net result that the Ni center donates more electrons to η^1-TEMPO.

Ni(η^2-TEMPO)(κ^1-TEMPOH)(κ^1-CCPh)	**Theory**	**Expt.**
Ni-O κ^1-TEMPOH r_e (Å)	1.9242	1.8927
Ni-O η^2-TEMPO r_e (Å)	1.9402	1.8868
Ni-N η^2-TEMPO r_e (Å)	1.8914	1.8608
N-O κ^1-TEMPOH r_e (Å)	1.3888	1.4048
N-O η^2-TEMPO r_e (Å)	1.3567	1.3869
N-H κ^1-TEMPOH r_e (Å)	1.0557	n.d.
Ni-C CCPh r_e (Å)	1.8385	1.8648
C-C CCPh r_e (Å)	1.2535	1.2205

Table 5.3. Geometric parameters of compound **5.3*c*** using the PBE level of theory.

In order to find out any observable differences in the reaction of **5.1*t*** in the abstraction of H/D, a 1:1 mixture of PhCCH and PhCCD in toluene-d_8 solvent was prepared and the reaction was monitored by ^{1}H NMR at room temperature. Integration of the resonances of the product showed approximately a 50:50 ratio for the formation of products **5.3*c*** and **5.3*c*-*d*$_1$**, indicating that there was no noticeable difference between the rates of formation of the products **5.3*c*** and **5.3*c*-*d*$_1$**. The reaction was also monitored by ^{2}H{^{1}H} NMR using toluene solvent, and the appropriate integration of the singlet deuterium resonances in the starting PhCCD verses the product N-D resonances in **5.3*c*-*d*$_1$** also showed approximately a 50:50 ratio. This reaction was also monitored using a 6:6 mixture of PhCCH and PhCCD, to give the same product ratio (see Appendix D Figure D.4 and D.5). This result is interpreted as being consistent with an addition mechanism that does not involve deprotonation of the C−H or C−D bond as the rate determining step,

in keeping with the computational results discussed in the section 'Kinetics Thermodynamics, and Selectivity of Substituted Species'.

Reaction of 5.1*t* with Trimethylsilyl acetylene, $Me_3SiC{\equiv}CH$ and Triisopropylsilyl acetylene, $^{i}Pr_3SiC{\equiv}CH$: Reactivity study of **5.1*t*** with alkynes was further extended to Me_3SiCCH and $^{i}Pr_3SiCCH$. These two silyl acetylenes are similar in structure with the only difference of steric crowdedness around the Si atom imparted by Me_3 groups in Me_3SiCCH (less bulky) and $^{i}Pr_3$ in $^{i}Pr_3SiCCH$ (more bulky).

When one equivalent of Me_3SiCCH was added to a room temperature hexane solution of **5.1*t*,** a color change from purple to light red occurred over a period of less than one hour. The reaction was almost instantaneous at 68 °C. The volatiles were removed in *vacuo* and the crystallization of solid residue in diethyl ether afforded bright red blocks of Ni(η^2-TEMPO)(κ^1-TEMPOH)(κ^1-$CCSiMe_3$), **5.4*c*** in 79 % yield. X-ray crystallographic analysis yielded the distorted square planar structure of shown in Figure 5.6. Further crystallographic information is provided in Appendix D Table D.2. This complex was characterized by ^{1}H NMR, FTIR, mass spectroscopy, and X-ray crystallographic analysis. Complex **5.4*c*** is stable in air compared to the previous compounds, and X-ray crystallographic data was collected successfully at ambient conditions with no apparent decomposition in the crystal.

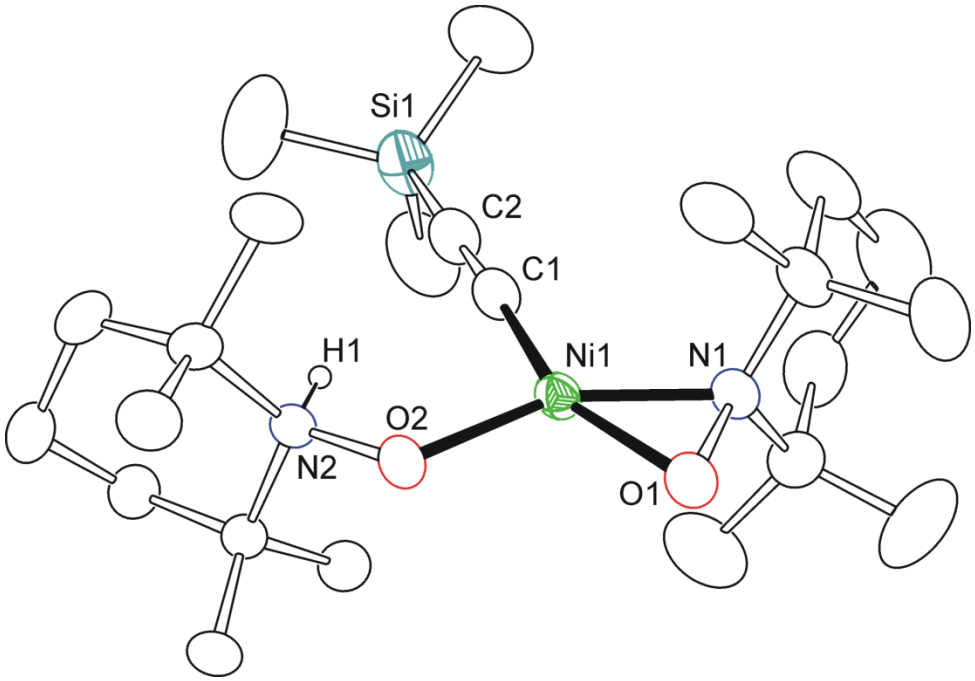

Figure 5.6. An ORTEP showing the molecular structure of Ni(η^2-TEMPO)(κ^1-TEMPOH)(κ^1-CCSiMe$_3$), **5.4*c*** at 30 % thermal ellipsoid probability. Selected bond distances and angles are as follows: Ni1−C1 = 1.860(3) Å, Ni1−N1 = 1.862(2) Å, Ni1−O1 =1.8701(17) Å, Ni1−O2 = 1.8871(15) Å, C1−C2 = 1.223(4) Å, N1−O1 = 1.388(2) Å, N2−O2 = 1.402(2) Å, and Si1−C2 = 1.806(3) Å;C1−Ni1−N1 = 111.84(9)°, C1−Ni1−O1 = 155.47(9)°, N1−Ni1−O1 = 43.66(7)°, C1−Ni1−O2 = 99.95(9)°, N1−Ni1−O2 =148.21(7)°, O1−Ni1−O2 = 104.56(7)°, N1−O1−Ni1 = 67.86(11)°,N2−O2−Ni1 = 117.07(12)°, O1−N1−Ni1 = 68.49(11)°.

As seen in Figure 5.6, the crystal structure of the compound **5.4*c*** is similar to compound **5.3*c*.** The alkyne hydrogen from C-H of Me_3SiCCH was again abstracted and bonded to N2. Its position was identified and refined using X-ray crystallographic analysis and further confirmed by ^{1}H NMR. The FTIR spectrum shows a single C≡C stretch at lower frequency 2009 cm^{-1} in hexane, compared to other Ni-TEMPO-acetylene derivatives which can be attributed to the electropositive silicon atom donating electron density into the triple bond and weakening it.

Though Me_3SiCCH reacts with **5.1*t***, $^{i}Pr_3SiCCH$ does not react with **5.1*t*** at all even under refluxing conditions to yield the expected product Ni(η^2-TEMPO)(κ^1-TEMPOH)(κ^1-CCSi^{i}Pr$_3$) similar to **5.4*c*.**

Reaction with symmetrical alkynes and dimerization reactions: After exploring the reaction of Ni(η^2-TEMPO)$_2$, **5.1*t*** with substituted alkynes where sp hybridized C-H bond was successfully activated to generate monomeric Ni-TEMPO products, the reactivity of **5.1*t*** has been extended to symmetrical alkynes with two sp hybridized C-H bonds to check the possibility of synthesizing bridged Ni-TEMPO products where two Ni metal atoms will be bridged with the carbon-carbon bonds; these type of compounds can be used for charge transfer reactions and also have the potential to further develop into molecular wires. The first symmetrical alkyne that has been tried is acetylene.

Reaction of Ni(η^2-TEMPO)$_2$ with Acetylene Gas, HC≡CH: When acetylene gas was purged through a hexane solution of **5.1*t***, a color change from purple to light red occurred over the period of one hour. The reaction was found to be almost instantaneous at 68 °C reflux. Removal of volatiles in *vacuo* followed by crystallization from diethyl ether afforded bright red blocks of Ni(η^2-TEMPO)(κ^1-TEMPOH)(κ^1-CCH), **5.5*c*** in 74 % yield. X-ray crystallographic analysis yielded the distorted square planar structure for the complex, **5.5*c***, shown in Figure 5.7. Further crystallographic information is provided in Appendix D Table D.2.

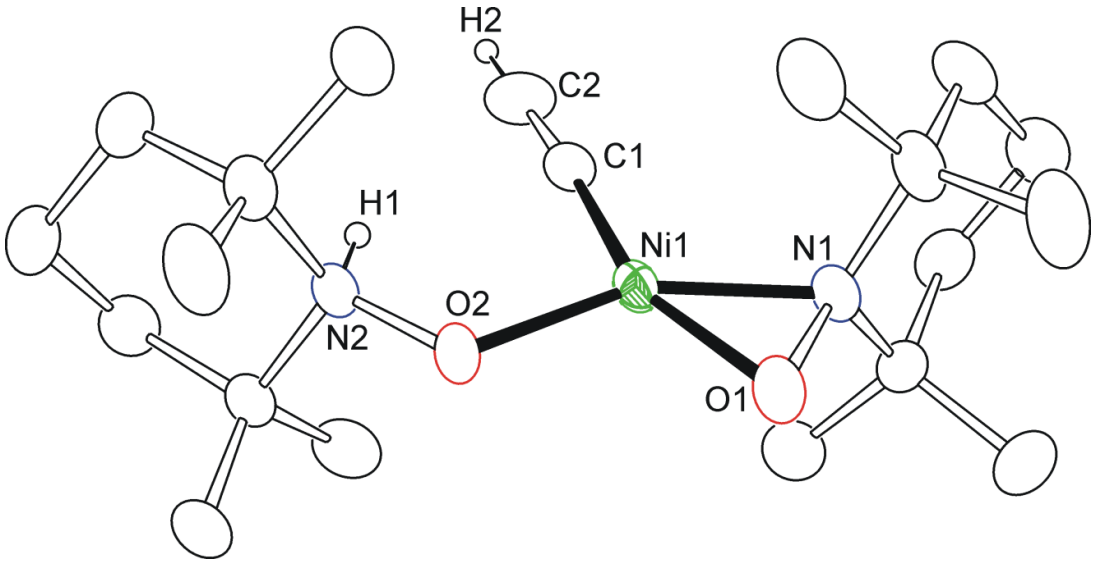

Figure 5.7. An ORTEP showing the molecular structure of Ni(η^2-TEMPO)(κ^1-TEMPOH)(κ^1-CCH), **5.5*c*** at 30 % thermal ellipsoid probability. Selected bond distances and angles are as follows: Ni1−O1 = 1.8614(12) Å, Ni1−C1 = 1.8708(15) Å, Ni1−N1= 1.8750(12) Å, Ni1−O2 = 1.8878(10) Å, N1−O1 = 1.3877(15) Å, N2−O2 = 1.4011(14) Å, and C1−C2 = 1.195(2) Å; O1−Ni1−C1 =157.23(5)°, O1−Ni1−N1 = 43.60(5)°, C1−Ni1−N1 = 113.66(6)°, O1−Ni1−O2 = 103.17(4)°, C1−Ni1−O2=99.59(5), N1−Ni1−O2 =146.73(5)°, N1−O1−Ni1 = 68.72(7)°, N2−O2−Ni1 = 117.22(8)°, N2−O2−Ni1 = 117.22(8)°, and O1−N1−Ni1 = 67.68(7)°.

Compound **5.5*c*** was characterized by ^{1}H NMR, FTIR, mass spectroscopy, and X-ray crystallographic analysis. The structure of compound is similar to **5.3*c*.** Interestingly, only one C-H bond of HC≡CH was activated and again the position of hydrogen on N2 was successfully identified and refined using X-ray crystallographic analysis and its presence was further confirmed by ^{1}H NMR which showed the usual N-H resonance at 7.64 ppm. A crystallographic database search provided very few examples of "end-on" group 10 metal-CCH compounds, all of which were synthesized by salt elimination.[256,267–269] We believe **5.5*c*** to be the first structurally characterized example of acetylene C-H bond activation to yield a Ni-(k^1-CCH) compound. The FTIR stretch for the C≡C bond is now found at 1933 cm^{-1} in hexane, significantly lower in energy than

any of the other Ni-acetylene compounds above. Literature values for these terminal acetylides are also around 1930 cm^{-1}.[270]

As seen in Figure 5.8, there is another terminal alkyne C-H bond available, and it could be considered that the reaction of **5.1*t*** with acetylene gas would also yield a product, where another molecule of **5.1*t*** reacts with **5.5*c***, to give compound **5.6*cc*** as shown in Scheme 5.4. However, we did not obtain this product. This is explainable in terms of steric crowding and repulsion between the approaching TEMPO moieties that is limiting the accessibility to the already coordinated acetylide ligand. Another possibility could be that the pKa for the second proton in acetylene is much higher (more basic). Though **5.6*cc*** could not be synthesized, we were able to obtain and study the computational structures (Scheme 5.3).

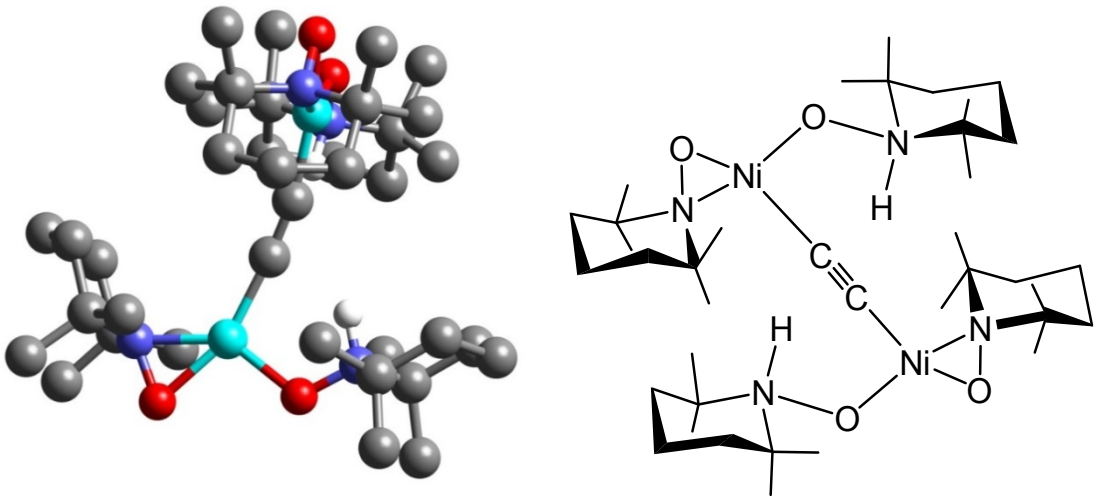

a **b**

Scheme 5.3. Structures of **5.6*cc*.** a) Computational structure (hydrogens omitted for clarity), b) Line drawing.

Unlike compound **5.8*cc*** (discussed below), one of the Ni(TEMPO)(TEMPOH) moieties in **5.6*cc*** is twisted 90 degrees (see computational structure) from the other to

relieve the pronounced steric repulsion. Compound **5.6*cc*** is not thermodynamically favored over its constituent monomers. The dimerization thermodynamics can be computed in two ways, via addition of two equivalents of **5.1*t*** and HCCH, or via the reaction of **5.1*t*** and **5.5*c***. The computed solution-phase free energy of reaction is quite large and positive for both cases: +5.4 and +9.2 kcal mol^{-1} (see Table 5.4 and Table D.4 in Appendix D).

Reaction	ΔG_{soln} (kcal mol^{-1})	$\Delta\Delta G_{soln}$ (kcal mol^{-1})
2 equiv **5.1*t*** + HCCH → **5.6*cc***	5.4	
5.5*c* + **5.1*t*** → **5.6*cc***	9.2	
5.8*cc* [a]		0
5.8*ct*		4.1
5.8*tt*		9.2
2 equiv **5.1*t*** + HCCPhCCH → **5.8*cc***	−5.2	
5.7*c* + **5.1*t*** → **5.8*cc***	−0.8	

[a] Isomer **5.8*cc*** is arbitrarily set to 0.0 kcal mol^{-1} .

Table 5.4. Solution-Phase reaction free energies (ΔGsoln in kcal mol^{-1}) of bimetallic complexes and the relative free energies (ΔΔGsoln in kcal mol^{-1}) of Isomers of **5.8*cc*.**

Reaction of 5.1*t* with 1, 4-Diethynylbenzene, HC≡C(C_6H_4)C≡CH: After learning that **5.1*t*** activates only one C-H bond of small acetylene molecule work has been extended to other interesting aromatic alkyne 1, 4-diethynylbenzene to further explore the efforts to link two Ni(TEMPO)$_2$ molecules. The alkyne, 1, 4-diethynylbenzene is an interesting

aromatic compound consisting of a benzene ring substituted with two acetylene groups positioned *para* to each other, shown in Figure 5.8.

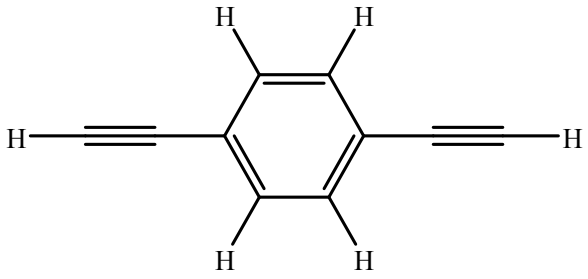

Figure 5.8. Line drawing of 1,4-diethynylbenzene.

When 1eq of 1,4-diethynylbenzne was added to a hexane solution of **5.1*t***, a color change from purple to auburn red occurred over a period of 1 hour. The reaction is nearly instantaneous at 68 °C. Removal of volatiles in *vacuo* and crystallization of solid residues from diethyl ether resulted in cherry red bars of Ni(η^2-TEMPO)(κ^1-TEMPOH)(κ^1-CC[C_6H_4]CCH), **5.7*c*** in 71% yield. X-ray crystallographic analysis yielded the anticipated distorted square planar structure as shown in Figure 5.10. Further crystallographic information is provided in Appendix D Table D.2. Compound **5.7*c*** was characterized by ^{1}H NMR, FTIR, mass spectroscopy, and X-ray crystallographic analysis. Complex **5.7*c*** is remarkably stable in air compared to the preceding compounds.

Similar to the compounds **5.3*c*, 5.4*c*** and **5.5*c***, there is only one acetylide group bonded to the Ni center in **5.7*c*** (see Figure 5.9). Again, the position of the H atom bonded to N2 atom was located and refined satisfactorily from the data collected using X-ray crystallographic analysis. ^{1}H NMR spectroscopy again shows evidence for the N-**H** at 7.65 ppm with exact integration of one H, as well as also showing the second acetylene

hydrogen intact at 3.26 ppm in C_6D_6. FTIR spectroscopy gives the broad hump suggestive of a N-**H** stretch around 3200 cm^{-1}.

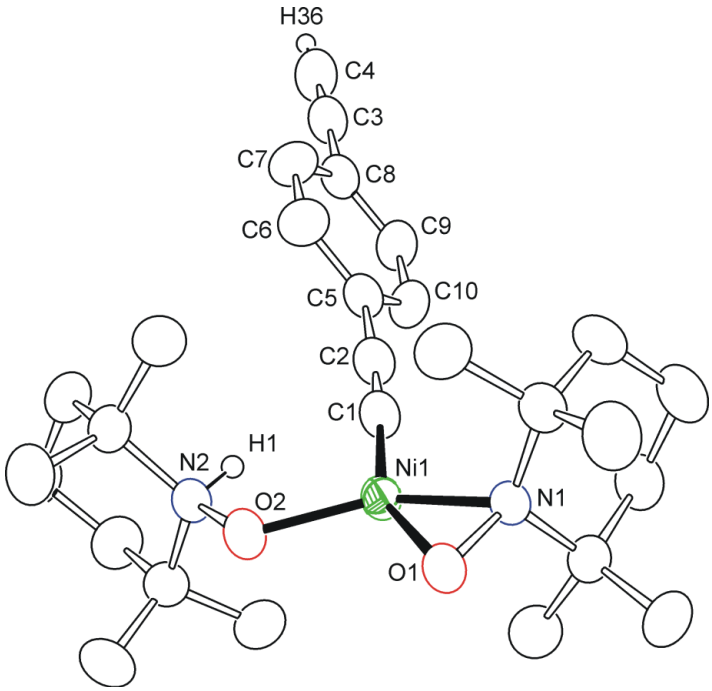

Figure 5.9. An ORTEP showing the molecular structure of Ni(η^2-TEMPO) (κ^1-TEMPOH)(κ^1-CC[C_6H_4]CCH), **5.7*c*** at 30 % thermal ellipsoid probability. Selected bond distances (Å) and angles (°) are: Ni1-N1=1.8605(9), Ni1-C1=1.8748(12), Ni1-O2=1.8890(8), Ni1-O1=1.8909(8), N1-O1=1.3840(11), N2-O2=1.4027(12), C1-C2=1.2146(17), N1-Ni1-C1=111.22(4), N1-Ni1-O2=149.15(4), C1-Ni1-O2=99.43(4), N1-Ni1-O1=43.29(3), C1-Ni1-O1=154.51(4), O2-Ni1-O1=106.02(3), O1-N1-Ni1=69.52(5), N1-O1-Ni1=67.19(5), N2-O2-Ni1=116.72(6).

The crystal structure of **5.7*c*** is similar to that of **5.3*c***, except now there is a free dangling alkyne hydrogen available for further reaction with another molecule of **5.1*t***. Assuming there is enough steric space to allow approach of **5.1*t***, this reaction should yield the dimeric product Ni(η^2-TEMPO)(κ^1-TEMPOH)[κ^1-κ^1-CC(C_6H_4)CC]Ni(η^2-TEMPO)(κ^1-TEMPOH), where two molecules of Ni(η^2-TEMPO)$_2$, **5.1*t*** are bridged by the dialkyne HC≡C(C_6H_4)C≡CH.

As expected, when the reaction was carried out with two equivalents of **5.1*t*** and one equivalent of 1,4-diethynylbenzne we did indeed obtain the complex Ni(η^2-TEMPO)(κ^1-TEMPOH)[κ^1-κ^1-CC(C_6H_4)CC]Ni(η^2-TEMPO)(κ^1-TEMPOH), **5.8*cc*** in 80 % yield where now two Ni(η^2-TEMPO)(κ^1-TEMPOH) groups are linked by a diacetylidebenzene group, see Figure 5.10. Consequently compound **5.8*cc*** is also synthesized by the reaction of compound **5.7*c*** with one equivalent of **5.1*t*** at room temperature.

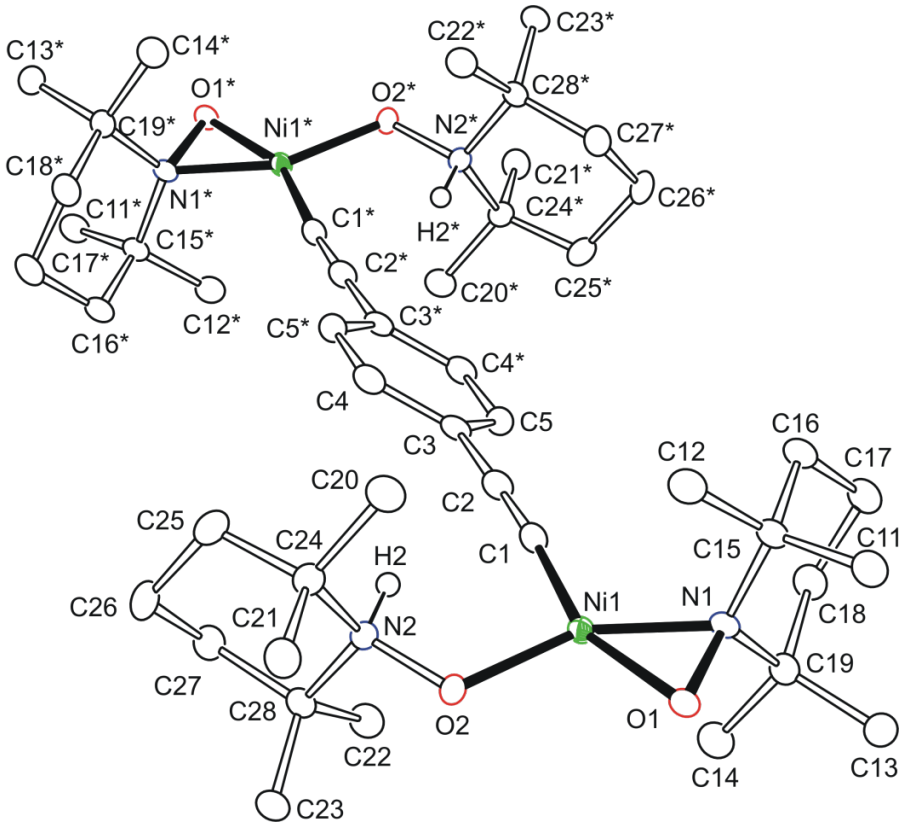

Figure 5.10. An ORTEP of the molecular structure of Ni(η^2-TEMPO)(κ^1-TEMPOH)[κ^1-κ^1-CC(C_6H_4)CC]Ni(η^2-TEMPO)(κ^1-TEMPOH), **5.8*cc*,** showing 50 % thermal ellipsoid probability. Selected bond distances (Å) and angles (°) are: Ni1-N1=1.8685(16), Ni1-C1=1.8582(19), Ni1-O2=1.8918(13), Ni1-O1=1.8795(13), N1-O1=1.3912(19), N2-O2=1.4114(19), C1-C2=1.217(3), N1-Ni1-C1=112.20(7), N1-Ni1-O2=149.13(6), C1-Ni1-O2=98.67(7), N1-Ni1-O1=43.58(6), C1-Ni1-O1=155.76(7), O2-Ni1-O1=105.56(5), O1-N1-Ni1=68.63(8), N1-O1-Ni1=67.79(8), N2-O2-Ni1=117.19(10).

Compound **5.8*cc*** is characterized by the combination of ^{1}H NMR, FTIR, mass spectroscopy, and X-ray crystallographic analysis. Compound **5.8*cc*** is highly stable and can be handled in air unlike previous compounds. Again positions of both the protons bonded to N2 and N2* as shown in Figure 5.10 were identified and refined satisfactorily using X-ray crystallographic analysis. Their presence was further confirmed by the ^{1}H NMR, which showed a peak at 7.66 ppm in C_6D_6 solvent with an appropriate integration of two H. As you see in Figure 5.10, the compound **5.8*cc*** is bridged by an aromatic link and these types of compounds are known to exhibit charge transfer in the near IR region.[271] Further experiments on this compound to study its charge transfer capabilities are underway in our lab.

While we have not attempted to model dimerization reaction kinetics or mechanisms, the various isomeric possibilities of **5.8** have been explored. Three possibilities arise, the *cis-cis*, *cis-trans*, or *trans-trans* isomers, which are labeled **5.8*cc***, **5.8*ct***, and **5.8*tt***, respectively (Scheme 5.4).

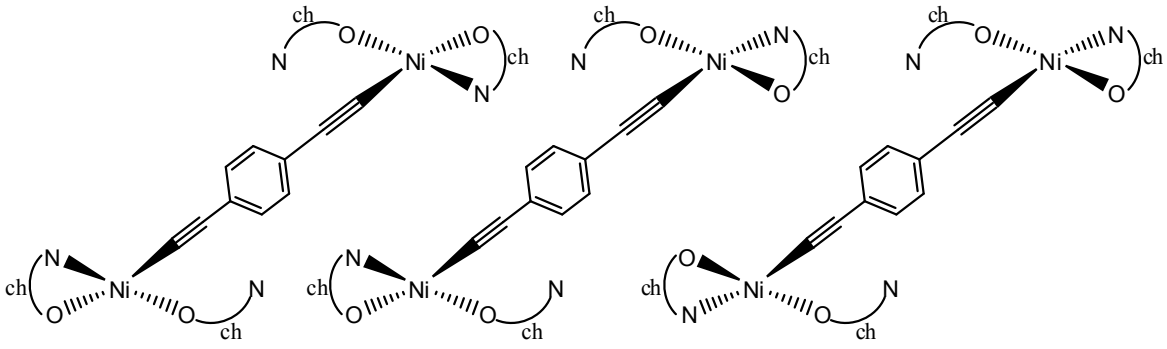

5.8*cc* **5.8*ct*** **5.8*tt***

Scheme 5.4. Possible isomers of compound **5.8.**

From Table 5.4, the **5.8*cc*** isomer is lowest in solution phase free energy by 4.1 and 9.1 kcal mol^{-1} compared to the **5.8*ct*** and **5.8*tt*** isomers, respectively, which is in agreement with the experimental characterization of **5.8***cc* The results from Table 5.4 also confirm that both experimental procedures for producing complex **5.8*cc***, addition of two equivalents of compound **5.1*t*** to $HCC(C_6H_4)CCH$ as well as addition of compound **5.7*c*** to compound **5.1*t***, have thermochemically favorable reaction free energies.

Reaction of Ni(η^2-TEMPO)$_2$, 5.1*t* with Pyridine: Except the compound **5.2*c***, all the products discussed so far are the result of reaction between **5.1*t*** and $1e^-$ donating reagents. Study has been extended to $2e^-$ donating ligands to further explore the reactivity of **5.1*t***. At room temperature when $2e^-$ donating ligand, pyridine, was added to the hexane solution of compound **5.1*t*,** an immediate color change from purple to dark brown/yellow occurred. During removal of volatiles in *vacuo* a partial regeneration of purple color on the Schlenk flask walls was observed. Recrystallization of solid residues from diethyl ether with a drop of pyridine afforded dark brown blocks of Ni(η^2-TEMPO)(k^1-TEMPO)(κ^1-NC_5H_5), **5.9*t*** in 95 % yield. X-ray crystallographic analysis yielded the expected distorted square planar structure as shown in Figure 5.11. Further crystallographic information is provided in Appendix D Table D.3. Compound **5.9*t*** was characterized by ^1H NMR, mass spectroscopy, and X-ray crystallographic analysis. Compound **5.9*t*** is highly air, moisture and temperature sensitive, and X-ray crystallographic data was collected at 100K under flow of N_2 to avoid crystal decomposition.

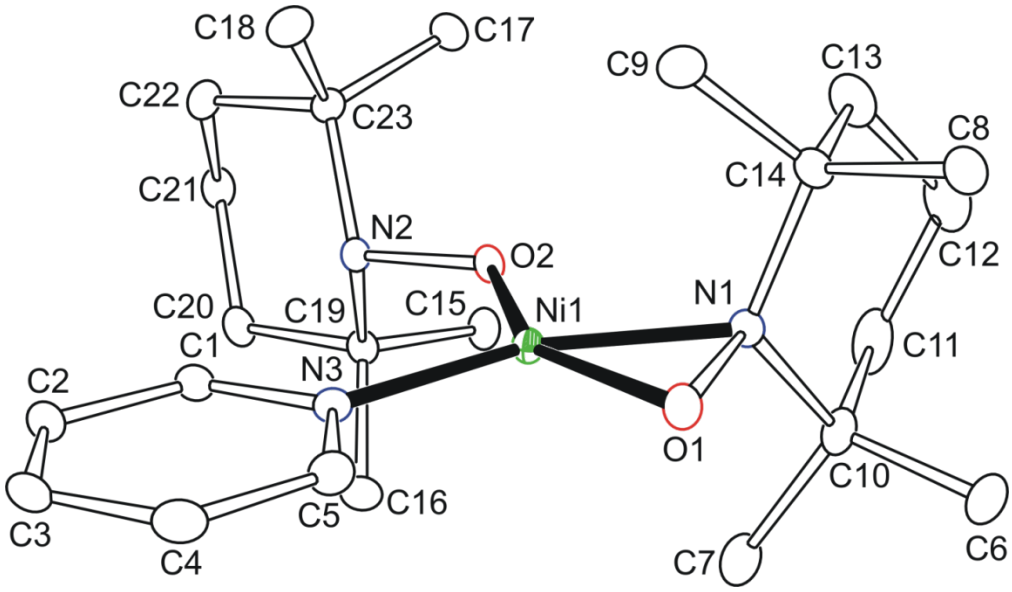

Figure 5.11. An ORTEP of the molecular structure of Ni(η^2-TEMPO)(k^1-TEMPO)(κ^1-NC_5H_5), **5.9*t*** showing 50 % thermal ellipsoid probability. Selected bond distances (Å) and angles (°) are: Ni1-O2=1.8407(10), Ni1-N1=1.9063(12), Ni1-O1=1.8690(10), Ni1-N3=1.9032(12), N1-O1=1.3946(15), N2-O2 =1.4308(15), O2-Ni1-O1=148.36(4), O2-Ni1-N3=108.55(5), O1-Ni1-N3=103.08(5), O2-Ni1-N1=105.04(5), O1-Ni1-N1=43.34(5), N3-Ni1-N1=146.23(5), O1-N1-Ni1=66.91(6), O1-N1-C14 =112.02(11), O1-N1-C10=112.71(11), O2-N2-C23=107.48(10).

A close look at the structure of compound **5.9*t*** reveals the unusual orientation of the TEMPO ligands. As you can see in the Figure 5.12, the oxygen atoms are not *cis* but rather *trans* as in the starting compound **5.1*t***. This kind of orientation had been expected for all the products, with the simple opening of one metallacycle and addition of a new ligand without flipping to yield *cis* oxygen atoms. Compound **5.9*t*** also contains an k^1-TEMPO ligand, and the orientation of the pyridine ring is coplanar with the distorted square planar geometry around nickel. Unlike the previous substituted complexes, the pyridine adduct is the only one observed in this study that retains the *trans*-disposition of the original complex.

As indicated earlier, compound **5.9*t*** appears to exist in equilibrium between starting material **5.1*t*** and its pyridine adduct. Removal of the solvent from the reaction mixture under reduced pressure always resulted in regeneration of some starting material **5.1*t***. In fact even crystallization at atmospheric pressure at room temperature results in regeneration of some starting material. Analysis by mass spectroscopy required addition of a drop of pyridine to the solution of compound **5.9*t*** to get the parent peak of 450 m/z which is a minor peak. Major peak corresponds to the mass of 370 m/z which is due to the starting material **5.1*t***.

The ^{1}H NMR analysis of **5.9*t*** was also difficult due to the reasons stated above. When pure crystal of compound **5.9*t*** were dissolved in any non-coordinating solvent such as toluene or benzene, it was immediately converted back to **5.1*t***, liberating free pyridine. The ^{1}H NMR spectrum of **5.9*t*** in pyridine-d5 solvent did not show the resonance of the pyridine ligand, because it was rapidly exchanged with pyridine-d5 from the solvent. In order to find out the binding strength of pyridine, a series of experiments for the addition of excess amounts of pyridine (49−294 equiv) to **5.1*t***, were monitored by ^{1}H NMR (see Figure D.6 in Appendix D), which did not show complete conversion of starting material **5.1*t*** to **5.9*t***. Using a rough estimate of ~80% conversion to **5.9*t*** in pure pyridine solvent, a K_{eq} value of 0.33 was estimated. This result suggests that binding of pyridine is very poor (in agreement with the computational results, vida infra). Furthermore, the ^{1}H NMR spectrum at room temperature showed broad, overlapping peaks indicative of fluxional processes associated with the TEMPO ligand. Variable-temperature ^{1}H NMR spectra in the range of −40° to 105 °C (see Figure D.7 in Appendix D) did not reveal a static spectrum that is consistent with the solid state structure of **5.9*t***. This fluxional process

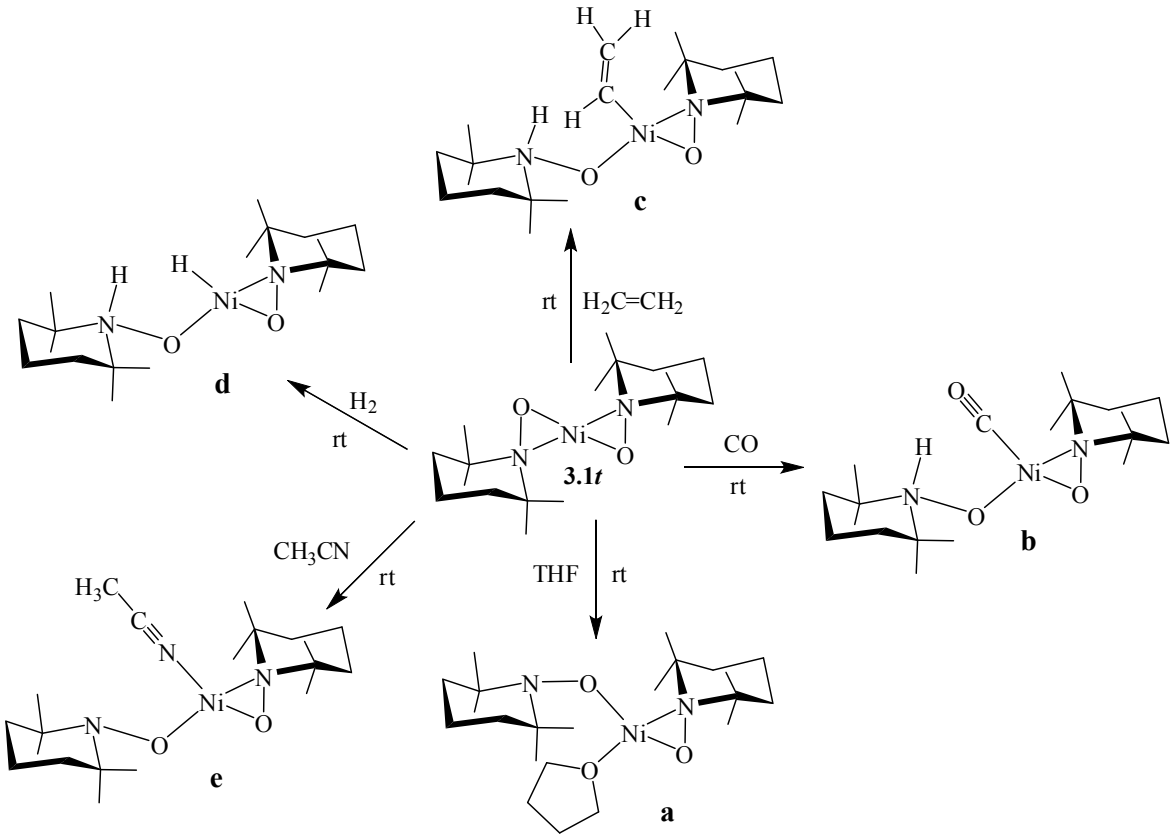

Scheme 5.5. Proposed line structures of products of **5.1*t*** with a) THF, b) CO, c) H_2CCH_2,

was also observed in the ^{1}H NMR spectrum of compound **5.2*c*** at room temperature. Variable-temperature ^{1}H NMR spectra in the range of 25°−90 °C resulted in some sharpening of the peaks. However, as shown in Figure D.7 in the Appendix D, some broadening remained, even at high temperature. At temperatures above 90 °C, **5.9*t*** decomposes. It is clear that some broadening and exchange occurs at higher temperatures as well. The exact nature of the fluxional processes in **5.2*c*** and **5.9*t*** remains unresolved at this point. While we are unable to unambiguously assign the dynamical process, work is underway to theoretically determine whether these processes occur due to η^1 (k^1) to η^2 exchange of the TEMPO ligands in solution or from conformational distortion of TEMPO.

Reaction of 5.1*t* with other small molecules and coordinating solvents: Based on the reaction of **5.1*t*** with Bu^tNC and acetylene gas to afford **5.2*c*** and **5.5*c***, work has been extended to activate other small molecules such as CO, C_2H_4, H_2 and coordinating solvents such as CH_3CN and THF. Scheme 5.5 depicts the conceivable (other possible isomers are not shown here) product types with these small molecules.

d) H_2, e) CH3CN.

Reaction with CO, H_2 and $H_2C=CH_2$: When Carbon monoxide gas was purged through a room-temperature hexane solution of **5.1*t*** an immediate color change to a dark reddish purple was observed, but within minutes, the solution becomes clear and a colorless solid precipitates at the bottom of the flask. Even at the depressed temperature of -78 °C, the same result was observed with no apparent signs of stabilization in the reaction mixture. This precipitate is not soluble in any of the tested solvents such as hexane, toluene, diethyl ether, tetrahydrofuran, dimethyl sulphoxide, methylene chloride, or water. The colorless product is yet be identified and efforts are underway in our lab to characterize it. Similarly when either H_2 or C_2H_2 gas is purged through the solution of **5.1*t***, even at depressed temperatures, there was rapid decolorization with precipitation of insoluble colorless solids. Again, there was no isolation of any new products.

It is possible that the proposed products with CO, H_2 and C_2H_2, lacks the sufficient steric volume to prevent further access to the unsaturated nickel center by the presence of excess amount of the reacting gasses but even the addition of equimolar amounts of gasses to the compound **5.1*t*** to get the above proposed products were unsuccessful. At

this time we are unsure as to why this product is so prone to decomposition, but as stated below, unstable reaction with small molecules is common for **5.1*t***.

Reaction of 5.1*t* with tetrahydrofuran (THF) and acetonitrile (CH_3CN) solvents: It has been observed that compound **5.1*t*** is stable in non-coordinating solvents such as hexane, benzene, toluene, methylene chloride and diethyl ether. However, after dissolving purple crystals of **5.1*t*** in either THF or CH_3CN solvent, the solution quickly becomes colorless and a colorless solid precipitates at the bottom of the reaction flask in a similar fashion to the reaction with CO gas, even at -78 °C. Again, no products were isolated from the reaction mixture. These observations of a strong reaction with coordinating solvents even at depressed temperature suggest that these reactions can be used for the synthesis of useful organic products in the presence of other reagents.

Exchange reactions between the acetylide products of compound 5.1*t*: It is evident from compounds **5.3*c*, 5.4*c*** and **5.5*c*,** that **5.1*t*** activates sp hybridized bond of symmetric and unsymmetric terminal alkynes. This is an essential step in the Sonogashira coupling reaction where a C-C bond is made. It is possible that the activated acetylides present on the Ni center can be coupled with other organic compounds to make new C-C, C-N, or C-O bonds and thus can be used to synthesize various useful organic products. Based on this idea, some interesting catalytic reactions were attempted to make new organic products with PhCCH and C_2H_2. Though, so far, the efforts to form new C-C bonds are unsuccessful, these attempts lead us to identify some interesting exchange reactions, occurring on the Ni center of these complexes as shown in equations 5.2 to 5.4.

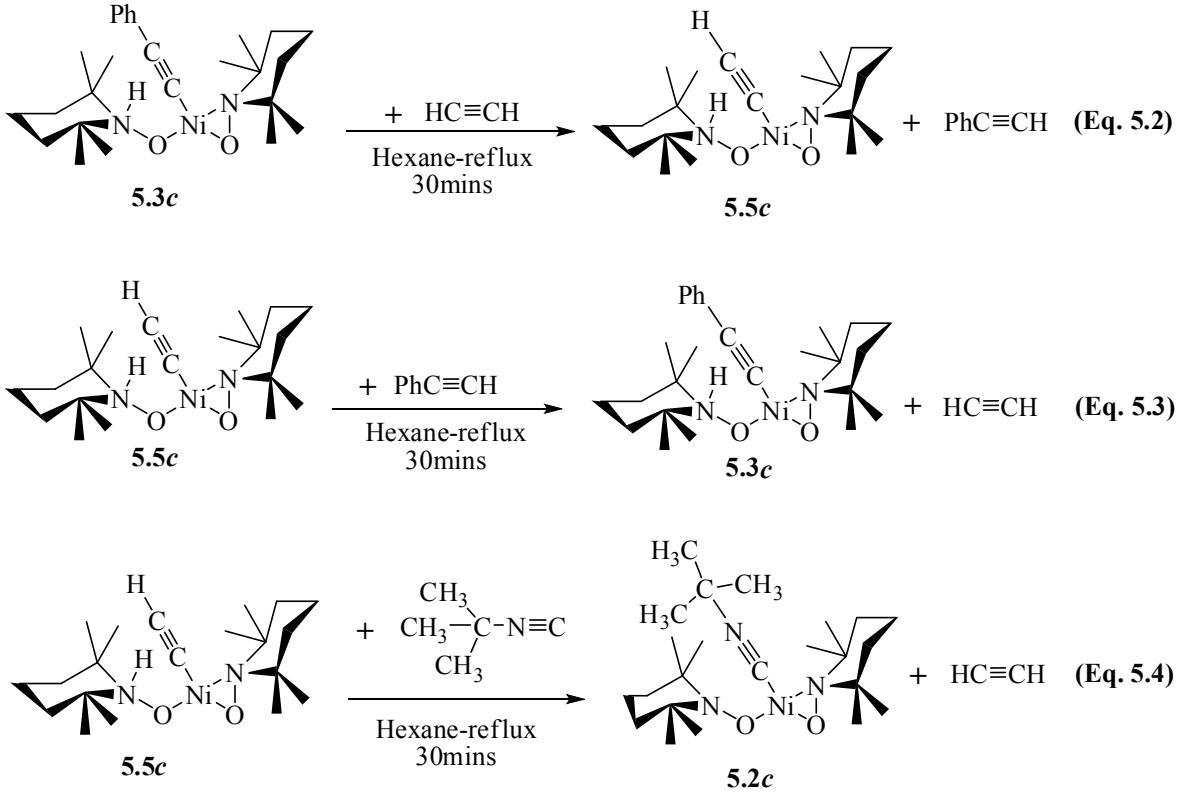

Phenyl acetylene and Bu^{t}NC replaces acetylene from 5.5*c*: When PhCCH and **5.5*c*** were reacted in 1:1 ratio, it was observed that PhCCH replaces the acetylene from **5.5*c*** and forms phenyl acetylide product **5.3*c*** within 30 minutes. These reactions were monitored by both IR and ^{1}H NMR which showed the resonances corresponding to both the products. This exchange reaction happens at RT and under refluxing conditions. A similar exchange phenomenon was observed with Bu^{t}NC, where it replaces acetylene and forms compound **5.2*c***. Unfortunately, these reactions do not go to the completion and stops after reaching some sort of equilibrium between the products. During this process unidentified black colored oily products were also observed.

Acetylene replaces phenyl acetylene from compound 5.3*c*. In this exchange reaction, acetylene gas is purged through the hexane solution of compound **5.3*c***. Interestingly,

acetylene gas replaces the phenyl acetylene from the compound **5.3*c*** only at refluxing temperature to form compound **5.5*c***. In this case, $CNBu^t$ does not replace Phenyl acetylide even under refluxing conditions. Again this reaction too does not go to the completion and stops after reaching some sort of equilibrium between both the products. Also, a black colored oily product was observed during the reaction.

5.4. Kinetics, thermodynamics, and selectivity of substituted species.

Mechanistic pathways of addition reactions of the various adducts (*tert*-butyl isocyanide, phenylacetylene, pyridine, acetylene, 1,4-diacetylenebenzene, and trimethylsilyl acetylene, respectively) are mapped out and discussed in the following section. First, transition states corresponding to the addition of the CN^tBu ligand to the *cis* and *trans* form of **5.1** have been computed and proceed via a simple association reaction. Both the *cis* and *trans* transition states (**TS-5.2*c*** and **TS-5.2*t***, respectively) possess an imaginary mode with Ni-N-O ring opening coupled to ligand addition. The PBE TS of the *trans* structure (Scheme 5.6) has a Ni-N bond distance of 2.427 Å versus 2.807 Å for the *cis*.

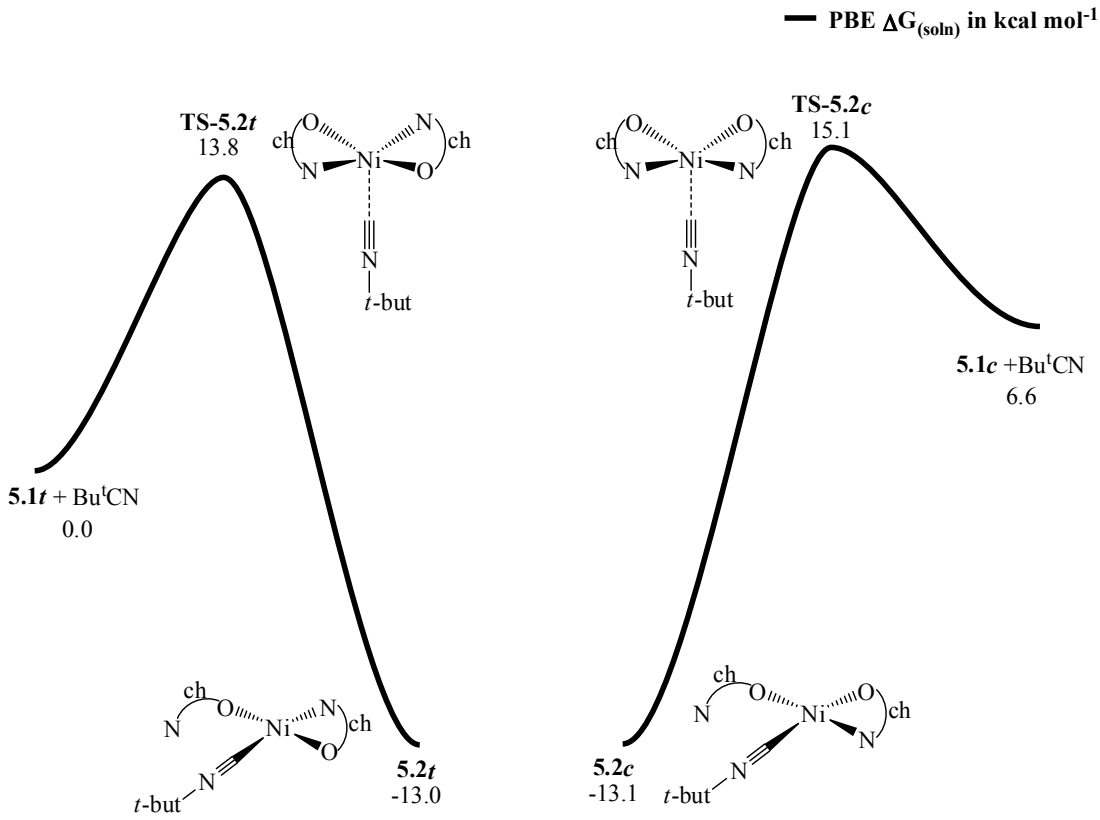

Scheme 5.6. Addition of $CNBu^t$ to compound **5.1*t*.**

From Scheme 5.7, it is evident that **5.2*c*** and **5.2*t*** are nearly isoenergetic. In the solution phase computations, the experimentally observed **5.2*c*** isomer is only 0.1 kcal mol^{-1} lower in free energy. Theory shows the experimentally observed isomer being slightly favored thermodynamically, but disfavored kinetically (the ΔG of **TS-5.2*c*** is 15.1 kcal mol^{-1} versus **TS-5.2*t*** with a ΔG of 13.8 kcal mol^{-1}). Among the complexes discussed in this paper, the **5.2*c*/5.2*t*** pair shows the closest relative free energies in terms of both kinetics and thermodynamics. However, attempts to force crystallization of the **5.2*t*** isomer under a variety of experimental conditions (variation of temperature and solvents) were unsuccessful and only resulted in formation of **5.2*c*** crystals.

In Scheme 5.7, the mechanism of phenylacetylene (PhCCH) addition to *trans*-Ni(η^2-TEMPO)$_2$ to form the *trans*-Ni(η^2-TEMPO)(k^1-TEMPOH)(η^1-CCPh) complex (**5.3*t***) is proposed. Note that intermediates in the addition reaction mechanism Schemes (both in the manuscript and in Appendix D) will be incrementally numbered starting after the first experimentally synthesized compound, *i.e.* starting with **10**.

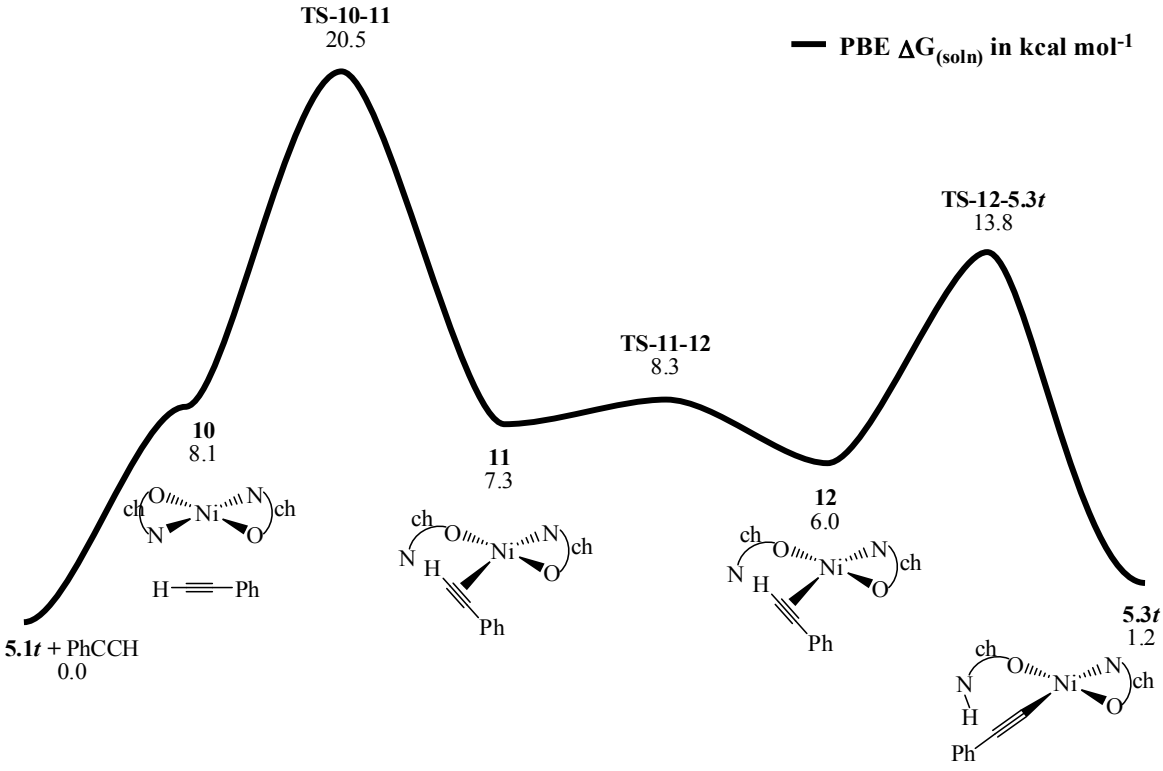

Scheme 5.7. Formation of **5.3*t*** from compound **5.1*t*.**

In Scheme 5.7 beginning with **5.1*t*** + PhCCH, a dipole-dipole intermediate (**10**) is obtained that is 8.1 kcal mol^{-1} higher in free energy than the infinitely separated *trans*-Ni(η^2-TEMPO)$_2$ and PhCCH. In this complex, a hydrogen atom from the phenyl ring is oriented towards one of the TEMPO oxygen atoms. The alkyl hydrogen of **10** is away from the complex at a distance of 5.811 Å from the Ni center. The phenyl of PhCCH

reorients significantly during **TS-10-11**, which has a ΔG of 20.5 kcal mol^{-1} compared to the separated species. The imaginary vibrational mode of **TS-10-11** corresponds to concerted ring opening of the Ni-O-N bond and formation of a single Ni-C bond with the terminal alkyl carbon. The subsequent intermediate (**11**) has the plane of the phenyl ring oriented parallel to the O-Ni-O plane (the out of plane angle is 17.5°). The intermediate **11** then undergoes a facile shift of the phenyl ring through the plane created by the Ni-O-N of the (k^1-TEMPO), **TS-11-12**, with ΔG = 8.3 kcal mol^{-1}. Finally, proton transfer of the alkyl hydrogen to the nitrogen atom on the (k^1-TEMPO) ligand occurs in **TS-12-5.3*t*** (ΔG = 13.8 kcal mol^{-1}) to give the final *trans*-Ni(η^2-TEMPO)(k^1-TEMPOH)(η^1-CCPh) product, **5.3*t***, with a ΔG of 1.2 kcal mol^{-1}.

In Scheme 5.8, the mechanism of PhCCH ligand addition to the *cis*-Ni(η^2-TEMPO)$_2$,**5.1*c*** complex is described. Upon association of the ligand, an interesting dipole-dipole species (**13**) is obtained where the hydrogen atom of the alkyne is oriented directly at the Ni-complex center, at a distance of 2.64 Å. This intermediate is 5.8 kcal mol^{-1} higher in free energy than the infinitely separated reactants (**5.1*c*** and PhCCH), and 12.4 kcal mol^{-1} higher in free energy than **5.1*t*** + PhCCH. The Ni-N bond of the TEMPO ligand opens and the Ni-C_{alkyl} bond forms in concert (**TS-13-14**). This transition state has a slightly higher free energy of activation than the equivalent *trans* TS (**TS-10-11**), with a $\Delta G_{(soln)}$ of 21.8 kcal mol^{-1}. The reaction pathway of **5.3*c*** has one less step when compared to **5.3*t***, as there is no reorientation of the alkyl bond needed to perform proton transfer (akin to **TS-11-12**). The intermediate **14** can directly transfer the proton to the TEMPO nitrogen atom (**TS-14-5.3*c***). This transition state has a lower free energy of activation (14.6 kcal mol^{-1}) and is quite early with a CH bond distance of 1.144 Å. The final product

5.3*c* has C_s point group symmetry and very closely resembles the X-ray crystal structure of the *cis*-Ni(η^2-TEMPO)(k^1-TEMPOH)(η^1-CCPh) complex (**5.3*c***).

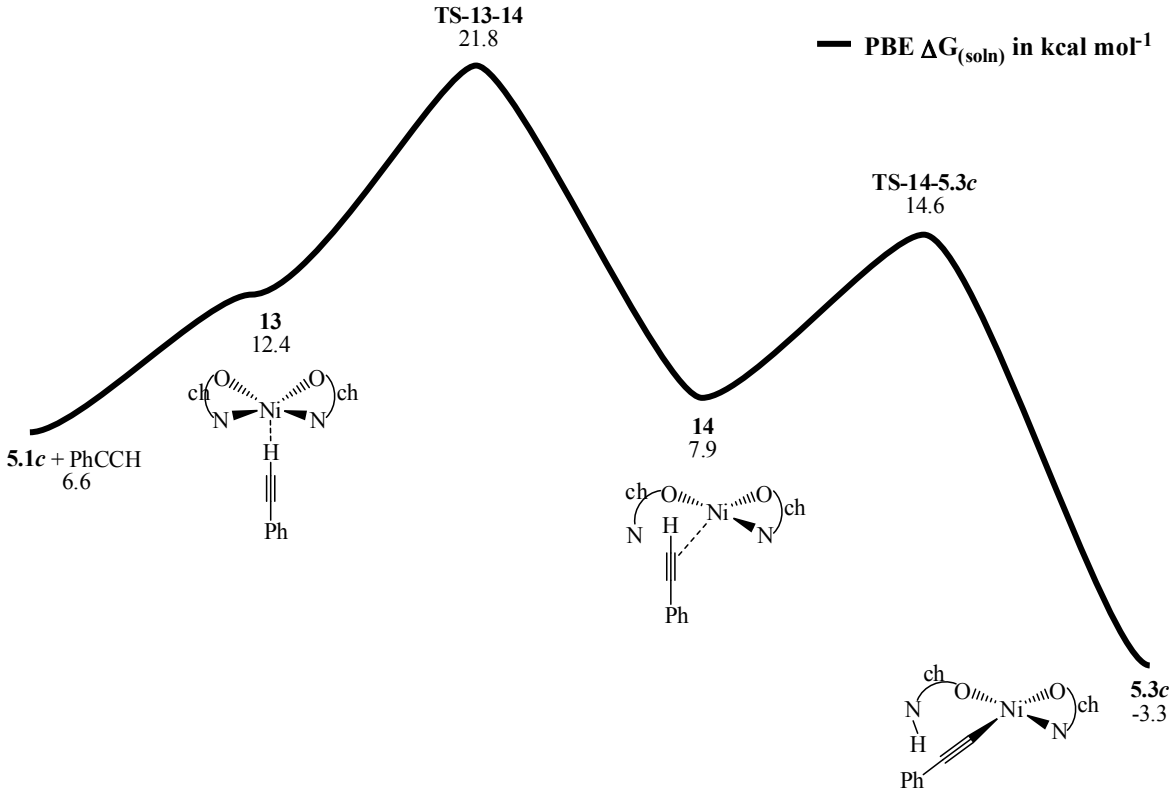

Scheme 5.8. Formation of **5.3*c*** from **5.1*c*.**

Addition of acetylene to complex **5.1*t*** and dddition of HCCH to **5.1*c*** is mechanistically very similar to the addition of PhCCH (see Appendix D, Schemes D.5 and D.6). The proposed mechanisms for the formation of **5.4*c***, **5.4*t***, **5.7*c***, and **5.7*t*** occur similarly to those described above, and are briefly discussed in Appendix Schemes D.1–D.4.

In Scheme 5.9, the thermodynamics of pyridine addition to complexes **5.1*t*** and **5.1*c*** to form complex **5.9*t*** and **5.9*c***, respectively, is shown. It is the least

thermodynamically stable of the product species, as it is the only one where the experimentally characterized structure has a computed positive binding energy (+2.1 kcal mol^{-1}). It is also the only adduct where the *trans* isomer has been isolated experimentally.

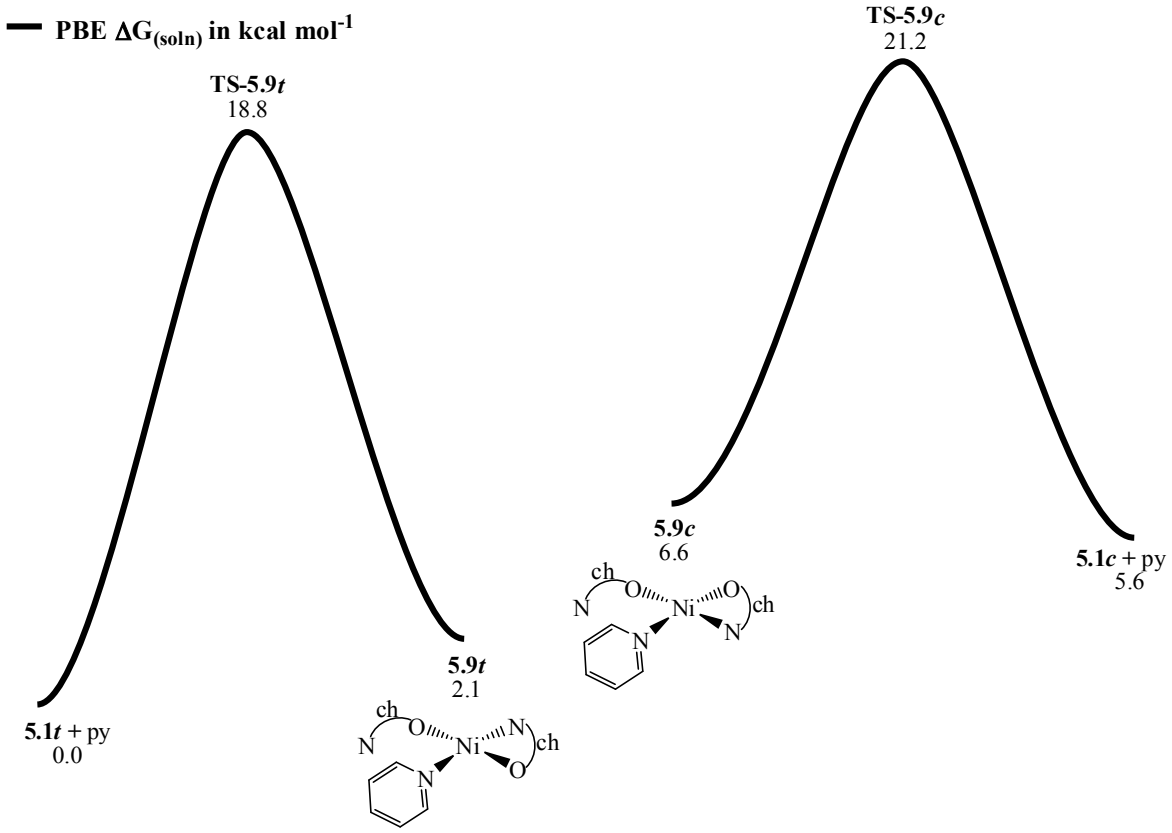

Scheme 5.9. Formation of **5.9*t*** from **5.1*t*.**

Kinetics, thermodynamics, and possible isomerization mechanisms: Table 5.5 shows the theoretical ligand binding energies for the addition of all substituents to complex **5.1** as well as solution phase activation free energies for the computed rate-limiting steps of the various addition reactions.

Reaction	Reaction free energy ΔG_{soln} (kcal mol^{-1})
5.1*t*	**0**
5.1*c*	4.0[b]
5.1*t* + $CNBu^t$ → **5.2*t***	−13.0
5.1*t* + $CNBu^t$ → **5.2*c***	**−13.1**
5.1*t* + PhCCH → **5.3*t***	1.2
5.1*t* + PhCCH → **5.3*c***	**−3.3**
5.1*t* + $HCCSi(CH_3)_3$ → **5.4*t***	−0.1
5.1*t* + $HCCSi(CH_3)_3$ → **5.4*c***	**−4.2**
5.1*t* + HCCH → **5.5*t***	−2.5
5.1*t* + HCCH → **5.5*c***	**−3.8**
5.1*t* + HCCPhCCH → **5.7*t***	−0.8
5.1*t* + HCCPhCCH → **5.7*c***	**−4.4**
5.1*t* + py → **5.9*t***	**2.1**
5.1*t* + py → **5.9*c***	5.6

Table 5.5. Theoretical PBE Solution-Phase Reaction Free Energies (ΔG_{soln}) for the Addition of All Ligands to Complex **5.1*t***[a] ([a] Further computational results for the gas-phase thermodynamics and gas-phase and solution-phase kinetics are included in the Appendix Table D.5. Included in the first rows are the relative energies of the *trans* and *cis* isomers of complex **5.1*t***. The reaction free energy of the experimentally observed isomer is shown in bold text. [b] The relative free energy of **5.1*c*** refers to the lowest energy conformer. The conformer that directly reacts to form the various addition products is slightly higher in free energy (ΔG_{soln} = 6.6 kcal mol−1); and this relative free energy is used along the reaction mechanisms shown in Schemes 5.7, 5.9, 5.11, 5.12, D.2 and D.4.

There are a few unexpected trends that have occurred in the reactions of the donator ligands with $Ni(TEMPO)_2$. First is that the *trans*-$Ni(TEMPO)_2$ complex (**5.1*t***) was isolated, but all adducts except for **5.9*t*** were crystallized in the *cis* form. The formation of **5.9*t*** is also unique because both *cis* and *trans* isomers are endergonic in the

solution phase computed pathways (ΔG = +5.6 and +2.1 kcal mol^{-1}, respectively). This corresponds well to the comparatively short lifetime, as well as the careful synthetic conditions necessary to isolate complex **5.9*t***. The second related phenomenon is that in all cases [again except for the addition of pyridine to the $Ni(TEMPO)_2$ complex (Scheme 5.10)] the PBE computations suggest that the experimentally observed product isomer is thermodynamically, but not kinetically controlled. In order to progress from the *trans* disposition of the reactant (**5.1*t***) versus the *cis* disposition of the various adducts (**5.2, 5.3, 5.4, 5.5, 5.7**), an isomerization must take place. There are three possibilities for an isomerization pathway, shown in Scheme 5.10.

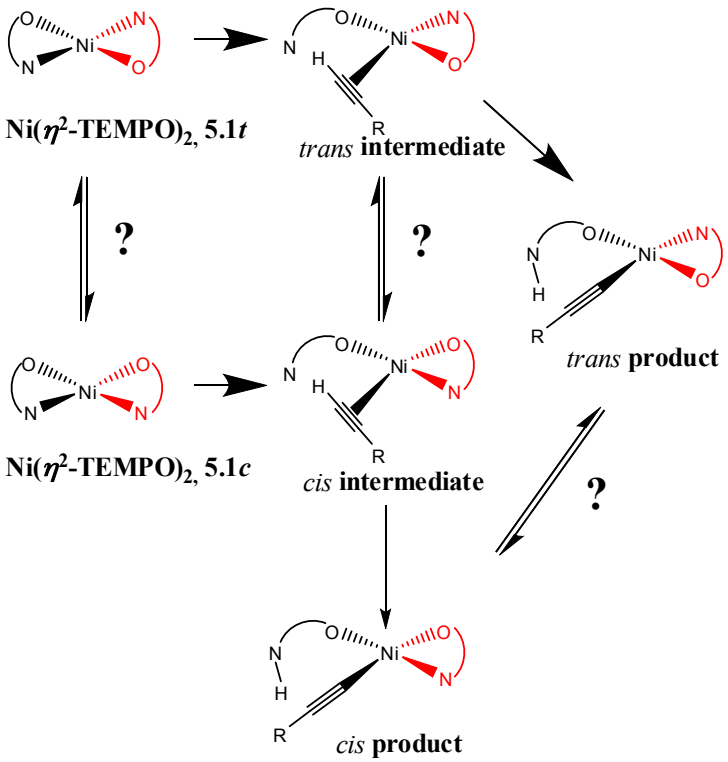

Scheme 5.10. Isomerization possibilities.

When does this isomerization occur? The first possibility is that isomerization takes place in the initial complex **5.1*t***, and then **5.1*c*** undergoes the addition reaction with

the alkyne substituent. The second possibility is that the isomerization occurs when the adduct is bound to the complex, but before the hydrogen transfer to the η1-TEMPO ligand, (i.e., a pathway connecting 11/12 to 14, 16 to 18, 20 to 22, or 24 to 26, shown in Schemes 5.8, 5.9 and in Schemes D.1 to D.6 in the Appendix D). Finally, there is the possibility that *trans*−*cis* isomerization can occur after the hydrogen transfer takes place (in a mechanism between **5.3*c*** and **5.3*t***, for example). All of this discussion of *trans*-to-*cis* isomerization is complicated by two factors: (1) the relative energy of the lowest energy **5.1*c*** isomer is 4.0 kcal mol−1 higher than the lowest energy isomer of **5.1*t*** and (2) astonishingly, the computed NMR spectrum of **5.1*c*** is very similar to the computed NMR spectrum of **5.1*t*** (which is in relatively good agreement with the experimentally observed NMR spectrum of 1t). Therefore, the very small amount of cis isomer produced from raising the temperature would only slightly alter the peak integrations. (See the Supporting Information for further discussion of these points).

5.5. Conclusions.

Synthesis and characterization of Ni(η^2-TEMPO)$_2$, **5.1*t***, the first literature example of an unsaturated transition metal complex with exclusively of TEMPO radicals as ligands, has been reported in this chapter. Complex **5.1*t*** is a 16electron unsaturated molecule with “bow-tie” type rectangular planar structure with oxygen atoms *trans* to each other. Complex **5.1*t*** is highly air and moisture sensitive. This simple molecule demonstrated a complex reactivity with a wide variety of small molecules (see Scheme 5.2) by displaying bifunctional cooperativity between the hemilabile TEMPO ligand and the Ni center in its reactivity with organic substrates at room temperature.

The reaction of **5.1*t*** with *tert*-butyl isocyanide to afford Ni(η^2-TEMPO)(η^1-TEMPO)(κ^1-CNBu^t), **5.2*c***, demonstrates one of several possible modes of reactivity. This reaction displays the ability of **5.1*t*** to transform one of the coordinated TEMPO ligand from η^2 to η^1 mode to yield a 16e$^-$ planar product, where now the oxygen atoms are *cis* to each other. This compound exhibited broadened ^{1}H NMR resonances suggestive of dynamical processes in solution suggestive of a fluxional equilibrium in solution. A similar dynamical process in solution was observed in case of reaction of **5.1*t***, with pyridine, though, here the mode of reactivity is completely different. Addition of pyridine to **5.1*t*** produces the dark brown product Ni(η^2-TEMPO)(k^1-TEMPO)(κ^1-NC_5H_5), **5.9*t*.** This is the only product synthesized which shows *trans* oxygen atoms as opposed to *cis* unlike other products of **5.1*t*.**

Compound **5.1*t*** reacts with terminal alkynes and activates sp hybridized C-H bond to yield acetylide products **5.3*c***, **5.4*c*,** **5.5*c*,** and **5.7*c***, which is rare, with the N atom on the TEMPO ligand acting as a base to deprotonate the alkyne. All these products contain *cis*-disposed oxygen atoms. Complex **5.8*cc***, is a good example where two terminal alkynes of same molecule are activated to link two Ni(η^2- TEMPO)(κ^1-TEMPOH) groups to form a bridging dinuclear complex.

Attempts to activate other small molecules such as H_2, C_2H_2, CO, CO_2, N_2 etc., by **5.1*t*** are unsuccessful. Compound **5.1*t*** is highly unstable in coordinating solvents such as tetrahydrofuran, acetonitrile, methanol etc., and forms unidentified products which are insoluble in all the tested solvents. These observations indicate a strong reaction of **5.1*t*** with above mentioned small molecules and solvents with the possibility to synthesize useful compounds by tweaking reaction conditions.

Density functional theory (DFT) has been employed to study the structural and thermochemical properties of the molecules shown in Scheme 5.2. Computed solution-phase relative free energies of the various characterized Ni-centered complexes are in agreement with the experimentally observed isomers. However, rate-limiting transition states of the addition reactions suggest that, in all cases except for the initial complex Ni(η^2-TEMPO)$_2$, **5.1*t*** and the product formed via the addition of pyridine (**5.9*t***), the experimentally observed isomer is always kinetically disfavored. The mechanism by which the *trans* complex **5.1*t*** isomerizes to the various *cis* product complexes upon substrate addition is still not completely understood. Further experimental and computational work will be performed in tandem to explore the fascinating conformational complexity of the isomerization reactions. Both theory and experiment also validate the formation of the bimetallic complex **5.8*cc*** (two C−H bond activations of 1,4-diethynylbenzene) and are correspondingly in agreement that the proposed bimetallic complex **5.6*cc*** (two C−H bond activations of acetylene) will be too sterically crowded to exist under the same experimental conditions used to isolate complex **5.8*cc***.

The reactions presented in this report are facile under mild conditions. The brief survey of contained reactions present a good start, in the wake of exchange reactions between dissimilar acetylide complexes of **5.1*t***, studies are planned in carbon−carbon bond coupling. Studies are also planned in the fields of homogeneous catalysis, targeting small molecules and C−H bond activation and oxygen atom transfer.

5.6. Experimental section.

General Data. Unless indicated otherwise, all reactions were performed under an atmosphere of argon. Reagent-grade solvents ere dried by the standard procedures and

were freshly distilled prior to use. Solution-phase infrared spectra were recorded on a Nicolet 380 FT-IR spectrophotometer. Single-crystal FTIR spectra were obtained on a Perkin−Elmer Spectrum 400 using a Perkin−Elmer Universal ATR Sampling Accessory. ^{1}H NMR spectra were recorded on a Bruker 400 spectrometer operating at 399.993 MHz. 2D [^{1}H, ^{15}N] HSQC NMR were collected on a Bruker Avance-IIIHD 500 NMR spectrometer operating at 500.21 MHz for ^{1}H and 50.69 MHz for ^{15}N at the University of South Carolina. Elemental analyses were performed by Columbia Analytical Services (Tucson, AZ). Electrospray mass spectrometric measurements were obtained on a Bruker micrOTOF-Q II. Bis(1,5-cyclooctadiene)nickel, Ni(COD)$_2$, was purchased from Strem Chemicals, used without further purification, and stored and handled in a drybox. TEMPO (2,2,6,6-tetramethylpiperidine-N-oxide), tert-butyl isocyanide, and phenylacetylene were purchased from Alfa Aesar and used without further purification. 1,4-Diethynylbenzene was purchased from TCI and used without further purification. Atomic-absorption-grade acetylene and argon (UHP grade) were purchased from AirGas and used without further purification. Phenylacetylene-d1 (99%), pyridine, and trimethylsilyl acetylene were purchased from Sigma−Aldrich and used without further purification.

Synthesis of Ni(η^2-TEMPO)$_2$,5.1*t*: A 100 mg (0.36 mmol) amount of Ni(COD)$_2$ and 115 mg (0.72 mmol) of TEMPO were loaded into a Schlenk flask. 30 mL of hexane solvent was then added to the flask using a cannula. The stirred solution changed color from light orange to deep purple as it was heated to reflux, for approximately 5 min. The solvent was then removed in *vacuo* and the residue was dissolved in 4 mL of diethyl ether, filtered into a glass vial, and placed in a -25 °C freezer in a drybox. Evaporation of

solvent afforded 105 mg (78% yield) of purple crystalline blocks of Ni(η^2-TEMPO)$_2$, **5.1*t***. Spectral data for **5.1*t***: ^{1}H NMR (C_6D_6 in ppm): δ = 2.39 (s, 12 H, 4 CH_3), 1.36 (s, 12 H, 4 CH_3), 1.40 – 1.25 (m, broad, 12 H, 6 CH_2). Mass Spec. ES^+/MS calcd for [M + CH_3CN], 412; found 412. The isotope distribution is consistent with the presence of one nickel atom.

Synthesis of Ni(η^2-TEMPO)(k^1-TEMPO)(κ^1-CNBu^t), 5.2*c*: A 40 mg (0.108 mmol) amount of Ni(η^2-TEMPO)$_2$ was loaded into a sidearm Schlenk flask and dissolved in 20 mL of hexane after which 10 mg (0.125 mmol) of Bu^{t}NC was added, resulting in an immediate color change from purple to dark red. The reaction mixture was stirred at room temperature for 10 min. The volatiles were removed in *vacuo* and the residue was dissolved in 2 mL of diethyl ether, filtered into a glass vial, and placed in a -25 °C freezer in a dry box. Evaporation of solvent afforded 44 mg (90% yield) of red crystalline blocks of Ni(η^2-TEMPO)(k^1-TEMPO)(κ^1-CNBu^t), **5.2*c***, Spectral data for **5.2*c*:** IR ν_{CN} (cm^{-1}, in hexane) 2169. ^{1}H NMR (toluene-d_8 in ppm): δ = 2.46 (s), 2.43-1.00 (broad), 1.55 (s), 1.50-1.20 (broad), 1.19 – 1.02 (broad multiplet), 0.95 (s). Note: The ^{1}H NMR spectrum at room temperature indicates some dynamical processes in solution, see text and supporting information. Mass Spec. EI/MS: *m/z* calcd for M^+= 453; found 453; calcd (M^+- ^{t}BuNC)= 370 (= Ni[η^2-TEMPO]$_2$); found 370. The isotope distribution is consistent with the presence of one nickel atom.

Synthesis of Ni(η^2-TEMPO)(κ^1-TEMPOH)(κ^1-CCPh), 5.3*c*: A 40 mg (0.108 mmol) amount of Ni(η^2-TEMPO)$_2$ was loaded into a sidearm Schlenk flask and dissolved in 20 mL of hexane. 12 mg (0.117 mmol) of phenylacetylene was added and the reaction mixture was stirred at room temperature for 1 hour, during which time the color changed

from purple to light red. The volatiles were then removed in *vacuo* and the residue dissolved in 2 mL of diethyl ether, filtered into a glass vial, and placed in a -25 °C freezer in a dry box. Evaporation of solvent afforded 37 mg (73% yield) of red crystalline blocks of Ni(η^2-TEMPO)(κ^1-TEMPOH)(κ^1-CCPh), **5.3*c*.** Spectral data for **5.3*c*:** FTIR (single crystal) $\nu_{(C\text{-}C)}$: 2079(s) cm^{-1}, $\nu_{(N\text{-}H)}$: 3675-3100 (broad) cm^{-1}. FTIR $\nu_{(C\text{-}C)}$ (cm^{-1} in hexane): 2074(s). ^1H NMR (C_6D_6 in ppm): δ= 7.62 (s, 1 H, N-H), 7.50 (d, 2 H, Ph), 7.10 (t, 2 H, Ph), 6.96 (t, 1 H, Ph), 3.10 (s, 6 H, 2 CH_3), 2.11 (s, 6 H, 2 CH_3), 1.76 (br, 2 H, CH_2), 1.29 (s, 8 H, 2 CH_3 and 1 CH_2), 1.08 (m, 6 H, 3 CH_2), 0.90 (s, 8 H, 2 CH_3 and 1 CH_2). Mass Spec. ES^+/MS calcd for $[M + H]^+$= 473; found 473. The isotope distribution is consistent with the presence of one nickel atom.

Synthesis of Ni(η^2-TEMPO)(κ^1-TEMPOH)(κ^1-CCSiMe$_3$), 5.4*c*: A 40 mg (0.108 mmol) amount of Ni(η^2-TEMPO)$_2$ was loaded into a sidearm Schlenk flask and dissolved in 20 mL of hexane. 12 mg (0.122 mmol) of trimethylsilyl acetylene was added and the reaction mixture was stirred at room temperature for 1 h, during which time the color changed from purple to light red. The volatiles were then removed in *vacuo* and the residue dissolved in 2 mL of diethyl ether, filtered into a glass vial, and placed in a -25 °C freezer in a dry box. Evaporation of solvent afforded 40 mg (79 % yield) of red crystalline blocks of Ni(η^2-TEMPO)(κ^1-TEMPOH)(κ^1-CCSiMe$_3$), **5.4*c***. Spectral data for **5.4*c*:** FTIR $\nu_{(C\text{-}C)}$ (cm^{-1} in hexane): 2009(s). ^1H NMR (C_6D_6 in ppm): δ= 7.69 (s, 1 H, N-H), 2.99 (s, 6 H, 2 CH_3), 2.09 (s, 6 H, 2 CH_3), 1.76 (m, 2 H, CH_2), 1.26 (s, 6 H, 2 CH_3), 0.91 (s, 6 H, 2 CH_3), 1.5-0.9 (m, broad, 10 H, 5 CH_2), 0.29 (s, 9 H, $SiMe_3$). Mass Spec. ES^+/MS calculated for $[M + H]^+$= 470 m/z; found 470 m/z. The isotope distribution is consistent with the presence of one nickel atom.

Synthesis of Ni(η^2-TEMPO)(κ^1-TEMPOH)(κ^1-CCH), 5.5*c*: A 40 mg (0.108 mmol) amount of Ni(η^2-TEMPO)$_2$ was loaded into a sidearm Schlenk flask and dissolved in 20 mL of hexane. Acetylene gas was purged through the reaction mixture and stirred at room temperature for 1 h, during which time the color changed from purple to light red. The volatiles were then removed in *vacuo* and the solid residue dissolved in 2 mL of diethyl ether, filtered into a glass vial, and placed in a -25 °C freezer in a dry box. Evaporation of solvent afforded 32 mg (74 % yield) of red crystalline blocks of Ni(η^2-TEMPO)(κ^1-TEMPOH)(κ^1-CCH), **5.5*c*.** Spectral data for **5.5*c*:** FTIR $\nu_{(C\text{-}C)}$ (cm^{-1} in hexane): 1933(s). ^{1}H NMR (C_6D_6 in ppm): δ= 7.64 (s, 1 H, N-H), 3.10 (s, 6 H, 2 CH_3), 2.08 (s, 6 H, 2 CH_3), 2.06 (s, 1 H, CCH), 1.78 (m, 2 H, CH_2), 1.26 (s, 6 H, 2 CH_3), 0.90 (s, 6 H, 2 CH_3), 1.4-0.8 (m, broad, 10 H, 5 CH_2). Mass Spec. ES^+/MS calculated for $[M + H]^+$= 397 m/z; found 397 m/z. The isotope distribution is consistent with the presence of one nickel atom.

Synthesis of Ni(η^2-TEMPO) (κ^1-TEMPOH)(κ^1-CC[C_6H_4]CCH), 5.7*c*: A 40 mg (0.108 mmol) amount of Ni(η^2-TEMPO)$_2$ was loaded into a sidearm Schlenk flask and dissolved in 20 mL of hexane. 15 mg (0.119 mmol) of 1,4-diethynylbenzene was added and the reaction mixture was stirred at room temperature for 1 h, during which time the color changed from purple to auburn red. The volatiles were then removed in *vacuo* and the residue dissolved in 2 mL of diethyl ether, filtered into a glass vial, and placed in a -25 °C freezer in a dry box. Evaporation of solvent afforded 38 mg (71 % yield) of red crystalline blocks of Ni(η^2-TEMPO) (κ^1-TEMPOH)(κ^1-CC[C_6H_4]CCH), **5.7*c***. Spectral data for **5.7*c*:** FTIR $\nu_{(C\text{-}C)}$ (cm^{-1} in hexane): 2071(s). ^{1}H NMR (C_6D_6 in ppm): δ= 7.65 (s, 1 H, N-H), 7.44-7.31 (d, 4 H, C_6H_4), 3.26 (s, 1 H, C≡CH), 3.08 (s, 6 H, 2 CH_3), 2.10 (s, 6

H, 2 CH_3), 1.76 (m, 2 H, CH_2), 1.28 (s, 6 H, 2 CH_3), 0.90 (s, 6 H, 2 CH_3), 1.5-0.8 (m, broad, 10 H, 5 CH_2). Mass Spec. ES^+/MS calculated for $[M + H]^+ = 497$; found 497. The isotope distribution is consistent with the presence of one nickel atom.

Synthesis of Ni(η^2-TEMPO)(k^1-TEMPOH)[k^1-k^1-CC(C_6H_4)CC]Ni(η^2-TEMPO)(k^1-TEMPOH), 5.8*cc*: To 48 mg (0.129 mmol) of Ni(η^2- TEMPO)$_2$ and 8 mg (0.063 mmol) of 1,4-diacetylenebenzene in a sidearm Schlenk flask, 20 mL of hexane was added. The reaction mixture was stirred at room temperature for 3 h, during which time the color changed from purple to auburn red. The volatiles were then removed in *vacuo* and the residue dissolved in approximately 2 mL of benzene, filtered into a glass vial, and placed in a dry box. Evaporation of solvent at room temperature afforded 44 mg (80 % yield) of pure red crystalline blocks of Ni(η^2-TEMPO)(k^1-TEMPO*H*)[η^1- η^1-CC(C_6H_4)CC]Ni(η^2-TEMPO)(η^1-TEMPOH). Spectral data for **9:** FTIR $\nu_{(C\text{-}C)}$ (cm^{-1} in hexane): 2073(s). ^{1}H NMR (C_6D_6): δ = 7.66 (s, 2 H, N-H), 7.43 (s, 4 H, C_6H_4), 3.09 (s, 12 H, 4 CH_3), 2.10 (s, 12 H, 4CH_3), 1.73 (t, 4 H, 2 CH_2), 1.29 (s, 12 H, 4 CH_3), 1.20 – 1.36 (br, 8 H, 4 CH_2), 1.00 – 1.15 (br, 12 H, 6 CH_2), 0.90 (s, 12 H, 4 CH_3). Mass Spec. ES^+/MS calculated for $[M + H]^+ = 868$; found 868. The isotope distribution is consistent with the presence of two nickel atoms.

Synthesis of Ni(η^2-TEMPO)(k^1-TEMPO)(κ^1-NC_5H_5), 5.9*t*: A 40 mg (0.108 mmol) amount of Ni(η^2-TEMPO)$_2$, **5.1*t*** was loaded into a sidearm Schlenk flask and dissolved in 20 mL of hexane. Excess pyridine (0.1 mL) was added and the reaction mixture immediately changed color from purple to dark brown. The volatiles were then removed in *vacuo* and the residue dissolved in 2 mL of diethyl ether with a drop of pyridine, filtered into a glass vial, and placed in a -25 °C freezer in a dry box. Evaporation of

solvent afforded 46 mg (95 % yield) of brown blocks of Ni(η^2-TEMPO)(k^1-TEMPO)(κ^1-NC_5H_5), **5.9*t***. Spectral data for **5.9*t*:** ^{1}H NMR (C_6D_6 in ppm, pyridine peaks and integrations not listed due to dynamical processes): δ= 2.96 (s), 2.35 (s), 3.0-1.8 (broad), 1.54 (s), 1.35 (s). ^{1}H NMR (NC_5D_5 in ppm, pyridine peaks and integrations not listed due to dynamical processes): δ= 3.03 (s), 2.38 (s), 3.0-1.8 (broad), 1.55 (s), 1.36 (s), 1.19 (s) (see Figure D.7 in Appendix D). Mass Spec. ES^+/MS calculated for $[M]^+$= 450 m/z; found 450 m/z. The isotope distribution is consistent with the presence of one nickel atom. NOTE: It should be noted that additional peaks with higher molecular weights were also present in the mass spectrum, presumably because of decomposition in the spectrometer. Similarly, reliable elemental analysis results were not obtained for this relatively unstable compound. Placing solid **5.9*t*** under vacuum, results in partial decomposition and regeneration of **5.1*t***. Dissolving **5.9*t*** in hexane or benzene appears to create equilibrium between starting **5.1*t*** and product **5.9*t***.

Conversion of 5.7*c* to 5.8*cc*: To 20 mg (0.040 mmol) of **5.7*c*** and 15 mg (0.040 mmol) of **5.1*t*** in a sidearm Schlenk flask, 20 mL of hexane was added. The reaction mixture was stirred at room temperature for 2 h. The volatiles were then removed in *vacuo* and the residue dissolved in approximately 2 mL of benzene, filtered into a glass vial, and placed in a dry box. Evaporation of solvent at room temperature afforded 22 mg (63 % yield) of pure red crystalline blocks of **5.8*cc***.

Addition of 1 equivalent each of PhCCH and PhCCD to 5.1*t* : To an equimolar mixture of PhCCH and PhCCD (7.5 μL, 0.069 mmol) dissolved in 0.5 mL of toluene-d_8 in a 5 mm NMR tube, 25.0 mg (0.068 mmol) of **5.1*t*** was added. ^{1}H NMR after approximately 10 min showed peaks corresponding to the product. Integration of the

resonances indicated approximately a 1:1 ratio for products **5.3*c*** and **5.3*c*-*d*$_1$**. Similarly when the reaction was carried out in non-deuterated toluene solvent, $^2H\{^1H\}$ NMR showed two singlet resonances for the starting PhCCD and product **5.3*c*-*d*$_1$** with relative intensities of approximately 1:1.

Reaction of 5.1*t* with 6 equiv PhCCH and 6 equiv PhCCD: To an equimolar mixture of PhCCH and PhCCD (44.4 μL, 0.404 mmol) dissolved in 0.6 mL of toluene-*d8* in a 5 mm NMR tube, 12.5 mg (0.034 mmol) of **5.1*t*** was added. 1H NMR after ~10 min showed peaks corresponding to the product. Integration of the resonances indicated an ~1:1 ratio for products **5.3*c*** and **5.3*c*-*d*$_1$**. Similarly, when the reaction was carried out in nondeuterated toluene solvent, 2H{1H} NMR showed two singlet resonances for the starting PhCCD and product **5.3*c*-*d*$_1$** with relative intensities of ~1:11 (see Figures D.4 and D.5 in Appendix D).

Reaction of 5.1*t* with Excess Pyridine: A stock solution of **5.1*t*** in C_6D_6 was prepared by dissolving 80.5 mg of **5.1*t*** in 5 mL of C_6D_6. In an NMR tube, to 0.5 mL of this solution (0.022 mmol), 87 μL of pyridine (1.06 mmol) was added, followed by the addition of C_6D_6, such that the total volume was 1.023 mL. Similarly, in a series of experiments, to 0.5 mL solution of **5.1*t***, pyridine in the amounts of 174, 349, and 523 μL, was added. ^1H NMR spectra are shown in Figure D.6 in Appendix D.

5.7. Crystallographic analysis.

Single crystals of **5.1*t*, 5.2*c*, 5.3*c*, 5.4*c*, 5.5*c*,** and **5.7*c*** suitable for X-ray diffraction (XRD) analysis were grown by evaporation of diethyl ether solutions at −25 °C. Single crystals of **5.9*t*** suitable for XRD analysis were grown by evaporation of a

diethyl ether solution with a drop of pyridine. Single crystals of **5.8*cc*** suitable for XRD analysis were grown by evaporation of a benzene solution. Single crystals of **5.10*t*** suitable for XRD analysis were grown by evaporation of mixture of CH_2Cl and hexane solution. Data crystals for **5.4*c*, 5.5*c*,** and **5.7*c*** were glued to the end of a thin glass fiber for data collection under ambient conditions. Data crystals for **5.1*t*, 5.2*c*, 5.3*c*, 5.8*cc*, and 5.9*t*** were mounted onto the end of a thin glass fiber using Paratone-N for data collection at 100 K under flow of N_2. X-ray intensity data were measured using a Bruker SMART APEX2 CCD-based diffractometer using Mo Kα radiation (λ = 0.71073 Å).[99] The raw data frames were integrated with the SAINT+ program by using a narrow-frame integration algorithm.[99] Corrections for Lorentz and polarization effects were also applied with SAINT+. An empirical absorption correction based on the multiple measurement of equivalent reflections was applied using the program SADABS. All structures were solved by a combination of direct methods and difference Fourier syntheses, and refined by full-matrix least-squares on F^2, by using the SHELXTL software package.[100,101] All non-hydrogen atoms were refined with anisotropic displacement parameters. Hydrogen atoms were located from the difference map and refined with isotropic thermal parameters. Crystal data, data collection parameters, and results of the analyses are listed in Tables D1 and D2 in Appendix D.

The compound Ni(η^2-TEMPO)$_2$, **5.1*t*,** crystallized in the monoclinic crystal system. The systematic absences in the intensity data were consistent with the unique space group $P2_1/n$. With $Z = 2$ the molecule is crystallographically centrosymmetrical and thus contains only one-half of the formula equivalent of the molecule in the asymmetric crystal unit.

The compound Ni(η^2-TEMPO)(k^1-TEMPO)(κ^1-CNBu^t), **5.2*c*,** crystallized in the monoclinic crystal system. The systematic absences in the intensity data were consistent with the unique space group $P2_1/n$.

Compound Ni(η^2-TEMPO)(κ^1-TEMPOH)(κ^1-CCPh), **5.3*c*,** crystallized in the triclinic crystal system. The space group $P\bar{1}$ was assumed and confirmed by the successful solution and refinement of the structure.

The compound Ni(η^2-TEMPO)(κ^1-TEMPOH)(κ^1-CCSiMe$_3$), **5.4*c*,** crystallized in the monoclinic crystal system. The systematic absences in the intensity data were consistent with the unique space group $P2_1/c$.

The compound Ni(η^2-TEMPO)(κ^1-TEMPOH)(κ^1-CCH), **5.5*c*** crystallized in the monoclinic crystal system. The systematic absences in the intensity data were consistent with the unique space group $P2_1/c$.

The compound and Ni(η^2-TEMPO) (κ^1-TEMPOH)(κ^1-CC[C$_6$H$_4$]CCH), **5.7*c*** crystallized in the triclinic crystal system. The space group $P\bar{1}$ was assumed and confirmed by the successful solution and refinement of the structure.

The compound Ni(η^2-TEMPO)(k^1-TEMPOH)[k^1-k^1-CC(C$_6$H$_4$)CC]Ni(η^2-TEMPO)(k^1-TEMPOH), **5.8*cc*** crystallized in the monoclinic crystal system. The systematic absences in the intensity data were consistent with the unique space group $P2_1/c$. The molecule is also crystallographically centrosymmetrical, and, moreover, the asymmetric unit contains two molecules of benzene from the crystallization solvent that co-crystallized with the complex.

The compound Ni(η^2-TEMPO)(k^1-TEMPO)(κ^1-NC_5H_5), **5.9*t*,** crystallized in the orthorhombic crystal system. The systematic absences in the intensity data were consistent with the unique space group Pbca.

Compounds Ni(η^2-TEMPO)$_2$, **5.1*t*,** Ni(η^2-TEMPO)(k^1-TEMPO)(κ^1-$CNBu^t$), **5.2*c*,** Ni(η^2-TEMPO)(κ^1-TEMPOH)(κ^1-CCPh), **5.3*c***, and Ni(η^2-TEMPO)(k^1-TEMPO)(κ^1-NC_5H_5), **5.9*t*,** decompose rapidly in air and thus their X-ray data collections were performed at 100 K under flow of N_2.

References.

1. "*Activation of Small Molecules*"; William, B. T., Ed.; WILEY-VCH: Weinheim, Germany, 2006, Chapter 1.

2. Yin, X.; Moss, J. R. *Coord. Chem. Rev.* **1999**, *181*, 27–59.

3. Herzog, H. J.; Drake, E. M. *Annu. Rev. Energy Environ.* **1996**, *21*, 145–166.

4. Herrmann, W. A.; Cornils, B. *Angew. Chem. Int. Ed. Engl.* **1997**, *36*, 1048–1067.

5. Zeise, W. C. *Ann. der Phys. und Chem.* **1831**, *21*, 497–541.

6. Love, R. A.; Koetzle, T. F.; Williams, G. J. B.; Andrews, L. C.; Bau, R. *Inorg. Chem.* **1975**, *14*, 2653–2657.

7. Mond, L.; Langer, C.; Quincke, F. *J. Chem. Soc. Trans.* **1890**, *57*, 749–753.

8. *Nature* **1898**, *59*, 63–64.

9. Abeles, R. H. *"Current Status of the Mechanism of Action of B12- Coenzyme" in Biological Aspects of Inorganic Chemistry, Addison, A. W.; Cullen, W. R.;Dolphin, D.; James, B. R. eds.,*; Wiley- Interscience,: New York, USA, 1977; pp. 245–260.

10. Gomez, M.; Muller, G.; Sainz, D.; Sales, J.; Solans, X. *Organometallics* **1991**, *10*, 4036–4045.

11. Gil, W.; Trzeciak, A. *Coord. Chem. Rev.* **2011**, *255*, 473–483.

12. Muñiz, K. *Angew. Chem. Int. Ed.* **2005**, *44*, 6622–6627.

13. Jira, R. *Angew. Chem. Int. Ed.* **2009**, *48*, 9034–9037.

14. Langmuir, I. *Science* **1921**, *54*, 59–67.

15. Jensen, W. B. *J. Chem. Educ.* **2005**, *82*, 28.

16. Blanchard, A. A.; Gilliland, W. L. *J. Am. Chem. Soc.* **1926**, *48*, 872–882.

17. Craig, D. P.; Doggett, G. *J. Chem. Soc.* **1963**, 4189–4198.

18. Mitchell, P. R.; Parish, R. V. *J. Chem. Educ.* **1969**, *46*, 811.

19. Miessler, G. L.; Tarr, D. A. In *Inorganic Chemistry*; Prentice-Hall: upper Saddle River, New Jersey-07458, USA, 1998; pp. 422–482.

20. Flood, T. C.; Jensen, J. E.; Statler, J. A. *J. Am. Chem. Soc.* **1981**, *103*, 4410–4414.

21. Day, J. P.; Basolo, F.; Pearson, R. G. *J. Am. Chem. Soc.* **1968**, *90*, 6927–6933.

22. Haim, A.; Wilmarth, W. K. *Inorg. Chem.* **1962**, *1*, 573–582.

23. Mays, M. J.; Simpson, R. N. F.; Stefanini, F. P. *J. Chem. Soc. Inorg. Phys. Theor.* **1970**, 3000–3002.

24. Miessler, G. L.; Tarr, D. A. In *Inorganic Chemistry*; Prentice-Hall: upper Saddle River, New Jersey-07458, USA, 1998; pp. 483–517.

25. Keitz, B. K.; Bouffard, J.; Bertrand, G.; Grubbs, R. H. *J. Am. Chem. Soc.* **2011**, *133*, 8498–8501.

26. Handbook of Metathesis by R. H. Grubbs. Wiley VCH: Weinheim. 2003. 1156 pp (3 volumes). ISBN 3-527-30616-1. *Org. Process Res. Dev.* **2003**, *8*, 294–294.

27. Nguyen, S. T.; Johnson, L. K.; Grubbs, R. H.; Ziller, J. W. *J. Am. Chem. Soc.***1992**, *114*, 3974–3975.

28. Dias, E. L.; Nguyen, S. T.; Grubbs, R. H. *J. Am. Chem. Soc.* **1997**, *119*, 3887–3897.

29. Jones, J. H. *Platin. Met. Rev.* **2000**, *44*, 94–105.

30. Cavallo, L.; Correa, A.; Costabile, C.; Jacobsen, H. *J. Organomet. Chem.* **2005**, *690*, 5407–5413.

31. Kelly III, R. A.; Clavier, H.; Giudice, S.; Scott, N. M.; Stevens, E. D.; Bordner, J. *Organometallics* **2007**, *27*, 202–210.

32. Huang, J.; Schanz, H.-J.; Stevens, E. D.; Nolan, S. P. *Organometallics*, **1999**, *18*, 5375–5380.

33. Tolman, C. A. *J. Chem. Educ.* **1986**, *63*, 199–201.

34. Tolman, C. A. *J. Am. Chem. Soc.* **1970**, *92*, 2956–2965.

35. Tolman, C. A. *Chem. Rev.* **1977**, *77*, 313–348.

36. Tolman, C. A.; Seidel, W. C.; Gosser, L. W. *J. Am. Chem. Soc.* **1974**, *96*, 53–60.

37. Sinfelt, J. H. *Bimetallic Catalysts. Discoveries, Concepts and Applications*; Wiley: New York, 1983.

38. Sachtler, W. M. H. *J. Mol. Catal.* **1984**, *25*.

39. Beuken, E. K. van den; Feringa, B. L. *Tetrahedron* **1998**, *54*, 12985–13011.

40. Guerrero-Ruiz, A. *Appl. Catal. A: Gen.* **1992**, *81*, 101–112.

41. Onda, A.; Komatsu, T.; Yashima, T. *Chem. Commun.* **1998**, 1507–1508.

42. Araña, J.; Ramirez de la Piscina, P.; Llorca, J.; Sales, J.; Homs, N.; Fierro, J. L. G. *Chem. Mater.* **1998**, *10*, 1333–1342.

43. Román-Leshkov, Y.; Barrett, C. J.; Liu, Z. Y.; Dumesic, J. A. *Nature* **2007**, *447*, 982–985.

44. Zhu, L.; Yempally, V.; Isrow, D.; Pellechia, P. J.; Captain, B. *J. Organomet.Chem.* **2010**, *695*, 1–5.

45. Parshall, G. W. *J. Am. Chem. Soc.* **1966**, *88*, 704–708.

46. Lindsey, R. V.; Parshall, G. W.; Stolberg, U. G. *J. Am. Chem. Soc.* **1965**, *87*, 658–659.

47. Holt, M. S.; Wilson, W. L.; Nelson, J. H. *Chem. Rev.* **1989**, *89*, 11–49.

48. Thomas, J. M.; Johnson, B. F. G.; Raja, R.; Sankar, G.; Midgley, P. A. *Acc.Chem. Res.* **2003**, *36*, 20–30.

49. Hermans, S.; Raja, R.; Thomas, J. M.; Johnson, B. F. G.; Sankar, G.; Gleeson, D. *Angew. Chem. Int. Ed.***2001**, *40*, 1211–1215.

50. Johnson, B. F. G.; Raynor, S. A.; Brown, D. B.; Shephard, D. S.; Mashmeyer, T.; Thomas, J. M.; Hermans, S.; Raja, R.; Sankar, G. *J. Mol. Catal. A: Chem.* **2002**, *182–183*, 89–97.

51. Hermans, S.; Johnson, B. F. G. *J. Chem. Soc. Chem. Commun.* **2000**, 1955–1956.

52. Huber, G. W.; Shabaker, J. W.; Dumesic, J. A. *Science* **2003**, *300*, 2075–2078.

53. Shabaker, J. W.; Simonetti, D. A.; Cortright, R. D.; Dumesic, J. A. *J. Catal.* **2005**, *231*, 67–76.

54. Rocha, W. R. *J Mol Stru-Theochem*, **2004**, *677*, 133–143.

55. Coupé, J. N.; Jordão, E.; Fraga, M. A.; Mendes, M. J. *Appl.Catal. A: Gen.* **2000**, *199*, 45–51.

56. West, N. M.; White, P. S.; Templeton, J. L. *Organometallics* **2008**, *27*, 5252–5262.

57. Muraza, O.; Rebrov, E. V.; Berenguer-Murcia, A.; de Croon, M. H. J. M. *Appl. Catal. A: Gen.* **2009**, *368*, 87–96.

58. Manzoli, M.; Shetti, V. N.; Blaine, J. A. L.; Zhu, L.; Isrow, D.; Yempally, V.; Captain, B. *Dalton. Trans.* **2012**, *41*, 982–989.

59. Yempally, V.; Zhu, L.; Isrow, D.; Captain, B. *J. Clust. Sci.* **2010**, *21*, 417–426.

60. Zhu, L.; Yempally, V.; Isrow, D.; Pellechia, P.; Captain, B. *J. Clust. Sci.* **2012**, *23*, 627–648.

61. Yempally, V.; Zhu, L.; Captain, B. *Inorg. Chem.* **2010**, *49*, 7238–7240.

62. Latif, L. A.; Eaborn, C.; Pidcock, A. P.; Weng, N. S. *J. Organomet. Chem.* **1994**, *474*, 217–221.

63. Baratta, W.; Stoccoro, S.; Doppiu, A.; Herdtweck, E.; Zucca, A.; Rigo, P. *Angew. Chem. Int. Ed.* **2003**, *42*, 105–109.

64. Hackett, M.; Ibers, J. A.; Jernakoff, P.; Whitesides, G. M. *J. Am. Chem. Soc.* **1986**, *108*, 8094–8095.

65. Hackett, M.; Whitesides, G. M. *J. Am. Chem. Soc.* **1988**, *110*, 1449–1462.

66. White, C. P.; Braddock-Wilking, J.; Corey, J. Y.; Xu, H.; Redekop, E.; Sedinkin, S.; Rath, N. P. *Organometallics* **2007**, *26*, 1996–2004.

67. Braddock-Wilking, J.; Corey, J. Y.; White, C.; Xu, H.; Rath, N. P. *Organometallics* **2005**, *24*, 4113–4115.

68. Adams, R. D.; Trufan, E. *Inorg. Chem.* **2009**, *48*, 6124–6129.

69. Calabrese, J. C.; Dahl, L. F.; Cavalieri, A.; Chini, P.; Longoni, G.; Martinengo, S. *J. Am. Chem. Soc.* **1974**, *96*, 2616–2618.

70. Cittadinia, V.; Leoni, P.; Marchetti, L.; Pasquali, M.; Albinati, A. *Inorganica Chim. Acta* **2002**, *330*, 25–32.

71. Nakazawa, H. *J. Organomet. Chem.* 2000, *611*, 349–363.

72. Levy, C. J.; Puddephatt, R. J. *Organometallics* **1997**, *16*, 4115–4120.

73. Bercaw, J. E.; Chen, G. S.; Labinger, J. A.; Lin, B.-L. *J. Am. Chem. Soc.* **2008**, *130*, 17654–17655.

74. Chen, G. S.; Bercaw, J. E.; Labinger, J. A. *Proc. Natl. Acad. Sci. United States Am.* **2007**, *104*, 6915–6920.

75. Rubinstein, L. I.; Pignolet, L. H. *Inorg. Chem.* **1996**, *35*, 6755–6762.

76. Sbraccia, C.; Zipoli, F.; Car, R.; Cohen, M. H.; Dismukes, G. C.; Selloni, A. *J. Phys. Chem. B* **2008**, *112*, 13381–13390.

77. Albinati, A.; Bakhmutov, V. I.; Caulton, K. G.; Clot, E.; Eckert, J.; Eisenstein, O.; Gusev, D. G.; Grushin, V. V.; Hauger, B. E. *J. Am. Chem. Soc.* **1993**, *115*, 7300–7312.

78. Ros, R. *J. Organomet. Chem.*, **1977**, *133*, 213–218.

79. Huang, Z.; White, P. S.; Brookhart, M. *Nature* **2010**, *465*, 598–601.

80. Conroy-Lewis, F. M.; Simpson, S. J. *J. Chem. Soc. Chem. Commun.* **1986**, 506–507.

81. Upmacis, R. K.; Poliakoff, M.; Turner, J. J. *J. Am. Chem. Soc.* **1986**, *108*, 3645–3651.

82. Kubas, G. J.; Unkefer, C. J.; Swanson, B. I.; Fukushima, E. *J. Am. Chem. Soc.* **1986**, *108*, 7000–7009.

83. Urey, H. C. *J. Chem. Soc*.**1947**, 562–581.

84. Isrow, D. Electronic unsaturation of organometallic complexes imparted by sterically demanding ligands, University of Miami, Coral Gables, FL, June, 2011.

85. Almeida, J. F.; Dixon, K. R.; Eaborn, C.; Hitchcock, P. B.; Pidcock, A. *J. Chem. Soc. Chem. Commun.* **1982**, 1315–1316.

86. Kirchmann, M.; Eichele, K.; Schappacher, F. M.; Pöttgen, R.; Wesemann, L. *Angew. Chem. Int. Ed.***2008**, *47*, 963–966.

87. Kirchmann, M.; Fleischhauer, S.; Wesemann, L. *Organometallics* **2008**, *27*, 2803–2808.

88. Permin, A.; Eisenberg, R. *Inorg. Chem.* **2002**, *41*, 2451–2458.

89. Garralda, M. A.; Hernández, R.; Ibarlucea, L.; Pinilla, E.; Torres, M. R. *Organometallics* **2003**, *22*, 3600–3603.

90. Kretschmer, M.; Pregosin, P. S. *J. Organomet. Chem.* **1985**, *281*, 365–378.

91. Glockling, F.; Pollock, R. J. I. *J. Chem. Soc., Dalton Trans.*, **1975**, 497–498.

92. Clemmit, A. F.; Glockling, F. *J. Chem. Soc. Chem. Commun.* **1970**, 705–706.

93. Tanabe, M.; Ito, D.; Osakada, K. *Organometallics* **2007**, *26*, 459–462.

94. Corey, J. Y. *Adv. Organomet. Chem.* **2004**, *51*, 1–52.

95. Curtis, M. D.; Epstein, P. S. *Adv. Organomet. Chem.* **1981**, *19*, 213–255.

96. Bertsch, S.; Braunschweig, H.; Forster, M.; Gruss, K.; Radacki, K. *Inorg. Chem.* **2011**, *50*, 1816–1819.

97. Spencer, J. L. *Inorg. Synth.* **1979**, *19*, 213.

98. Gynane, M. J. S.; Lappert, M. F.; Riley, P. *J. Organomet. Chem.* **1980**, *202*, 5–12.

99. *Apex2 Version 2.2-0 SAINT+ Version 7.46A; Bruker Anal. X-ray Syst. Inc., Madison, Wisconsin, USA,* **2007**.

100. Sheldrick, G. M. *Acta Crystallogr. Sect.* **2008**, *64*, 112–122.

101. *Sheldrick, G. M. SHELXTL Version 6.1; Bruker Anal. X-ray Syst. Inc., Madison, Wisconsin, USA,* **2000**.

102. Díez-González, S.; Marion, N.; Nolan, S. P. *Chem. Rev.* **2009**, *109*, 3612–3676.

103. Öfele, K. *J. Organomet. Chem.* **1968**, *12*, P42–P43.

104. Wanzlick, H.-W.; Schönherr, H.-J. *Angew.Chem. Int. Ed. Engl*.**1968**, *7*, 141–142.

105. Lappert, M. F. *J. Organomet. Chem.* **1988**, *358*, 185–213.

106. Arduengo, A. J.; Harlow, R. L.; Kline, M. *J. Am. Chem. Soc.* **1991**, *113*, 361–363.

107. Dorta, R.; Stevens, E. D.; Hoff, C. D.; Nolan, S. P. *J. Am. Chem. Soc.* **2003**, *125*, 10490–10491.

108. Naziruddin, A. R.; Hepp, A.; Pape, T.; Hahn, F. E. *Organometallics*, **2011**, *30*, 5859–5866.

109. Viciu, M. S.; Germaneau, R. F.; Nolan, S. P. *Org. Lett.* **2002**, *4*, 4053–4056.

110. Herrmann, W. A. *Angew. Chem. Int. Ed.* **2002**, *41*, 1290–1309.

111. Díez-González, S.; Nolan, S. P. *Coord. Chem. Rev.* **2007**, *251*, 874–883.

112. Jacobsen, H.; Correa, A.; Poater, A.; Costabile, C.; Cavallo, L. *Coord. Chem. Rev.* **2009**, *253*, 687–703.

113. Frenking, G.; Solà, M.; Vyboishchikov, S. F. *J. Organomet. Chem.* **2005**, *690*, 6178–6204.

114. Herrmann, W. A.; Elison, M.; Fischer, J.; Köcher, C.; Artus, G. R. J. *Angew.Chem. Int. Ed. Engl*. **1995**, *34*, 2371–2374.

115. Fürstner, A.; Leitner, A. *Synlett* **2001**, 290–292.

116. McGuinness, D. S.; Cavell, K. J. *Organometallics*, **2000**, *19*, 741–748.

117. Chatterjee, A. K.; Grubbs, R. H. *Org. Lett.* **1999**, *1*, 1751–1753.

118. Keitz, B. K.; Bouffard, J.; Bertrand, G.; Grubbs, R. H. *J. Am. Chem. Soc.* **2011**, *133*, 11006–11006.

119. Clavier, H.; Urbina-Blanco, C. A.; Nolan, S. P. *Organometallics*, **2009**, *28*, 2848–2854.

120. Jafarpour, L.; Nolan, S. P. *Organometallics*, **2000**, *19*, 2055–2057.

121. Rix, D.; Caijo, F.; Laurent, I.; Boeda, F.; Clavier, H.; Nolan, S. P.; Mauduit, M. *J. Org. Chem.* **2008**, *73*, 4225–4228.

122. Hadei, N.; Kantchev, E. A. B.; O'Brie, C. J.; Organ, M. G. *Org. Lett.* **2005**, *7*, 3805–3807.

123. Hadei, N.; Kantchev, E. A. B.; O'Brie, C. J.; Organ, M. G. *J. Org. Chem.* **2005**, *70*, 8503–8507.

124. Hadei, N.; Kantchev, E. A. B.; O'Brie, C. J.; Organ, M. G. *Org. Lett.* **2005**,*7*, 1991–1994.

125. Cai, X.; Majumdar, S.; Fortman, G. C.; Cazin, C. S. J.; Slawin, A. M. Z.; Lhermitte, C.; Prabhakar, R.; Germain, M. E.; Palluccio, T.; Nolan, S. P.; Rybak- Akimova, E. V.; Temprado, M.; Captain, B.; Hoff, C. D. *J. Am. Chem. Soc.* **2011**, *133*, 1290–1293.

126. Lee, C. H.; Laitar, D. S.; Mueller, P.; Sadighi, J. P. *J. Am. Chem. Soc.* **2007**, *129*, 13802–13803.

127. Wu, J.; Faller, J. W.; Hazari, N.; Schmeier, T. J. *Organometallics*, **2012**, *31*, 806–809.

128. Fantasia, S.; Egbert, J. D.; Jurčík, V.; Cazin, C. S. J.; Jacobsen, H.; Cavallo, L.; Heinekey, D. M.; Nolan, S. P. *Angew. Chem. Int. Ed.* **2009**, *48*, 5182–5186.

129. Wu, J.; Hazari, N.; Incarvito, C. D. *Organometallics*, **2011**, *30*, 3142–3150.

130. Praetorius, J. M.; Crudden, C. M. *Dalton. Trans.* **2008**, 4057–4180.

131. Nolan, S. P. *Accounts Chem. Res.* **2011**, *44*, 91–100.

132. Veige, A. S. *Polyhedron*, **2008**, *27*, 3177–3189.

133. Llewellyn, S. A.; Green, M. L. H.; Cowley, A. R. -*t. Trans.* **2006**, 4164–4168.

134. Marko, I. E. *Science*, **2002**, *298*, 204–206.

135. Jung, I. G.; Seo, J.; Lee, S. I.; Choi, S. Y.; Chung, Y. K. *Organometallics*, **2006**, *25*, 4240–4242.

136. Marx, T.; Wesemann, L.; Hagen, S.; Pantenburg, I. *Z. Naturforsch*, **2003**, *58*, 147–150.

137. Auburn, M.; Ciriano, M.; Howard, J. A. K.; Murray, M.; Pugh, N. J.; Spencer, J. L.; Stone, F. G. A.; Woodward, P. *J. Chem. Soc., Dalton Trans.* **1980**, 659–666.

138. *Theory Appl. Comput. Chem. Chapter 40 – Forty years Fenske-Hall Mol. orbital Theory* **2005**, 1143–1165.

139. Hall, M. B.; Fenske, R. F. *Inorg. Chem.* **1972**, *11*, 768–775.

140. Furlani, A.; Licoccia, S.; Russo, M. V. New Platinum Hydrido Acetylides. Crystal and Molecular Structure. *J. Chem. Soc., Dalton Trans.***1982**, 2449–2453.

141. Darensbourg, D. J.; Hyde, C. L. *J. Chem. Phys.* **1973**, *59*, 3869–3870.

142. Gründemann, S.; Kovacevic, A.; Albrecht, M.; Faller, J. W.; Crabtree, R. H. *J. Am. Chem. Soc.* **2002**, *124*, 10473–10481.

143. Nuzzo, R. G.; McCarthy, T. J.; Whitesides, G. M. *Inorg. Chem.* **1981**, *20*, 1312–1314.

144. Hunt, L. B.; Lever, F. M. *Platin. Met. Rev.* **1969**, *13*, 126–138.

145. Burge, H. D.; Collins, D. J.; Davis, B. H. *Ind. & Eng. Chem. Prod. Res. Dev.* **1980**, *19*, 389–391.

146. Raney, M. "*Method of Producing Finely Divided Nickel*" **1927**, U.S. Patent1, 628,190.

147. Silgel, A.; Sigel, H. *Met. Ions Life Sci.* **2007**, *2*.

148. Jolly, P. .; Wilke, G. *"The organic chemistry of Nickel"*; Academic Press: New york, USA, 1974.

149. In *Jolly, P. W., in "Comprehensive Organometallic Chemistry",*; Wilkinson, G.; Stone, F. G. A.; Abel, E. W., Eds.; Pergamon: Oxford, UK, 1982; Vol. 8, pp. 773–797.

150. Amer, I.; Alper, H. *J. Organomet. Chem.* **1990**, *383*, 573–577.

151. Fontaine, F.-G.; Nguyen, R.-V.; Zargarian, D. *Int. J. Chem.* **2003**, *81*, 1299–1306.

152. Wilke, G. *Angew.Chem. Int. Ed. Engl*. **1988**, *27*, 185–206.

153. Alonso, F.; Riente, P. *Tetrahedron*, **2009**, *65*, 10637–10643.

154. Choi, H.; Hershberger, J. W.; Pinhas, A. R.; Ho, D. M. *Organometallics*, **1991**, *10*, 2930–2936.

155. Negishi, E.; Takahashi, T.; Akiyoshi, K. *Chem. Ind.* **1988**, *33*, 381.

156. Negishi, E. *Accounts Chem. Res.* **1982**, *15*, 340–348.

157. Kumada, M. *Pure Appl. Chem.* **1980**, *52*, 669–679.

158. Hoberg, H.; Peres, Y.; Krüger, C.; Tsay, Y.-H. *Angew.Chem. Int. Ed. Engl*. **1987**, *26*, 771–773.

159. Hoberg, H.; Ballesteros, A.; Sigan, A.; Jégat, C.; Bärhausen, D.; Milchereit, A. *J. Organomet. Chem*. **1991**, *407*, C23–C29.

160. Hoberg, H.; Ballesteros, A.; Sigan, A.; Jégat, C.; Bärhausen, D.; Milchereit, A. *J. Organomet. Chem.*, 1991, *407*, C23–C29.

161. Walther, D.; Bräunlich, G. *J. Organomet. Chem.* **1992**, *436*, 109–119.

162. Morgenstern, D. A.; Wittrig, R. E.; Fanwick, P. E.; Kubiak, C. P. *J. Am. Chem. Soc.* **1993**, *115*, 6470–6471.

163. Yempally, V. Synthesis and characterization of transition metal complexes with bulky ligands for application in small molecule activation, University of Miami, Coral Gables, Fl, June, 2012.

164. Fox, B. J.; Millard, M. D.; DiPasquale, A. G.; Rheingold, A. L.; Figueroa, J. S. *Angew. Chem. Int. Ed.* **2009**, *48*, 3473–3477.

165. Day, V. W.; Day, R. O.; Kristoff, J. S.; Hirsekorn, F. J.; Muetterties, E. L. *J. Am. Chem. Soc.* **1975**, *97*, 2571–2573.

166. Wrighton, M. *Chem. Rev.* **1974**, *74*, 401–430.

167. Puff, H.; Breuer, B.; Gehrke-Brinkmann, G.; Kind, P.; Reuter, H.; Schuh, W.; Wald, W.; Weidenbrück, G. *J. Organomet. Chem.* **1989**, *363*, 265–280.

168. Buschhaus, H.-U.; Neumann, W. P.; Apoussidis, T. *Liebigs Ann. Chem.***1981**, *1981*, 1190–1197.

169. Kerschl, S.; Wrackmeyer, B. *Z. Naturforsch, B: Chem. Sci*. **1987**, *42*, 387–394.

170. Mindiola, D. J.; Waterman, R.; Jenkins, D. M.; Hillhouse, G. L. *Inorg. Chim. Acta* **2003**, *345*, 299–308.

171. Blanchard, S.; Neese, F.; Bothe, E.; Bill, E.; Weyhermüller, T.; Wieghardt, K. *Inorg. Chem.* **2005**, *44*, 3636–3656.

172. Davies, A. G. "*Organotin chemistry"*; Weinheim : Wiley-VCH, 2004.

173. Lebedev, O. L.; Kazarnovskii, S. N. *Zhur. Obshch. Khim.* **1960**, *30*, 1631–1635.

174. Barriga, S. *Synlett*, **2001**, *4*, 563.

175. Mahanthappa, M. K.; Huang, K.-W.; Cole, A. P.; Waymouth, R. M. *Chem.Commun.* **2002**, 502–503.

176. Zhu, Z.; Fettinger, J. C.; Olmstead, M. M.; Power, P. P. *Organometallics*, **2009**, *28*, 2091–2095.

177. Ito, M.; Matsumoto, T.; Tatsumi, K. *Inorg. Chem.* **2009**, *48*, 2215–2223.

178. Laugier, J.; Latour, J. M.; Caneschi, A.; Rey, P. *Inorg. Chem.* **1991**, *30*, 4474–4477.

179. Sekiguchi, A.; Fukawa, T.; Lee, V. Y.; Nakamoto, M. *J. Am. Chem. Soc.* **2003**, *125*, 9250–9251.

180. Meier, K. *Coord. Chem. Rev.* **1991**, *111*, 97–110.

181. Yamamoto, M.; Oster, G. *J. Polym. Sci., Part A-1: Polym. Chem.* **1966**, *4*, 1683–1688.

182. Tehfe, M. A.; Louradouremail, F.; Lalevée, J.; Fouassieremail, J.-P. *Appl. Sci.* **2013**, *3*.

183. Fouassier, J.; Allonas, X.; Burget, D. *Prog. Org. Coatings* **2003**, *47*, 16–36.

184. Li, P.; Qiu, K.-Y. *Polymer* **2002**, *43*, 5873–5877.

185. Dolinsky, M. C. B.; Lin, W. O.; Dias, M. L. *J. Mol. Catal. A-chemical* **2006**, *258*, 267–274.

186. Jiang, H.; Xiao, J.; Lu, J. *E-polymers* **2011**, *11*, 454–462.

187. Merlin, A.; Lougnot, D.; Fouassier, J. *Polym. Bull.* **1980**, *3*, 1–6.

188. Ciriminna, R.; Pagliaro, M. *Org. Process. Res. & Dev.* **2010**, *14*, 245–251.

189. Keana, J. F. W. *Chem. Rev.* **1978**, *78*, 37–64.

190. Lagunas, A.; Mairata i Payeras, A.; Jimeno, C.; Pericàs, M. A. *Org. Lett.* **2005**, *7*, 3033–3036.

191. Hoffman, B. M.; Eames, T. B. *J. Am. Chem. Soc.* **1971**, *93*, 3141–3146.

192. Forbes, G. C.; Kennedy, A. R.; Mulvey, R. E.; Rodger, P. J. A. *J. Chem. Soc. Chem. Commun.* **2001**, 1400–1401.

193. Scepaniak, J. J.; Wright, A. M.; Lewis, R. A.; Wu, G.; Hayton, T. W. *J. Am. Chem. Soc.* **2012**, *134*, 19350–19353.

194. Wright, A. M.; Zaman, H. T.; Wu, G.; Hayton, T. W. *Inorg. Chem.* **2013**, *52*,3207–3216.

195. Dickman, M. H.; Doedens, R. J. *Inorg. Chem.* **1982**, *21*, 682–684.

196. Dong, T. Y.; Hendrickson, D. N.; Felthouse, T. R.; Shieh, H. S. *J. Am. Chem. Soc.***1984**, *106*, 5373–5375.

197. Farnaby, J. H.; Fang, M.; Ziller, J. W.; Evans, W. J. *Inorg. Chem.* **2012**, *51*, 11168–11176.

198. Georges, M. K.; Lukkarila, J. L.; Szkurhan, A. R. *Macromolecules*, **2004**, *37*, 1297–1303.

199. Maehata, H.; Buragina, C.; Cunningham, M.; Keoshkerian, B. *Macromolecules*, **2007**, *40*, 7126–7131.

200. Hawker, C. J. *Accounts Chem. Res.* **1997**, *30*, 373–382.

201. Benoit, D.; Chaplinski, V.; Braslau, R.; Hawker, C. J. *J. Am. Chem. Soc.* **1999**, *121*, 3904–3920.

202. Hu, S.; Gao, W.; Kumar, R.; Gross, R. A.; Gu, Q.-M.; Cheng, H. N. *Biocatalysis in Polymer Science;* 2002, Chapter 21; pp.253–264.

203. Michaud, A.; Gingras, G.; Morin, M.; Béland, F.; Ciriminna, R.; Avnir, D.; Pagliaro, M. *Org. Process. Res. & Dev.* **2007**, *11*, 766–768.

204. Bordenave, N.; Grelier, S.; Coma, V. *Biomacromolecules*, **2008**, *9*, 2377–2382.

205. De Nooy, A. E. J.; Besemer, A. C.; van Bekkum, H. *Synthesis-stuttgart*, **1996**, 1153–1174.

206. Sheldon, R. A.; Arends, I. W. C. E. *Adv. Synth. Catal.* **2004**, *346*, 1051–1071.

207. Recupero, F.; Punta, C. *Chem. Rev.* **2007**, *107*, 3800–3842.

208. Gamez, P.; Arends, I. W. C. E.; Reedijk, J.; Sheldon, R. A. *Chem. Commun.* **2003**, 2414– 2415.

209. Cheng, L.; Wang, J.; Wang, M.; Wu, Z. *Inorg. Chem.* **2010**, *49*, 9392–9399.

210. Semmelhack, M. F.; Schmid, C. .; Cortes, D. A. *Tetrahedron Lett.* **1986**, *27*, 1119–1122.

211. Borbat, P. P.; Costa-Filho, A. J.; Earle, K. A.; Moscicki, J. K.; Freed, J. H. *Science*, **2001**, *291*, 266–269.

212. Chen, J. Y.-C.; Jayaraj, N.; Jockusch, S.; Ottaviani, M. F.; Ramamurthy, V.; Turro, N. J. *J. Am. Chem. Soc.* **2008**, *130*, 7206–7207.

213. Jayaraj, N.; Porel, M.; Ottaviani, M. F.; Maddipatla, M. V. S. N.; Modelli, A.; Da Silva, J. P.; Bhogala, B. R.; Captain, B.; Jockusch, S.; Turro, N. J.; Ramamurthy, V. *Langmuir*, **2009**, *25*, 13820–13832.

214. Yi, S.; Captain, B.; Ottaviani, M. F.; Kaifer, A. E. *Langmuir*, **2011**, *27*, 5624–5632.

215. Dane, E. L.; Maly, T.; Debelouchina, G. T.; Griffin, R. G.; Swager, T. M. *Org. Lett.* 2009, *11*, 1871–1874.

216. Angelin, M.; Hermansson, M.; Dong, H.; Ramström, O. *Eur. J. Org. Chem.* **2006**, *2006*, 4323–4326.

217. Pervukhina, N. V.; Romanenko, G. V.; Podberezskaya, N. V. *J. Struct. Chem.* 1994, *35*.367-390

218. Felthouse, T. R.; Dong, T. Y.; Hendrickson, D. N.; Shieh, H. S.; Thompson, M. R. *J. Am. Chem. Soc.* **1986**, *108*, 8201–8214.

219. Dickman, M. H.; Porter, L. C.; Doedens, R. J. *Inorg. Chem.* **1986**, *25*, 2595–2599.

220. Caneschi, A.; Grand, A.; Laugier, J.; Rey, P.; Subra, R. *J. Am. Chem. Soc.* **1988**, *110*, 2307–2309.

221. Jaitner, P.; Huber, W.; Gieren, A.; Betz, H. *Z. Anorg. Allg. Chem.* **1986**, *538*, 53–60.

222. Jaitner, P.; Huber, W. *J. Organomet. Chem.* **1986**, *311*, 379–385.

223. Jaitner, P.; Huber, W. *J. Organomet. Chem.* **1983**, *259*, C1–C5.

224. Evans, W. J.; Perotti, J. M.; Doedens, R. J.; Ziller, J. W. *Chem. Commun.* **2001**, 2326–2327.

225. Huang, K.-W.; Han, J. H.; Cole, A. P.; Musgrave, C. B.; Waymouth, R. M. *J. Am. Chem. Soc.* **2005**, *127*, 3807–3816.

226. Hoover, J. M.; Ryland, B. L.; Stahl, S. S. *J. Am. Chem. Soc.* **2013**, *135*, 2357–2367.

227. Belanzoni, P.; Michel, C.; Baerends, E. J. *Inorganic Chemistry*, **2011**, *50*, 11896–11904.

228. Ragagnin, G.; Betzemeier, B.; Quici, S.; Knochel, P. *Tetrahedron* **2002**, *58*, 3985–3991.

229. Lu, Z.; Costa, J. S.; Roubeau, O.; Mutikainen, I.; Turpeinen, U.; Teat, S. J.; Gamez, P.; Reedijk, J. *Dalton Trans.***2008**, 3567–3573.

230. Smith, J. M.; Mayberry, D. E.; Margarit, C. G.; Sutter, J.; Wang, H.; Meyer, K.; *J. Am. Chem. Soc.***2012**, *134*, 6516–6519.

231. Isrow, D.; Captain, B. *Inorg. Chem.* **2011**, *50*, 5864–5866.

232. Hoover, J. M.; Stahl, S. S. *J. Am. Chem. Soc.* **2011**, *133*, 16901–16910.

233. Capiomont, P.; Lajzerowicz-Bonneteau, J. *Acta Crystallogr., Sect. B: Crystallogr. Cryst. Chem.* **1974**, *30*, 2160–2166.

234. Porter, L. C.; Doedens, R. J. *Acta Crystallogr. Sect. C Cryst. Struct. Commun.* **1985**, *41*, 838–840.

235. Isrow, D.; DeYonker, N. J.; Koppaka, A.; Pellechia, P. J.; Webster, C. E.; Captain, B. *Inorg. Chem.* **2013**, *52*, 13882–13893.

236. Fullmer, B. C.; Fan, H.; Pink, M.; Caulton, K. G. *Inorganica Chim. Acta.* **2011**, *369*, 49–54.

237. Frisch, M. J. *Frisch, M. J. Gaussian 09, Rev. B.01; Gaussian, Inc.: Wallingford, CT, 2009.*

238. Parr, R. G.; Yang, W. *Density Functional Theory of Atoms and Molecules; Oxford University Press*; New York, 1989.

239. Becke, A. D. *J. Chem. Phys.* **1993**, *98*, 5648–5652.

240. Lee, C.; Yang, W.; Parr, R. G. *Phys. Rev. B, Condens. Matter.* **1988**, *37*, 785–789.

241. Perdew, P.; Burke, K.; Ernzerhof, M. *Phys. Rev. Lett.* **1997**, *78*, 1936.

242. Hay, P. J.; Wadt, W. R. *J. Chem. Phys.* **1985**, *82*, 299–310.

243. Wadt, W. R.; Hay, P. J. *J. Chem. Phys.***1985**, *82*, 284–298.

244. Couty, M.; Hall, M. B. *J. Comput. Chem.* **1996**, *17*, 1359–1370.

245. Hariharan, P. C.; Pople, J. A. *Theor. Chim. Acta.* **1973**, *28*, 213–222.

246. Foresman, J. B.; Frisch, Æ. In *Exploring Chemistry with Electronic Structure Methods, 2nd Ed.*; Pittsburgh, PA, 1996; p. 110.

247. Marenich, A. V.; Cramer, C. J.; Truhlar, D. G. *J. Phys. Chem. B* **2009**, *113*, 6378–6396.

248. Sgro, M. J.; Stephan, D. W. *-t. Trans.* **2010**, *39*, 5786–5794.

249. Huffman, M. A.; Liebeskind, L. S. *J. Am. Chem. Soc.* **1991**, *113*, 2771–2772.

250. Ervin, K. M.; Gronert, S.; Barlow, S. E.; Gilles, M. K.; Harrison, A. G.; Bierbaum, V. M.; DePuy, C. H.; Lineberger, W. C.; Ellison, G. B. *J. Am. Chem.Soc.* **1990**, *112*, 5750–5759.

251. Segall, J.; Lavi, R.; Wen, Y.; Wittig, C. *J. Phys. Chem.* **1989**, *93*, 7287–7289.

252. Groux, L. F.; Zargarian, D. *Organometallics*, **2003**, *22*, 4759–4769.

253. Khairul, W. M.; Fox, M. A.; Zaitseva, N. N.; Gaudio, M.; Yufit, D. S.; Skelton, B. W.; White, A. H.; Howard, J. A. K.; Bruce, M. I.; Low, P. J. *-t. Trans.* **2009**, 610–620.

254. Burling, S.; Elliott, P. I. P.; Jasim, N. A.; Lindup, R. J.; McKenna, J.; Perutz, R. N.; Archibald, S. J.; Whitwood, A. C. *Dalton Trans.* **2005**, 3686–3695.

255. Goicoechea, J. M.; Sevov, S. C. *J. Am. Chem. Soc.* **2006**, *128*, 4155–4161.

256. Walther, D.; Stollenz, M.; Görls, H. *Organometallics*, **2001**, *20*, 4221–4229.

257. Yam, V. W.-W.; Tao, C.-H.; Zhang, L.; Wong, K. M.-C.; Cheung, K.-K. *Organometallics*, **2001**, *20*, 453–459.

258. Yam, V. W.-W.; Zhang, L.; Tao, C.-H.; Man-ChungWong, K.; Cheung, K.-K. *J. Chem. Soc. Dalton Trans.***2001**, 1111–1116.

259. Müller, C.; Iverson, C. N.; Lachicotte, R. J.; Jones, W. D. *J. Am. Chem. Soc.* **2001**, *123*, 9718–9719.

260. Banditelli, G.; Bandini, A. L. *Organometallics*, **2006**, *25*, 1578–1582.

261. Cao, D. H.; Stang, P. J.; Arif, A. M. *Organometallics*, **1995**, *14*, 2733–2740.

262. Bax, A.; Griffey, R. H.; Hawkins, B. L. *J. Magn. Reson. (1969)*, **1983**, *55*, 301–315.

263. Carlton, L.; Staskun, B.; van Es, T. *Magn. Reson. Chem. : MRC*, **2006**, *44*, 510–514.

264. Chaudhry, A. F.; Mandal, S.; Hardcastle, K. I.; Fahrni, C. J. *Chem. Sci.* **2011**, *2*, 1016–1024.

265. Hetterscheid, D. G. H.; Kaiser, J.; Reijerse, E.; Peters, T. P. J.; Thewissen, S.; Blok, A. N. J.; Smits, J. M. M.; de Gelder, R.; de Bruin, B. *J. Am. Chem. Soc.* **2005**, *127*, 1895–1905.

266. Ahlers, C.; Dickman, M. H. *Inorg. Chem.* **1998**, *37*, 6337–6340.

267. Phillips, J. R.; Trogler, W. C.; Miller, G. A. *Acta Crystallogr. Sect. C Cryst. Struct. Commun.* **1990**, *46*, 1648–1650.

268. Janka, M.; Anderson, G. K.; Rath, N. P. *Organometallics*, **2004**, *23*, 4382–4390.

269. Butler, P.; Gallagher, J. F.; Manning, A. R.; Mueller-Bunz, H.; McAdam, C. J.; Simpson, J.; Robinson, B. H. *J. Organomet. Chem.* 2005, *690*, 4545–4556.

270. Bruce, M. I.; Ellis, B. G.; Low, P. J.; Skelton, B. W.; White, A. H. *Organometallics*, **2003**, *22*, 3184–3198.

271. Cardolaccia, T.; Li, Y.; Schanze, K. S. *J. Am. Chem. Soc.* **2008**, *130*, 2535–2545.

Appendix A: Supporting Information for Chapter 2.

Table A.1. Crystallographic data for compounds **2.1, 2.3** and **2.4.**

Compound	**2.1**	**2.3**	**2.4**
Empirical formula	$PtSnC_{20}H_{40}$	$Pt_2Sn_4C_{40}H_{94}$	$Pt_2Sn_4C_{42}H_{94}O_2$
Formula weight	594.30	1440	1496
Crystal system	Monoclinic	Monoclinic	Triclinic
Lattice parameters			
a (Å)	11.1084(4)	9.2175(8)	9.1706(3)
b (Å)	12.6969(4)	18.2662(15)	11.9962(4)
c (Å)	15.4779(5)	16.2599(13)	12.7070(5)
α (deg)	90.00	90.00	97.1493(5)
β (deg)	102.2130(10)	104.7720(10)	99.4757(5)
γ (deg)	90.00	90.00	102.9447(5)
V ($Å^3$)	2133.63(12)	2647.2(7)	1324.75(8)
Space group	$P2_1/n$ (# 14)	$P2_1/n$ (# 14)	$P\bar{1}$ (# 2)
Z value	4	4	1
ρ_{calc} (g / cm^3)	1.850	1.802	1.870
μ (Mo K_α) (mm^{-1})	7.717	7.144	7.144
Temperature (K)	100	296	100
$2\Theta_{max}$ (°)	63.98	54.00	60.00
No. Obs. (I > 2σ(I))	212	223	7055
No. Parameters	5996	3979	245
Goodness of fit GOF*	1.019	1.003	1.042
Max. shift in cycle	0.001	0.001	0.001
Residuals*: R1; wR2	0.0183; 0.0382	0.0299; 0.0589	0.0391; 0.0974
Absorption Correction, Max/min	Multi-scan 0.8609/0.3715	Multi-scan 0.9320/0.7631	Multi-scan 0.7465/0.4005
Largest peak in Final Diff. Map (e^- / $Å^3$)	0.737	0.994	0.995

*$R = \Sigma_{hkl}(\,|\,|F_{obs}|-|F_{calc}|\,|)/\Sigma_{hkl}|F_{obs}|$; $R_w = [\Sigma_{hkl}w(|F_{obs}|-|F_{calc}|)^2/\Sigma_{hkl}wF_{obs}^2]^{1/2}$, $w = 1/\sigma^2(F_{obs})$; $GOF = [\Sigma_{hkl}w(|F_{obs}|-|F_{calc}|)^2/(n_{data} - n_{vari})]^{1/2}$.

Table A.2. Crystallographic data for compounds **2.5, 2.6** and **2.8.**

Compound	**2.5**	**2.6**	**2.8**
Empirical formula	$PtSn_2N_2C_{34}H_{74}{\cdot}Et_2O$	$PtSn_2N_2C_{34}H_{72}$	$PtSn_3N_2C_{64}H_{64}$
Formula weight	1017.54	941.41	1412.33
Crystal system	Orthorhombic	Monoclinic	Orthorhombic
Lattice parameters			
a (Å)	13.1534(7)	13.6893(6)	13.2568(6)
b (Å)	19.3120(10)	15.7758(7)	18.3985(8)
c (Å)	9.2366(5)	19.1337(8)	24.2209(11)
α (deg)	90.00	90.00	90
β (deg)	90.00	91.0532(7)	90
γ (deg)	90.00	90.00	90
V ($Å^3$)	2346.3(2)	4131.4(3)	5907.6(5)
Space group	*Pmmn* (# 59)	$P2_1/n$ (# 14)	$P2_12_12_1$(#19)
Z value	2	4	4
ρ_{calc} (g / cm^3)	1.440	1.514	1.588
μ (Mo K_α) (mm^{-1})	4.056	4.598	3.653
Temperature (K)	100	100	296
$2\Theta_{max}$ (°)	60.00	60.00	54.00
No. Obs. ($I > 2\sigma(I)$)	2959	9231	10594
No. Parameters	120	376	636
Goodness of fit GOF*	1.080	1.015	1.047
Max. shift in cycle	0.001	0.002	0.004
Residuals*: R1; wR2	0.0437; 0.1062	0.0293; 0.0552	0.0487; 0.1075
Absorption Correction, Max/min	Multi-scan 0.9223/0.4690	Multi-scan 0.9136/0.4311	Multi-scan 0.7457/0.5079
Largest peak in Final Diff. Map (e^- / $Å^3$)	3.100	1.867	1.311

*$R = \Sigma_{hkl}(\,|\,|F_{obs}| - |F_{calc}|\,|)/\Sigma_{hkl}|F_{obs}|$; $R_w = [\Sigma_{hkl}w(|F_{obs}| - |F_{calc}|)^2/\Sigma_{hkl}wF_{obs}^2]^{1/2}$, $w = 1/\sigma^2(F_{obs})$; $GOF = [\Sigma_{hkl}w(|F_{obs}| - |F_{calc}|)^2/(n_{data} - n_{vari})]^{1/2}$.

Table A.3. Crystallographic data for compounds **2.9, 2.10** and **2.11.**

Compound	**2.9**	**2.10**	**2.11**
Empirical formula	$PtSn_2N_2C_{46}H_{48}$	$PtSn_2N_2C_{49}H_{78}$	$PtSn_2N_2C_{64}H_{84}$
Formula weight	1061.33	1127.60	1313.80
Crystal system	Triclinic	Monoclinic	Trigonal
Lattice parameters			
a (Å)	9.9845(6)	12.5045(3)	22.0027(12)
b (Å)	10.4305(6)	21.6120(6)	22.0027(12)
c (Å)	11.9205(7)	21.7113(6)	24.3085(13)
α (deg)	65.6890(1)	90	90
β (deg)	75.8450(1)	99.923(1)	90
γ (deg)	86.2710(1)	90	120
V ($Å^3$)	1096.11(11)	5779.6(3)	10191.6(10)
Space group	$P\ \bar{1}$ (# 2)	$P2_1/n$ (# 14)	$P\ \bar{3}c1$ (# 165)
Z value	1	4	6
ρ_{calc} (g / cm^3)	1.608	1.296	1.284
μ (Mo K_α) (mm^{-1})	4.344	3.299	2.817
Temperature (K)	296	296	296
$2\Theta_{max}$ (°)	56.00	56.00	52.00
No. Obs. ($I > 2\sigma(I)$)	4290	10472	6676
No. Parameters	250	487	324
Goodness of fit GOF*	1.054	1.105	1.165
Max. shift in cycle	0.001	0.001	0.001
Residuals*: R1; wR2	0.0296; 0.0684	0.0387; 0.1350	0.0431; 0.1245
Absorption Correction, Max/min	Multi-scan 0.7461/0.5677	Multi-scan 0.8524/0.5583	Multi-scan 0.7659/0.3987
Largest peak in Final Diff. Map (e^- / $Å^3$)	0.756	1.471	1.751

*$R = \Sigma_{hkl}(\,|\,|F_{obs}| - |F_{calc}|\,|)/\Sigma_{hkl}|F_{obs}|$; $R_w = [\Sigma_{hkl}w(|F_{obs}| - |F_{calc}|)^2/\Sigma_{hkl}wF_{obs}^2]^{1/2}$, $w = 1/\sigma^2(F_{obs})$; $GOF = [\Sigma_{hkl}w(|F_{obs}| - |F_{calc}|)^2/(n_{data} - n_{vari})]^{1/2}$.

Table A.4. Crystallographic data for compounds **2.12** and **2.13.**

Compound	**2.12**	**2.13**
Empirical formula	$PtSn_2C_{26}H_{54}O_2$	$PtSn_2C_{35}H_{72}N_2O$
Formula weight	831.16	969.42
Crystal system	Monoclinic	Orthorhombic
Lattice parameters		
a (Å)	15.3248(2)	13.9304(9)
b (Å)	9.19810(10)	19.0073(13)
c (Å)	24.1611(3)	9.4382(6)
α (deg)	90.00	90.00
β (deg)	98.2477(6)	90.00
γ (deg)	90.00	90.00
V (Å^3)	3370.50(7)	2499.0(3)
Space group	*C*2/*c* (# 15)	*Pmmn* (# 59)
Z value	4	2
ρ_{calc} (g / cm^3)	1.638	1.288
μ (Mo K_α) (mm^{-1})	5.627	3.805
Temperature (K)	296	296
$2\Theta_{max}$ (°)	60.00	56.00
No. Obs. ($I > 2\sigma(I)$)	152	115
No. Parameters	4301	2477
Goodness of fit GOF*	1.199	1.133
Max. shift in cycle	0.001	0.001
Residuals*: R1; wR2	0.0455; 0.1165	0.0442; 0.1369
Absorption Correction, Max/min	Multi-scan 0.7468/0.4928	Multi-scan 0.7461/0.5194
Largest peak in Final Diff. Map (e$^-$ / Å^3)	1.064	1.492

*$R = \Sigma_{hkl}(\,|\,|F_{obs}| - |F_{calc}|\,|)/\Sigma_{hkl}|F_{obs}|$; $R_w = [\Sigma_{hkl}w(|F_{obs}| - |F_{calc}|)^2/\Sigma_{hkl}wF_{obs}^2]^{1/2}$, $w = 1/\sigma^2(F_{obs})$; $GOF = [\Sigma_{hkl}w(|F_{obs}| - |F_{calc}|)^2/(n_{data} - n_{vari})]^{1/2}$.

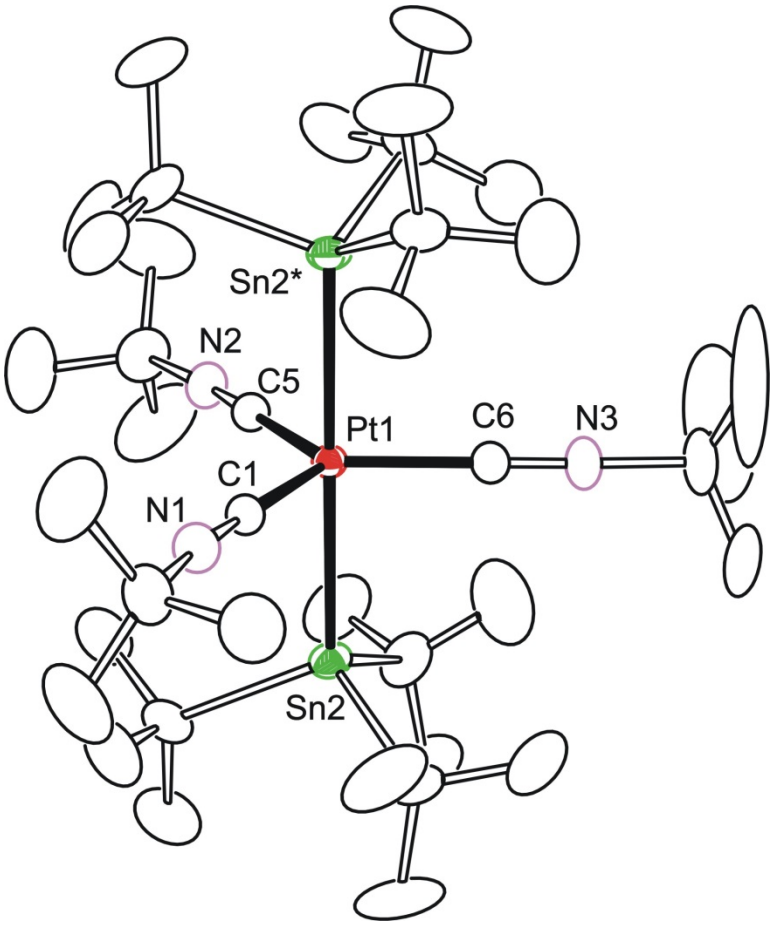

Figure A.1. An ORTEP of the molecular structure of $Pt(SnBu^t_3)(CNBu^t)$, **2.7** showing 30 % thermal ellipsoid probability.

Appendix B: Supporting Information for Chapter 3

Table B.1. Crystallographic data for compounds **3.1** and **3.3.**

Compound	**3.1**	**3.3**
Empirical formula	$Pt_2Sn_2C_{46}H_{96}N_4$	$PtSnC_{24}H_{48}N_2O$
Formula weight	1332.83	694
Crystal system	Triclinic	Monoclinic
Lattice parameters		
a (Å)	10.17420(10)	12.6631(3)
b (Å)	11.76800(10)	27.5135(7)
c (Å)	13.5031(2)	17.6146(4)
α (deg)	102.1810(10)	90.00
β (deg)	106.6930(10)	104.69
γ (deg)	113.1550(10)	90.00
V ($Å^3$)	1324.02(3)	5936.3(2)
Space group	$P\ \bar{1}$ (# 2)	$P2_1/c$ (# 14)
Z value	1	8
ρ_{calc} (g / cm^3)	1.672	1.553
μ (Mo K_α) (mm^{-1})	6.230	5.564
Temperature (K)	100(2)	296(2)
$2\Theta_{max}$ (°)	58.0	54.0
No. Obs. ($I > 2\sigma(I)$)	262	557
No. Parameters	6906	9939
Goodness of fit GOF*	1.072	1.018
Max. shift in cycle	0.002	0.005
Residuals*: R1; wR2	0.0145; 0.0366	0.0279; 0.0562
Absorption Correction, Max/min	Multi-Scan 0.7062/0.3163	Multi-scan 0.8969/0.2690
Largest peak in Final Diff. Map (e^- / $Å^3$)	1.000	1.000

*$R = \Sigma_{hkl}(\ |\ |F_{obs}| - |F_{calc}|\ |\ )/\Sigma_{hkl}|F_{obs}|$; $R_w = [\Sigma_{hkl}w(\ |F_{obs}| - |F_{calc}|\ )^2/\Sigma_{hkl}wF_{obs}^2]^{1/2}$, $w = 1/\sigma^2(F_{obs})$; $GOF = [\Sigma_{hkl}w(\ |F_{obs}| - |F_{calc}|\ )^2/(n_{data} - n_{vari})]^{1/2}$.

Table B.2. Crystallographic data for compounds **3.5** and **3.7.**

Compound	**3.5**	**3.6**
Empirical formula	$PtSnC_{25}H_{52}N_2$	$PtSnC_{24}H_{74}N_2O$
Formula weight	694.7	977.39
Crystal system	Triclinic	Orthorhombic
Lattice parameters		
a (Å)	9.3026(3)	11.9259(5)
b (Å)	12.3233(5)	13.9050(6)
c (Å)	14.8142(6)	26.0856(10)
α (deg)	96.2210(10)	90.00
β (deg)	93.0120(10)	90.00
γ (deg)	110.3320(10)	90.00
V ($Å^3$)	1575.66(10)	4325.8(3)
Space group	$P\ \bar{1}$ (# 2)	P2(1)2(1)2(1)
Z value	2	4
ρ_{calc} (g / cm^3)	1.464	1.501
μ (Mo K_α) (mm^{-1})	5.238	4.397
Temperature (K)	100(2)	296
$2\Theta_{max}$ (°)	55.0	64.0
No. Obs. ($I > 2\sigma(I)$)	289	402
No. Parameters	6755	11995
Goodness of fit GOF*	1.118	1.005
Max. shift in cycle	0.001	0.002
Residuals*: R1; wR2	Multi-scan 0.0294; 0.0988	Multi-scan 0.0330; 0.0665
Absorption Correction, Max/min	0.7461/0.5448	0.9172/ 0.1778
Largest peak in Final Diff. Map ($e^- / Å^3$)	0.996	1.262

*$R = \Sigma_{hkl}(\ |\ |F_{obs}| - |F_{calc}|\ |\ )/\Sigma_{hkl}|F_{obs}|$; $R_w = [\Sigma_{hkl}w(|F_{obs}| - |F_{calc}|)^2/\Sigma_{hkl}wF_{obs}^2]^{1/2}$, $w = 1/\sigma^2(F_{obs})$; $GOF = [\Sigma_{hkl}w(|F_{obs}| - |F_{calc}|)^2/(n_{data} - n_{vari})]^{1/2}$.

Appendix C: Supporting Information for Chapter 4.

Table C.1. Crystallographic data for compounds $Ni(SnBu^t_3)_2(CNBu^t)_3$, **4.1** and $Ni(SnBu^t_3)_2(CNBu^t)_2(CO)$,**4.2.**

Compound	**4.1•C_6H_6**	**4.2•Et_2O**
Empirical formula	$NiSn_2N_3C_{45}H_{87}$	$NiSn_2N_2O_2C_{39}H_{82}$
Formula weight	966.27	907.19
Crystal system	Orthorhombic	Orthorhombic
Lattice parameters		
a (Å)	13.6127(5)	13.3434(6)
b (Å)	19.6978(8)	19.3749(9)
c (Å)	39.0026(15)	9.2939(4)
α (deg)	90.00	90.00
β (deg)	90.00	90.00
γ (deg)	90.00	90.00
V ($Å^3$)	10458.1(7)	2402.72(19)
Space group	*Cmca* (# 64)	*Pmmn* (# 59)
Z value	8	4
ρ_{calc} (g / cm^3)	1.227	2.344
μ (Mo Kα) (mm^{-1})	1.333	2.470
Temperature (K)	296	296
$2\Theta_{max}$ (°)	56.00	56.00
No. Obs. ($I > 2\sigma(I)$)	4627	2706
No. Parameters	254	133
Goodness of fit	1.098	1.006
Max. shift in cycle	0.001	0.045
Residuals*:R1; wR2	0.0529; 0.1344	0.0303; 0.0759
Absorption Correction, Max/min	Multi-scan 0.7465; 0.5501	Multi-scan 0.7465, 0.5695
Largest peak in Final Diff. Map ($e^- / Å^3$)	2.098	0.569

*$R = \Sigma_{hkl}(\,|\,|F_{obs}| - |F_{calc}|\,|\,)/\Sigma_{hkl}|F_{obs}|$; $R_w = [\Sigma_{hkl}w(|F_{obs}| - |F_{calc}|)^2/\Sigma_{hkl}wF_{obs}^2]^{1/2}$, $w = 1/\sigma^2(F_{obs})$; $GOF = [\Sigma_{hkl}w(|F_{obs}| - |F_{calc}|)^2/(n_{data} - n_{vari})]^{1/2}$.

Table C.2 Crystallographic data for compounds $[Ni(Sn^tBu_3)(^tBuNC)_2(CO)]_2$, **4.4** and $Ni(\eta^2$-TEMPO)$(SnBu^t_3)$ $(CNBu^t)$, **4.5.**

Compound	**4.4**	**4.5**
Empirical formula	$Ni_2Sn_2N_4O_2C_{46}H_{90}$	$NiSnON_2C_{26}H_{54}$
Formula weight	1086.02	588.11
Crystal system	Monoclinic	Monoclinic
Lattice parameters		
a (Å)	10.2875(5)	17.2516(7)
b (Å)	15.7767(7)	11.3442(4)
c (Å)	17.8035(8)	17.5158(7)
α (deg)	90.00	90.00
β (deg)	94.1568(8)	109.8390(6)
γ (deg)	90.00	90.00
V ($Å^3$)	2882.0(2)	3224.5(2)
Space group	$P2_1/n$ (# 14)	$P2_1/c$ (# 14)
Z value	2	4
ρ_{calc} (g / cm^3)	1.251	1.211
μ (Mo Kα) (mm^{-1})	1.533	1.375
Temperature (K)	296	296
$2\Theta_{max}$ (°)	56.00	56.00
No. Obs. (I > 2σ(I))	4826	6236
No. Parameters	268	296
Goodness of fit	1.012	1.015
Max. shift in cycle	0.059	0.004
Residuals*:R1; wR2	0.0317; 0.0782	0.0292; 0.0750
Absorption Correction, Max/min	Multi-scan 0.7465, 0.6127	Multi-scan 0.7457; 0.5671
Largest peak in Final Diff. Map (e^- / $Å^3$)	0.438	0.857

*$R = \Sigma_{hkl}(\,|\,|F_{obs}|-|F_{calc}|\,|\,)/\Sigma_{hkl}|F_{obs}|$; $R_w = [\Sigma_{hkl}w(|F_{obs}|-|F_{calc}|)^2/\Sigma_{hkl}wF_{obs}^2]^{1/2}$, $w = 1/\sigma^2(F_{obs})$; $GOF = [\Sigma_{hkl}w(|F_{obs}|-|F_{calc}|)^2/(n_{data} - n_{vari})]^{1/2}$.

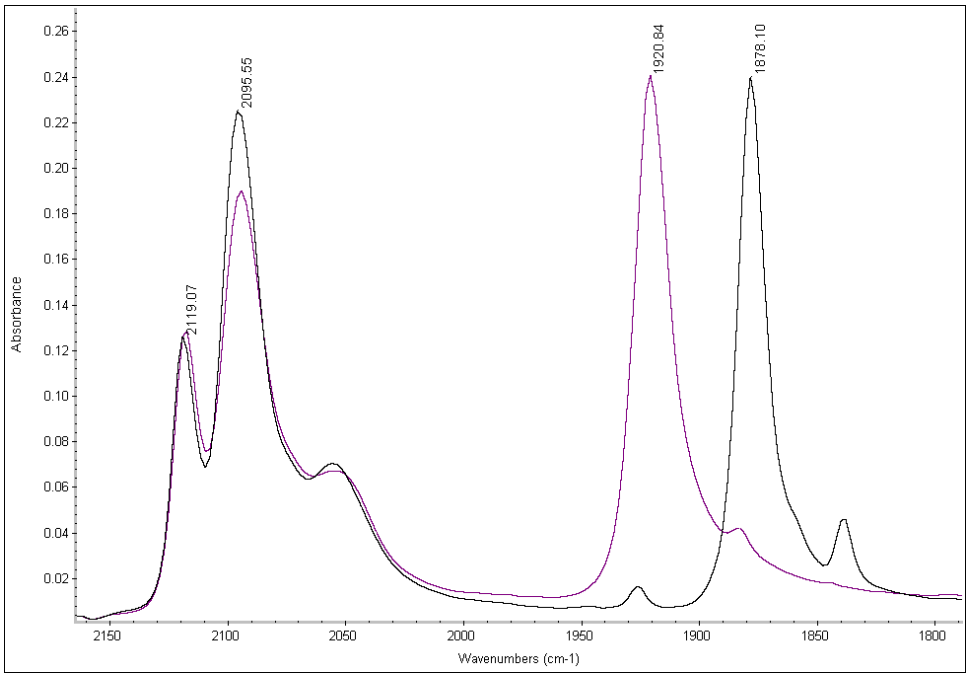

Figure C.1. Single crystal FTIR spectrum of $Ni(SnBu^t_3)_2(CNBu^t)_2(CO)$ (purple) vs ^{13}CO-$Ni(SnBu^t_3)_2(CNBu^t)_2(CO)$ (black).

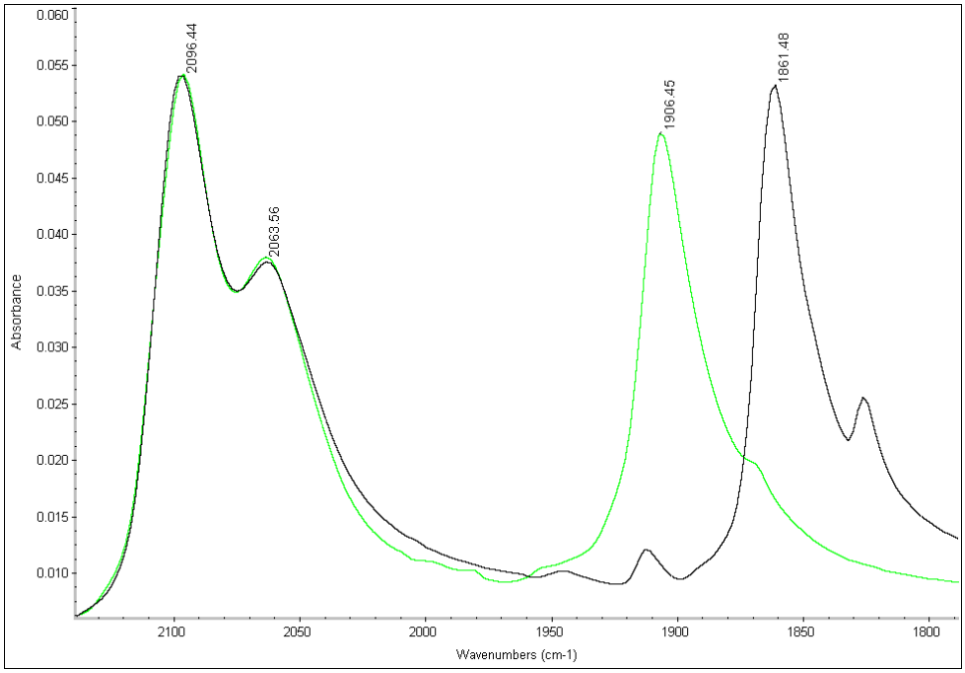

Figure C.2. Single crystal FTIR spectrum of $[Ni(SnBu^t_3)(CNBu^t)_2(CO)]_2$ (green) vs ^{13}CO-$[Ni(SnBu^t_3)(CNBu^t)_2(CO)]_2$ (black).

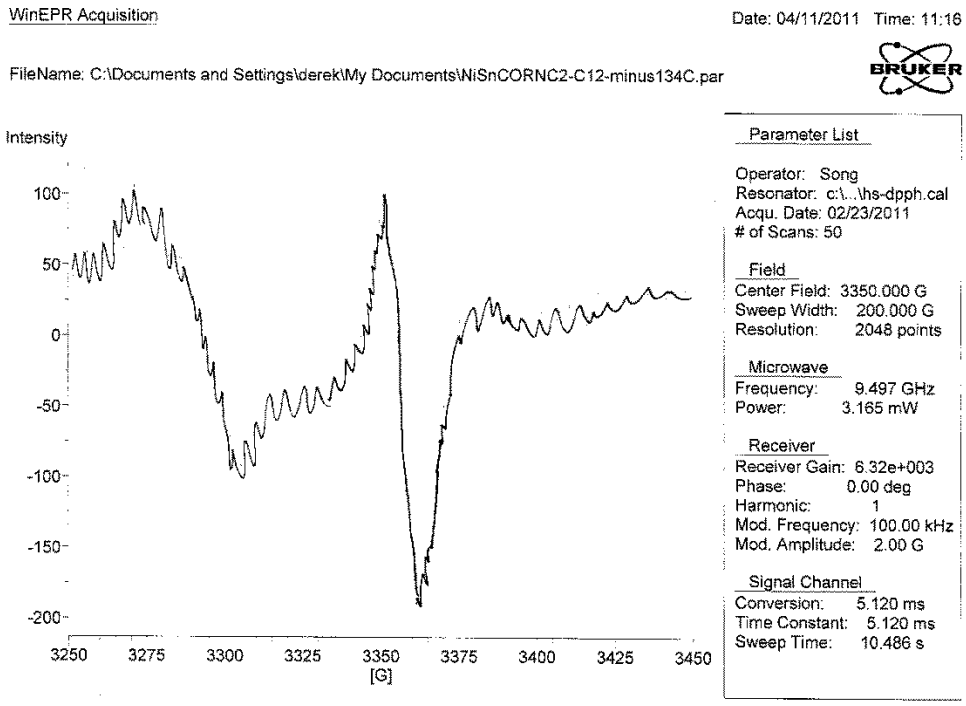

Figure C.3. ESR spectrum of ^{12}CO-[Ni($SnBu^t_3$)($CNBu^t$)$_2$(CO)]$_2$ in toluene at 134 K.

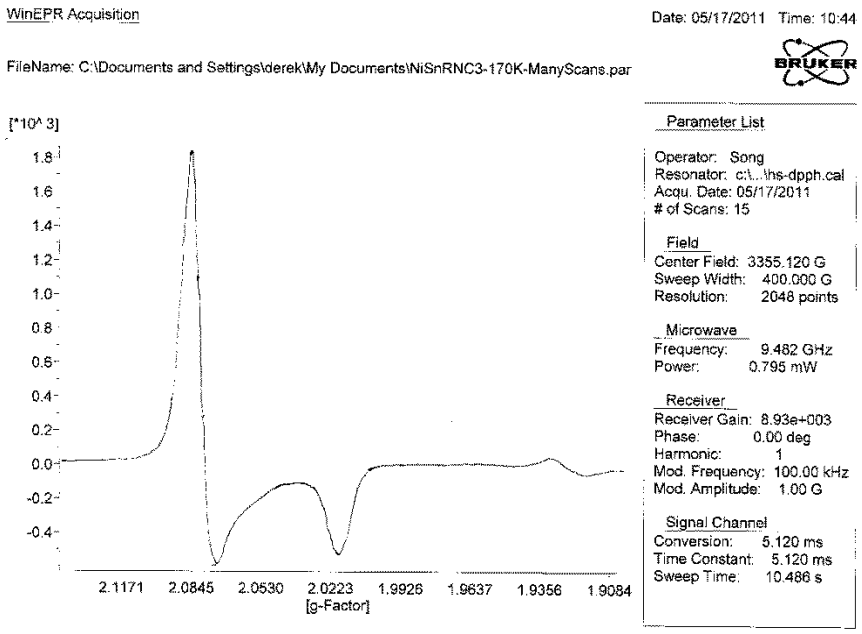

Figure C.4. ESR spectrum of proposed Ni(Sn^tBu_3)(^{t}BuNC)$_3$ in toluene at 170 K.

Appendix D: Supporting Information for Chapter 5.

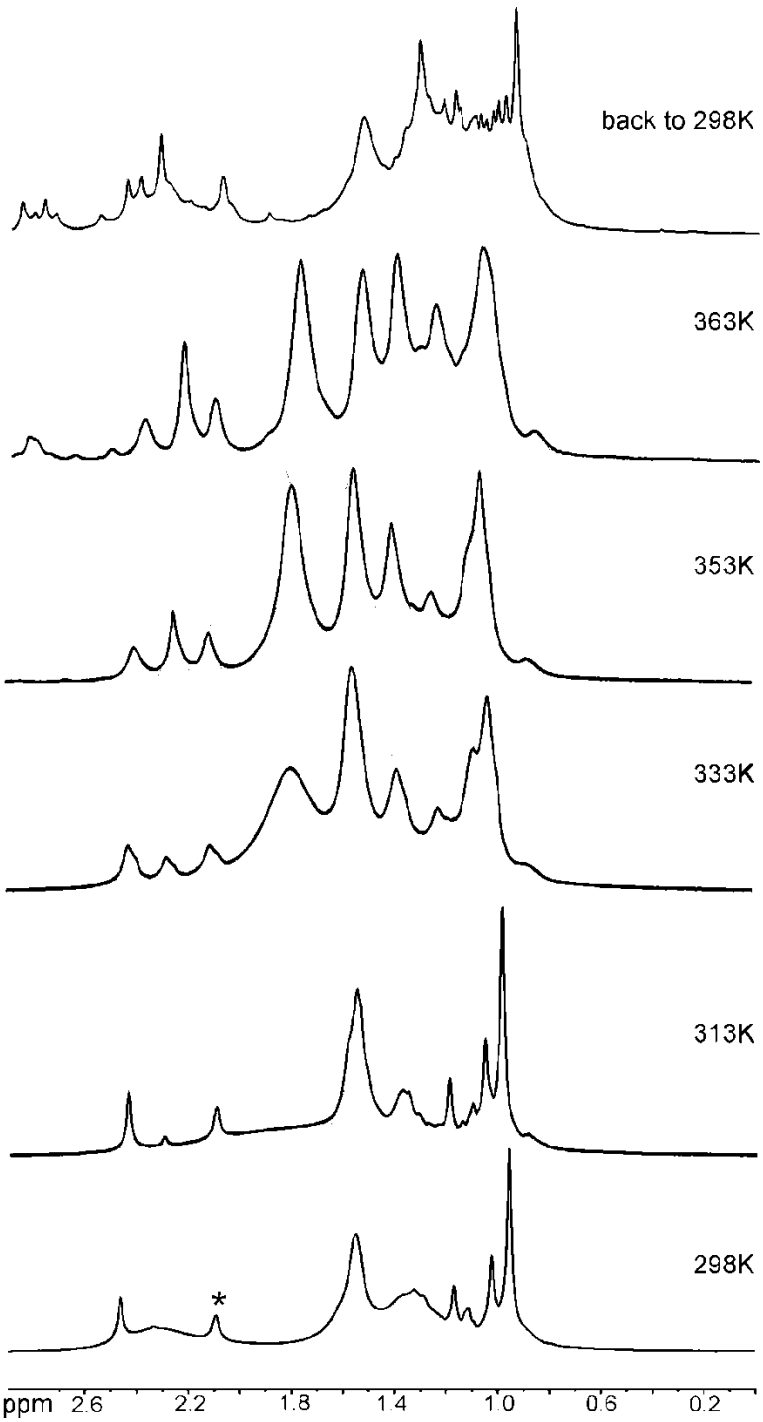

Figure D.1. ^{1}H NMR spectra at 400 MHz of Ni(η^2-TEMPO)(κ^1-TEMPO)(CN^{t}Bu), **5.2*c*** at various temperatures in toluene-d_8 solvent. * denotes the methyl peak from toluene-d_8 solvent.

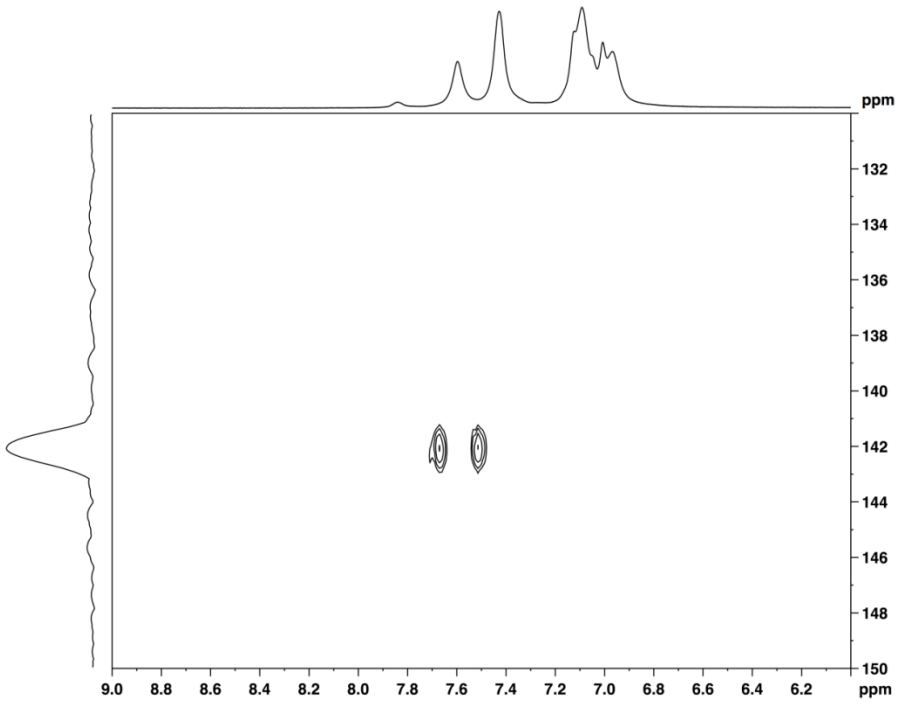

Figure D.2. 2D [^{1}H, ^{15}N] HSQC NMR spectra of Ni(η^2-TEMPO)(κ^1-TEMPOH)(κ^1-CCPh), **5.3*c*** in toluene-d_8. The ^{15}N chemical shift is with reference to liquid NH_3.

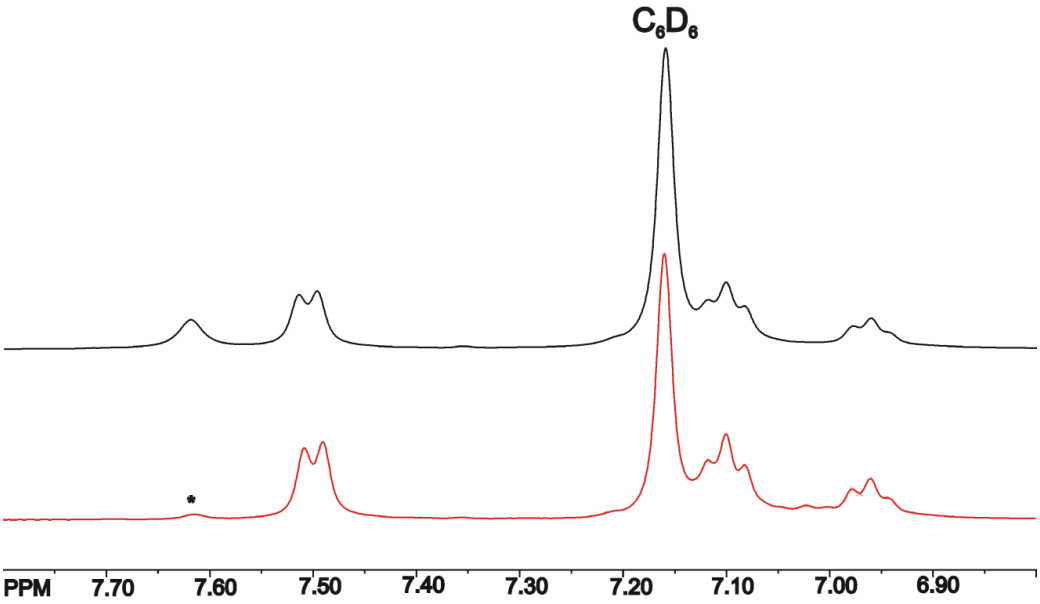

Figure D.3. ^{1}H NMR spectrum of Ni(η^2-TEMPO)(κ^1-TEMPOH)(κ^1-*C*CPh), **5.3*c*** (black) and Ni(η^2-TEMPO)(κ^1-TEMPOD)(κ^1-*C*CPh), **5.3*c*-*d*$_1$** (red). * denotes acetylene hydrogen now on TEMPO nitrogen N2.

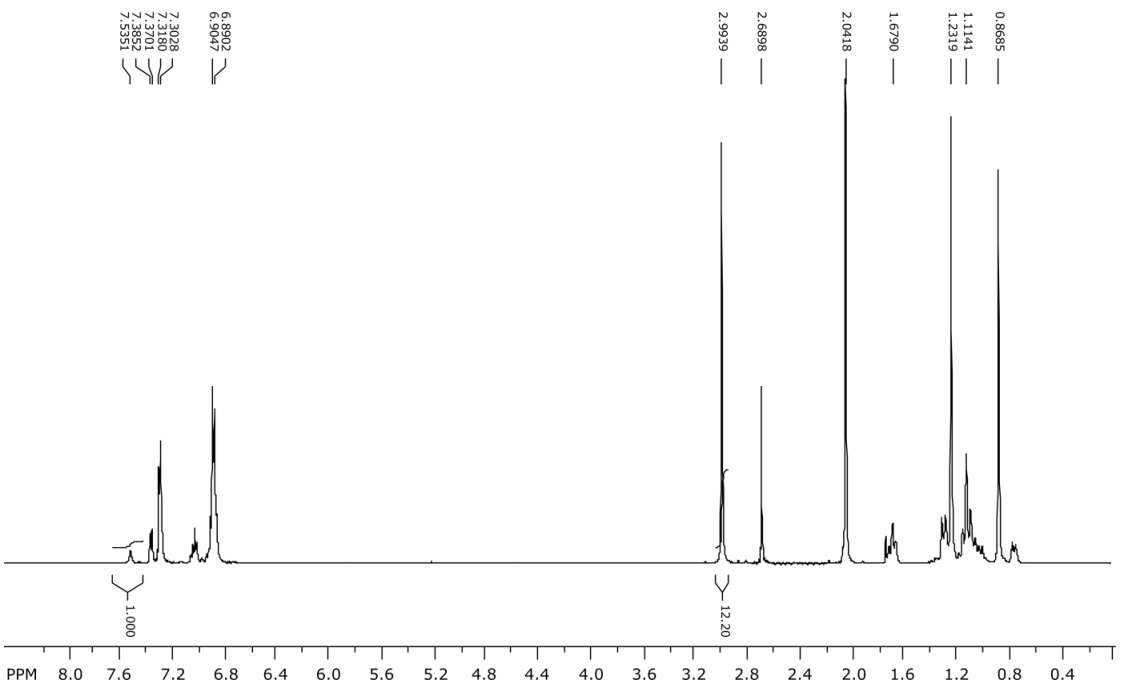

Figure D.4. ^{1}H NMR spectrum of **5.1*t*** plus a 6:6 mixture of PhCCH and PhCCD in toluene-d_8 solvent at room temperature.

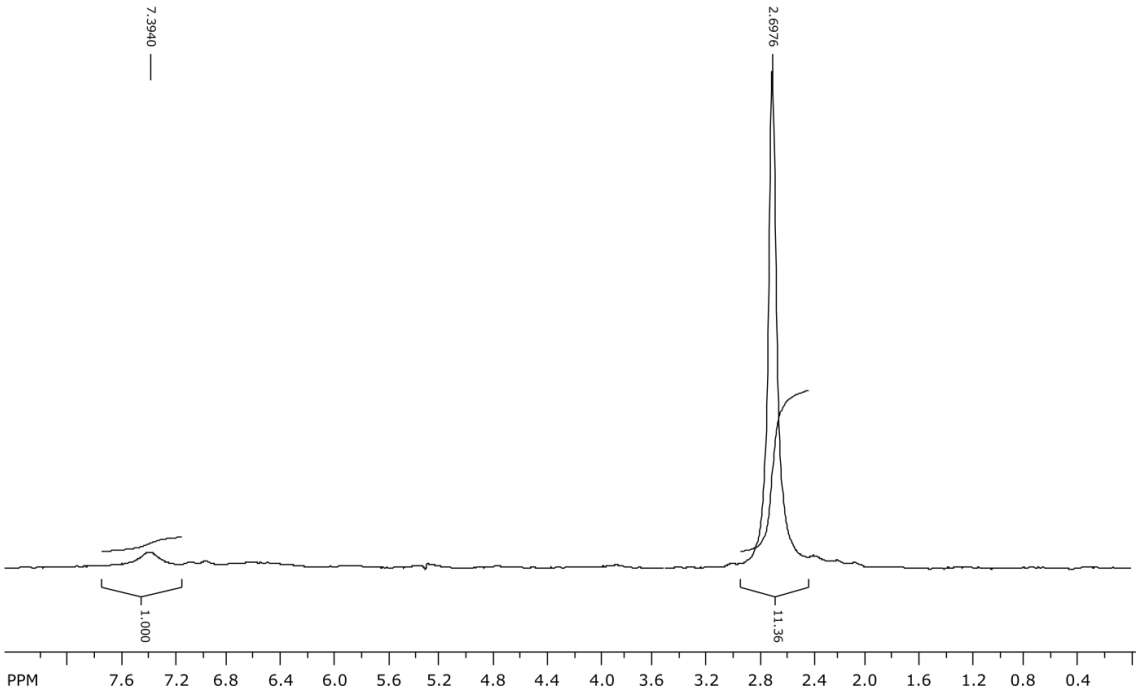

Figure D.5. ^{2}H NMR spectrum of **5.1*t*** plus a 6:6 mixture of PhCCH and PhCCD in toluene solvent at room temperature

Table D.1. Crystallographic data for compounds **5.1*t***, **5.2*c*** and **5.3*c***.

Compound	**5.1*t***	**5.2*c***	**5.3*c***
Empirical formula	$NiO_2N_2C_{18}H_{36}$	$NiO_2N_3C_{23}H_{45}$	$NiO_2N_2C_{26}H_{42}$
Formula weight	371.20	454.33	473.33
Crystal system	Monoclinic	Monoclinic	Triclinic
Lattice parameters			
a (Å)	8.1165(4)	7.7242(3)	8.3519(3)
b (Å)	10.6126(5)	21.8142(8)	12.3164(4)
c (Å)	11.6382(6)	15.2535(6)	14.5401(5)
α (deg)	90.00	90.00	111.5580(5)
β (deg)	107.224(3)	92.041(7)	95.8880(5)
γ (deg)	90.00	90.00	107.7300(4)
V (Å^3)	957.52(8)	2568.54(17)	1285.55
Space group	$P2_1/n$ (# 14)	$P2_1/n$ (# 14)	$P\bar{1}$ (# 2)
Z value	2	4	2
ρ_{calc} (g / cm^3)	1.287	1.175	1.223
μ (Mo Kα) (mm^{-1})	1.024	0.777	0.778
Temperature (K)	100	100	100
$2\Theta_{max}$ (°)	57.00	58.00	56.00
No. Obs. (I > 2σ(I))	2139	6360	5974
No. Parameters	178	442	448
Goodness of fit	1.057	1.075	1.043
Max. shift in cycle	0.001	0.003	0.002
Residuals*:R1; wR2	0.0315; 0.0830	0.0234; 0.0581	0.0217; 0.0569
Absorption Correction, Max/min	Multi-scan 0.7465/0.4399	Multi-scan 0.7465/0.5552	Multi-scan 0.7465/0.6322
Largest peak in Final Diff. Map (e$^-$ / Å^3)	0.966	0.423	0.346

*$R = \Sigma_{hkl}(\,|\,|F_{obs}|-|F_{calc}|\,|)/\Sigma_{hkl}|F_{obs}|$; $R_w = [\Sigma_{hkl}w(|F_{obs}|-|F_{calc}|)^2/\Sigma_{hkl}wF_{obs}^2]^{1/2}$, $w = 1/\sigma^2(F_{obs})$; GOF = $[\Sigma_{hkl}w(|F_{obs}|-|F_{calc}|)^2/(n_{data} - n_{vari})]^{1/2}$.

Table D.2. Crystallographic Data for compounds **5.4*c***, **5.5*c*** and **5.7*c***.

Compound	**5.4*c***	**5.5*c***	**5.7*c***
Empirical formula	$NiSiO_2\ N_2C_{23}H_{46}$	$NiO_2N_2C_{20}H_{38}$	$NiO_2N_2C_{28}H_{42}$
Formula weight	469.42	397.23	497.345
Crystal system	Monoclinic	Monoclinic	Triclinic
Lattice parameters			
a (Å)	7.8725(3)	13.6684(6)	7.7421(3)
b (Å)	10.8105(4)	11.5267(5)	12.3093(5)
c (Å)	33.0125(13)	14.3518(6)	15.1659(6)
α (deg)	90.00	90.00	74.2830(5)
β (deg)	93.253(1)	92.658(1)	77.757(1)
γ (deg)	90.00	90.00	84.2730(6)
V ($Å^3$)	2805.02(19)	2258.72(17)	1358.25(9)
Space group	$P2_1/c$ (# 14)	$P2_1/c$ (# 14)	$P\ \bar{1}$ (# 2)
Z value	4	4	2
ρ_{calc} (g / cm^3)	1.112	1.168	1.216
μ (Mo Kα) (mm^{-1})	0.753	0.873	0.740
Temperature (K)	296	296	296
$2\Theta_{max}$ (°)	54.00	56.00	56.00
No. Obs. ($I > 2\sigma(I)$)	5114	4597	6003
No. Parameters	277	242	466
Goodness of fit	1.046	1.018	1.042
Max. shift in cycle	0.003	0.001	0.001
Residuals*:R1; wR2	0.0459; 0.1231	0.0307; 0.0813	0.0275; 0.0757
Absorption Correction, Max/min	Multi-scan 0.9285/0.7047	Multi-scan 0.9178/0.7216	Multi-scan 0.9640/0.8086
Largest peak in Final Diff. Map (e^- / $Å^3$)	0.931	0.260	0.371

*$R = \Sigma_{hkl}(\ |\ |F_{obs}|\ -\ |F_{calc}|\ |\ )/\Sigma_{hkl}|F_{obs}|$; $R_w = [\Sigma_{hkl}w(\ |F_{obs}|\ -\ |F_{calc}|\ )^2/\Sigma_{hkl}wF_{obs}^2]^{1/2}$, $w = 1/\sigma^2(F_{obs})$; $GOF = [\Sigma_{hkl}w(\ |F_{obs}|\ -\ |F_{calc}|\ )^2/(n_{data} - n_{vari})]^{1/2}$.

Table D.3. Crystallographic data for compounds **5.8*cc***, and **5.9*t*.**

Compound	**5.8*cc***	**5.9*t***
Empirical formula	$Ni_2O_4N_4C_{46}H_{78}•2C_6H_6$	$NiO_2N_3C_{23}H_{41}$
Formula weight	1024.76	450.30
Crystal system	Monoclinic	Orthorhombic
Lattice parameters		
a (Å)	13.7972(7)	14.7413(6)
b (Å)	10.8726(6)	14.8196(6)
c (Å)	18.9646(9)	22.0621(9)
α (deg)	90	90.00
β (deg)	101.396(1)	90.00
γ (deg)	90	90.00
V (Å^3)	2788.8(2)	4819.7(3)
Space group	$P2_1/c$ (# 14)	*Pbca* (# 61)
Z value	2	8
ρ_{calc} (g / cm^3)	1.220	1.241
μ (Mo Kα) (mm^{-1})	0.722	0.827
Temperature (K)	100	100
$2\Theta_{max}$ (°)	56.00	57.00
No. Obs. (I > 2σ(I))	5391	4852
No. Parameters	315	270
Goodness of fit	1.018	1.012
Max. shift in cycle	0.001	0.001
Residuals*:R1; wR2	0.0376; 0.0895	0.0296; 0.0671
Absorption Correction, Max/min	Multi-scan 0.7461/0.6645	Multi-scan 0.9677/0.8137
Largest peak in Final Diff. Map (e$^-$ / Å^3)	1.247	0.340

*$R = \Sigma_{hkl}(\,|\,|F_{obs}|-|F_{calc}|\,|)/\Sigma_{hkl}|F_{obs}|$; $R_w = [\Sigma_{hkl}w(|F_{obs}|-|F_{calc}|)^2/\Sigma_{hkl}wF_{obs}^2]^{1/2}$, $w = 1/\sigma^2(F_{obs})$; GOF = $[\Sigma_{hkl}w(|F_{obs}|-|F_{calc}|)^2/(n_{data} - n_{vari})]^{1/2}$.

Table D.4. Solution-phase reaction free energies (ΔG_{soln} in kcal mol^{-1}) of bimetallic complexes and relative free energies ($\Delta\Delta G_{soln}$ in kcal mol^{-1}) of isomers of complex **5.8** (isomer **5.8*cc*** is arbitrarily set to 0.0 kcal mol^{-1}).

PBE	**B3LYP**
2 equiv **5.1*t*** + HCCH → **5.6*cc*** 5.4	2 equiv **5.1*t*** + HCCH → **5.6*cc*** 14.4
5*c* + **5.1*t*** → **5.6*cc*** 9.2	**5*c*** + **5.1*t*** → **5.6*cc*** 15.8
5.8*cc* **5.8*ct*** **5.8*tt*** 0.0 4.1 9.2	**5.8*cc*** **5.8*ct*** **5.8*tt*** 0.0 3.3 5.6
2 equiv **5.1*t*** + HCCPhCCH → **5.8*cc*** -5.2	2 equiv **5.1*t*** + HCCPhCCH → **5.8*cc*** -0.3
5.7*c* + **5.1*t*** → **5.8*cc*** -0.8	**5.7*c*** + **5.1*t*** → **5.8*cc*** 1.1

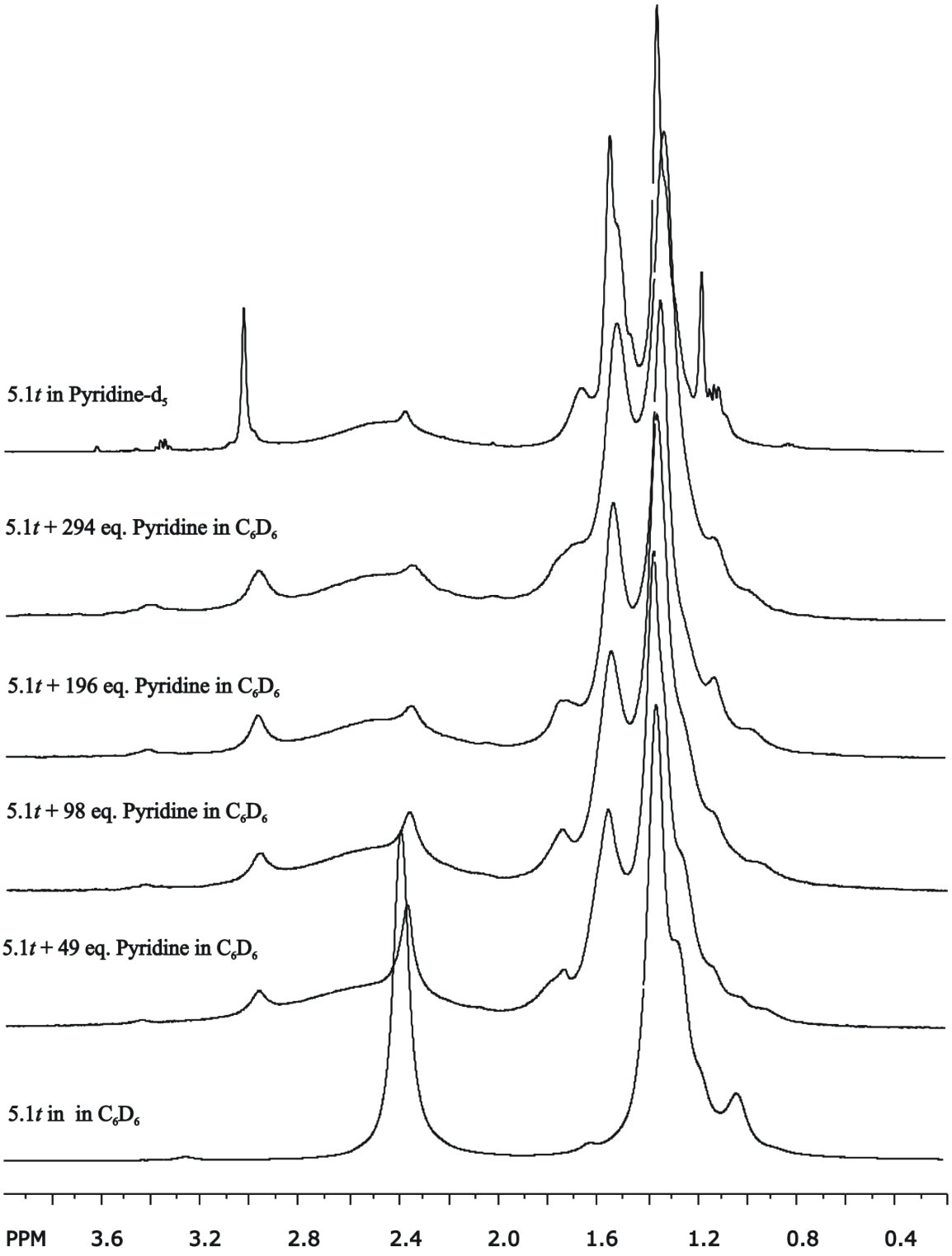

Figure D.6. ^{1}H NMR spectra for the addition of excess amounts of pyridine to **5.1*t*** at room temperature.

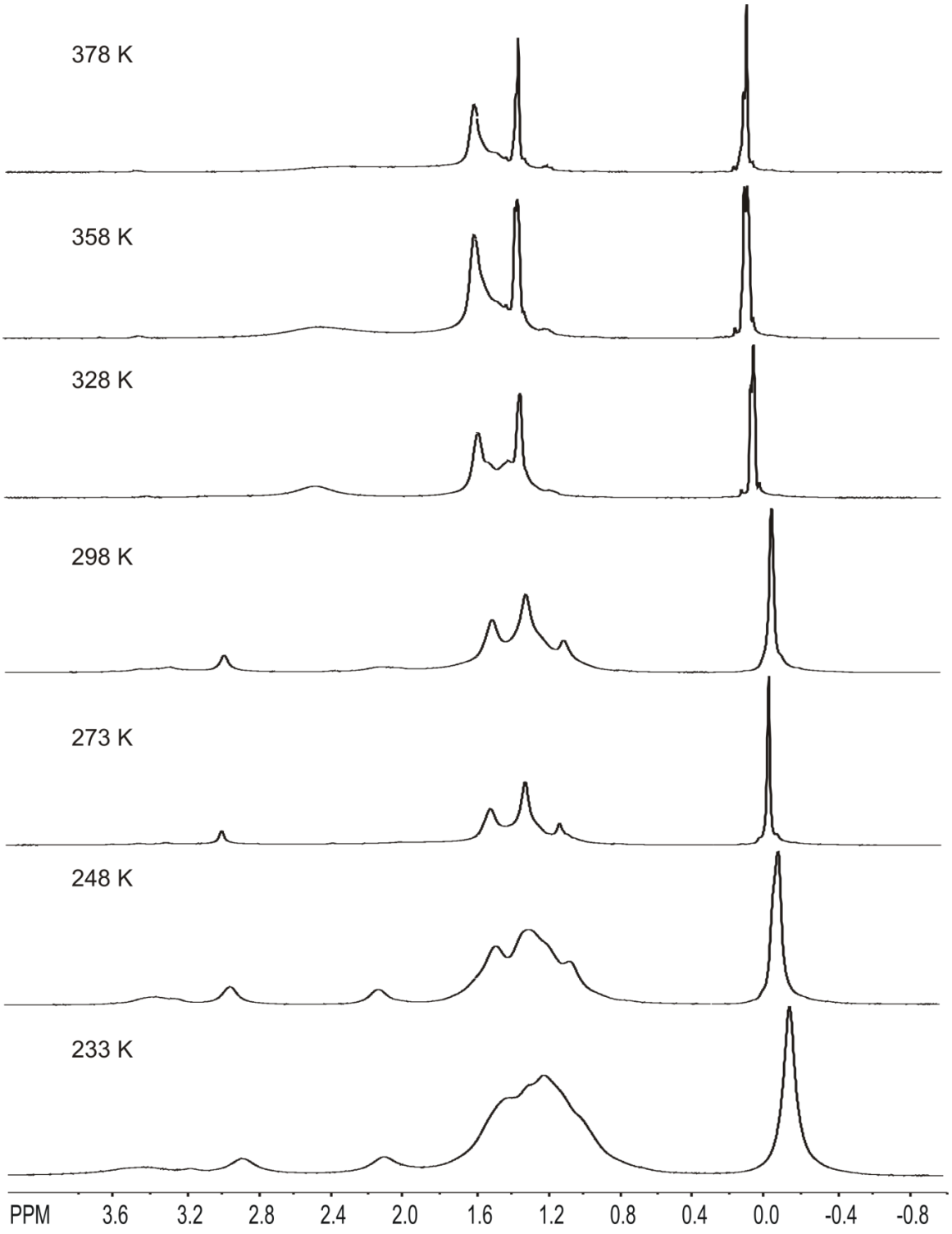

Figure D.7. ^{1}H NMR spectra at 400 MHz of compound Ni(η^2-TEMPO)(η^1-TEMPO)(κ^1-NC$_5$H$_5$), **5.9*t*** at various temperatures in toluene-d_8 solvent.

Table D.5. Relative free energies and energies of activation (in kcal mol^{-1}). Experimentally observed isomer is in bold.

	5.1*t*				**5.1*c***			
	$\Delta G_{(g)}$	$\Delta G_{(soln)}$			$\Delta G_{(g)}$	$\Delta G_{(soln)}$		
B3LYP	**0**	**0**			4.2	4		
PBE	**0**	**0**			4	4		
	5.1*t* + $CNBu^t$ → **5.2*t***				**5.1*t*** + $CNBu^t$ → **5.2*c***			
	$\Delta G_{(g)}$	$\Delta G_{(soln)}$	$\Delta G^{‡}_{(g)}$	$\Delta G^{‡}_{(soln)}$	$\Delta G_{(g)}$	$\Delta G_{(soln)}$	$\Delta G^{‡}_{(g)}$	$\Delta G^{‡}_{(soln)}$
B3LYP	-6.9	-5.3	14.4	16.7	**-3.5**	**-2.8**	**15.5**	**16.3**
PBE	-15.3	-13	11.1	13.8	**-14.4**	**-13.1**	**13.6**	**15.1**
	5.1*t* + PhCCH → **5.3*t***				**5.1*t*** + PhCCH → **5.3*c***			
	$\Delta G_{(g)}$	$\Delta G_{(soln)}$	$\Delta G^{‡}_{(g)}$	$\Delta G^{‡}_{(soln)}$	$\Delta G_{(g)}$	$\Delta G_{(soln)}$	$\Delta G^{‡}_{(g)}$	$\Delta G^{‡}_{(soln)}$
B3LYP	2.5	2	20.6	22.7	**0**	**-0.6**	**24**	**25.3**
PBE	1.3	1.2	18.5	20.5	**-3.1**	**-3.3**	**20.3**	**22**
	5.1*t* + $HCCSi(CH_3)_3$ →**5.4*t***				**5.1*t*** + $HCCSi(CH_3)_3$ → **5.4*c***			
	$\Delta G_{(g)}$	$\Delta G_{(soln)}$	$\Delta G^{‡}_{(g)}$	$\Delta G^{‡}_{(soln)}$	$\Delta G_{(g)}$	$\Delta G_{(soln)}$	$\Delta G^{‡}_{(g)}$	$\Delta G^{‡}_{(soln)}$
B3LYP	2.7	2.1	21.5	23.8	**-0.2**	**-0.8**	**24.9**	**25.9**
PBE	0.2	-0.1	18.9	21.3	**-3.9**	**-4.2**	**22.9**	**24.2**
	5.1*t* + HCCH → **5.5*t***				**5.1*t*** + HCCH → **5.5*c***			
	$\Delta G_{(g)}$	$\Delta G_{(soln)}$	$\Delta G^{‡}_{(g)}$	$\Delta G^{‡}_{(soln)}$	$\Delta G_{(g)}$	$\Delta G_{(soln)}$	$\Delta G^{‡}_{(g)}$	$\Delta G^{‡}_{(soln)}$
B3LYP	1.5	0.6	18.2	19.8	**-0.6**	**-1.4**	**22.2**	**22.8**
PBE	-1.9	-2.5	17	18.5	**-3.3**	**-3.8**	**20.7**	**21.2**
	5.1*t* + HCCPhCCH → **5.7*t***				**5.1*t*** + HCCPhCCH → **5.7*c***			
	$\Delta G_{(g)}$	$\Delta G_{(soln)}$	$\Delta G^{‡}_{(g)}$	$\Delta G^{‡}_{(soln)}$	$\Delta G_{(g)}$	$\Delta G_{(soln)}$	$\Delta G^{‡}_{(g)}$	$\Delta G^{‡}_{(soln)}$
B3LYP	1.7	1.2	20.6	22.7	**-0.8**	**-1.4**	**23.5**	**24.8**
PBE	-0.6	-0.8	17.9	19.9	**-4.1**	**-4.4**	**20.2**	**21.7**
	5.1*t* + py → **5.9*t***				**5.1*t*** + py → **5.9*c***			
	$\Delta G_{(g)}$	$\Delta G_{(soln)}$	$\Delta G^{‡}_{(g)}$	$\Delta G^{‡}_{(soln)}$	$\Delta G_{(g)}$	$\Delta G_{(soln)}$	$\Delta G^{‡}_{(g)}$	$\Delta G^{‡}_{(soln)}$
B3LYP	**1.5**	**3.8**	**16.8**	**18.5**	8.6	9.8	21.2	21.9
PBE	**-0.5**	**2.1**	**17**	**18.8**	4	5.6	20.3	21.2

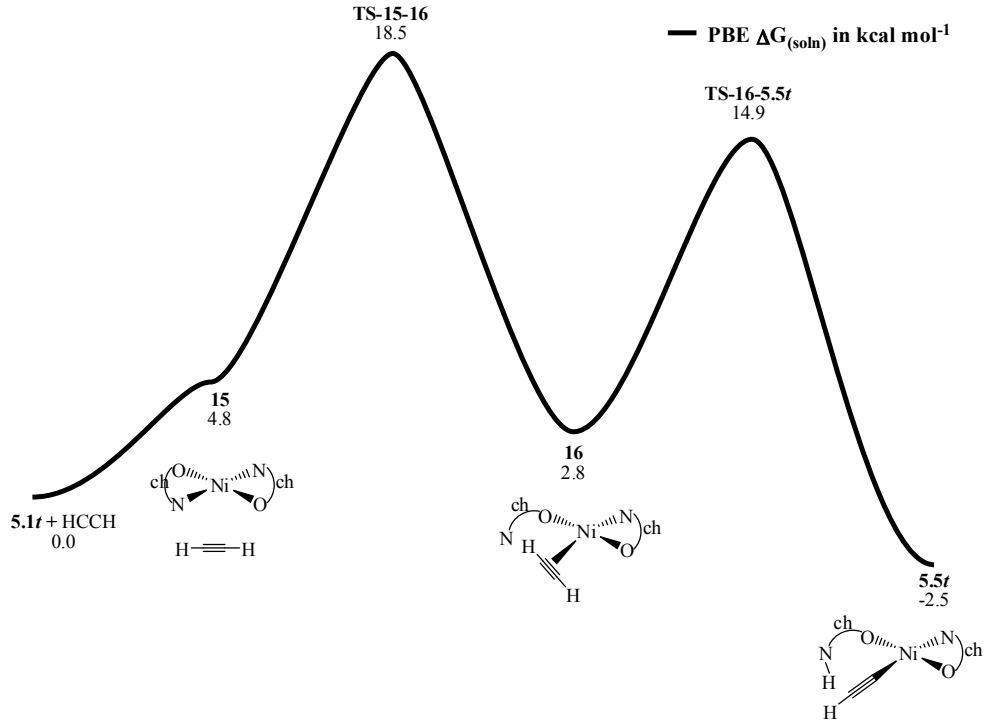

Scheme D.1. Addition of HCCH to **5.1*t*.**

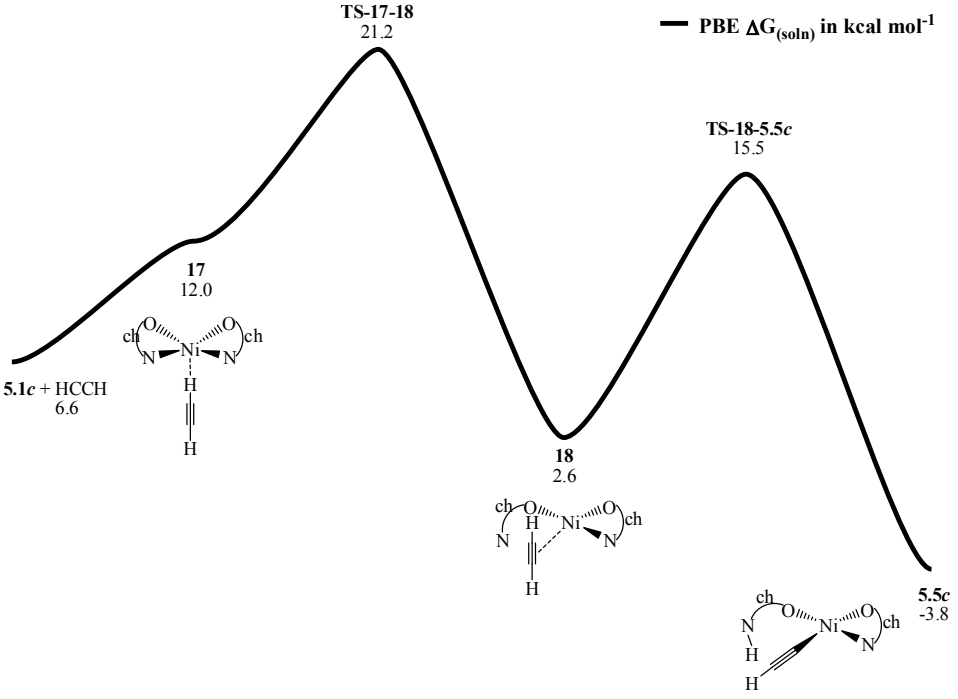

Scheme D.2. Addition of HCCH to **5.1*c*.**

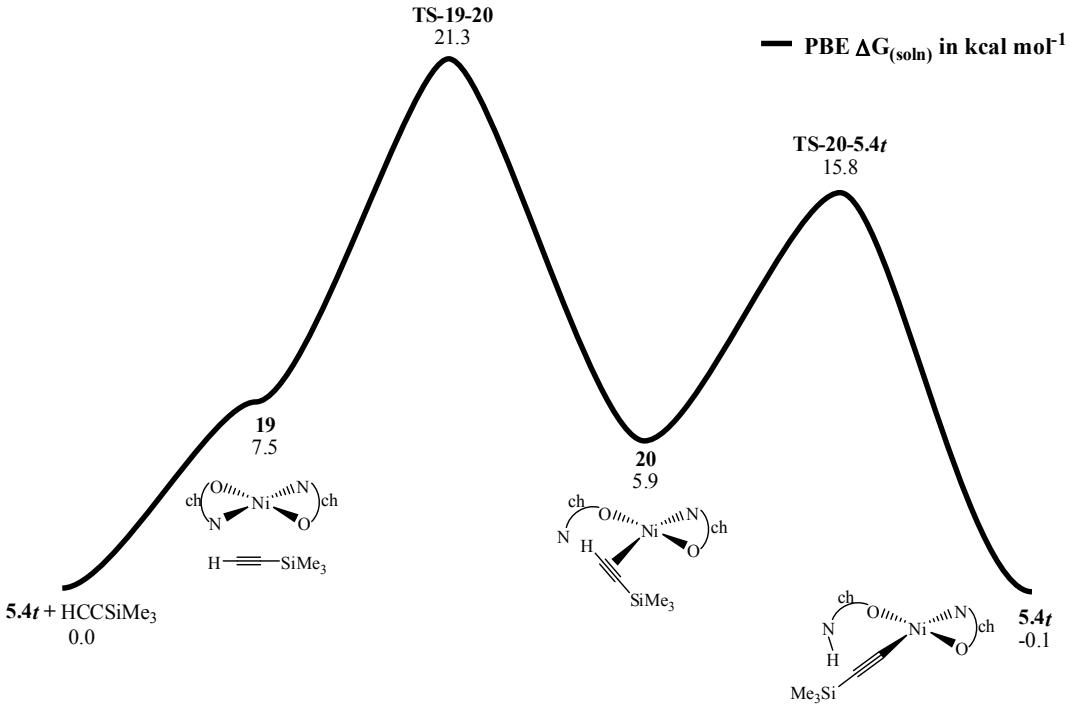

Scheme D.3. Addition of $HCCSiMe_3$ to form **5.4*t***.

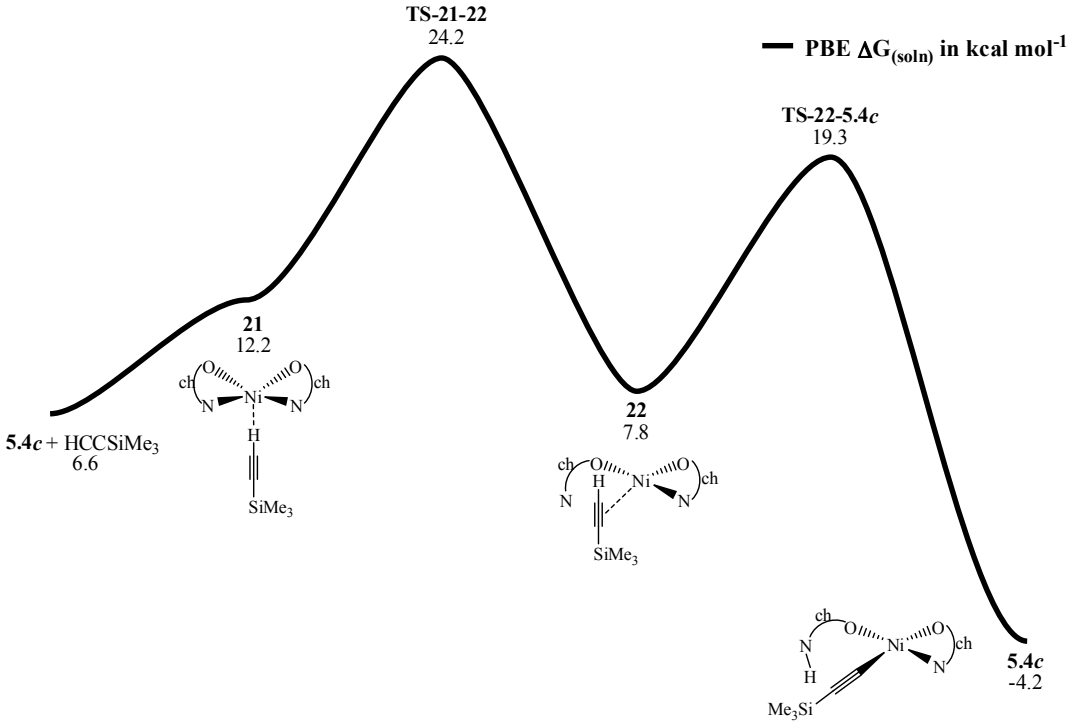

Scheme D.4. Addition of $HCCSiMe_3$ to form **5.4*c*.**

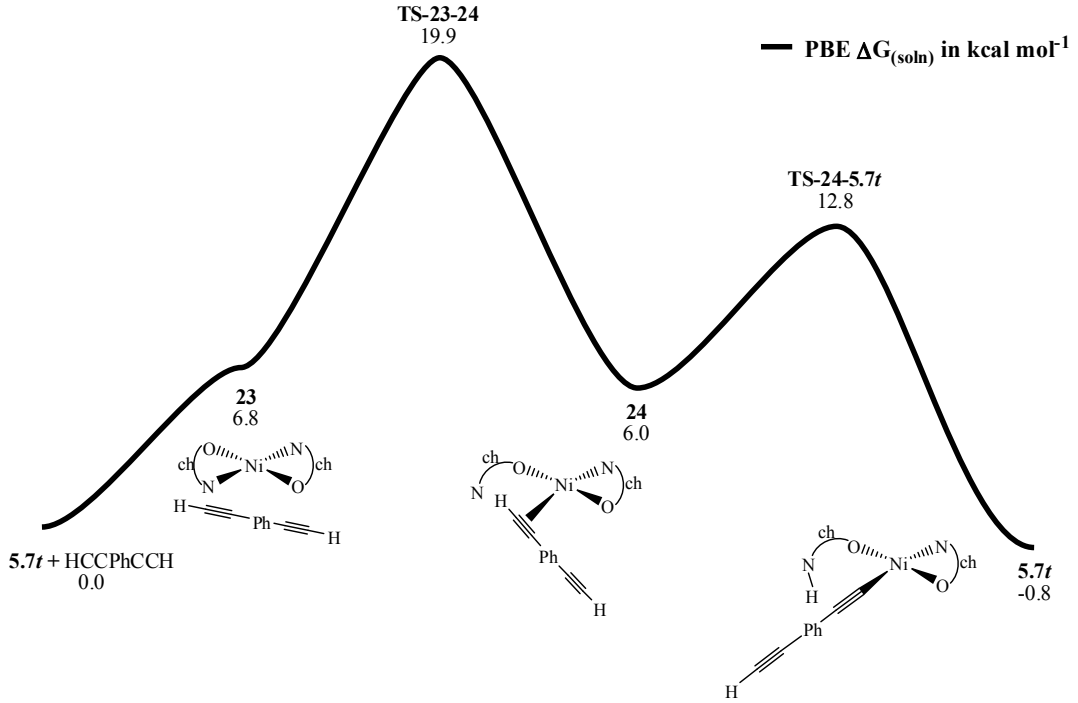

Scheme D.5. Addition of HCC(Ph)CCH to form **5.7*t***

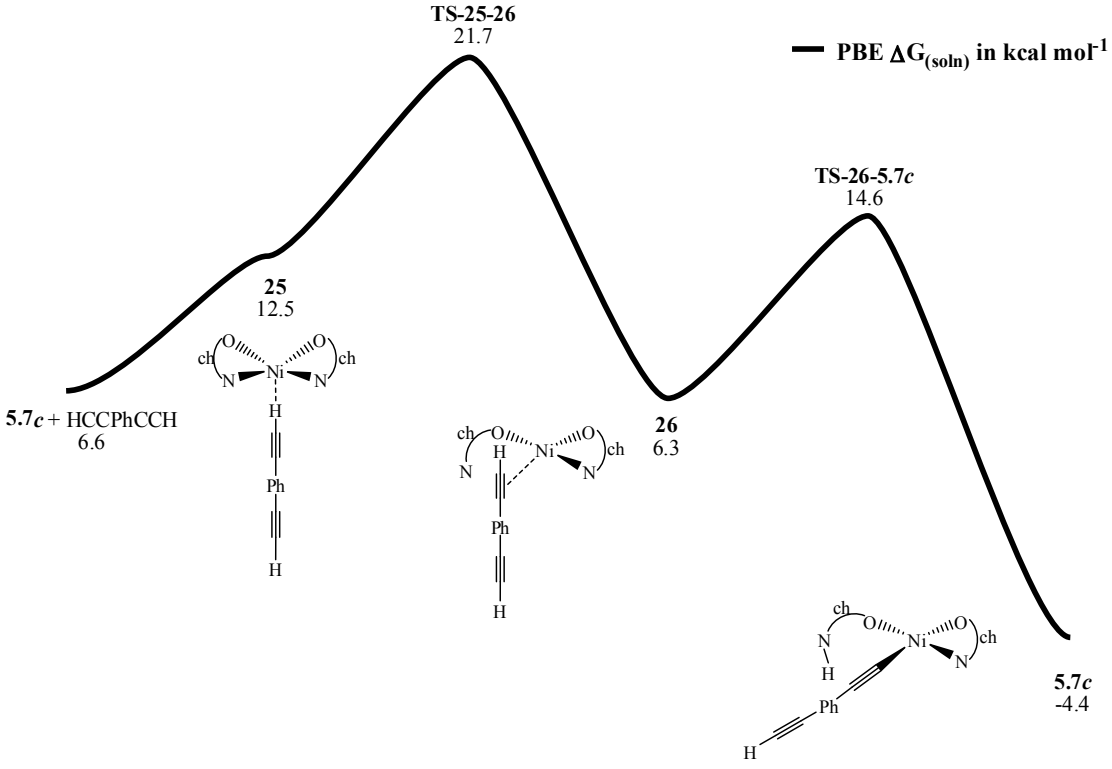

Scheme D.6. Addition of HCC(Ph)CCH to form **5.7*c*.**

Table D.6. Computed total dipole moments (in Debye).

	5.1*t*		**5.1*c***		
B3LYP	0.000	B3LYP	4.095		
PBE	0.000	PBE	3.989		
	5.2*t*		**5.2*c***		
B3LYP	3.310	B3LYP	7.692		
PBE	1.907	PBE	5.945		
	5.3*t*		**5.3c**		
B3LYP	6.307	B3LYP	3.322		
PBE	6.176	PBE	2.433		
	5.4*t*		**5.4*c***		
B3LYP	6.323	B3LYP	3.031		
PBE	6.078	PBE	2.422		
	5.5*t*		**5.5*c***		
B3LYP	6.182	B3LYP	3.651		
PBE	5.774	PBE	3.085		
	5.7*t*		**5.7*c***		
B3LYP	6.775	B3LYP	2.864		
PBE	6.964	PBE	2.412		
	5.8*tt*		**5.8*ct***		**5.8*cc***
B3LYP	1.821	B3LYP	5.338	B3LYP	0.000
PBE	0.823	PBE	5.637	PBE	0.000
	5.9*t*		**5.9*c***		
B3LYP	2.621	B3LYP	6.753		
PBE	1.280	PBE	4.877		

Description of computed NMR spectra for complex 5.1

Computed NMR data shows the lowest energy conformers of both *cis* and *trans* isomers of **5.1** have fortuitously similar chemical shifts. The isomerization of *cis* and *trans* isomers of **5.1** is possible at room temperature but would not be observed in the VT NMR because the coalescence of peaks would not produce new chemical shifts different

than those already present in the spectrum. Our hypothesis derived from the computational results is that the only expected alteration in the spectrum would be a visually imperceptible change in the peak integrations. The NMR chemical shift computations rely upon a variety of approximations and the absolute chemical shift values are difficult to accurately compute. Organometallic complexes present even further challenges in accurately computing chemical shifts. Therefore, we will rely more heavily upon the differences in chemical shifts.

One would reasonably expect obvious and quantitative differences in the spectra of **5.1*t*** and **5.1*c***. However, the results of the NMR computations are surprising. From the experimental NMR spectra, the two sets of four methyls have averaged chemical shifts of 2.39 and 1.36 ppm, respectively. The computed values for **5.1*t*** (chair/chair) are 2.10 and 1.18 ppm. Again, even though we expect to not as accurately compute the chemical shift, the placement of the peaks in the spectrum for **5.1*t*** still compare fairly well. The differences in these shifts (1.03 versus 0.92) are in excellent agreement (for computed NMR chemical shifts). For **5.1*t***, the experimental propylene CH2 proton range is 1.40 – 1.25 ppm. The computed chemical shifts are computed to be more downfield, ranging from 1.69 – 1.52 ppm.

The "chair-axial/chair" form is the lowest energy conformation of the *cis* isomer of **5.1** (**5.1*c***) and is computationally determined to be ~ 4 kcal mol-1 less stable than the lowest energy conformation of the *trans* isomer of **5.1** (**5.1*t*** - "chair/chair" form). Assume the isomerization to the lowest-energy *cis* form is possible at slightly elevated temperatures (as our computations indicate). At room temperature, approximately 0.1% of the complex in solution will be in the **5.1*c*** form. The detection limit for NMR is

typically considered to be in the parts per thousand. Even considering this detection limit, the range of the propylene proton chemical shifts for *both* the "chair" and "chair-axial" side (1.74 – 1.57 ppm) of **5.1*c*** fall within or are very close to the computed range for **5.1*t***. More importantly, the "chair" side methyl protons of **5.1*c*** have *essentially the same chemical shift* as the **5.1*t*** isomer, and the "chair-axial" side proton chemical shifts (1.73 and 1.49 ppm) now overlap with the propylene-type proton chemical shifts (further leading to the experimentally observed broadened peaks). Therefore, **5.1*c*** will not significantly contribute to the observed NMR spectrum.

Table D.7. Computed chemical shifts (in ppm) of complex **5.1*t***, **"chair/chair"**

H type	chemical shift	average of unique H shifts
CH3–	2.9	2.1
	0.89	
	2.5	
–CH2–	1.72	1.18
	0.42	
–CH2–	1.39	1.69
	1.79	
CH3–	1.59	1.52
	1.77	
	1.27	

Table D.8. Computed chemical shifts (in ppm) of complex **5.1*c***, **"chair-axial/chair"**

chair-axial H type	chemical shift	chair H type	chemical shift	chair-axial side average of unique H shifts	chair side average of unique H shifts
CH3–	1.67	CH3–	2.59	1.73	2.15
	0.41		2.89		
	3.1		0.97		
–CH2–	1.71	–CH2–	1.84	1.49	1.25
	0.91		0.44		
–CH2–	1.86	–CH2–	1.47	1.61	1.74
	1.64		1.78		
CH3–	1.58	CH3–	1.71	1.58	1.57
	1.83		1.31		
	1.33		1.84		

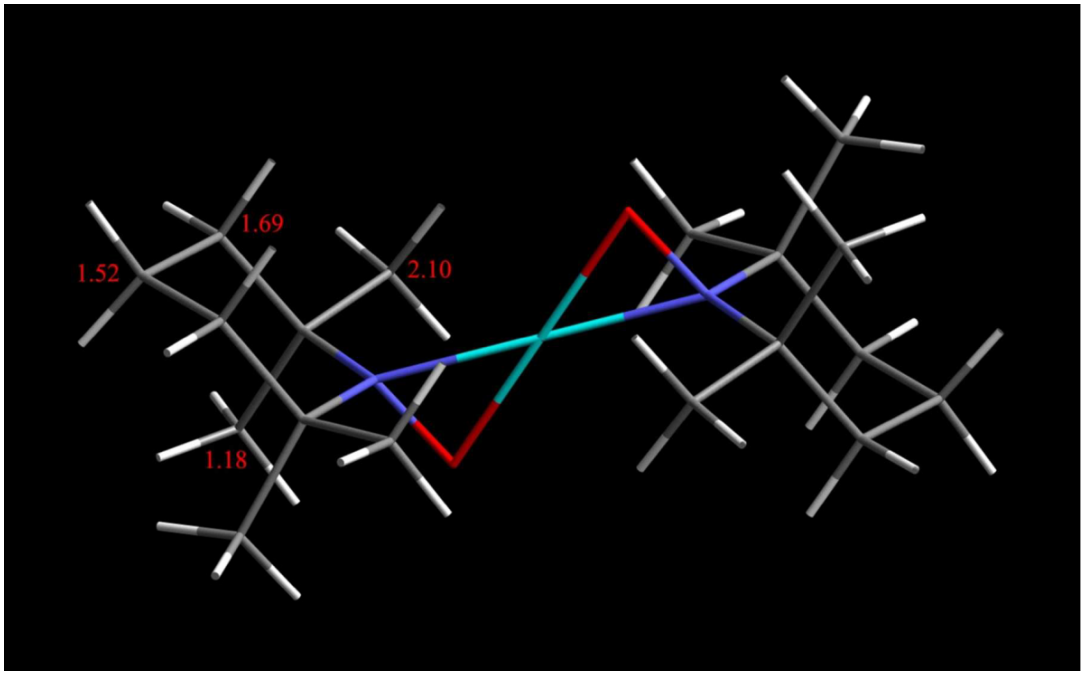

Figure D.8. Complex **5.1*t*** "chair/chair" – C_{2h} symmetric chemical shifts are omitted

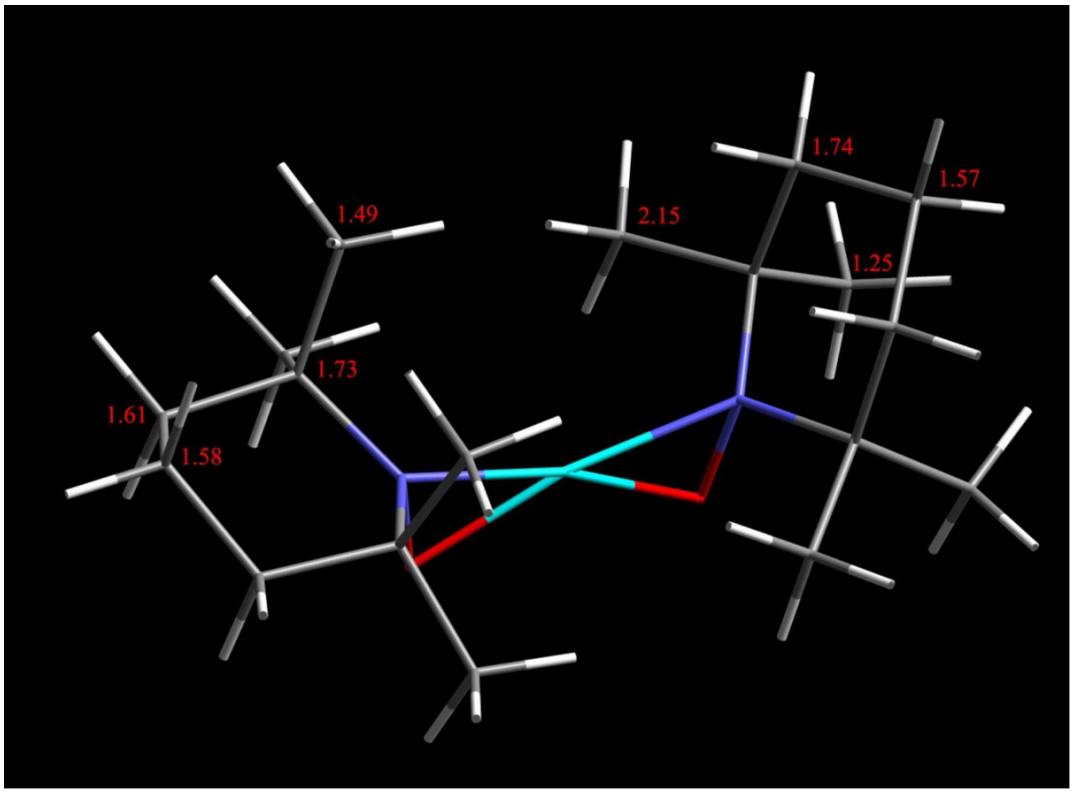

Figure D.9. Complex **5.1*c*** "chair-axial/chair" – C_S symmetric chemical shifts are omitted